الجمهورية الجزائرية الديمقراطية الشعبية

PEOPLE'S DEMOCRATIC REPUBLIC OF ALGERIA

وزارة التعليم العالي والبحث العلمي

MINISTRY OF HIGHER EDUCATION AND SCIENTIFIC RESEARCH

Badji Mokhtar Annaba University

Faculty of Engineering Sciences

Hydraulics department

جامعة باجي مختار – عنابـــة

كلية علـــوم الهندســـة

قســـم الـــــــــري

Thesis

Presented to obtain the diploma of

Doctorate

Specialty: Hydraulics

Field: Urban hydraulics

By: **BOUDIAF Besma**

Theme:

Contribution to the study of variability and climate change in the North-East of Algeria

Doctoral thesis defended on

in front of the jury composed of:

N°	Name and surname	Grade	Establishment	Quality
01	HANI Azzeddine	Pr.	Annaba University	President
02	BOUTAGHANE Hamouda	MCA	Annaba University	Supervisor
03	LAKEHAL Moussa	MCA	Annaba University	Examinator
04	MRAD Dounia	MCA	Souk Ahras University	Examinator
05	HEDDAM Salim	Pr.	Skikda University	Examinator
06	ŞEN Zekai	Pr.	Istanblul Medipol Universty	Guest member

Contribution to the study of variability and climate change in the North-East of Algeria

Abstract

Climate change impacts affect hydrological cycle and hence water resources availability and management works. Rainfall, as the most important hydro-meteorological event and as the main source of water, may have increasing or decreasing trends depending on the location, general air circulation, closeness to the coastal area and geomorphology. Algeria being adjacent to the mediterranean sea is under the effect of rainfall variations. A study of trends and possible risks is required in order to preserve the area against climate change impacts. There are many studies for monotonic trend analysis in the literature, but it is important to assess trends at different levels of records. For this purpose, in this thesis instead of monotonic trend search, partial trends are sought at "Low", "Medium" and "High" rainfall records groups, which is possible through the innovative trend analysis (ITA) methodology. The application of ITA methodology with the risk assessment is presented for 16 Algerian annual rainfall records from 1982 to 2019 in the North-Eastern part of the country close to the Mediterranean basin. Furthermore, the polygon trend analysis is applied to inspect the interannual changeset. Partially increasing, decreasing or no trend pieces are identified at each station. It is concluded that in the future at some stations there are dry spell or drought dangers at "Low" data groups, and significant flood cases at "High" rainfall amount group. In general, the study area is subject to increasing rainfall trend. This is due to the mountainous surface features in the study area and confrontation with cold air movements from European continent during winter periods.

Keywords: Algeria, classification, climate change, high, low, medium, rainfall, trend.

المساهمة في دراسة التقلبات والتغير المناخي في شمال شرق الجزائر

الملخص :

يؤثر تغير المناخ على الدورة الهيدرولوجية للمياه مما يؤدي إلى عدم استقرار للموارد المائية و ينتج عن ذلك تذبذب في تساقط الأمطار التي تعد مصدرا رئيسيا للمياه. يختلف الاتجاه العام لتساقط الأمطارح حسب الموقع الجغرافي للمنطقة ، وباعتبار الجزائر تنتمي لدول البحر المتوسط هذا يجعلها عرضة لأضرار التغير المناخي المتوقعة حسب الدراسات الحديثة،لذلك فإنه من المهم جدا التوسع في الدراسات الخاصة بالاتجاه العام لسلوك تساقط الامطار هل هو في تزايد ام تناقص و هذا بغرض تجنب العواقب المحتملة لهذه التغيرات. توجد العديد من الدراسات السابقة لتحليل الاتجاه الرتيب ، ولكن من المهم تقييم الاتجاهات على مستويات مختلفة من السجلات. لهذا الغرض ، في هذه الأطروحة بدلاً من البحث عن الاتجاه الرتيب ، تم البحث عن اتجاهات جزئية في مجموعات "منخفضة" و "متوسطة" و "عالية"، و هو أمر ممكن من خلال المنهجية المبتكرة لتحليل الاتجاهات مع تقييم للمخاطر المحتملة ل 16 محطة متواجدة بالشمال الشرقي الجزائري لمدة38سنة منذ 1982 الى 2019، علاوة على ذلك تم تطبيق اتجاه المضلعات لتحليل التغير الحاصل خلال السنة من شهر الى آخر و خلص البحث إلى أنه في المستقبلممكن ان تتعرض بعض المحطات إلى مخاطر الجفاف في مجموعات البيانات ذات القيم "المنخفضة" ، وحالات الفيضانات الكبيرة في مجموعة كميات الأمطار ذات القيم "العالية". بشكل عام ، تخضع منطقة الدراسة لاتجاه متزايد لهطول الأمطار. ويرجع ذلك إلى الخصائص السطحية الجبلية في منطقة الدراسة وتعرضها لتحركات الهواء البارد من القارة الأوروبية خلال فترات الشتاء.

الكلمات المفتاحية: الاتجاه، الجزائر، تصنيف، تغير المناخ ، هطول الأمطار، متوسط، مرتفع، منخفض.

Contribution à l'étude de la variabilité et du changement climatique dans le Nord-Est de l'Algérie

Résumé

Les impacts du changement climatique affectent le cycle hydrologique et donc la disponibilité des ressources en eau et les travaux de gestion. Les précipitations, en tant qu'événement hydrométéorologique le plus important et en tant que principale source d'eau, peuvent avoir des tendances à la hausse ou à la baisse en fonction de l'emplacement, de la circulation générale de l'air, de la proximité de la zone côtière et de la géomorphologie. L'Algérie étant adjacente à la mer méditerranée est sous l'effet des variations pluviométriques. Une étude des tendances et des risques possibles est nécessaire afin de préserver la zone contre les impacts du changement climatique. Il existe de nombreuses études sur l'analyse des tendances monotones dans la littérature, mais il est important d'évaluer les tendances à différents niveaux d'enregistrements. À cette fin, dans cette thèse, au lieu de la recherche de tendances monotones, des tendances partielles sont recherchées dans les groupes d'enregistrements de précipitations « faibles », « moyennes » et « élevées », ce qui est possible grâce à la méthodologie innovante d'analyse des tendances (ITA). L'application de la méthodologie ITA à l'évaluation des risques est présentée pour 16 relevés annuels de précipitations algériens de 1982 à 2019 dans la partie Nord-Est du pays proche du bassin méditerranéen. De plus, l'analyse de tendance polygonale est appliquée pour inspecter l'ensemble de modifications interannuelles. Des éléments de tendance partiellement croissants, décroissants ou inexistants sont identifiés à chaque station. On en conclut qu'à l'avenir, dans certaines stations, il y a des périodes de sécheresse ou des risques de sécheresse pour les groupes de données « faibles » et des cas d'inondations importants pour le groupe de précipitations « élevées ». En général, la zone d'étude est soumise à une tendance à la hausse des précipitations. Cela est dû aux caractéristiques de surface montagneuse de la zone d'étude et à la confrontation avec les mouvements d'air froid du continent européen pendant les périodes hivernales.

Mots clés : Algérie, changement climatique, classification, élevé, faible, moyen, précipitations, tendance.

Acknowledgment

Alhamdulillah, thank you Allah for all the blessing You had given me. The ability, courage, endurance, and patience You put inside me strengthening me in completing this study and research.

I would like to show my deepest appreciation to my supervisor, Dr Hamouda BOUTAGHANE (Badji Mokhtar Annaba University) for his precious and continuous guidance and support throughout the course of this study. His dedicated supervision and constant encouragement towards the completion of this thesis encouraged me to do my best, It will never leave my thoughts the day he suggested me to choose the field hydraulics and promised to guide me until I become a doctor like himself, may Allah bless him.

I would like to express my deep and sincere gratitude to my co-supervisor whose sincerity and encouragement I will never forget, Prof ZEKAI ŞEN (Istanbul Medipol University, School of Engineering and Natural Sciences, Civil Engineering Department, Kavacık, Istanbul, Turkey) has been an inspiration as I hurdled through the path of this thesis. He is the true definition of a leader and the ultimate role model.

I would like to thank Istanbul Medipol University, Climate Change Researches Application and Research Center, (IKLIMER) Kavacık, Istanbul, Turkey, for having welcomed me and gave me the opportunity to be complete this work.
I would like to warmly thank the members of the jury: Pr. HANI Azzeddine, Dr. LAKEHAL Moussa, Dr. MRAD Dounia and Pr. HEDDAM Salim for having accepted to preside the defense jury.

I would like to dedicate my thesis to my father Rachid who passed away 21 years ago from now, may Allah grant him the highest level of Paradise. I am grateful for my mother Guenfoudi Yasmina whose constant love and support keep me motivated and confident.

My accomplishments and success are because she believed in me. Deepest thanks to my siblings, Sofiane, Naouel, Yazid and my brother and in low Mehdi, whom kept me grounded, reminded me of what is important in life, and were always supportive of my adventures. Special thanks to my dearest friend Peter Dimitriou for being so supportive and helpful during this journey.

Finally, I acknowledge the generous financial support from the Algerian ministry of higher education and scientific research by giving me the chance to gain a scholarship PNE 2019/2020 for 10 months in Istanbul Medipol University,Turkey.

بِسْمِ اللَّهِ الرَّحْمَٰنِ الرَّحِيمِ

In the Name of Allāh, the Most Gracious, the Most Merciful

Contents

List of Figures

List of Tables

Problem statement

PROBLEM STATEMENT

The Earth and the moon have basically the same distance from the sun, yet temperature on the moon average is unlivable (-18°C) and even deadlier, they range from -170°C during lunar night to 100°C at the lunar noon, regularly exceeding both the coldest -89°C and the hottest 71°C temperatures ever recorded on Earth. And while the days and nights on the moon are about 14 times longer than those on Earth, our planet's relatively fast rotation isn't what spares us from those loony temperatures. What protect us is our atmosphere. By day, it serves as a shield, blocking out the most harmful and energetic of the sun's rays and about 1/3 of the less-intense visible light. At the same time, it traps the infrared radiation radiating out from Earth's sun warmed surface, keeping us from freezing solid at night.

The atmosphere of Earth, commonly known as air, the three major constituents of Earth's atmosphere are nitrogen, oxygen, and argon, the remaining gases are known as greenhouse gases, absorbs and emits radiant energy within the thermal infrared range, causing the greenhouse effect, The primary greenhouse gases in Earth's atmosphere are water vapor (H_2O), carbon dioxide (CO_2), methane (CH_4), nitrous oxide (N_2O), and ozone (O_3). Without greenhouse gases, the average temperature of Earth's surface would be about −18 °C.

Human activities since the beginning of the Industrial Revolution (around 1750) have increased the atmospheric concentration of carbon dioxide by almost 50%, from 280 ppm in 1750 to 419 ppm in 2021. The last time the atmospheric concentration of carbon dioxide was this high was over 3 million years ago. This increase of greenhouses produced the phenomenon called global warming.

The global warming is the increasing of annual temperature has increased in total by a little more than 1 degree Celsius, or about 2 degrees Fahrenheit. Between 1880—the year that accurate recordkeeping began—and 1980, it rose on average by 0.07 degrees Celsius (0.13 degrees Fahrenheit) every 10 years. Since 1981, however, the rate of increase has more than doubled: For the last 40 years, we've seen the global annual temperature rise by 0.18 degrees Celsius, or 0.32 degrees Fahrenheit, per decade, this significant increasing has led to changing climate,

Climate change is a long-term change in the average weather patterns that have come to define Earth's local, regional and global climates. Scientists use observations from the ground, air and space, along with theoretical models, to monitor and study past, present and future climate change. Climate data records provide evidence of climate change key indicators, such as global land and ocean temperature increases; rising sea levels; ice loss at Earth's poles and in mountain glaciers; frequency and severity changes in extreme weather such as hurricanes, heatwaves, wildfires, droughts, floods and precipitation.

Current climate models indicate that rising temperatures will intensify the Earth's water cycle, increasing evaporation. Increased evaporation will result in more frequent and intense storms, but will also contribute to drying over some land areas. As a result, storm-affected areas are likely to experience increases in precipitation and increased risk of flooding, while areas located far away from storm tracks are likely to experience less precipitation and increased risk of drought.

The increase in the average temperature in the lower atmosphere caused by climate change triggers changes in various elements of the hydrological cycle at different scales depending on location in the world.

Warm atmosphere can sustain a higher concentration of water vapor than cooler air without becoming saturated. Consequently, as air warms, for whatever reason, more evaporation may take place and the concentration of water vapor may increase. An increase in water vapor enhances the greenhouse effect and gives rise to further warming. This positive feedback, warming from increased greenhouse gases leading to an increase of water vapor and therefore even more warming, is a feature of climate models used for estimating the effect of increased greenhouse gases.

Every change in the climatic system induces a change in the water system. The likelihood of deleterious impacts, as well as the cost and difficulty of adaptation, would increase with the extent and the speed of global climate change.

Among the proceedings of the hydrological cycle, the impact of climate change produced a conspicuous effect on precipitations, which is vitally important for human civilization. Although numerous published studies are concerned with the effect of climate change on hydrological elements such as precipitation, unfortunately, the performance of water engineering structures is not taken into consideration. Nevertheless, as an integral part of the whole water resources systems, engineering structures such as dams, canals, culverts, and wells are also subject to climate change impacts. This examines the performance of engineering structures by taking into account how climate change impacts on the risk assessment formulation. The construction of these engineering structures needs a comprehensive understand of possible trends in order to make the optimum predictions.

In addition, variability of rainfall patterns is a fact of life in the Mediterranean Sea region which includes Algeria. In this region, climate change impact may aggravate the situation as in much the rest of the world. The statistical values that are used before must therefore be constantly updated with a view to a better understanding the current climate

and moreover make predictions for the future, and eventually, take precautions against possible climate damages.

Through this thesis we aim to contribute modestly to make available to the institutions concerned with this aspect of a trend analysis of the precipitation time series in order to detect the impact of climate change in the North Eastern part of Algeria using new and Innovative methods where each one will be discussed in separate chapter.

This thesis is structured in five chapters:

Chapter 1: Introduction to climate change composed of background, listing previous studies related to the subject, history and basic notions.

Chapter 2: devoted to the area of study along with the utilized data.

Chapter 3: A general risk assessment procedure implemented from a climate change perspective along with dry and wet spells examination, the work presented in this chapter was published on February 14, 2020 as an original article in Earth Systems and Environment Journal DOI:https://doi.org/10.1007/s41748-019-00136-7, (Boudiaf et al., 2020).

Chapter 4: Trend analysis application for annual data using the innovative trend analysis (ITA) methodology in partial manner with "low", "medium" and "high" precipitation groups, the research made in this chapter has been published on March 14, 2021 in Arabian Journal of Geosciences DOI: 10.1007/s12517-021-06644-z, (Boudiaf et al., 2021).

Chapter 5: Trend analysis application for interannual data using the innovative polygon trend analysis (IPTA) methodology. The results of this chapter are in process of publishing in Arabian Journal of Geosciences.

Finally, in order to summarize the impact of climate change over the North Eastern part of Algeria, a general conclusion is given as well as the perspective.

Chapter I
Introduction to Climate Change

CHAPTER I: INTRODUCTION TO CLIMATE CHANGE

1.1 INTRODUCTION AND BACKGROUND

Our Earth in its aluminous bubble of air, under this protective layer, life is grown and thrived over the last 10.000 years, this unusually stable climate system has allowed for the rise of human civilization, until now, with over seven billion people consuming the world's resources economic viability is now pitted against the environment with little concern for the next generation, people are starting to feel the effects of poor harvests, mega droughts and extreme floods.

In 1988 worried scientist established the Intergovernmental Panel on Climate Change (IPCC) to monitor Earth's changes from the rapid retreat of the Himalaya's glaciers thawing of Arctic permafrost to ocean acidification, rising CO2 levels threaten our very survival, scientists across the planet are gathering to ring the warming bell.

The consequences of our worming atmosphere are impacting the major water towers on the planet. Thousands of research hours have highlighted potential water security, floods, droughts, all symptoms of changing climate system there requires our great understanding. For Dr. Pachauri the head of the IPCC, the water shortage is both of local and global concern. Higher temperatures in the ocean load the atmosphere with vapor, worldwide we are experiencing rising numbers of heavy local rainfall can devastate entire regions. Precipitation is constrained additionally by the need for condensation heating in the atmosphere to balance with radiative cooling to space. The amount of change in precipitation associated with a specific amount of change in surface temperature is of critical importance to understanding the global hydrological system and to climate model development and validation (Ren et al., 2013).

Surface temperature and precipitation are arguably the most basic climatic parameters. Precipitation variations control freshwater availability, food production, disease outbreaks, floods, and droughts. Models suggest that precipitation will change with global temperature, and monitoring is critical for assessing changes both globally and regionally (Smith et al., 2012). The global mean annual anomalies of reconstructed precipitation REC indicate a general increasing tendency over both land and ocean from 1900 to 2008, the trend over land is 0.03 mm day-1 per 100a (100 years), which is slightly weaker than that over the ocean (0.04 mm day-1 per 100a). the global mean annual mean anomalies including both land and ocean in REC precipitation variations are generally correlated with the temperature variations over the century with the temporal correlation of 0.60. such correlation increases to 0.80 with 9-year Gaussian filtering and decreases to 0.28 after de-trending, which suggest that correlation between the global precipitation and surface temperature is dominated by the long-term trend but does include some correspondence on shorter time scales. The trend in temperature is 0.7°C per 100a (Ren et al., 2013).

Positive trends, largely weak, were observed over much of North America (except Southwest United States), much of Eurasia, and northern Australia, negative trends are observed across northern Africa and much of eastern South America. The examination of global trends in the 20th century from the REC provides the foundation of our understanding of the trends. As future climate projections rely on coupled climate model simulations, the assessment of coupled model simulations of trends in the past century helps establish confidence in future projections. Ren et al. (2013)examined both CMIP5 and CMIP3 models in the 20th century. In CMIP5 models, the global precipitation anomaly averages show significant drops in 1902, 1963, 1982, and 1991, those drops are coincident with and presumably associated with the aerosols resulting from volcanic eruptions of Pelee/Sourfiere/Santa Maria, Agung, El Chichon, and Pinatubo in 1902, 1963, 1982, and 1991, respectively. The CMIP3 models show weaker volcanic signals. The volcanic effects on global precipitation may lessen the trends in the CMIP5 models. For example, more than 3 years after in 1963 Agung event, global

precipitation over both land and ocean still had nor recovered to the pre-eruption state, which suggests that the model volcanic aerosols remain in the atmosphere longer than in nature, reducing the global precipitation accordingly (Ren et al. 2013).

According to independent analyses by NASA and the National Oceanic and Atmospheric Administration (NOAA), Earth's surface temperatures in 2019 were the second warmest since modern recordkeeping began in 1880. Globally, 2019 temperatures were second only to those in 2016 and continued the planet's long-term warming trend. The past five years have been the warmest of the past 140 years.

In 2019, global temperatures were 0.98 degrees Celsius (1.8 degrees Fahrenheit) warmer than the 1951 to 1980 mean. "The decade that just ended is clearly the warmest decade on record," said (Goddard Institute for Space Studies: GISS) Director Gavin Schmidt. "Every decade since the 1960s clearly has been warmer than the one before." The average global surface temperature has risen since the 1880s and is now more than 2 degrees Fahrenheit (a bit more than 1 degree Celsius) above that of the late 19th century. For reference, the last Ice Age was about 10 degrees Fahrenheit colder than pre-industrial temperatures (Schmidt et al., 2006).

Using climate models and statistical analysis of global temperature data, scientists have concluded that this increase has been driven mostly by increased emissions into the atmosphere of carbon dioxide and other greenhouse gases produced by human activities.

Africa is often identified as the most vulnerable region to climate change, rainfall is below 100mm per year in part of Sahara, one of the driest, hottest regions of the world, with average temperatures around 30 degrees centigrade. Meanwhile the southern Sahel receives between 700mm and 1000mm per year. By contrast, parts of Tunisia receive 1500mm per year and about 2000mm of precipitation per year fall in Atlas Mountain in Morocco, where skiing is possible in winter (Oli Brown, 2019).

Over the last 50 to 100 years temperatures in Africa increased by 0.5 degrees centigrade (IPCC, 2014). The climate that the region can expect in future depends, in large part,

on the level of continuing emissions of greenhouse gases (GHG) and their complex interactions with the interlinked factors (land cover, pollution levels, tipping points and so on) that combine to determine average temperatures and precipitation levels (The international community uses climate models, known as Representative Concentration Pathways (RCPs), to describe four different 21st century 'futures' depending on GHG emissions and atmospheric concentrations, air pollutant emissions and land-use. The RCPs include a stringent mitigation scenario (RCP2.6 - representing ambitious international action to mitigate climate change), two intermediate scenarios (RCP4.5 and RCP6.0) and one scenario with very high GHG emissions (RCP8.5 - in effect a business-as-usual scenario) (IPCC, 2014)).

Temperatures in the region are predicted to rise faster than the global average (IPCC, 2014). Under a high emissions scenario the mean average temperature across Africa is likely to rise by more than 2 degrees centigrade above the temperatures at the end of the twentieth century, increasing heat stress on people, plants and livestock and possibly making some currently inhabited areas unlivable. Meanwhile, sea level rise and possible reductions in the flow of the Nile could have significant impacts on Egypt, in particular the area of the Nile Delta (Alda, 2014).

Further warming is projected to occur in Africa during the 21st century, with plausible increases of 4–6°C over the subtropics and 3–5°C over the tropics by the end of the century relative to present-day climate under the A2 (a low mitigation) scenario of the Special Report on Emission Scenarios. High impact climate events such as heat-wave days and high fire-danger days are consistently projected to increase drastically in their frequency of occurrence. General decreases in soil-moisture availability are projected, even for regions where increases in rainfall are plausible, due to enhanced levels of evaporation (Engelbrecht et al., 2015).

In Mediterranean areas, some decreases in annual precipitation have been detected by several researchers. Buffoni et al. (1999) investigated series of annual and seasonal

precipitation from 32 stations for the period 1833–1996. They observed some decreasing trends in the annual series, which were statistically significant, only in central southern Italy. On the seasonal basis, a decreasing trend was significant only for spring in the central south and for autumn in the North of Italy. Caloiero et al. (2011)performed a statistical analysis of annual and seasonal precipitation over 109 rainfall series with more than 50 years of data observed in southern Italy (Calabria). The employed rainfall data were first processed using a pre-whitening technique in order to reduce the autocorrelation of rainfall series. This study showed a decreasing trend for annual and winter-autumn and an increasing trend for summer precipitation. Moreover, high percentages of rainfall series show breaks during the decade 1960–1970 (Hamlaoui-Moulai et al., 2013).

A study of changes in data series of climatic variables at annual and monthly scales in the western part of the French Mediterranean area showed that annual precipitation did not evidence any trend (Chaouche et al., 2010). However, monthly rainfall has been found to decrease in June and increase in November throughout the area. Changes in precipitation for the Balearic Islands (Spain) have been analyzed by (Homar et al., 2009). They used daily time series during the period 1951–2006. The results showed a negative tendency for annual precipitation. An abrupt decrease in mean yearly precipitation of 65 mm has been detected in the time series around 1980 (Hamlaoui-Moulai et al., 2013).
According to IPCC reports, the Mediterranean basin and particularly the North African area are amongst the most vulnerable regions to climate change. However, the information concerning the North African zone is very limited, and studies on climate change have never been conducted in North-East Algeria up to now.

The issue of climate change is in Algeria an important and new challenge. A large part of Algeria belongs to the Mediterranean basin which is a "hot spot" of climate change and should therefore be protected. Algeria, ratified in April 1993, the United Nations Framework Convention on Climate Change (UNFCCC), and fully subscribes to

commitments relating to the stabilizing emissions of greenhouse gases to prevent anthropogenic interference with the climate system (Sahnoune et al., 2013).

Algeria has developed an initial strategy against climate change and developed numerous projects for adaptation and mitigation of changes climate. The national strategy is based primarily on four areas: institutional strengthening, adaptation to climate change, mitigation of emissions of greenhouse gas GHG and human capacity building. Its implementation mainly concerns the sectors of energy, industry, transport, waste, water resources, agriculture and forests. In this context, there was creation in 2007 of the National Agency for climate change and inventories of greenhouse gas (GHG) emission are carried out periodically (Sahnoune et al., 2013). The annual and seasonal drying/warming signal over the North African region is a consistent feature in the climate change projections for the twenty-first century under the A1B and A2 scenarios.

Numerous studies have been conducted on the northern regions of Algeria regarding precipitation and temperature, but they are directed more towards the west than the east. Elmeddahi et al. (2016) analyzed the trends in rainfall and stream flows across the Cheliff basin situated in northwest Algeria employing Sen's non-parametric estimator of slope to estimate the extent of tendencies, whose statistical significance was measured by the Mann-Kendall (MK) and the Modified Mann-Kendall (MMK) test where results showed that the annual rainfall had a statistically significant downward trend in the whole basin.

Bessaklia et al. (2018) studied 23 rainfall stations in the extreme north-east of Algeria over the period 1970–2010 and concluded that the results of Mann-Kendall test show that areas of high precipitation concentration tend to increase.

Merabti et al. (2018) examined 5 locations spread over the Northeast part of the country and inferred those arid and semi-arid zones have experienced a larger number

of drought events while the humid and sub-humid locations received greater precipitation events.

A study of precipitation variability on the massif forest of Mahouna (North Eastern-Algeria) has been made by Beldjazia Amina (2016) found strong tendency at the beginning and bit of weakness in the end of the seasons of winter and spring.

1.2 HISTORY OF CLIMATE CHANGE

65 million years ago, the dinosaurs were the unchallenged masters of the prehistoric world until their sudden demise. A medial strike triggered volcanic eruptions and earthquakes; the ensuing climatic chain reaction wiped out the giant reptile. After the age of the dinosaurs, the earth cooled. Climate change also affected our ancestors, early hominids had to survive periods of both extreme heat and extreme cold, most were unable to adapt and died out.
Then, over thousands of years, the polar ice caps expanded as did the Earth's alpine glaciers (Glen, 1994).

Around 60000 BC, average temperatures were about five 5 degrees colder than they are today, this had a huge impact. Arctic sea ice extended all way to Europe, so much water frozen but sea levels become up to 100 meters lower. The icy temperatures also affected the land, the ground was not only frozen solid, but also extremely dry. Where the ice ended, there were stretches of Tundra and Taiga (The Taiga is a forest of the cold subarctic region. The subarctic is an area of Northern hemisphere that lies of the arctic circle. Tundra and Taiga are the two coldest land biomes on the planet Earth). But one hominid genus was resistant to these stresses (Thorne et al., 2011).

The Neanderthals were suited to these extreme conditions, they were the first hominids to develop successful strategies for coping with climatic variations where summer had max temperature 10 degree. The Neanderthals adapted, survived and thrived in the ice

ages while the climate was stable, but quite suddenly it changed. The climate has always been subject to large but predictable fluctuations (Staubwasser et al., 2018).

Most of these are caused by the sun, the center of our solar system, as the Earth revolves, the sun's rays strike its surface, at some times, orbits are more circular, at others more elliptical. One orbital cycle takes 100 000 years. The angle of the Earth's axis also moves in a 40 000 years cycle. These changes caused regular climatic variations on Earth as the intensity of solar radiations increases and decreases. Other influences on the Earth's climate such as fluctuation in sea currents are irregular.
The Gulf stream for example works like a giant heat pump moving warms water toward Europe. The Gulf stream is our main factor. Other aspects of the climate system, such as the sun, change the climate by two degrees at most. When the Gulf stream speeds up or slows down, it causes changes of six to eight degrees in the North Atlantic "which is a lot more" (Dong et al., 2019).

About 60000 years ago, the climate change suddenly with dramatic consequences for the Neanderthals, evidence have been founded of rapid climate change with a quick alternation of warm and cold phases, 10 cold and hot phases in quick succession. The landscape and the vegetation changed rapidly, humans and nature were under constant stress, this climate chaos pushed the Neanderthals to their limits and threatened their very existence (Staubwasser et al., 2018).

Around 45000 BC, Homosapiens evolved in the warm climate of East Africa and slowly migrated all the way to Europe. The new comers seemed completely unsuited to this harsh and changeable climate, but they overcame this disadvantage thanks to a new skill. After migrating to Europe from Africa, Homosapiens spread to India and Asia then by land bridges to Australia and America, during this mass migration they settled in some of the most remote corners of the earth (Shea, 2008).

A key to that was the adaptability, the ability to understand the environment how it's changing and to work with large social groups to be able to actually deal with that changing landscape. This is the point when humans first started to adapt to the climate and use the climate for their own good. During a time of unprecedented climate, surviving in changing climates, this allowed them to withstand the last millennia of the Ice Age, a time of extreme cold. The ice age gradually came to an end (Millar and Woolfenden, 1999).

Around 17000 BC, due to changes in the Earth's orbit. As the Earth moves closer to the sun as explained in Figure 1-1, life changed dramatically. The sun light grew stronger particularly in summer (Quinn et al., 1991).

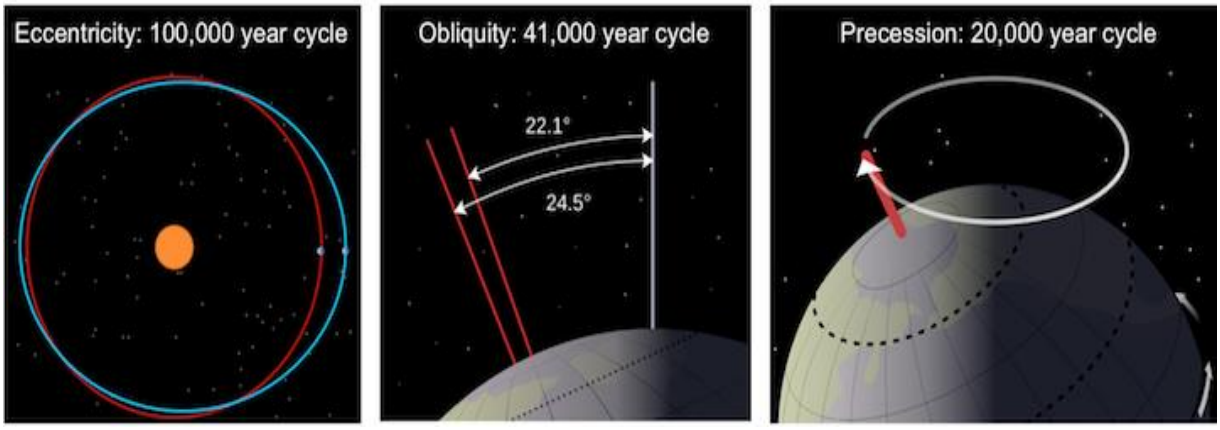

Left: The shape of Earth's orbit (its eccentricity) changes over 100,000 year cycles from more circular to more elliptical. Middle: Over 41,000 year periods, Earth's axis of rotation nods toward and away from the sun. Right: Over 21,000 year cycles, Earth wobbles on its axis of rotation. Source: Karla Panchuk (2017) CC BY 4.0. Modified after Steven Earle (2015) CC BY 4.0

Figure 1-1: Cycles in Earth's orbit

The icy planet was about to experience a global spring. It took several thousand years for the sun to warm the entire globe. As the earth's climate became much milder, a new era began and has continued until the present day. Warmer temperatures led to changes in the environment. First the ice sheets in the arctic and Antarctic began to melt. The oceans also began to warm and Gulf stream began to flow again. As

temperatures rose, more and more moisture evaporated into the atmosphere, this led to regular rainfall, which triggered a burst of planet growth. There were increased biodiversity mixed forests spread across Europe and North America and subtropical forests flourished closer to the equator, new animals' species started to populate the fertile plain. The biosphere began to flourish, there were more grasslands and more animal herds. Humans had much richer environment than at the end of the ice age, particularly in terms of plant foods they found themselves in paradise. Along the Tigris and Euphrates rivers and in the eastern Mediterranean, abundant natural resources created ideal living conditions (Paillard, 2010).

Around the same time, a disaster was looming in North America, part of continental ice sheets melted and created a vast lake, it continued to grow until it covered an area of 440000 Km^2, far bigger than any lake existing today the intense sunlight caused the lake to grow as more and more melt water flowed into it from the mountains. At first ice barriers held back this huge volume of water, but around 6200 BC they too began to melt and disaster was inevitable, the barriers around of icy water was released, it flooded large parts of North America, and eventually drained into the Atlantic. The immense inflow of cold water upset the currents in Atlantic, it disrupted the Gulfstream which ceased to have a warming effect, temperatures dropped all across Europe, in the fertile crescent where agriculture had so recently allowed humans to make enormous progress, the weather suddenly became cold and dry, this led to devastating droughts and crops failed, the new agrarian societies lost their livelihood (Harris, 2020).

Sea levels rose 120 meters, all over the world humans found their very existence threatened, gradually the theory claimed vast tracts of fertile land and rising sea levels flooded settlements in river deltas and a long coast. The Qu'ran tells of these events in one of its best-known stories, Allah Almighty told the prophet Noah peace be upon him to gather all the world's animals on his ark, two of each kind, and take them to safety, the rest of humanity was to be punished in a devastation deluge, Noah did Allah's bidding Harris (2020).

Around 6000 BC, the rising sea levels changed the map of the world. In North America Hudson Bay and the Great Lakes came into being. In Northern Europe the Baltic Sea was formed. Japan, Indonesia and Australia became Islands. The great glacial melt did not always bring devastation, one place that benefited was the Sahara. Today it's a hot, arid and inhospitable region, but the Sahara may once have been very different (Nicholls, 2011, Erlandson, 2008).

To change in this region climate was influenced by another factor, monsoon winds, the Northern hemisphere was receiving more heat from the sun because of a change in the tilt of the Earth's axis, land masses store more heat than oceans creating temperature differences that produce monsoon winds brought rain and moist air inland, these winds brought rain and abundant life to what is now desert. When monsoon rains fail, it takes only six weeks to three for plants to die from drought. If that happens over consecutive years, seeds also die and a steppe soon turns into a desert (Emeis et al., 1995).

It wasn't just Egypt that flourished other civilization are runs between the latitudes of 20 and 40 degrees North in Mesopotamia and Persia, in Northern India, in Karakoram in China, in Mexico and Pero and in the Mediterranean, the Mycenaeans, Minoan, Thracians and Etruscan, all these cultures had similar climates, scientists call that period the Bronze age. During the late bronze age, the climate became drier, a drought affected the entire Mediterranean region. Kingdoms fell because of the climate anomaly. Rainfall dropped substantially and temperatures were the lowest since the end of the Ice Age. It wasn't until about 300 BC that the Earth's alignment again made the climate more favorable, with milder temperatures and regular rainfall.

Climate change is influenced by astronomical forces, it depends on the Earth's orbit around the Sun, the tilt of the Earth's axis and the level of solar activity all of which vary, sometimes the Earth's orbit is almost circular and others more elliptical, one orbital cycle takes 100.000 years, during a 40000 years cycle, the angle of the Earth's

axis also changes in the Earth's climate as the intensity of solar radiation increases and decreases (Gaffney and Steffen, 2017, Lambeck et al., 2002, Kelsey et al., 2015).

At about the time of Christ's (peace be upon him) birth, solar radiation probably decreased, the Gulfstream cooled and the Earth's climate became much colder, crops died all across North Africa when the summer rains faild. As Europe entered the Middle Age the climate was still unstable until particularly the spring of 536, the Sun suddenly darkened and temperatures dropped. The Ilopango volcano (figure 1-2) what is now El Salvador erupted leaving a caldera 17 km wide and killing 100.000 people, Robert Dahl a climatologist believes that the volcano caused the climate crisis in the early Middle Ages.

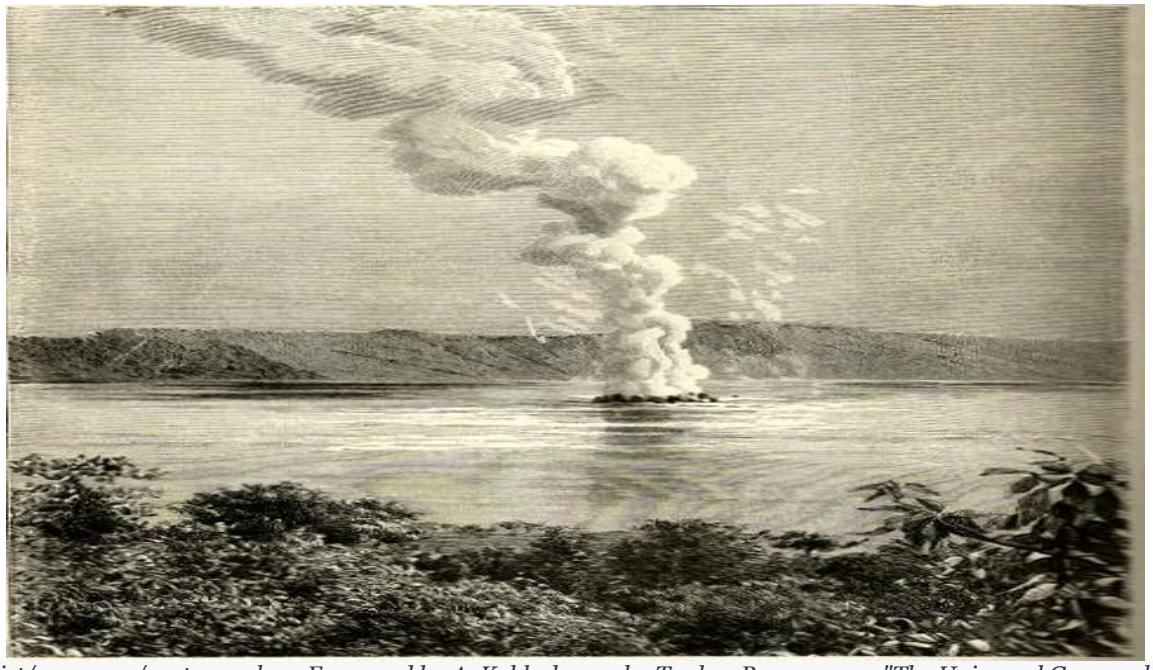

Artist/engraver/cartographer: Engraved by A. Kohl; drawn by Taylor. Provenance: "The Universal Geography"; by Élisée Reclus, Edited by A.H. Keane, Published by J.S. Virtue & Co., London /Central America/ [Universal Geography]. Type: Antique wood-engraved print.

Figure 1-2: Ilopango Volcano, El Salvador; 19th century engraving

The amount of material that was erupted during the eruption of Ilopango was at least 84 km^3, a massive amount of rock thrown into atmosphere at once, some of those materials have blasted horizontally into the landscape but a large amount would have gone up through the lower atmosphere into the stratosphere, when that happens, the climate cools which is exactly what happened after the Ilopango eruption. During the eruption, enormous quantity of ash and sulfur dioxide were propelled into the stratosphere (the region of atmosphere above about 10 km in altitude), typically these particles remain in the stratosphere for several years before they fall into lower atmosphere and will quickly washed out by rainfall, during this period they disperse around the whole globe and cut out some radiation from the sun, thus tending to cool the lower atmosphere (Dull et al., 2001).

Ilopango lies close to the equator, from there winds carried the ash and sulfurous gases to both the North and South poles, within weeks the blue planet was enveloped in a cloud of ash that blocked virtually all sunlight, a volcanic winter is lasted for 18 months, and made the natural environment much more inhospitable, the ash cloud not only blocked the sun, but also brought cold and rain, it had a devastating effect on human population.
After the volcanic winter it reclaimed its territory, only few decades later dense forest had grown across vast of Europe.

The sun continuously produces vast amounts of energy, which are released on its surface in the form of solar flares and geomagnetic storms, this heat energy affects the amount of solar radiation that reaches the Earth, this radiation is strong at sometimes and weaker at others, this is because solar activity is always fluctuating (Baker, 2000).

A beak occurred in 880 AD, solar activity was at maximum levels and solar radiation particularly intense. The Earth began to heat up. The North Atlantic which had been covered in solid pack Ice became navigable all year round (Liu et al., 2011).

Since 1000 AD, as the increased solar activity continue, temperature continue to rise, forest began to grow at altitudes above 2000 meters, the dark year of hardship and hunger were over, conditions for agriculture were the best they'd been for centuries. Spring, summer, autumn, and winter came and went in a predictable pattern (Gorney, 1990).

By 1250 AD, kingdom had been established all over Europe, the Roman Empire expanded and was bigger than ever, but then everything changed, once again climate was to make history, in the second half of the thirteenth century Europe cooled significantly, the trigger for this was a number of volcanic eruptions in different parts of the world's largest volcanic belts, the pacific ring of fire. First erupt in 1257 with Samalas volcano in Indonesia on Lombok that adversely affected climate and harvests around the world , in 1453 the violently, finally the lake fissure in Iceland, erupted continuously for eight 8 months, all these eruptions spew ash and sulfur dioxide into the stratosphere, they affected the world's climate for almost 500 years (Bankoff and Christensen, 2016).

The mid 13 the century, marked the start of the longest cold period since the end of the Ice Age, more than 10.000 years before "little Ice Age" (Ogilvie and Jónsson, 2001). **1342 AD,** a flood hit central Europe on an unprecedented scale, Rudriger Glaser from university of Freiburg considered this year the greatest hydrological catastrophe for 1000 years (Herget et al., 2015).

In the summer for 1586, the citizens of Ghent feared for their lives, a ferocious storm struck the city, people and even buildings were washed away, evidence suggests it was the tornado that tore through dent, the storm had long-term effects on the city's inhabitants because essential structures had been destroyed, it often took up to two

generations to repair such extensive damage. During the 500 years of little Ice Age unstable climatic conditions made life a daily struggle for survival (de Kraker, 2015).

In 1815, the little Ice Age enter the final dark phase triggered by another geological disaster, Indonesia's mount Tambora erupted the massive explosions rejected almost twice as much material of Ilopango in 536 including vast clouds of fine ash that remained in the atmosphere for months, that ash worked its way around the globe in upper atmosphere as a dust fail and that dust reflected the sun's radiation in a way that would cause climate cooling. 1816 was a year without a summer all over the planet, unseasonal frost and snow caused crop values and disastrous famines in Europe (Brázdil et al., 2016, Stothers, 1984, Bernice de Jong, 1995).

Finally, the cold eased in about 1850, a warm phase began bringing stable, moderate temperatures, it has shaped our climate ever since, just before this warm period began, humans embarked on time of dramatic technological and social change, the industrial revolution ever since, technological progress has brought prosperity, to industrial nations but it has also caused human induced climate change on an alarming and unprecedented scale, natural disasters are nature's way of sounding the alarm bell. Our planet has heated up and struggling to cope with global warming, for some time scientists have been asking us to acknowledge these sings and change course (Frisken, 1971, Stern and Rydge, 2012, Martinez, 2005).

We are at that point where we can decide what sort of climate want to have in the future, if we as a collective in the world all the nations actually reduce climate change, that would be amazing because what it means is for first time instead of climate controlling us our global society has decided we are going to control the climate and we are going to make sure that we have a stable climate for all future.
All climate change affects life on Earth. Climate makes history, it always has done and it always will.

1.3 THE REMARKABLE LAST DECADES OF THE TWENTIETH CENTURY

The 1980s and 1990s were unusually warm. Globally speaking, the decades have been the warmest since accurate records began somewhat over a hundred years ago and these unusually warm years are continuing into the twenty-first century. In terms of global average near-surface air temperature, the year 1998 was the warmest in the instrumental record and the nine warmest years in that record have occurred since 1990 (Philander, 2018).

The period has also been remarkable (just how remarkable will be considered later) for the frequency and intensity of extremes of weather and climate. For example, periods of unusually strong winds have been experienced in western Europe (Wang et al., 2011). During the early hours of the morning of 16 October 1987, over fifteen million trees were blown down in southeast England and the London area (Burt and Mansfield, 1988). The storm also hit Northern France, Belgium and The Netherlands with ferocious intensity; it turned out to be the worst storm experienced in the area since 1703. Storm-force winds of similar or even greater intensity but covering a greater area of western Europe have struck since – on four occasions in 1990 and three occasions in December 1999 (Brade et al., 2009).

But those storms in Europe were mild by comparison with the much more intense and damaging storms other parts of the world have experienced during these years. About eighty hurricanes and typhoons – other names for tropical cyclones – occur around the tropical oceans each year, familiar enough to be given names. Hurricane Gilbert that caused devastation on the island of Jamaica and the coast of Mexico in 1988 (Bellingham et al., 1992, Wunderle et al., 1992), Typhoon Mireille that hit Japan in 1991 (Takemi et al., 2016), Hurricane Andrew that caused a great deal of damage in Florida and other regions of the southern United States in 1992 Willoughby and Black (1996) and Hurricane Mitch Hellin et al. (1999), Morris et al. (2002) that caused great devastation in Honduras and other countries of central America in 1998 are notable

recent examples. Low-lying areas such as Bangladesh are particularly vulnerable to the storm surges associated with tropical cyclones; the combined effect of intensely low atmospheric pressure, extremely strong winds and high tides causes a surge of water which can reach far inland. In one of the worst such disasters in the twentieth century over 250 000 people were drowned in Bangladesh in 1970. The people of that country experienced another storm of similar proportions in 1999 as did the neighboring Indian state of Orissa also in 1999, and smaller surges are a regular occurrence in that region (Chowdhury, 2021).

1.4 BASIC NOTIONS

1.4.1 Atmospheric measurements

How does scientists know that climate change is taking place or that the factors they believe to be driving climate change such as greenhouse gas concentrations are themselves changing?

The answer lies in observational data. In the coming sections, we turn to instrumental measurements documenting changes in the properties of atmosphere over time, measurements have uncertainties. Goal of the measurements to assess whether there appear to be trends in measures of climate and the factors governing climate and whether the trends are consistent with our expectations of what the response of the climate system to human impacts ought to look like.

These measurements come from a variety of sources, from measurements of changes of CO2 in the atmosphere to observations and records of extreme weather events. Let's begin with the fundamental question: is there evidence that greenhouse gases, purportedly responsible for observed warming, are actually changing in the first place? Is there evidence that there is actually more CO2 in the atmosphere at the beginning of

the 21st century than at the beginning of the 20th century? Yes. Roger Revelle and Charles David Keeling made direct measurements of CO2 levels in the atmosphere from the same sites over decades the Mauna Loa Observatory in Hawaii. They made continuous measurements of atmospheric CO2 from 1958 henceforth, and the result is the most famous curve in all of atmospheric science, the so-called Keeling curve (figure 1-3) (Harris, 2010).

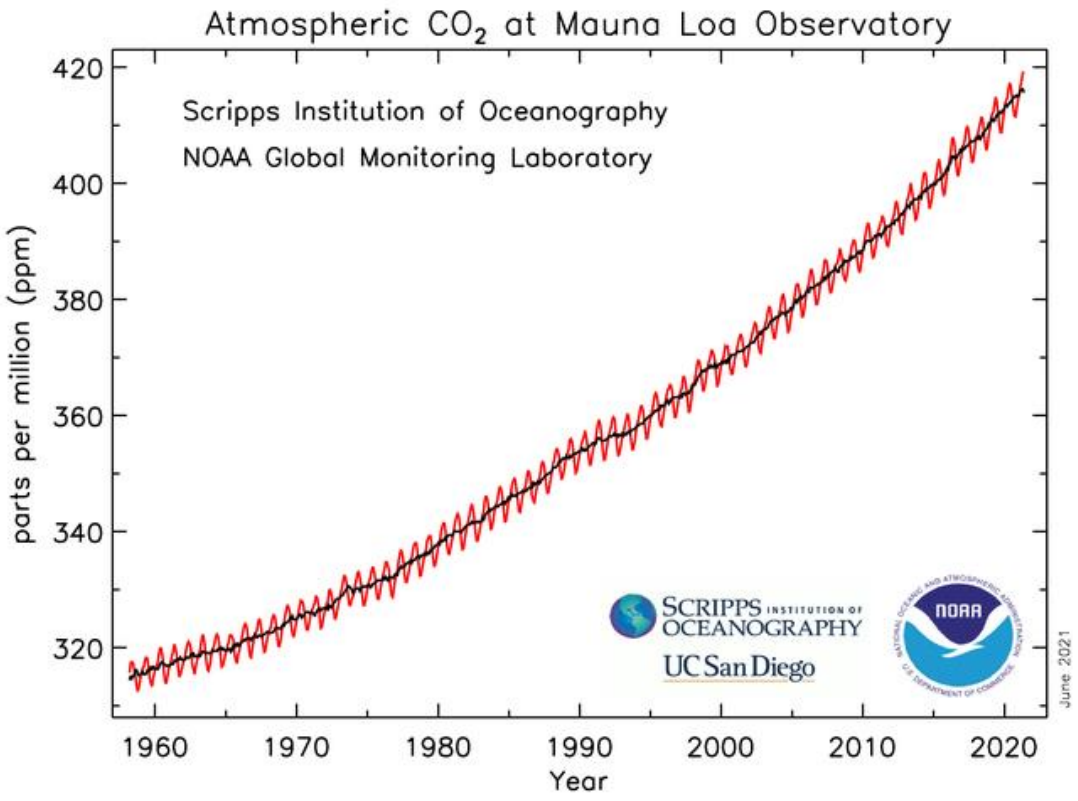

Figure 1-3: Keeling curve

That curve shows a steady increase in atmospheric CO2 concentrations in the atmosphere from about 315 parts per million when the measurements began in 1958 to over 410 parts per million in 2020.
It continues to climb. Long term records have been established in other locations over the globe. There are also ice core records that tell us that CO2 levels were lower about 280 parts per million in the atmosphere at the dawn of the Industrial Revolution. And the 410 parts per million CO2 in the atmosphere that we see in 2020 nearing 420 parts per million co2 in the atmosphere in the year 2021, that is the highest level we see in ice cores and other indirect measurements that take us back over several million years.

So, the CO2 levels in the atmosphere today are literally the highest that we have seen in millions of years. How do we know that the increase in CO2 in the atmosphere is from humans not natural? Well, there are a variety of sources of evidence that that's the case. Carbon that gets buried in the earth from dying organic matter and eventually turns into fossil fuels tends to be what we call isotopic lee light. Fossil fuels are thus relatively rich in the lighter isotope of carbon, carbon 12 rather than carbon 13. However natural atmospheric CO2 produced by respiration has more of the heavier carbon, the carbon 13 isotope.

If the CO2 increases were from natural sources, we would therefore expect the ratio of the heavy isotope carbon 13 to the light isotope carbon 12 to be getting higher over time, but instead the ratio is getting lower, as CO2 builds up in the atmosphere. The ratio bares the fingerprint of an anthropogenic source anthropogenic fossil fuel burning. In summary greenhouse gas concentrations including atmospheric CO2 and methane are increasing dramatically, and these increases are unprecedented over a very long-time frame and we know they are associated with human activity (ACS, 2015).

1.4.2 Rising surface temperatures

In addition to CO2 measurements from the atmosphere, there are also evidence of rising surface temperatures from more than a century of widespread measurements around the globe. There is over a century of thermometer records from land-based stations, islands, and shipboard measurements of ocean surface temperatures. They provide the scientists with more than a century of reasonably global estimates of surface temperature changes.

The earth has warmed about a degree Celsius, a little more than a degree Celsius since the mid-19th century, as far back as the surface temperature observations go. Natural sources of warming give rise to different patterns of temperature change than human sources, such as increasing greenhouse gases. This is particularly true when we look at the vertical pattern of warming in the atmosphere.

There are different layers of the atmosphere, the troposphere the stratosphere, troposphere being the lower part that we live in, the stratosphere the layer above it. The upper air temperature amounts have been estimated from weather balloons and satellite measurements, that measure temperatures both in the troposphere and stratosphere, and they revealed a remarkable pattern, the lower part of the atmosphere the troposphere has been warming along with the surface. However, once we get into the stratosphere, temperatures have actually been decreasing (NOAA).

In summary the surface of the earth is warming, and certain regions such as the Arctic or warming even faster than others. The vertical pattern of the warming indicates that the surface and lower atmosphere are warming up, while the atmosphere is cooling at altitude a pattern that is consistent with greenhouse warming.

1.4.3 Ocean warming

The surface of the earth is warmed by about 1 degree Celsius this past century, the ocean is warm too, though a bit less than the land (NASA, 2020). Why does the ocean warm more slowly than the land?

Thermal inertia. Due to the depth of the ocean heat diffuses more slowly downward through the layers of the ocean. The slower rate of warming of the ocean, the slower rate of response to radiative forcing leads, to another key concept called committed climate change. The process is small-scale convection and diffusion by which this heat penetrates down through the ocean or slow. Sea water expands with warming, ocean levels continue to slowly rise as the heating penetrates down through the deep ocean (Cowan et al., 2012).
Even if we stop all CO2 emissions now global sea level will continue to rise for several centuries. There are more changes in the pipeline that we haven't seen the effects of yet, but that we are already committed to. It's key to remember that oceans are not passive, they are active dynamic systems. They transport heat from low latitudes to high latitudes to relieve the imbalances of solar heating through two primary mechanisms ocean gyres and the conveyor belt ocean circulation system. Do we see any changes in these mechanisms as an indication of climate change?

Let's first talk about the gyres. Now the gyres, the horizontal ocean jars are governed primarily by the latitudinal variation in surface winds. Climate change may be altering prevailing wind patterns somewhat, and that could lead to changes in these wind-driven gyres, but the gyres are fairly robust. Regardless of how temperature patterns change and wind patterns change, these horizontal ocean gyres will continue to transport heat poleward. The conveyor belt ocean circulation, or thermohaline circulation, is a different matter there's quite a bit of evidence not only that that circulation pattern could weaken because of climate change, but it may actually be

already weakening. It is a combination of the salty and cold properties of surface waters in the subpolar North Atlantic that leads to their high density and the sinking motion.

That sinking motion forms the descending limb of the thermohaline circulation, so any substantial freshening and warming of these waters could inhibit that sinking. It has long been suspected that global warming, through the influx into the North Atlantic of fresh water, in particular from the melting of the Greenland ice sheet, well that that could inhibit or even shut down the thermohaline circulation (Di Lorenzo et al., 2010, Kim et al., 2007).
There's been some debate in the past about whether or not there's evidence of this happening, the most recent observations seemed to indicate that we are now seeing a weakening of that ocean circulation pattern, and it may be a result of the ice that is melting from Greenland, that is already flowing into the North Atlantic and freshening those surface waters (Caesar et al., 2018).

About observations of extreme weather, and in particular hurricanes and tropical storms. During the past several years, a strongest storm globally ever recorded, that was hurricane Patricia in the North Pacific (Knutson et al., 2010). Also during that period the strongest storm ever in the southern hemisphere that was hurricane Winston that made landfall on Fiji (Sattler et al., 2018). And in the open Atlantic that was Irma (Radabaugh et al., 2020). So, there's a trend towards more extreme and more intense hurricanes where scientists have estimated that for each degree Celsius warming of ocean surface temperatures there would be an overall increase of about seven percent in the maximum wind speeds of those storms (Holland and Bruyère, 2014).

The destructive potential of a hurricane goes as the third power of the wind speed, which translates to a 23% increase in destructive potential. So, it's probably not a coincidence that there is a trend towards more intense more destructive storms as ocean surface temperatures have warmed. There is some disagreement among

scientists as to whether the number of tropical storms is increasing both globally and in regions like the North Atlantic, and whether expect the number of those storms to increase with global warming. But where there seems to be quite a consensus now within the scientific community is that as surface temperatures warm, we will see more intense destructive hurricanes (Dinan, 2017, Hallegatte, 2007, Marsooli et al., 2019).

In summary, land regions over the globe have warmed on average a little more than 1 degrees Celsius, the oceans have warmed a little less than 1 degrees Celsius. The oceans thermohaline circulation appears to be slowing down, it appears to be decreasing, and certain types of extreme weather events, and in particular hurricanes, have become more extreme. We see an increase in the intensity of hurricanes that is correlated with the warming of the oceans.

1.4.4 Changes in precipitation patterns

Climate change isn't just about temperature changes, it's about changes in rainfall patterns. From the observed trends in rainfall and precipitation around the globe over the past century, it is obvious that the trends are fairly heterogeneous (New et al., 2001).
As the atmosphere warms up, it can hold more moisture, and more expected intense hydrological cycle overall. Meaning larger amounts of rainfall globally. But those trends vary markedly with region, and it's especially useful to average into latitudinal bands and to see how rainfall is changing in certain latitudinal bands over time.

As the surface is warming up and there is more moisture in the atmosphere, in those regions which usually tend to have rainfall because of rising motion, like in the Intertropical Convergence zone in the tropics, it may actually get more rainfall because the atmosphere has more moisture to turn into rainfall, but also there will be an expansion of the descending limb of that so-called Hadley cell circulation (Frierson et

al., 2007, Lu et al., 2007). And as that descending limb spreads to higher latitudes, we see a decrease in rainfall in the sub tropics and part of the mid latitudes. And then finally as getting to the highest latitudes, as the storm tracks move poleward with changing atmospheric circulation patterns, rainfall increase once again in subpolar regions (Trenberth, 1998).

So, when we look at precipitation, the global pattern shows a small overall increase, but there are large regional trends in opposite directions, with the tropics becoming wetter the sub tropics getting less rainfall, and finally the subpolar latitudes, associated with the poleward migrating polar front, once again seeing more precipitation in the form of rainfall and snow. Now when we look at patterns of drought, we see something a little bit different because drought reflects not only the precipitation that's coming down to the surface, but the loss of moisture back up into the atmosphere through evaporation. And as the earth warms up and as soils and vegetation warm up, they evaporate more moisture into the atmosphere. So even some regions in the mid latitudes that have shown small increases in rainfall, are seeing worse droughts because of the lost moisture associated from warming soils and increased evaporation. So, when it comes to rainfall and drought, we see what sometimes appears to be a paradox. Some regions that see worse summer droughts also see more intense rainfall events (Trenberth, 2011).

1.4.5 Extreme precipitation events

Extreme precipitation events, includes both rainfall and snow falls. As the earth warms up, as the oceans warm up and evaporate more moisture into the atmosphere, there is a potential for more intense precipitation events, even in regions that see more widespread drought, may see more intense rainfall events and more intense snowfall events because a warmer atmosphere holds more moisture, so, when conditions

happen to be conducive to getting precipitation, when there is rising motion in the atmosphere, it brings more precipitation out of the atmosphere, and if that happens when it is warm that will be rainfall, and when it happens in the winter it will be snowfall.

The 2003 European heat wave Bouchama (2004) said that the worst heat wave on record for Europe, 30,000 people perished in that heat wave. And they have records of temperatures going back hundreds of years, and there were upward trend in the record, and it tells that it was an unprecedented extreme heat event. The entire summer was warmer than average, and the extreme heat in that heat wave was embedded in what was otherwise a very warm summer that is part of a trend towards warmer and warmer summers. So that small shift in the bell curve (Normal distribution) took a 1,000-year event, an event that the historical records tell us shouldn't happen more often than once in a thousand years, and it turned it into a 20-year event. An event that's likely to happen every 20 years. And that tells us once again about the profound impact that even modest warming can have on the so-called tail of the distribution, where the extreme events happen. By later this century, that same event could become a two-year event, a summer like the 2003 European summer may occur once every two years. A catastrophic heat wave would become a biannual event for Europe and in many other regions around the world (Van Aalst, 2006, Banholzer et al., 2014, Pinault, 2012, D'Aleo and Khandekar, 2016).

Chapter II
Study Area Presentation and Data

2 CHAPTER II: STUDY AREA PRESENTATION AND DATA

2.1 INTRODUCTION

Algeria is a semi-arid to arid north to south, water availability per capita is 600 m3/hab./an, placing it in the category of poor countries in water resources under the shortage threshold set by the UNDP or the scarcity set by the World Bank in 1000 m3/hab./year. With 71 dams of a capacity of 7.1 billion m3 (Sahnoune et al., 2013).
A study made by Nouaceur and Murărescu (2016) over 12 station situated in Algeria revealed that during the period 1987-2002 there was a drying trend, however from 2002 until 2013, 82% of the years described as rainy.
Another study made by Hassini et al. (2011) about the precipitation received in northern Algeria found a succession of episodes of excessive and deficient precipitation compared to normal with a great variability. In addition, the average annual rainfall increases along two main directions, namely from west to east and from south to north.

2.2 LOCATIONS

The localities surveyed are located in three climatic stages, Mediterranean a climate distinguished by warm, wet winters under prevailing westerly winds and calm, hot, dry summers. Sub-humid with mild but cool winters and a slight risk of frost, and Semi-dry zone is characterized by cool winters, summers with a temperature of the hottest month (July) of 26.8 ° C in Tebessa and Khenchela, and relative humidity not exceeding 38% (Louadi et al., 2008).

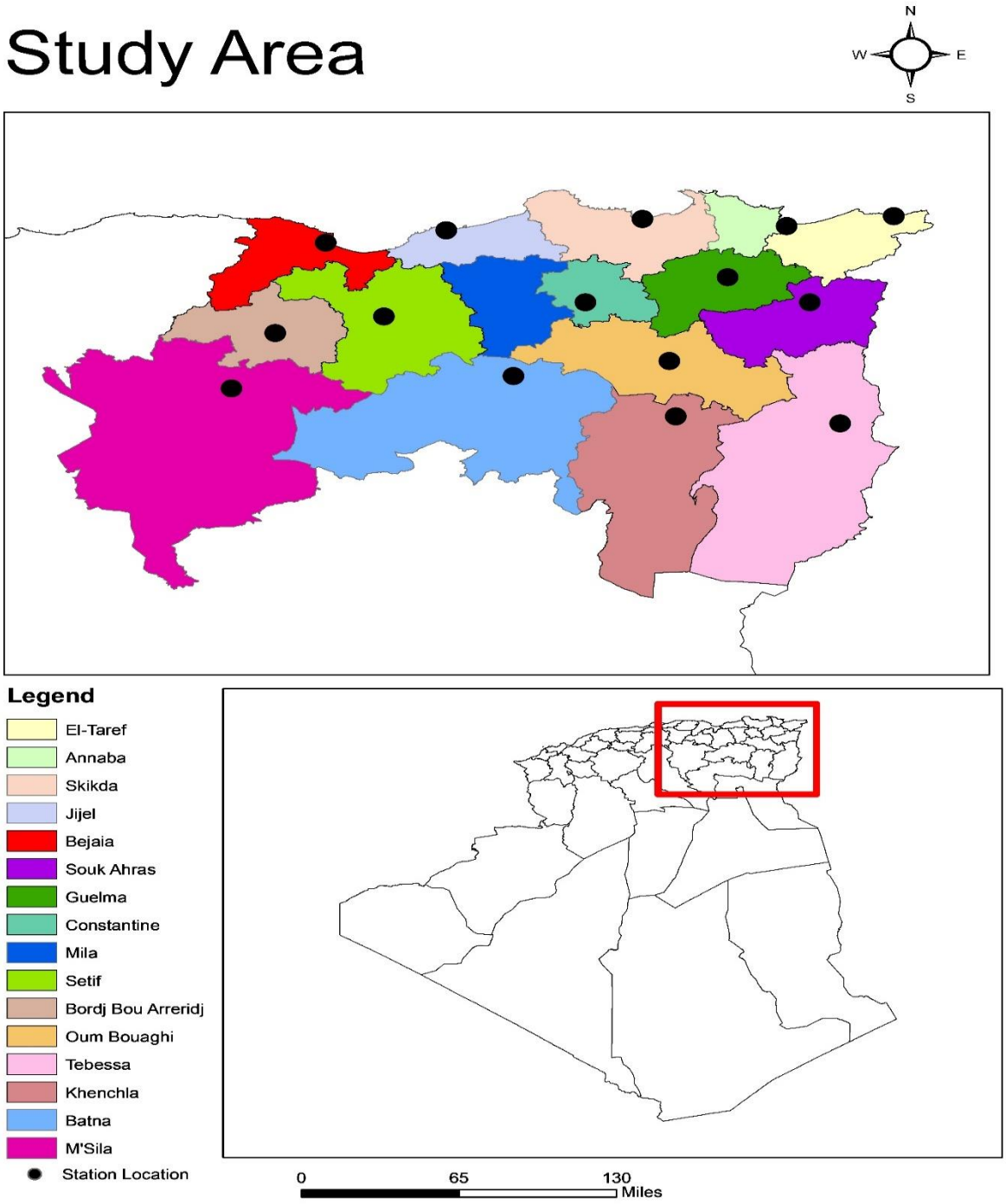

Figure 2-1: Representation of the study area

Table 2-1: Localities of the study area

Locality	coordinates			Geographic situation	Climate	Area (Km²)	Population (Habitat)
	Latitude	Longitude	Altitude				
El Taref	36° 46′ 07N	8° 19′ 00E	14	littoral	Mediterranean	3 339	408 414
Annaba	36° 53′ 59N	7° 46′ 00E	0	littoral	Mediterranean	1 439	609 499
Skikda	36° 51′ 44N	6° 56′ 50E	25	littoral	Mediterranean	4 026	898 680
Jijel	36° 47′ 59N	5° 46′ 00E	47	littoral	Mediterranean	2 577	636 948
Bejaia	36° 45′ 00N	5° 04′ 59E	0	littoral	Mediterranean	3 268	912 577
Souk Ahras	36° 16′ 07N	7° 56′ 08E	686	High Tellian plain	Sub-humid	4 541	438 127
Guelma	36° 27′ 58N	7° 26′ 02E	256	Middle position between the North of the country, the Highlands and the South.	Sub-humid	4 101	482 430
Constantine	36° 21′ 54N	6° 36′ 53E	626	High Tellian plain	sub-humid	2 187	938 475
Setif	36° 11′ 29N	5° 24′ 34E	1080	High Tellian plain	Semi-dry	6 504	1 489 979
Bordj Bouarreridj	36° 04′ 00N	4° 46′ 00E	900	High Tellian plain	Semi-dry	4 115	628 475
Oum Bouaghi	35° 52′ 39N	7° 06′ 49E	902	High Tellian plain	Semi-dry	7 638	621 612
Mila	36° 27′ 04N	6° 15′ 55E	486	High Tellian plain	Sub-humid	3 407	766 886
M'Sila	35° 43′ 32N	4° 31′ 40E	475	High Tellian plain	Semi-dry	18 718	990 591
Batna	35° 33′ 19N	6° 10′ 43E	1048	High Tellian plain	Semi-dry	12 192	1 119 791
Tebessa	35° 24′ 15N	8° 07′ 27E	851	High Tellian plain	semi-dry	14 227	648 703
Khenchla	35° 26′ 09N	7° 08′ 36E	1152	High Tellian plain	semi-dry	9 811	386 683
Total						**102090**	**11 977 879**

Administratively, the study area is compounded of sixteen provinces located as shown in the Figure 2-1 occupying 102 090 Km² and containing almost 12 million habitats which reflect the importance of making a full study about climate change impact on this region, more details are mentioned in Table *2-1*.

2.3 AVAILABLE DATA

The basic data are obtained from Algerian Meteorological Organization (ONM) and the National Agency for Hydraulic Resources (ANRH). The available monthly precipitation record for the majority of the study area were from 1982 to 2019, Table *2-2* present the record duration for each station.

Note: the missing data were removed from the time series.

Table 2-2: Meteorology station characteristics

Station name	Station code	Record duration (year)	Start of recording	End of recording	Missing years	Min value (mm)	Max value (mm)	Mean Value (mm)	Standard Deviation	Coefficient of variation %
El Taref	031717	16	1992	2008	1995	392.2	1040.2	729.3	186.2	25.5
Annaba	603600	38	1982	2019	No gaps	235.2	1008.5	643.3	161	25
Skikda	603550	38	1982	2019	No gaps	342.9	964.3	656.2	146.2	22.3
Jijel	603510	38	1982	2019	No gaps	101.1	1352.3	850.4	281.5	33.1
Bejaia	604020	38	1982	2019	No gaps	259.5	1570.8	745.6	252.8	33.9
Souk Ahras	120101	32	1982	2013	No gaps	176.7	991.3	576.3	183.1	31.8
Guelma	604030	16	2004	2019	No gaps	346.2	869.4	575.5	150.3	26.1
Constantine	604190	38	1982	2019	No gaps	210.1	904.2	489.7	159.6	32.6
Mila	100620	26	1978	2011	1980-1981-1983-1992-1998-1999-2000-2003	302.5	955.3	580.7	164.9	28.4
Setif	604450	38	1982	2019	No gaps	118.4	614.8	382.3	99	25.9
Bordj Bouarreridj	604440	38	1982	2019	No gaps	104.9	655.2	337.3	118.6	35.2
Oum Bouaghi	070707	44	1960	2012	1962-1966-1977-1979-1981-1982-1987-1992-1995	155	594.1	390.6	106.4	27.2
Tebessa	604750	38	1982	2019	No gaps	187.4	640	356.7	101.8	28.5
Khenchla	/	34	1970	2004	No gaps	149.8	753.7	413.5	166.5	40.3
Batna	604680	38	1982	2019	No gaps	106.2	610.9	289.3	112.4	38.9
M'Sila	051005	22	1975	2004	1993-1994-1995-1996-1997-1998-2000-2001	108.4	367.1	216.5	58.4	27

Chapter III
Risk
Assessment

3 CHAPTER III: RISK ASSESSMENT

3.1 ABSTRACT

Climate change impacts on social, economic, industrial, agricultural, and water resource systems tend to increase incrementally with each passing day. Therefore, it is necessary to plan to control its effects, especially with regard to rainfall events impacting future water resource operation, maintenance and management works. Climate change has a direct influence at the trend of both precipitation in increasing or decreasing manner depending on the study area. Engineering risk management is very significant factor in climate change assessment and impact intensity calculations on engineering water structures.

In order to enhance and perform a better idea about the impacts of the climate change fact, 1) A trend analysis technique was employed along with risk assessment. The modified risks associated with 2-, 5-, 10-, 25-, 50-, 100-, 250, and 500-year return periods are then calculated for each station. 2) Wet and dry spells identification. These methodologies were applied to precipitation records for sixteen different meteorological stations situated in Northeast Algeria. This study confirms that climate change has and will continue to have an impact on precipitation and that should be considered for all infrastructure planning, design, construction, operation, maintenance and optimum management studies in future.

3.2 INTRODUCTION

One of the most concerning aspects of climate change is the changes in water cycle. These projected changes can perturb the hydrological cycle; higher temperatures are likely to speed up evaporation from water and land surfaces and speed up transpiration from

plants. No matter what happens to precipitation, increased evapotranspiration will dry out soils and leave less water available to flow to streams as well as less water available to infiltrate into the ground and recharge aquifers (Stagl et al., 2014). Warmer temperatures will also cause a shift in precipitation toward less snow and more rain and will lead to earlier and more rapid melting of both the seasonal snowpack and glaciers that have persisted for many years (Hoegh-Guldberg et al., 2018). Melting glaciers might cause increased runoff in glacier-fed streams in the short run, but in the long run as glaciers shrink, the melt water runoff will diminish. Along the coasts, rising sea levels are likely to inundate more low-lying land (Stagl et al. 2014).

Water quality is likely to be affected too (Xia et al., 2015), with warmer temperatures, muddier water from increased erosion, more pollutants from storm water runoff during heavy rains, and in some places, higher contaminant levels due to less stream flow available due to diluting waste water discharges.

Considering the impacts of both climate change and population growth, water scarcity is projected to rise significantly, according to population action international based on the United Nations Medium Population Projections of 1998, more than 2.8 billion people in 48 countries will face water stress or scarcity conditions by the year 2015, of these countries, 40 are in Western Asia, Africa, or Sub-Saharan Africa.

By 2050, the number of countries facing water stress or scarcity could rise to 54 with combined population of 4 billion people, about 40% of the projected global population of 9.4 billion (Gardner-Outlaw and Engleman, 1997). Climate change effects will vary significantly, severely affecting infrastructure in different regions of the world (IPCC, 2014). As climate change progresses, an important question must be asked—how to modify urban infrastructure dimensions to adapt to these expected impacts (Carter et al., 2015). Usually, urban infrastructure is constructed, assuming a stable climate and until recently climate change has not been taken into account by engineers during the design stage. Now, changes in the frequency and intensity of hydroclimatic averages and

extremes will probably change the critical design parameters. For this reason, a simple risk formulation, which takes into consideration the impact of climate change, must be developed to adapt for these vulnerabilities (Şen, 2014, Şen, 2017).

The objective of this study is to generate a relationship between the climate trends and the corresponding risk levels for precipitation data in Northeast region of Algeria. This relationship is required to establish precautionary boundaries to account for climate change impacts.
Many people (particularly politicians) want scientists to tell when to expect a flood, but that unfortunately is a question scientist cannot answer, they can communicate the probability of an extreme event to occur, but not easily the moment when it will occur.

3.3 RISK DEFINITION

A risk is the measure of the probability and severity of an adverse effect to property such as water resources engineering structures. It is estimated by the mathematical expectation (arithmetic average) of the consequences of an adverse event occurrence (i.e., the product of the probability of occurrence and the consequence). It is also defined as the chance (probability) of something happening that will have an undesirable impact on the objectives. Risk is measured in terms of a combination of the likelihood that a hazard gives rise to an undesirable outcome and the seriousness (consequences) of that undesirable outcome.

3.3.1 Risk acceptability

It is the acceptability of the risk by the stakeholders, water system designers and those who will bear the consequences.

3.3.2 Risk analysis

In its context are the actual determination of the likelihood and consequences of undesirable effects on the water resources system.

3.3.3 Risk assessment

This is defined as the overall process of hazard identification, risk estimation, and risk evaluation (may be qualitative, semiquantitative, or quantitative).

3.3.4 Risk management

It is the processes and structures to manage potential adverse impacts.

3.3.5 Safe water structure

Any water structure does not impose an unacceptable risk to people or property and meets safety criteria that are acceptable to the government, the engineering profession and the public.

3.3.6 Threat

An action or activity that has the capacity to adversely affect an ecological value or asset. The chief characteristic of a heavy rainfall event as flash flooding and such an event (in any region) can be described as a natural hazard that causes major floods and severe destruction, often resulting in loss of lives and damage to property.

It is, therefore, necessary to understand and be able to follow the evolution of a heavy rainfall event at the event scale. Such an assessment provides considerably beneficial information to scientists, in general, and to the administrative authorities of a region, in particular. Sudden and rapid occurrences of flash floods in natural channels present technical challenge to scientific modelers and decision-making administrations.

3.4 RISK CALCULATION

There are different contexts, but in very simple terms, it is how likely is it that someone will be exposed to a bad consequence:
Risk = likelihood * consequence.
Likelihood == hazard.
Consequence == how bad the outcome will be.

Since the consequences of climate impacts can be so catastrophic for those exposed to the risk, it is important to urgently commit resources to develop a greater understanding of the risk as far as possible, to fill data gaps and overcome key weaknesses in our understanding and act in a precautionary manner rather than postpone action until better data are collected.

Risk assessment and risk models cannot make decisions but they can inform policymakers. As well as encouraging and developing a culture of risk identification and understanding making it more resilient and saving lives, livelihoods and property.

In this chapter, a general risk assessment procedure is implemented from a climate change perspective. Climate change is expected to affect all hydroclimatic variables at many different levels. Theoretically several convenient formulations have been generated for precipitation design values. Climate change effects are ignored in most calculation procedures.

3.4.1 CDF curves generation

Any engineering structure with a design capacity should not be exceeded during its economic life, but may be subject to extreme events risk, which should be taken into consideration before any infrastructure construction.

The classical risk is the probability of dangerous event occurrence only once during the entire life of the infrastructure. In this chapter, the risk calculations are not based only on the life span, but additionally on the slope of possible trend in the precipitation records. An extreme event is defined as the occurrence of a variable value above (or below) a threshold near the upper (or lower) ends of its observed range in a specific region.
The MATLAB software was used to determine risk values based on different risk levels and cumulative distribution function (CDF curves) for each station, the program will be added as appendix, see section 8.1.1.

In order to calculate the risk under climate change effect, a climate factor α, which is the slope of the trend component within the hydro-meteorological time series that needs to be added to the numerator of the classical risk formulation. If α = 0, there is no climate change expectation trend, otherwise, in increasing and decreasing cases α takes positive and negative value, respectively.
The time series plots of each station with the corresponding CDF curves for exceedance probability calculations for precipitation records are presented in a set of figures: Figure 3-1, Figure 3-2, Figure *3-3*, Figure *3-4* and Figure *3-5* (Şen et al., 2017, Boudiaf et al., 2020).
Note: the plots of the remaining stations will be added as appendix, see section 8.1.2.

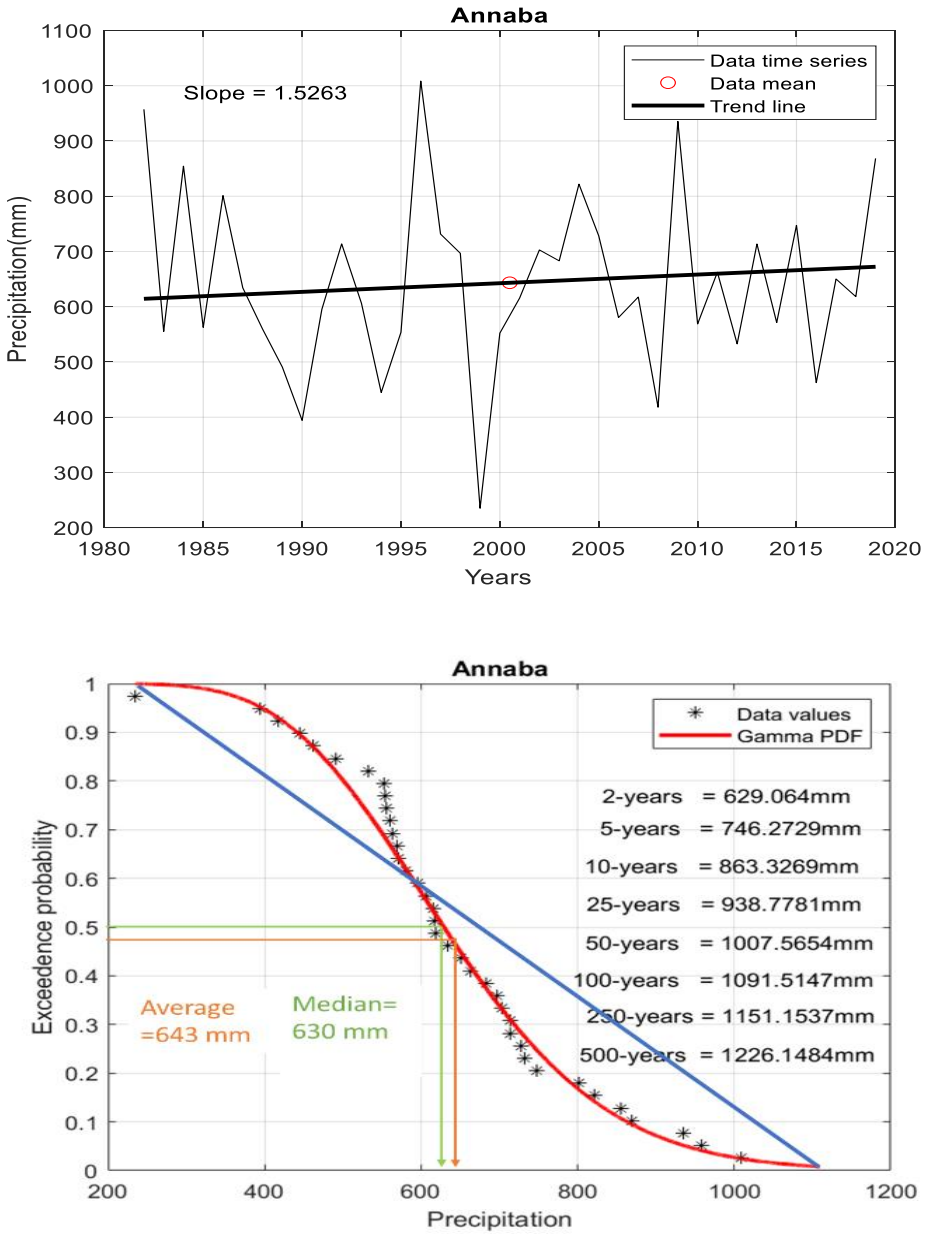

Figure 3-1: Precipitation time series plot with CDF curve of Annaba Station

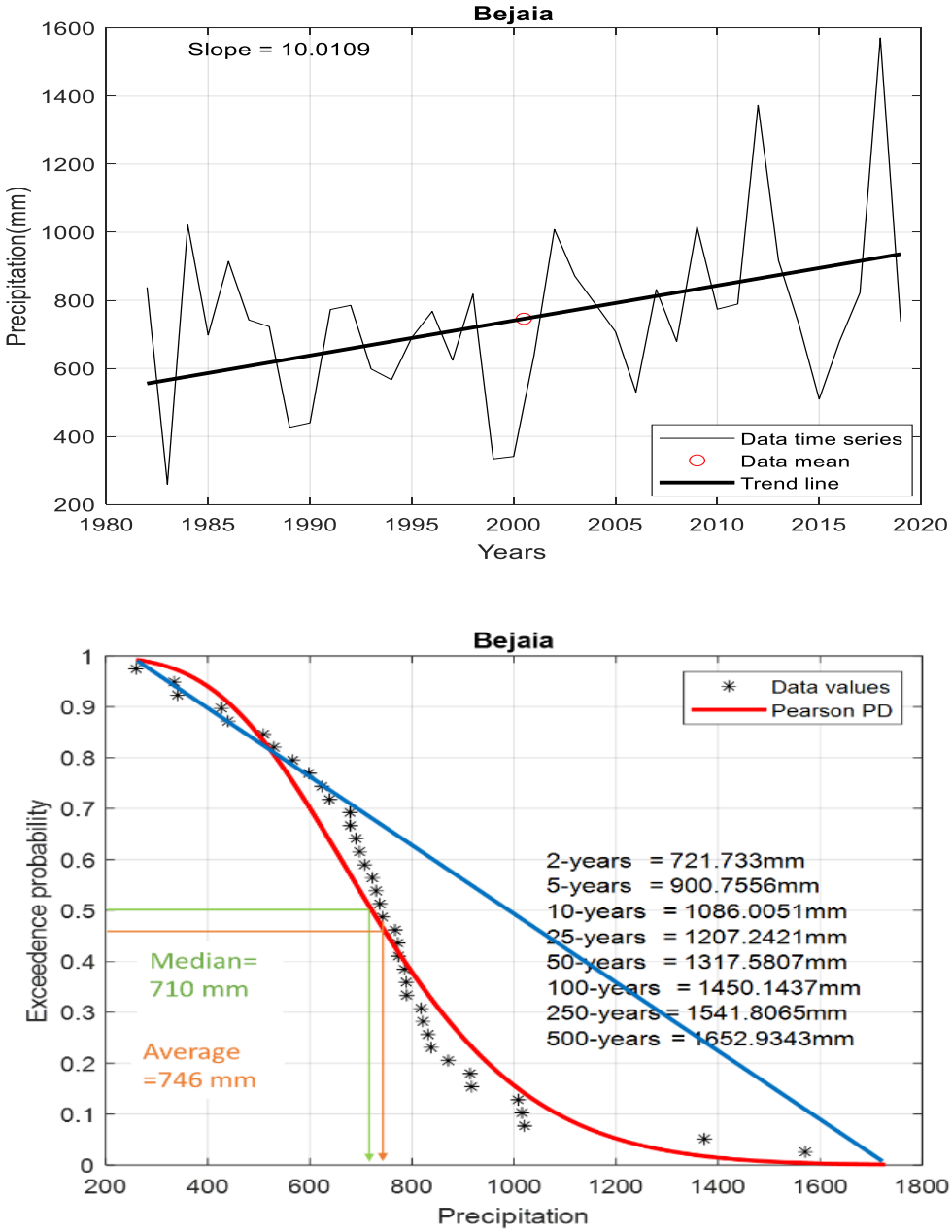

Figure 3-2: Precipitation time series plot with CDF curve of Bejaia Station

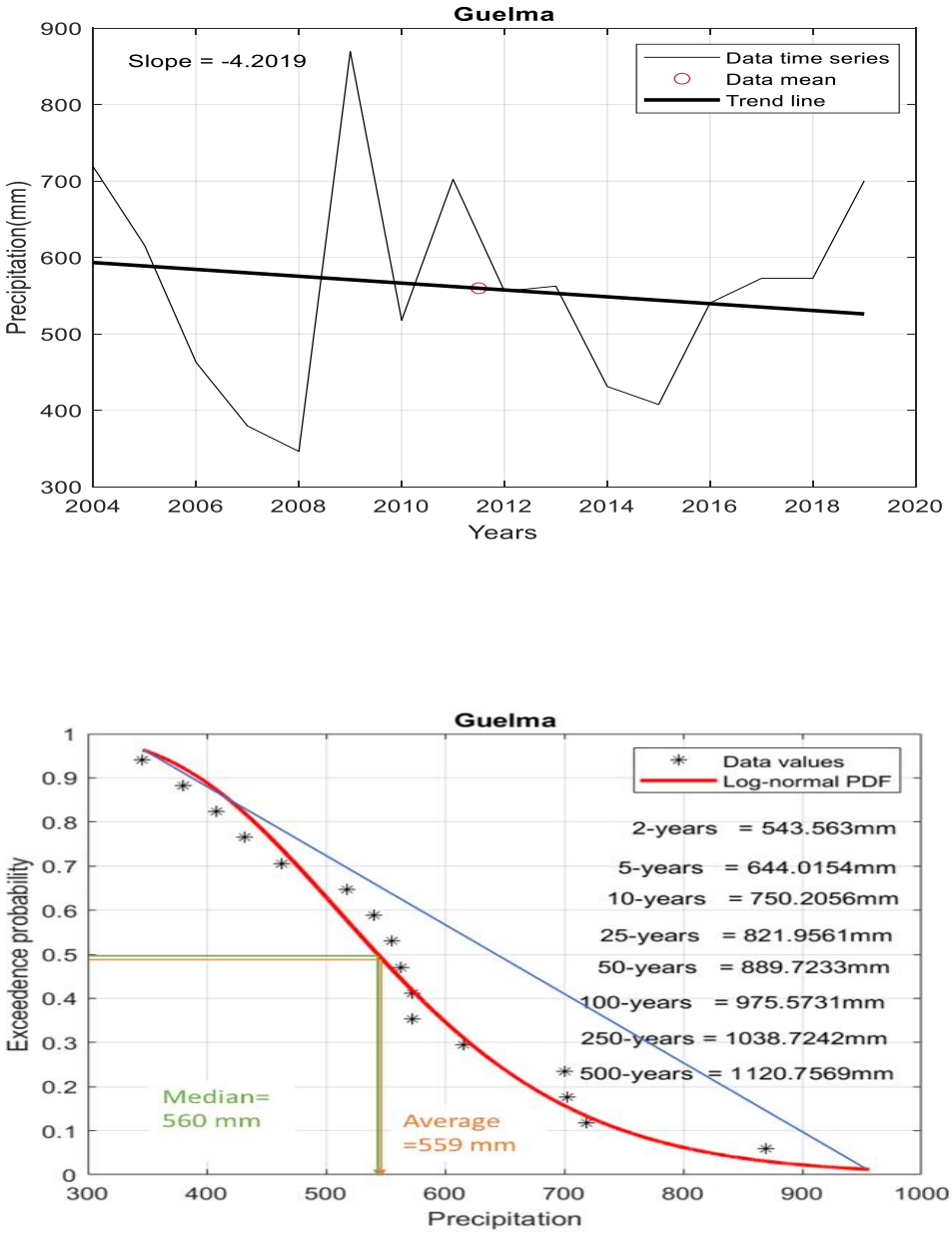

Figure 3-3: Precipitation time series plot with CDF curve of Guelma Station

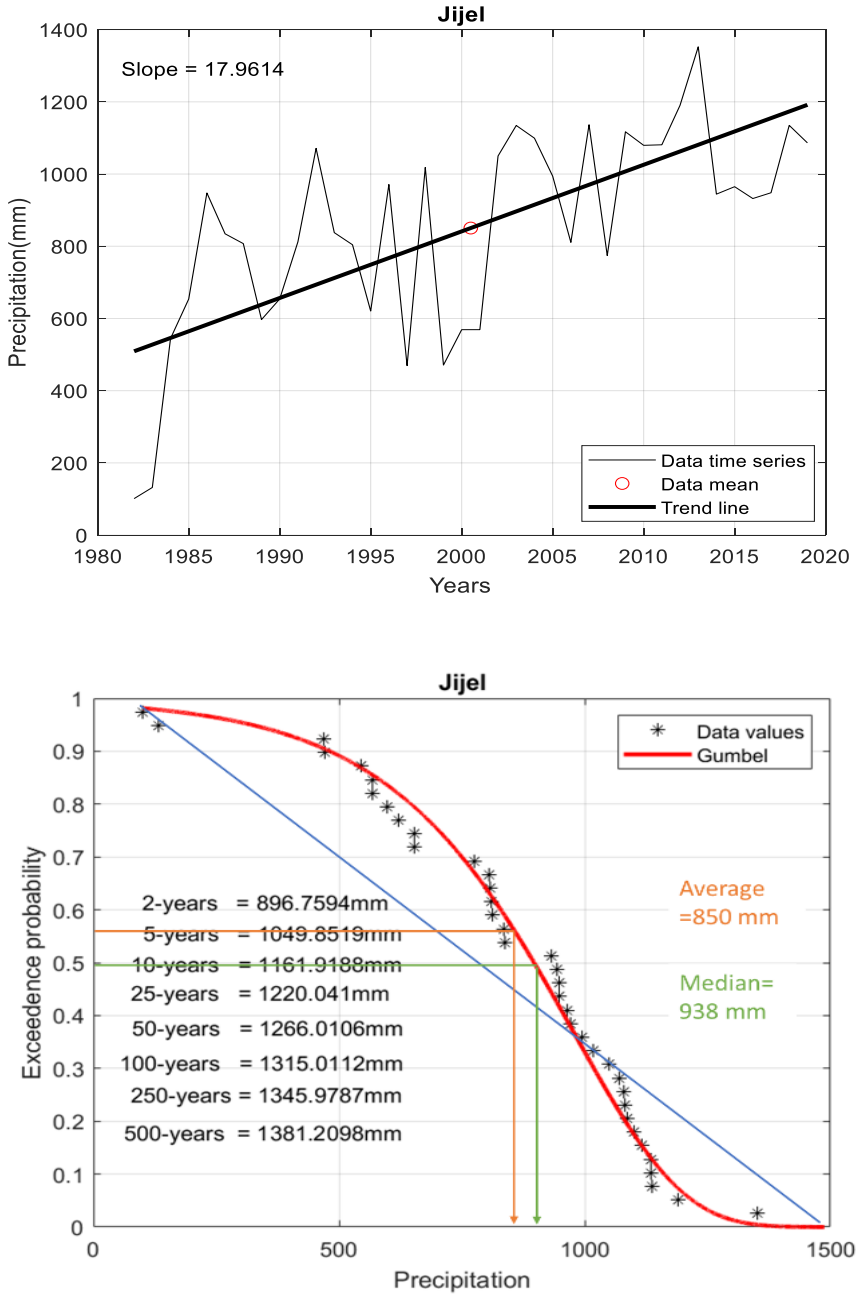

Figure 3-4: Precipitation time series plot with CDF curve of Jijel Station

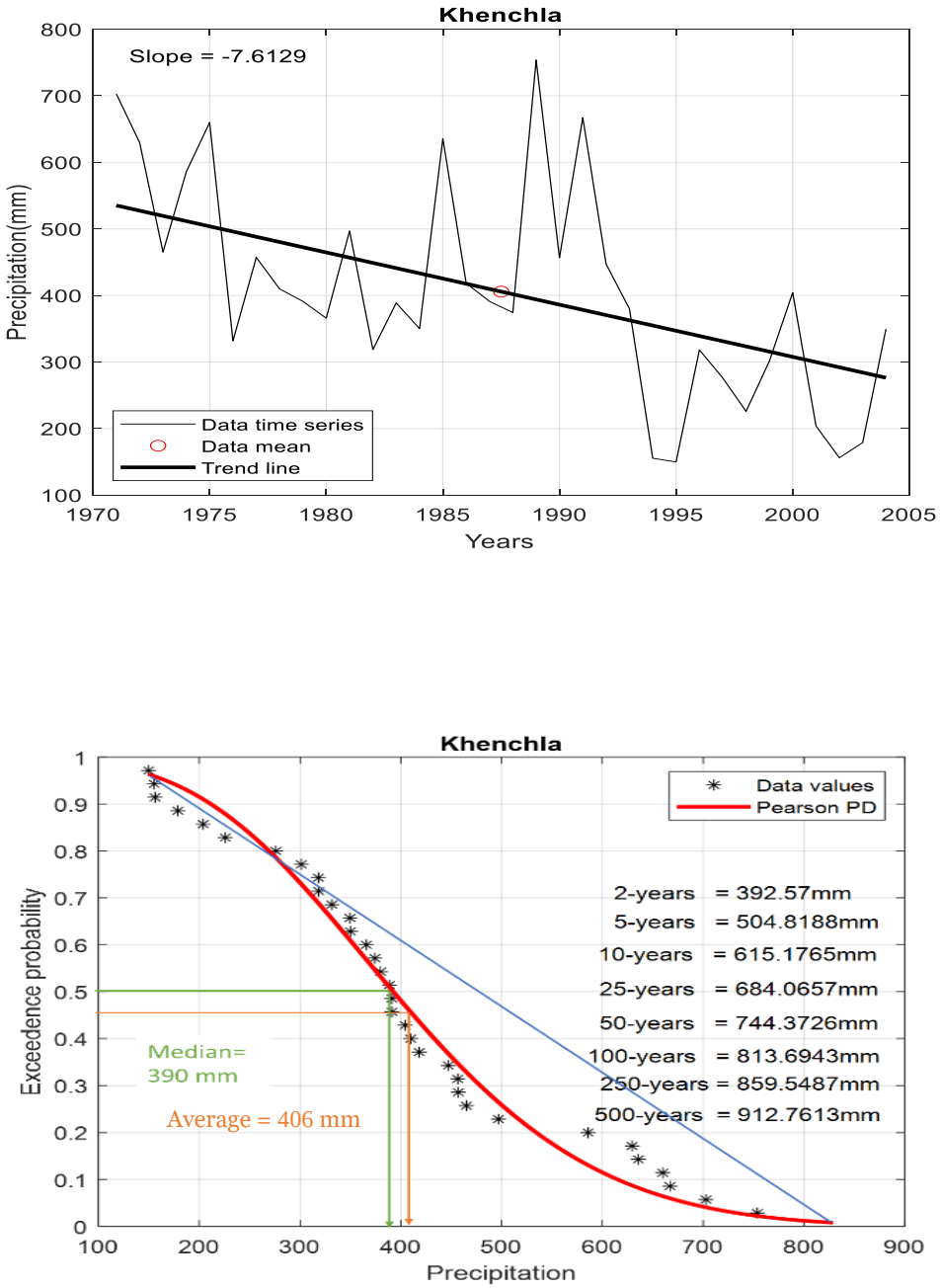

Figure 3-5: Precipitation time series plot with CDF curve of Khenchla Station

3.4.2 Interpretation

3.4.2.1 Precipitation time series plots

Relying on the slope value, the trend is categorized as increasing if the slope is positive and decreasing if it is negative. For example, Annaba station have a slope of 1.5, that should mean there is an increasing by 1.5 mm per year, however, Khenchla station have a slope of -7.6, that should mean there a decreasing by of 7.6 mm per year. The more sloping upward, the more the increment we have and vice versa.

We can arrange the resulted plots into four (4) categories as in Table *3-1*:

Table 3-1: Plot's calcification

Positive and significant trend	Positive but not significant trend	Negative significant trend	Negative but not significant trend
Souk Ahras Bejaia Mila El Taref Jijel	Constantine Borj Bouarriridj Skikda Annaba Oum Bouaghi Setif Tebessa Batna	Khenchla Guelma	M'Sila

3.4.2.2 Description of CDF curves interpretation

The Cumulative Distribution Function (CDF) very powerful tool to visually represent the distribution, and its interpretation rely on four Moments:

3.4.2.2.1 Central tendency (Mean, Median)

Figure *3-6* shows the basic characteristics of the CDF, where the vertical axis is the cumulative probability, going from 0% to 100%, and the x-axis shows the numerical values in the distribution.

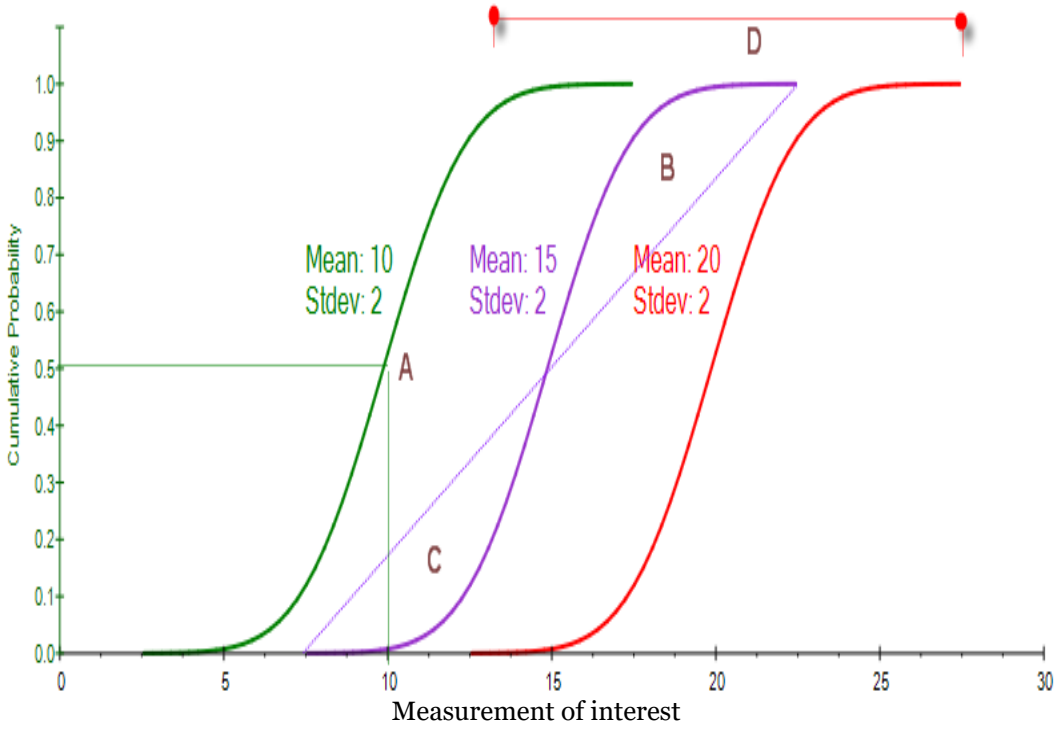

Figure 3-6: Interpreting S-Curves

The center of the S-Curve is the median or 50th percentile (A), and we can clearly see that the central tendency of the three curves is shifted away from one another, indicating a different median and mean (and because the Normal distribution is symmetrical, the mean is exactly at the median). The equal areas above (B) and below (C) the 45-degree line indicate a symmetrical distribution, where we have equally likely outcomes above and below the median. Finally, the length from one end to another (D) measures the spread, or risk, and we see that these three curves have similar widths or lengths, indicating similar risk levels (identical standard deviations).

3.4.2.2.2 Risk spread (Standard Deviation)

Figure *3-7.* shows the corresponding S-Curves. We see that the steeper the slope of the S-Curve, the less risk, or width, of the distribution.

The longer or wider the S-Curve, and the flatter the S-Curve, the higher the standard deviation (second moment, measuring risk, dispersion, and range of possible outcomes).

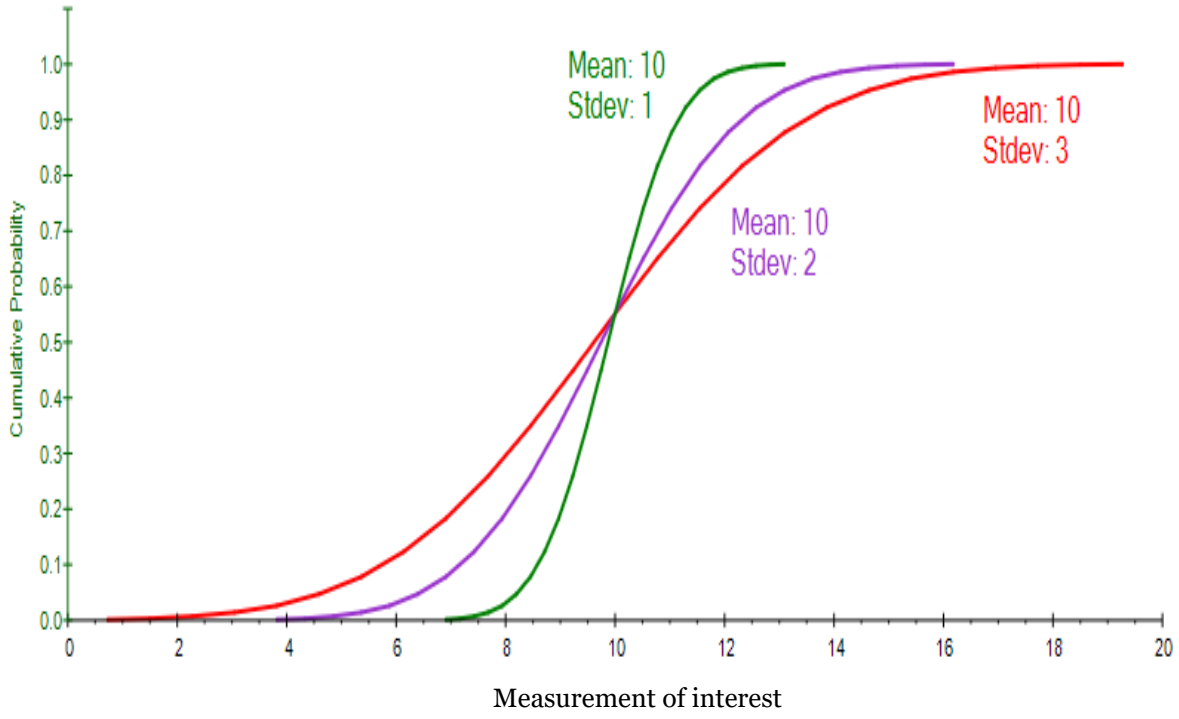

Figure 3-7: CDFs of Three Normal Distributions (Identical Means, Different Standard Deviations)

3.4.2.2.3 Directional Probabilistic Weights (Skew)

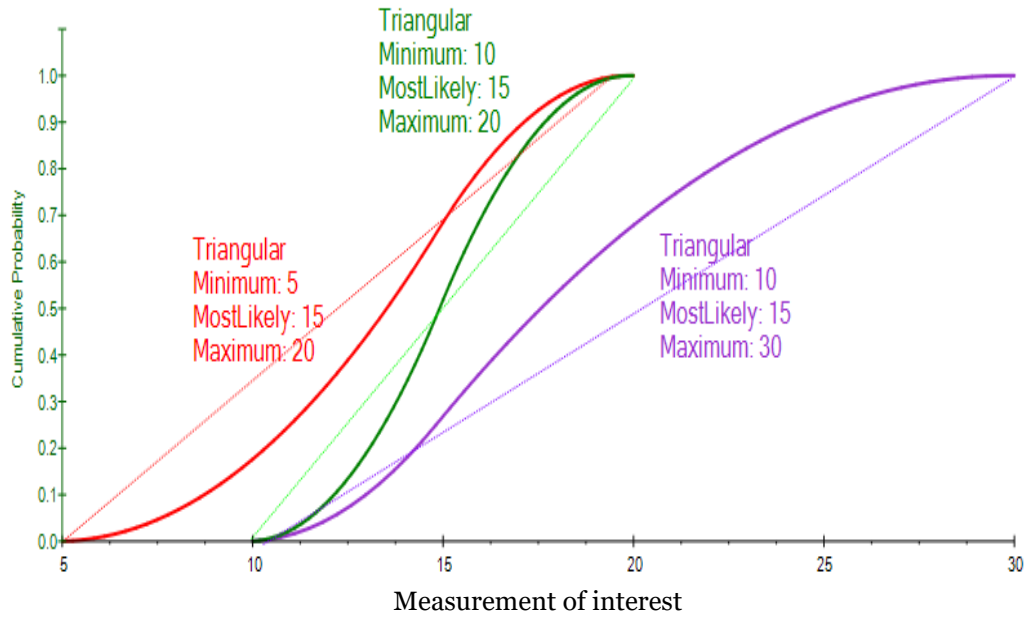

Figure 3-8: CDFs of Three Triangular Distributions (Different Skew and Asymmetry)

Figure *3-8* shows the corresponding S-Curves. We see that when we draw a 45-degree line (starting from the minimum and ending at the maximum of the S-Curve), the area above/below the 45-degree line provides an insight into the skewness of the distribution. We see that the negative skew distribution (red) has greater area below the 45-degree line than above, whereas the inverse is true for the positive skew (purple). The symmetrical distribution (green) has equal areas above and below the 45-degree line.

3.4.2.2.4 Extreme Tail Events (Kurtosis)

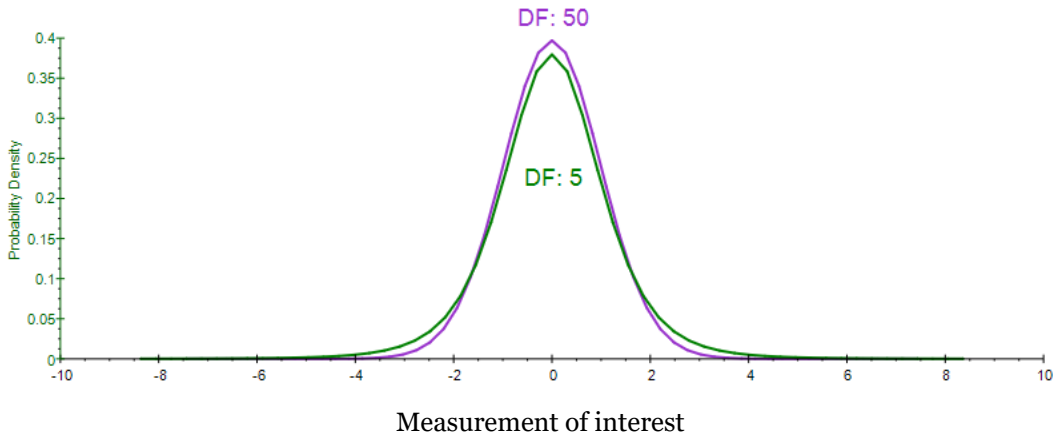

Figure 3-9: PDFs of Two T-Distributions (Illustrates Kurtosis or Excess Tail Probabilities)

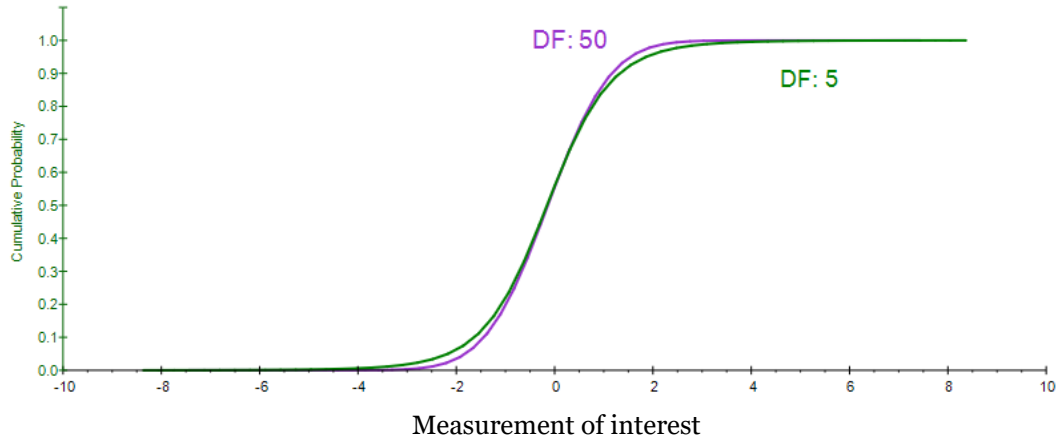

Figure 3-10: CDFs of Two T-Distributions (Illustrates Kurtosis or Excess Tail Probabilities)

Figure 3-9 shows the PDF interpretation of the fourth moment of a distribution (or its kurtosis, measuring the extreme values in the tails). The T distribution with a higher degree of freedom (purple curve with the DF of 50) is closer to a normal distribution, with zero excess kurtosis, whereas the fatter-tailed distribution (green curve with the DF of 5) has a higher kurtosis (higher probabilities of occurrence of extreme events in the tails). Figure 3-10 shows the corresponding CDF, and we see that the distribution with the fatter tails (higher kurtosis), indicating higher probabilities of extreme events, will have longer

tails at the extreme low and extreme high (green curve) as compared to another distribution with less kurtosis (purple curve).

3.4.2.3Interpretation of the resulted figures:

Visually, most of the stations represent an increasing trend, moreover, 75% of the resulted CDF curves are positively skewed which means most of data, means that highest number of data points have low values, the rest of data represent negative skewness reflecting that large number of data points have higher values. Skikda and Souk Ahras have -0.01 and 0.01 (nearly zero) skewness respectively implying the existence of a normal distribution for these two-time series.

The Table *3-2* show the extracted values of each moment and its interpretation

Table 3-2: Extracted values of each moment and its interpretation

Station name	Average	STD	Median	Skewness	Kurtosis	Interpretation
Annaba	643.31	160.96	617.88	0.14	0.49	positively approximately skewed, a little pointy not far from normal.
M'Sila	216.49	58.38	208.88	0.69	0.91	positively moderately skewed, a bit pointy but not significant.
Oum Bouaghi	396.02	104.62	386.10	0.64	0.22	positively moderately skewed with presence of significant kurtosis.
Mila	580.68	164.90	575.10	0.41	-0.04	positively approximately skewed with kurtosis very close to normal
El Taref	729.26	186.25	756.60	-0.06	-0.81	slight negative skewness with relatively high negative kurtosis could reveal a flatness of PDF curve
Jijel	850.40	281.48	938.27	-0.87	0.66	negatively with quite elevated skewness, however the kurtosis is positive but remains close to normal
Guelma	559.75	139.99	559.21	0.48	0.10	positively approximately skewed with kurtosis very close to normal
Setif	382.30	99.00	385.56	-0.12	1.29	negative but not significant skewness with relatively high kurtosis where the PDF seems to be pointy
Tebessa	357.11	101.39	346.09	0.66	0.54	Moderately positive skewed with slight pointy PDF curve
Constantine	490.24	159.48	472.81	0.78	0.31	Moderately positive skewed with slight pointy PDF curve
Bejaia	745.59	252.78	739.78	0.94	2.77	positive with 0.94 value of skewness it approaches to the highly skewed zone, also represent very high kurtosis revealing a very peaky Pdf curve
Bordj Bouarreridj	337.51	118.66	317.92	0.81	1.17	Moderately positive skewed with relatively high kurtosis
Skikda	656.22	146.25	644.52	-0.01	-0.68	it's skewness almost 0 where the kurtosis is below 0 indicating flat curve skewness is almost negligeable
Batna	289.31	112.43	282.46	0.90	1.50	the skewness factor approaches to highly skewed zone which is beyond the absolute value of 1, the kurtosis is high as well.
Khenchla	405.74	162.41	389.85	0.40	-0.38	positively approximately skewed with slight flatted curve
Souk Ahras	576.2725	183.0559	561.0903	-0.01091	0.134462	pretty much close to normal PDF curve

3.4.3 Risk assessment

3.4.3.1 Extreme events determination

Each chart contains several return periods associated with their extreme precipitation that can happen once during that period, for example, in Bejaia station chart, the extreme precipitation that may happen during 2 years is almost equal to 722 mm, while within 100 years an amount of 1450 mm can be reached at least once. And so on for the other charts. Table *3-3* represent the annual precipitation records of each meteorological station with its statistics for different return periods.

Table 3-3: Annual records at different return period

Return Period	2 years	5 years	10 years	25 years	50 years	100 years	250 years	500 years
Risk = 1/Return period	0.5	0.2	0.1	0.04	0.02	0.01	0.004	0.002
Annaba	629	746	863	939	1008	1092	1151	1226
Tebessa	348	418	488	534	575	626	663	708
Constantine	466	579	704	791	876	986	1068	1177
Bejaia	722	901	1086	1207	1318	1450	1542	1653
Borj Bouarriridj	326	408	494	550	600	662	704	755
Setif	384	452	509	541	568	598	618	642
Souk Ahras	576	703	814	877	927	979	1010	1043
M'Sila	209	251	296	327	356	393	420	456
Oum Bouaghi	383	456	533	584	632	690	730	780
Guelma	544	644	750	822	890	976	1039	1121
Jijel	897	1050	1162	1220	1266	1315	1346	1381
Batna	275	354	436	491	542	605	650	708
El Taref	758	872	956	999	1033	1070	1093	1119
Mila	583	698	796	852	899	953	988	1029
Khenchla	393	505	615	684	744	814	860	913
Skikda	658	757	841	887	923	959	980	1002

3.4.3.2 Calculations of the new risk with taking into consideration climate change impact

In water resource projects, risk levels are determined based on the available methods which currently ignore climate change influence.

Logically, since the simple and classical risk, R, without taking climate change into consideration, is equal to the probability of the occurrence of the dangerous event, P, only once during the entire existence of the structure, R, its notational definition is given as equation (3.1) (Benjamin and Cornell, 1970),

$$R = \frac{1}{T} \qquad \textbf{(3.1)}$$

R= Risk without climate change impact

T= Return period

This simple risk approach is modified by Şen et al. (2017) to equation (3.2)by taking into consideration the climate change effect as follows:

$$Rcc = \frac{1+\alpha}{T} \qquad \textbf{(3.2)}$$

Rcc: is the risk under climate change effect.

α = Climate factor (trend line slope).

using the equation (3.2), risk level under climate change effect is calculated for each station, all the results are presented in Table *3-4*.

Table 3-4: Risk levels under climate change effect using the equation (3.2)

Return Period	2 years	5 years	10 years	25 years	50 years	100 years	250 years	500 years
Risk = 1/Return period	0.5	0.2	0.1	0.04	0.02	0.01	0.004	0.002
Annaba	1.263	0.505	0.253	0.101	0.051	0.025	0.010	0.005
Tebessa	1.715	0.686	0.343	0.137	0.069	0.034	0.014	0.007
Constantine	0.886	0.355	0.177	0.071	0.035	0.018	0.007	0.004
Bejaia	5.505	2.202	1.101	0.440	0.220	0.110	0.044	0.022
Borj Bouarriridj	1.124	0.450	0.225	0.090	0.045	0.022	0.009	0.004
Setif	1.663	0.665	0.333	0.133	0.067	0.033	0.013	0.007
Souk Ahras	5.061	2.025	1.012	0.405	0.202	0.101	0.040	0.020
M'Sila	0.156	0.062	0.031	0.012	0.006	0.003	0.001	0.001
Oum Bouaghi	1.336	0.535	0.267	0.107	0.053	0.027	0.011	0.005
Guelma	-1.601	-0.640	-0.320	-0.128	-0.064	-0.032	-0.013	-0.006
Jijel	9.481	3.792	1.896	0.758	0.379	0.190	0.076	0.038
Batna	2.301	0.920	0.460	0.184	0.092	0.046	0.018	0.009
El Taref	6.388	2.555	1.278	0.511	0.256	0.128	0.051	0.026
Mila	5.664	2.265	1.133	0.453	0.227	0.113	0.045	0.023
Khenchla	-3.306	-1.323	-0.661	-0.265	-0.132	-0.066	-0.026	-0.013
Skikda	1.252	0.501	0.250	0.100	0.050	0.025	0.010	0.005

3.4.3.3 Calculations of the new return period with taking into consideration climate change impact:

By taking into consideration the climate change risk level calculations from Eq. (3.2), one can calculate the return periods according to the standard formulation in Eq. (3.1) as if there is no climate change impact, results are shown in Table *3-5*.

Table 3-5: Return periods under climate change effect using equation (3.1)

Old Return Period	2 years	5 years	10 years	25 years	50 years	100 years	250 years	500 years
Annaba	0.8	2.0	4	10	20	40	99	198
Tebessa	0.6	1.5	3	7	15	29	73	146
Constantine	1.1	2.8	6	14	28	56	141	282
Bejaia	0.2	0.5	1	2	5	9	23	45
Borj Bouarriridj	0.9	2.2	4	11	22	44	111	222
Setif	0.6	1.5	3	8	15	30	75	150
Souk Ahras	0.2	0.5	1	2	5	10	25	49
M'Sila	6.4	16.1	32	80	161	321	803	1607
Oum Bouaghi	0.7	1.9	4	9	19	37	94	187
Guelma	-0.6	-1.6	-3	-8	-16	-31	-78	-156
Jijel	0.1	0.3	1	1	3	5	13	26
Batna	0.4	1.1	2	5	11	22	54	109
El Taref	0.2	0.4	1	2	4	8	20	39
Mila	0.2	0.4	1	2	4	9	22	44
Khenchla	-0.3	-0.8	-2	-4	-8	-15	-38	-76
Skikda	0.8	2.0	4	10	20	40	100	200

3.4.4 Discussion

Table *3-5* revealed dangerous presumptions, in 13 stations, an extreme event that should happen once in a while will occur much sooner, where some of them can reach a creepy level such as Jijel which present a return period equal to 5 years instead of 100!!! Same as El Taref, Bejaia, Mila, Souk Ahras show a dramatic decrease in their return periods. Less significant shift in return periods for (Annaba, Tebessa, Constantine, Bordj Bouarreridj, Setif, Oum Bouaghi, Batna and Skikda).

On the other hand, three 3 stations performed counteractively, which they show longer return period, for example M'Sila station return period increases three times longer than it should be without climate impact assumption, Khenchla and Guelma present negative numerical values because the slope goes below -1, in that case the return periods will be longer same as M'Sila station and even beyond that.

3.5 WET AND DRY PERIODS

Wet spell is the period of excessive precipitation amount that cause water surplus which might lead to floods. Where the term dry spell is related to periods where there is deficit in precipitation which cause droughts (Şen, 2015). In general, wet and dry spells are identified by duration, intensity, severity, and spatio-temporal extent.

One of the characteristics of many precipitation regimes throughout the world is that wet spells occur in a variety of durations. Monthly precipitation records may be analyzed simply using a certain risk level, which helps to identify also the critical magnitudes of monthly wet and dry spells at a truncation level (Şen, 2019). Full information about the wet and dry spell numbers become more pressing in water resources management projects, agricultural planning, flood and drought studies. The geographical distribution of these meteorological parameters helps to plan and manage water resources related projects. Figure 3.11 gives detailed information about wet and dry periods of a time series, X_i (i = 1, 2, …, n) at a truncation (threshold) level, X_0.

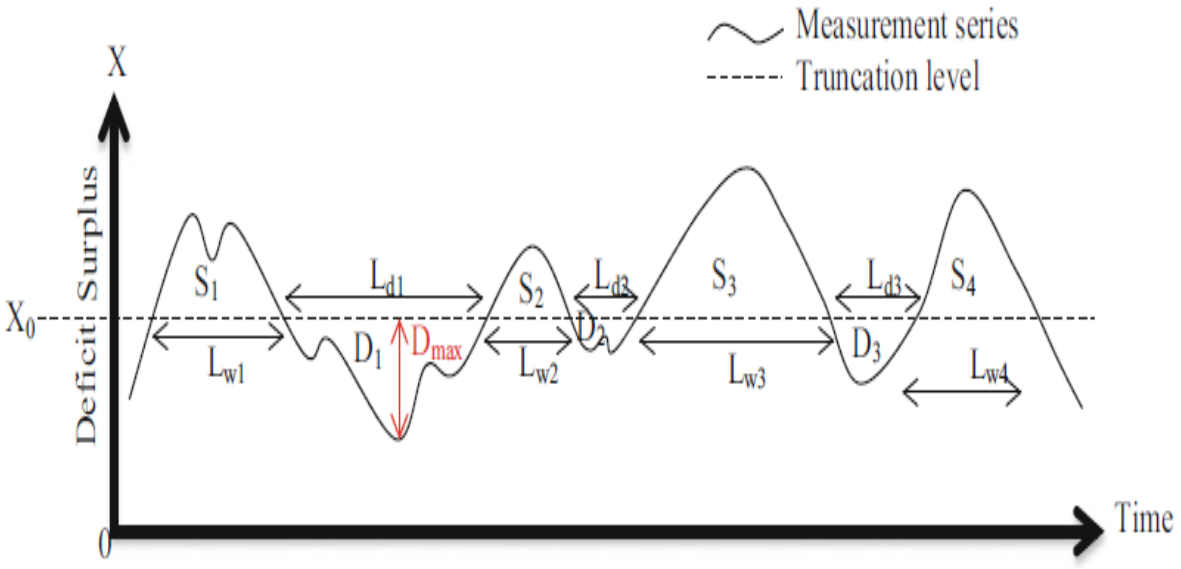

Figure 3-11: Wet and dry periods of time series Xi(i=1, 2, …,n)

In this figure, sequences of surplus and deficit periods are given on a certain truncation level, X0, which may be the arithmetic average or any other supply or demand level. Above and below given truncation levels, there are various dry and wet period specifications.

In Figure 3-11 dry periods are referred to as the drought representatives and their lengths (L_{d1}, L_{d2}, …) are the drought durations. In the figure, three distinctive drought durations are shown. These durations are very important in cases of water scarcity, and in a given record, there are many of them. The question is which one of these drought durations to adapt in practical applications.

The sequence of such durations provides a basis for probabilistic and statistics methodological applications. One may take the arithmetic average as the representative drought duration, but in practical applications, it is better to adapt a value that

corresponds to a certain risk level such as 5 or 10%. All what has been said for drought duration the same arguments are valid for wet durations. In Figure 3-11, each deficit spell has differences of X values from X_o and their summation is referred to as the drought magnitude, D_M, which can be expressed as equation (3.3),

$$\boldsymbol{D_M = \sum_{i=1}^{L_d}(X - X_0)} \qquad \textbf{(3.3)}$$

D_M = Drought magnitude.

L_d = Drought length (duration).

X = Precipitation amount (mm).

X_o = truncation level usually is the average of the time series, in this case average precipitation (mm).

It shows the total deficit amount along any drought duration. Among all the drought magnitudes within the historical data, the maximum one may be taken as the most dangerous case that may appear in the future. There is another description of the drought, which corresponds to the maximum deficit, D_{MAX}, value during any drought duration.
After knowing the drought magnitude and its duration, the drought intensity, DI, is defined as the drought magnitude divided by the corresponding drought duration. For instance, according to Figure 3-11 the first drought intensity, D_{I1}, is calculated as equation (3.4),

$$\boldsymbol{D_{I1} = \frac{Dmax}{L_{d1}}} \qquad \textbf{(3.4)}$$

D_I= Drought intensity.

D_{MAX}= Maximum deficit.

L_d= Drought length (duration)

It is possible to calculate each one of the drought quantities at risk levels (0.50, 0.20 0.10, 0.04, 0.02, and 0.01) corresponding to a set of return periods respectively (2-year, 5-year, 10-year, 25-year, 50-year, and 100-year) (Şen, 2019).

3.5.1 Drought Indices

There are many drought indices in practical use for different purposes including engineering, agricultural, irrigation, meteorology, soil moisture, and other activities. The most widely used alternatives are either the classical approach as explained above or the standard precipitation index, which is effective in meteorological applications for depicting the effects of meteorological droughts.

I. A "wet" state ($X_i > X_0$) occurs at any time interval, i, with its "surplus" amount as ($X_i - X_0 > 0$.
II. Otherwise, a "dry" state ($X_i < X_0$) exists with its corresponding "deficit" amount ($X_i - X_0 < 0$.
III. A "wet spell" is defined as the delimitation of consecutive uninterrupted wet spells by at least one "wet" state. If the dry state locations at the beginning and the end of a "wet spell" are ($X_i < X_0$) and ($X_j < X_0$), respectively, then the duration of this wet spell is defined quantitatively as ($j - i$).
IV. Likewise, "dry spell" is defined as an uninterrupted sequence of "dry" states that are delimited at the two ends by at least one "wet" state. If the "wet" state locations at the beginning and the end of a "dry spell" are "wet" states as ($X_k > X_0$) and ($X_l > X_0$), then the "dry spell" duration is equal to ($l - k$).
V. If there is a transition from a "dry spell" to subsequent "wet spell," then such a transition point is defined by two successive states as "dry" ($X_i < X_0$) and "wet" ($X_{i+1} > X_0$). This means that at i-th location there is an up-crossing point, ui.
VI. Similarly, any transition between "wet spell" and the following "dry spell" implies a down-crossing, di, point defined by a "wet" state ($X_i > X_0$) and the next "dry" state ($X_{i+1} < X_0$).
VII. Among the "dry spell" durations at a given truncation level there is one, which is the maximum (minimum), and this duration is referred to as the "critical dry duration" ("critical wet duration"). Such critical periods play a significant role in

any capacity design in water structures (dams, canals, dikes, levees, etc.) and especially in the water resources operations and management.

VIII. The summation of surpluses (deficits) along any wet duration (dry duration) is referred to as the "surplus magnitude," S_M ("drought magnitude," D_M, as in Eq. 3-4). These are also known as the total surplus and total deficit amounts, respectively, in practical studies.

It is also possible to consider the "gross deficit," D_G ("gross surplus," S_G) by considering the totals over the whole record period. Comparison of these two gross values leads to the following three alternatives.

- **(a)** If $D_G = S_G$ then at this location, temporarily, the summation of deficits is in balance with surpluses during the whole record or planned period considered. It is possible to balance the whole deficit occurrence during this duration by surplus amounts provided that the surpluses are stored in convenient storage. For instance, if the water demand level of a settlement area is considered as the truncation level, then the total surplus around this level can meet the whole deficit (water shortage) occurrences without any water shortage provided that proper storage units are constructed. Such a situation corresponds to ideal reservoir design, which is referred to as the Ripple diagram in hydrology.

- **(b)** If $D_G > S_G$, then at this location one expects drought effect, and in order to offset such a case, it is necessary to transfer water from other locations.

- **(c)** If $D_G < S_G$, there is a wet spell expectation at this location with extra water amounts and it may be possible to transfer the extra water to nearby water-shortage or drought-stricken areas.

Each one of the drought definitions can be calculated, if there is a reliable sequence of data at hand with objectively defined threshold level. It is also possible to make future

predictions of these quantities for different return periods (design durations) such as 5-year, 10-year, 25-year, 50-year, or 100-year.

3.5.2 Application of the drought indexes calculation application

Seeking the optimal results, MATLAB software was used to write the appropriate program which will be added as appendix, see section 8.1.3 .
Note: this program should be associated with the probability density function program.
The truncation level used here is equal to the average precipitation of the whole time series.

The results related to Annaba station are presented in Figure 3-13 and Table *3-6*.

Annaba Station

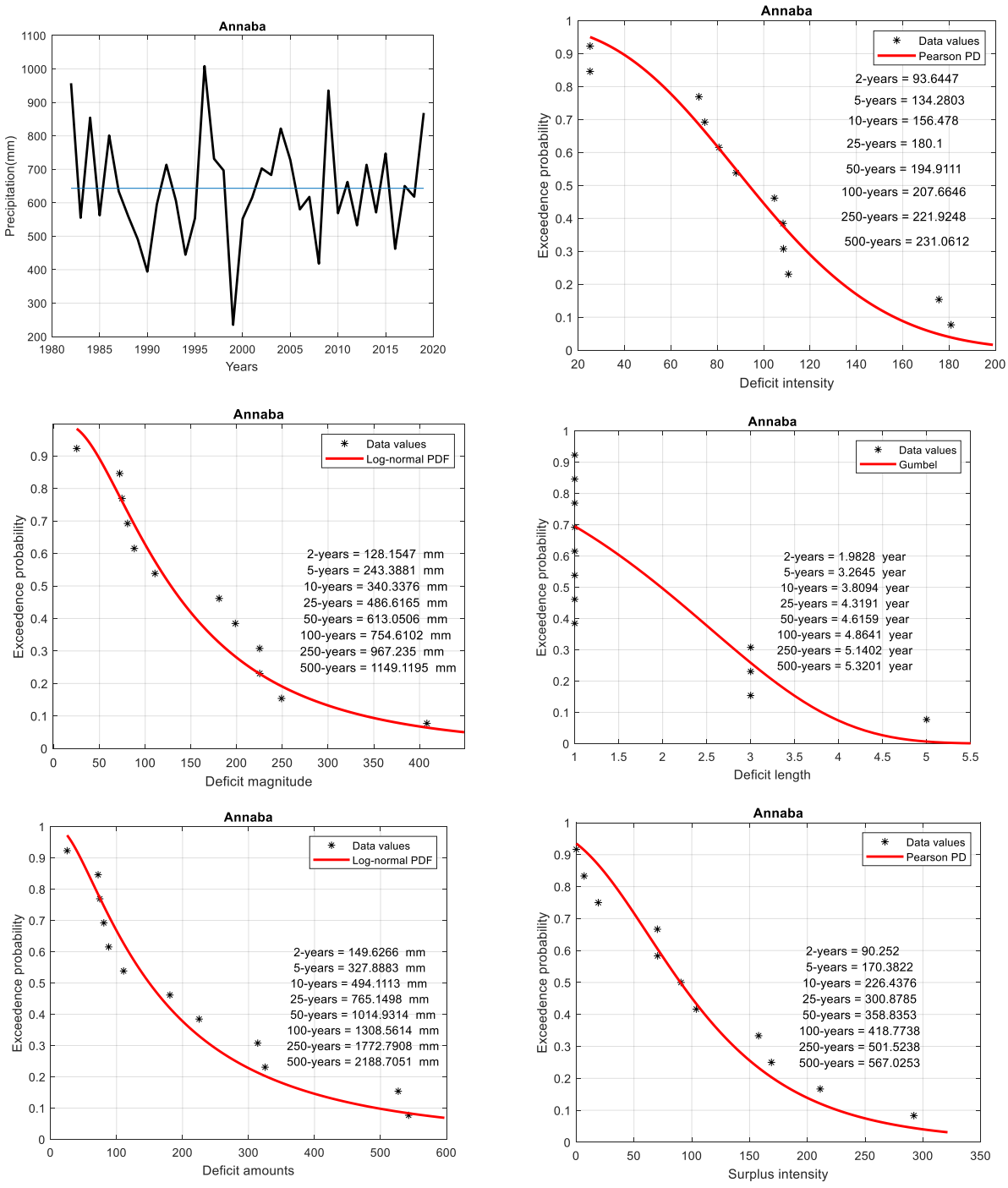

Figure 3-12: Annaba's drought indexes.

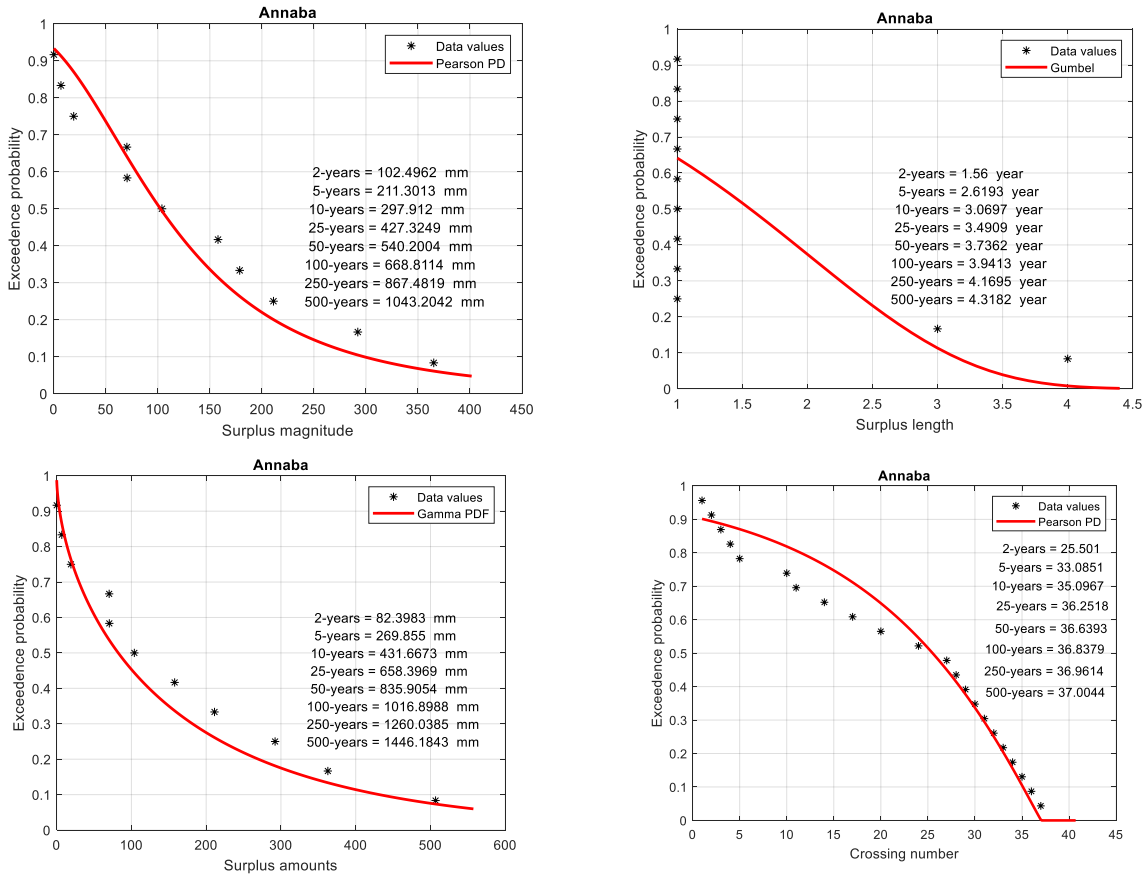

Figure 3-13 (suite and end): Annaba's drought indexes.

Table 3-6: Annaba's drought indexes result

D magnitude (mm)	88.1	80.7	542.6	325.1	526.8	313.9	74.6	110.7	72.1	180.8	25.1	Total = 2340.4	Gross= 111
D intensity(mm/year)	88.1	80.7	108.5	108.4	175.6	104.6	74.6	110.7	72.1	180.8	25.1		
D length (year)	1	1	5	3	3	3	1	1	1	1	1	Total = 21	
D max (mm)	88.1	80.7	249.1	198.6	408.1	225.2	74.6	110.7	72.1	180.8	25.1		
S magnitude (mm)	0.1	211.1	157.8	70.4	506.8	362.7	292.2	19.1	70.2	103.9	6.9	Total = 1801.4	Gross = 113
S intensity (mm/year)	0.1	211.1	157.8	70.4	168.9	90.7	292.2	19.1	70.2	103.9	6.9		
S length (year)	1.0	1.0	1.0	1.0	3.0	4.0	1.0	1.0	1.0	1.0	1.0	Total = 16	
S max (mm)	0.1	211.1	157.8	70.4	365.2	178.6	292.2	19.1	70.2	103.9	6.9		

The results of the remaining stations are added as appendix, see section 8.1.4.

3.5.3 Interpretation

The precipitation plot can be interpreted as demonstrated in the Figure 3-14.

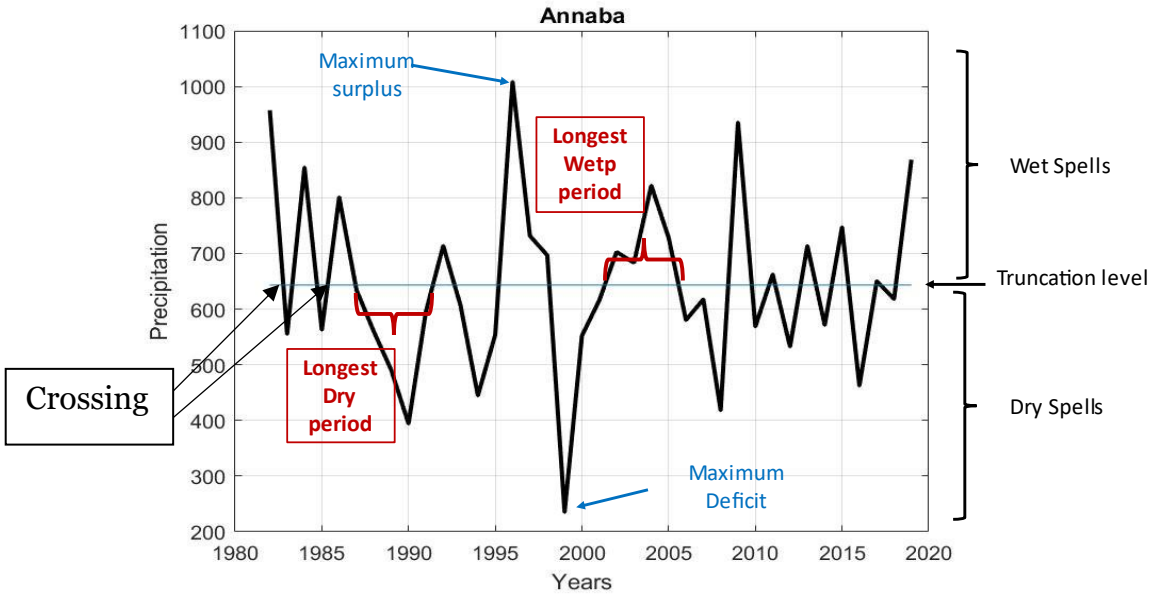

Figure 3-14: Annaba's plot demonstration

Visually, there are a lot of crossings reflecting the unsteady climate, especially the period 1995-2002 there were noticeable shift from a very wet season to a very dry one, longest dry period was between 1987-1992, where the wet one was between 2001-2005.

From the table, one is able to calculate the Total wet = 16 years (Dry= 21 years) spell durations. Moreover, one can extract the gross surplus SG as well as the gross deficit DG and compare theme the each other.
SG = 111 mm, DG = 113 mm.

DG > SG: there is drought expectation at this location.

The droughts are longer than the wet spells, but with the increasing trend (see table 4-1) the wet spells may expand in the future.
The CDF curves are tools to calculate the associated risk levels for each attribute.
The results of the other stations will be added as appendix (see section 8.1.4).

3.6 CONCLUSION

It is well known precipitation has been steadily increasing across the globe, and especially, in the Mediterranean basin over the last 3 decades. The most important factor in the design of any water resource system is the risk associated with hydrometeorological events.

The purpose of this study is to analyze trends in precipitation records and incorporate these into risk assessments by factoring in the changing climate for the Northeast of Algeria over the 38-year period (1982–2019). For the purpose of this study, a climate change factor is incorporated into the classical formulation, based on the trend slope in historical records. The risks associated with 2-, 5-, 10-, 25-, 50-, 100-, 250-, and 500-year return periods are then calculated for each station. Furthermore, multiple wet and dry spells have been examined as part of drought indexes calculations.

It has been determined that 81% of the study area is experiencing an increasing trend in rainfall, with certain regions in the study area experiencing speedier return periods, with some of them seeing return periods as much as 95% sooner. The regions in first position include, Souk Ahras, Bejaia, Mila, El Teref and Jijel since they are in the flash flood prone areas, in second position under the flood threat are Constantine, Bordj Bouarreridj, Skikda, Annaba, Oum Bouaghi, Setif Tebessa, and Batna. In contrast, three stations (Khenchla, Guelma, and M'Sila) perform contrarily toward drought as they present a decreasing trend.

By digging deeper into the details and finding that drought indexes especially the gross deficit D_G (gross surplus S_G) index, for ten 10 stations Annaba, Oum Bouaghi, Mila, Jijel, Ttebessa, Constantine, Bejaia, Bordj Bouarreridj, Skikda, and Khenchla were found with $S_G > D_G$ referring to the more frequent wet spells bringing extra amounts of water to nearby water-shortage or drought-stricken areas. On the other hand, dry spells dominate the five 5 other stations El Taref, Guelma, Setif, Souk Ahras and Batna) where M'Sila remaining in balance.

The superposing of the two conclusions above uncovers an important inference that is: Regions with both increasing trends especially if it is significant with prevailed surplus are continuously under threat because additional precipitation is expected, far apart from areas who have decreasing trends where the surplus may get reduced as long as the precipitation decreases like Khenchla station. Concerning the locations where drought spells take over, if they present a decreasing trend, then this region should be stated as drought prone like Guelma station.

Finally, the study made in this chapter revealed that climate change will aggravate situations in the study area, and the top three locations needing quick rehabilitation against floods are Bejaia, Mila and Jijel, where Constantine, Bordj Bouarreridj, Skikda, Annaba, Oum Bouaghi, and Tebessa come in second position, Khenchla already under flood risk but it tends to get less rainy while Guelma station need solutions for droughts because they tend to be more frequent.

Chapter IV
Innovative Trend Analysis (ITA)

4 CHAPTER IV: INNOVATIVE TREND ANALYSIS (ITA)

4.1 ABSTRACT

Climate change impacts affect the hydrological cycle and hence the availability of water resources and their management. Rainfall, is the most important hydro-meteorological event and as the main source of water, may have increasing or decreasing trends depending on geography and location, general air circulation, proximity to coastal areas and geomorphology. There are many studies using monotonic trend analysis in the literature, but it is important to assess these trends at different levels for proper recording. For this purpose, in this paper, instead of using monotonic trend analysis, partial trends will be sought at “Low”, “Medium” and “High” rainfall records groups, which is possible through the innovative trend analysis (ITA) methodology.

Algeria being adjacent to the Mediterranean Sea is impacted by variations in rainfall. In the present chapter, the application of the ITA methodology will be presented for 16 different Algerian annual rainfall records from 1982 to 2019 in the North-Eastern region of the country which is in proximity to the Mediterranean basin. Partially increasing, decreasing or no trend pieces are identified at each station. It is concluded as assuming the future will keep the same pattern some stations will record dry spell or drought dangers for “Low” data groups, and significant flood danger for the “High” rainfall amount data group. In general, the study area is known to be subject to an increasing rainfall trend. This is due to the mountainous terrain in the study area and makes for confrontation with cold air movements from the European continent during winter periods.

4.2 INTRODUCTION

The Eastern Mediterranean and the North African areas are considered to be by IPCC (2014) the region's most vulnerable to anthropogenic greenhouse gas (GHG) emissions, which will in turn lead to widespread climate change impacts. Numerous studies have mentioned the decrease in rainfall in Maghreb countries (Hallouz et al., 2018, Mahe et al., 2013, Meddi et al., 2010b). The north Algerian parts are next to the Mediterranean basin, and therefore, subject to these climate change effects. Since 1993 Algeria is incorporated within the United Nations Framework Convention on Climate Change (UNFCCC), and adheres to the UNFCCC commitments to stabilize GHG emissions to prevent anthropogenic interference within the climate system (Sahnoune et al., 2013).

Algeria has a large coastal area in the Western Mediterranean region subject to climate change impacts (Hadour et al., 2020, Hallouz et al., 2020, Khedimallah et al., 2020, Taïbi et al., 2018, Zeroual et al., 2019), and therefore, needs protection against these hazardous effects such as rainfall reductions, droughts and floods. Sahnoune et al. (2013) mentioned that Algeria has shown its determination to participate in the international effort to fight climate change and its potential impacts on water resources, natural ecosystems and continued economic development.

The initial strategy used to combat climate change is discussed in various project documents for adaptation and mitigation strategies. These national strategies are based primarily on four concepts: institutional strengthening; adaptation to climate change; mitigation of GHG emissions and human capacity building.

Elmeddahi et al. (2016) presented the effect of climate change on Algerian water resources through streamflow monotonic trend analysis. IPCC (2014) reports indicate that in general, the Mediterranean basin and in particular the North African countries including Algeria are more vulnerable to climate change. Oli Brown (2019) stated that among the continents, Africa in general and North Africa in particular are the regions most exposed

to climate change impacts, because within the continent exists the driest and hottest regions of the world. Along the Mediterranean coastal areas annual rainfall amounts are comparatively very high reaching to 1,500 mm/year in Tunisia and Algeria, whereas it reaches to about 2,000 mm/year in Morocco due to the Atlas Mountain. Inside the continent, the amounts are much less than 100 mm.

Numerous studies have been conducted in the northern regions of Algeria regarding precipitation and temperature, but they are concentrated more towards the western regions than in the east. Elmeddahi et al. (2016) analyzed monotonic trends in rainfall and stream flows across the Cheliff basin in northwest Algeria employing non-parametric trend slope estimator for the extent of tendencies whose statistical significance was measured by the Mann-Kendall (MK) and the Modified Mann-Kendall (MMK) tests (Mann, 1945, Kendall, 1975), where results indicated statistically significant monotonic downward trend in the annual rainfall over the entire basin (Sen, 1968).

Over the period 1970–2010, Bessaklia et al. (2018) studied 23 rainfall station records in the extreme North-East of Algeria. They concluded that according to MK test, there is an increasing trend in high precipitation records.

Another 5 locations covering the northeast part of the country were studied by Merabti et al. (2018) with the inference that arid and semi-arid zones have experienced a larger number of drought events, while the humid and sub-humid locations received more precipitation events.

An additional study of precipitation variability on the Massif Forest of Mahouna (Northeastern Algeria) has been presented by Beldjazia Amina (2016) who found strong tendency at the beginning and bit of weakness at the end of the winter and spring seasons. The most important impacts on potential water resources are across temporal and spatial scales, especially floods, droughts and sea level rise (Mimura, 2013). Global warming increases evaporation from water surfaces (sea, lake, and river), which end up with more

extreme rainfall events in ever increasing or decreasing trend forms depending on the land surface morphology (Trenberth, 2011). The amount of change in precipitation associated with a specific change in surface temperature is critically important to understanding the global hydrological system and for climate model development and validation (Ren et al., 2013).

The objective assessment of climate change impacts is possible by employing trend analyses methodologies, which have been in frequent use for nearly three decades. In the past, hydro-meteorological time series records were considered as stationary without any trend component, often with a seasonality component attached for use in future studies.

Trend studies exist in different parts of the world, because of the variety of climate change impacts, search Funk et al. (2015), Ishida et al. (2017), Madsen et al. (2014), Şen (2012), in all these studies monotonic trends are identified and interpreted for the different study areas.

It is the main purpose of this chapter to identify trend features for a set of meteorological station precipitation records in North-East Algeria, the records are subjected to innovative trend analysis (ITA) methodology to identify partial rainfall trends, depending on "Low", "Medium" and "High" data classifications (Şen, 2012, Şen, 2017). Each record provides necessary information on pertinent precautions to take during dry and wet period events, as is necessary to mitigate against droughts and floods. Each class trend components are identified with relevant interpretations.

4.3 DEFINITION OF TREND ANALYSIS

A temporal trend is any systematic and continuous increase or decrease along time axis, which may be in the linear or nonlinear forms. Definitions of trend generally fall into two categories: to describe variation from a constant population over time and to describe the

numeric change in population over a specific time period. Trends are almost everywhere. There is a variety of trend definition depending on the purpose and circumstances. In general, it is a tendency in which some event develops as increasing (upward) or decreasing (downward) changes. Each trend has a general direction, which may also be expressed in terms of drift, shift, swing, course, current, leaning, tendency, and inclination and synonymously as bias and bend. The term trend may also have social context as modern model, fashion, mode, type, style, vogue, and rage. Some examples are increasing as warming trend, fashion trend, upwards economic trend, downward trade trend, quality trend, stock market trend, business trend, etc.

4.3.1 Goals of trend analysis

Some possible goals when analyzing a time series would be the following:

1. Detection of trend.
2. Estimation of the magnitude of trend.
3. Identification of time periods when change is the greatest.
4. Identification of time periods in which there was substantial trend and times in which there was negligible trend.
5. Prediction or forecasting of trend.

4.3.2 Conceptual and Visual Trends

In any scientific work, provided that the numerical data are available, the preliminary work is to try, visualize and explore the data behavior in graphical forms, which trigger the mind and creative thinking through the geometrical shapes. This is already reflected in saying that one picture is worth of thousand words. Especially, in the time series analysis, the temporal evolution of the phenomenon concerned can be grasped through the relevant graphs so as to see the random and systematic (trend, seasonality, sudden

jumps) behaviors. The graphical representation and its visual interpretation provide valuable qualitative (verbal, linguistically) information, which are the basic ingredients of original scientific developments prior to any quantitative evaluation. Qualitative information deduction from the temporal behavior of a time series depends on the grasp and intuitive ability of a person, and although a set of subjective information are derived, among them there are also objective supportive ones.

Without any specialization, if someone is asked, say, about the possible relationship between the rainfall and its consequent runoff event, then s/he responds that there is a direct relationship, which means that increase in the former variable implies increase in the other in the form of increasing trend. After the decision on the direct or inverse relationship, the next question is whether this relationship is in the linear or nonlinear form? Another alternative to these questions is that there might not be any relationship between the two variables. As a result of these two questions, there are six possible and simple alternatives, each one of which is the answer for dependent and independent variable, Y and time, t, and evolution in the form of two-variable relationship in any discipline with mathematical certainty as in Figure *4-1*.

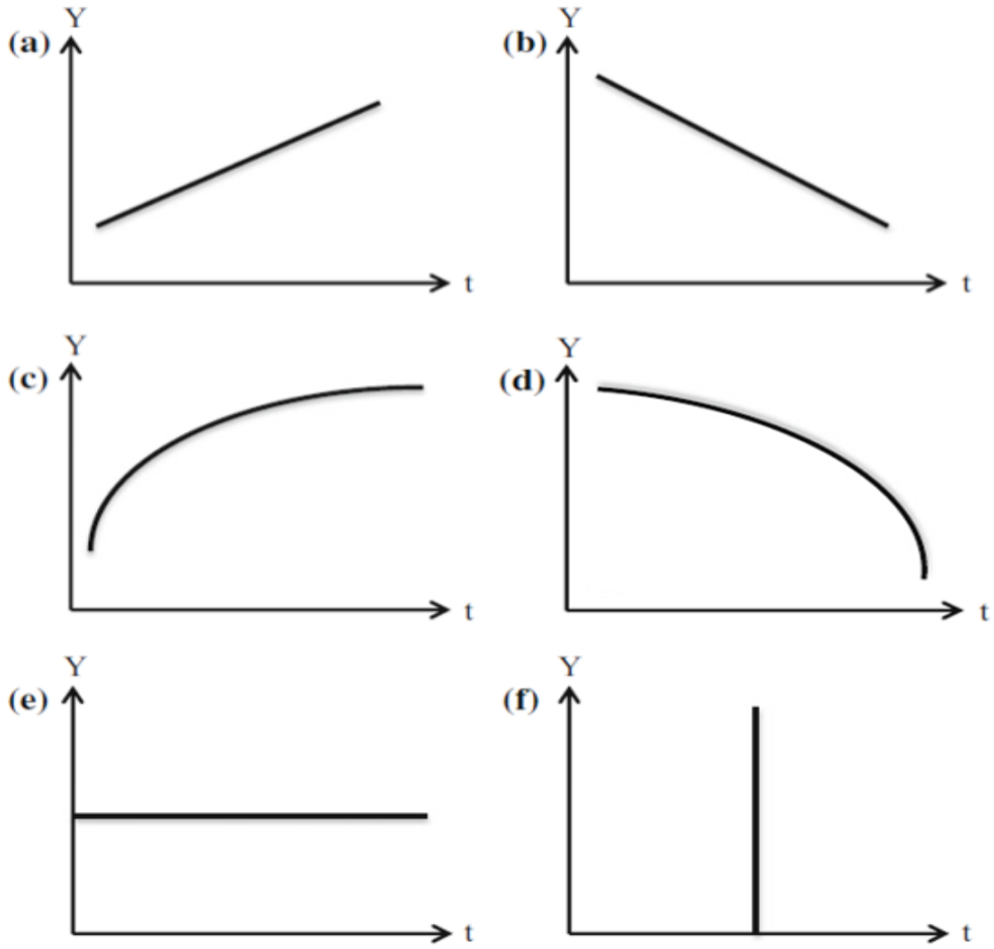

Figure 4-1: Proportionality and geometry relationship, a direct-linear, b inverse-linear, c direct-nonlinear, d inverse-non-linear, e no relation, f no relation

After the aforementioned conceptualizations and explanations, one can conclude that mentally, there are two questions; what are the proportionality relationships between two variables and what the shape (geometry) of the relationship is?

On the other hand, one can visualize temporal evolution of an event, provided that there are measurements, which help to fix the position, if the event performs on the event variable-time coordinate system. If there are no random errors in the measurements and the system is performing deterministically without any random component then the plot of the measurement data appears as a systematic scatter of

points along one of the graphs in Figure *4-1*. However, in case of random variabilities in addition to the systematic variations, the resulting scatter of points appears in one of the six alternatives as in Figure 4-2.

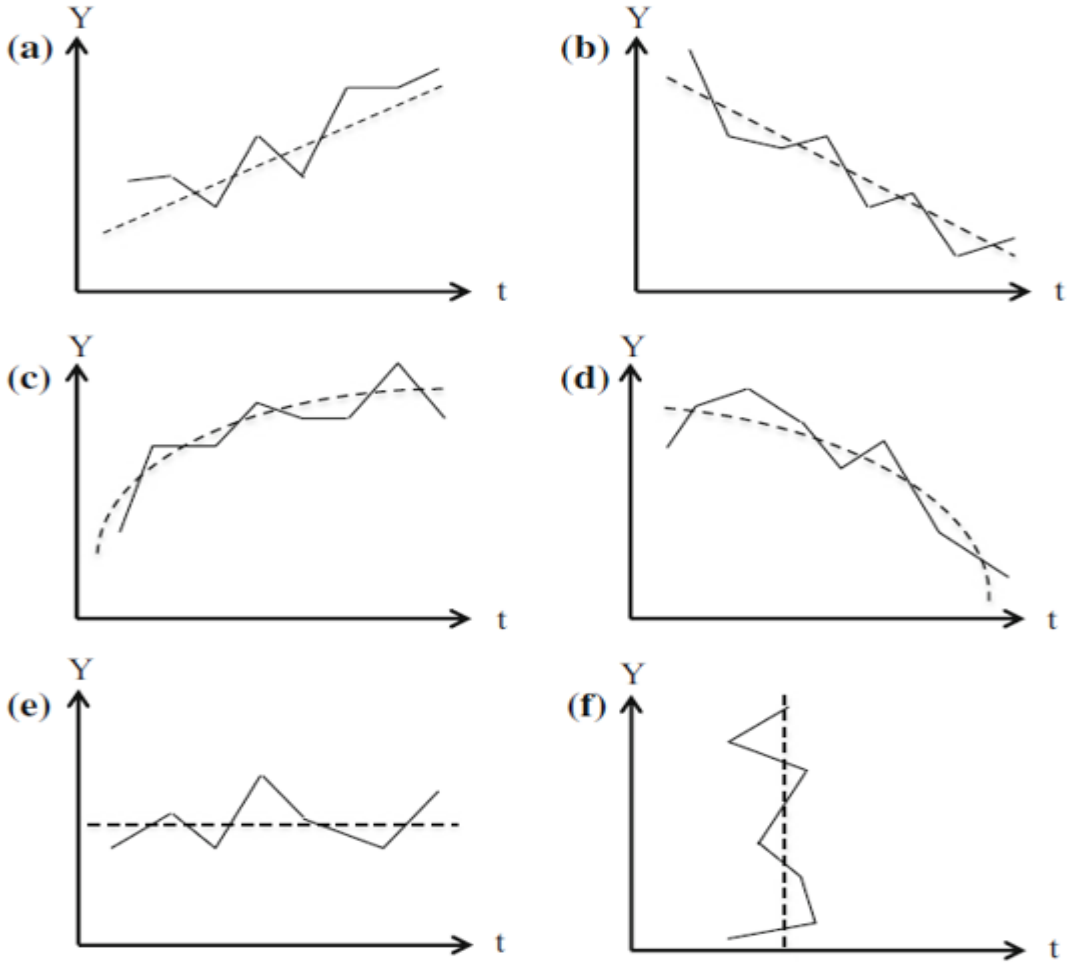

Figure 4-2: Different time series and trends, a linearly increasing, b linearly decreasing, c nonlinearly increasing, d nonlinearly decreasing, e no trend (independence), and f no trend

The trends in each one of these graphs are obvious and naked eye transforms visual information into mind and then appropriate qualitative interpretations can be deduced accordingly and they pave way toward probabilistic, statistical, stochastic or mathematical assessment. As for the measurements, whatever is the sensitivity, there are

always measurement errors or inherent structural randomness during the evolution of the event. Trends in these graphs are representatives of systematic variability and deviations from each trend are the random or stochastic component of the variable.

Conceptual and visual trend evaluations provide linguistic (verbal) and partially fuzzy knowledge and information, which are qualitative, but they are the fundamentals of subsequent mathematical and statistical trend deduction, identification, determination and quantitative assessments as well as interpretations that are the main topics in this chapter. It should be emphasized at this junction that expertise about an event can be gained through such basic human intuitional and visual conceptions prior to any mathematical and statistical data treatment (Şen, 2017).

4.3.3 Mathematical Trend

Conceptual and visual trend alternatives provide the geometrical (functional) relationships of different forms without symbolic (mathematical) expressions, which provide preliminary objective definition, identification and description of a trend. If digital data are available in the form of time series, then their treatment through scientific methodologies require first the establishment of mathematical foundations. For this purpose, simple mathematical functions must be kept in the library to study a time series for trend analysis. In practical applications, most often trend implies linear forms as increasing or decreasing tendencies. Hence, frequent trend searches are confined to Figure *4-1* a, b mathematically and Figure 4-2 a, b statistically. These have the simplest mathematical forms with two parameters a and b. For the linear trends in Figure *4-1*, the trend components are completely deterministic without random deviations, and therefore, the mathematical form is given as equation (4.1),

$$Y = a \pm bt \qquad \textbf{(4.1)}$$

where positive (negative) sign is for increasing (decreasing) trend. Equation (4.1) is the mathematical expression of Figure *4-1* a, b. The parameter values represent the intercept on the vertical axis and the slope of the line, respectively (see Figure 4-3). Equation (4.1) takes an uncertainty form by addition of an uncertain (random) element, u, with zero arithmetic average into the deterministic trend component as equation (4.2)

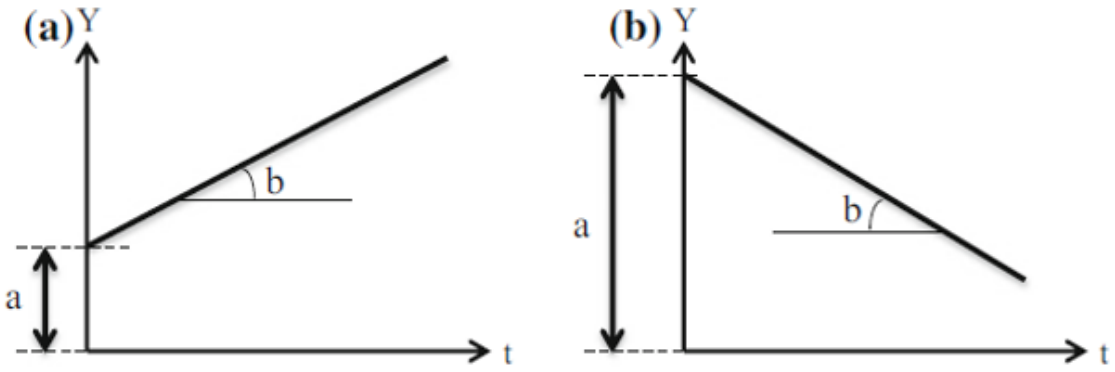

Figure 4-3: Linear trend parameters

$$\boldsymbol{Y = a \pm bt + u} \qquad \textbf{(4.2)}$$

This expression represents Figure 4-2 a, b, because of its linear structure.

In conceptual trend works, sometimes it is possible to judge the parameter values, although there is no measurement. For instance, if there is no currency in the credit card one cannot buy goods, but depending on the amount of credit the amount of shopping increases, and therefore, the parameter a is equal to zero. Another example is the relationship between the rainfall, R, and the surface water flow, F, over a land piece, where there is no surface flow prior to the rainfall.

Logically, one can conceptualize that the surface flow cannot be more than the rainfall, and hence, the slope parameter, b, value must be less than 1. In this example, the linear line also passes through the origin, and consequently, the trend line between the rainfall

and surface water flow passes through the origin (a = 0) with slope b < 1. However, precise determination of the slope value necessitates simultaneous rainfall and surface flow measurements.

As for the nonlinearity trends, mathematical functions may be in different forms including polynomial, exponential, power, logarithmic and other functions, but they are not frequently used in practice. The most widely used nonlinear trend description is in the form of second order polynomial function as equation (4.3),

$$Y = a \pm bt \pm ct^2 \qquad \textbf{(4.3)}$$

where c is an additional parameter that indicates the curvature of the nonlinear trend. It is the mathematical formulation of Figure *4-1*c, d. In case of uncertainty ingredient component existence, it can be rewritten as equation (4.4),

$$Y = a \pm bt \pm ct^2 + u \qquad \textbf{(4.4)}$$

This is the valid mathematical counterpart of Figure 4-2c, d. It is also possible to describe the trend components mathematically by differential equations. The first order differential expression represents linear trend and depending on its sign, it may be increasing (positive sign) or decreasing (negative sign) trend. However, the second order differential equation represents the nonlinear form again depending on the sign, where positive (negative) sign implies concave upward (downward) curvature. These alternatives are presented in Figure 4-4.

The first order differential term of Eq. (4.1) leads to the equation (4.5) that is in accordance with Figure 4-4a, b

$$\frac{dY}{dt} = \pm b \qquad (4.5)$$

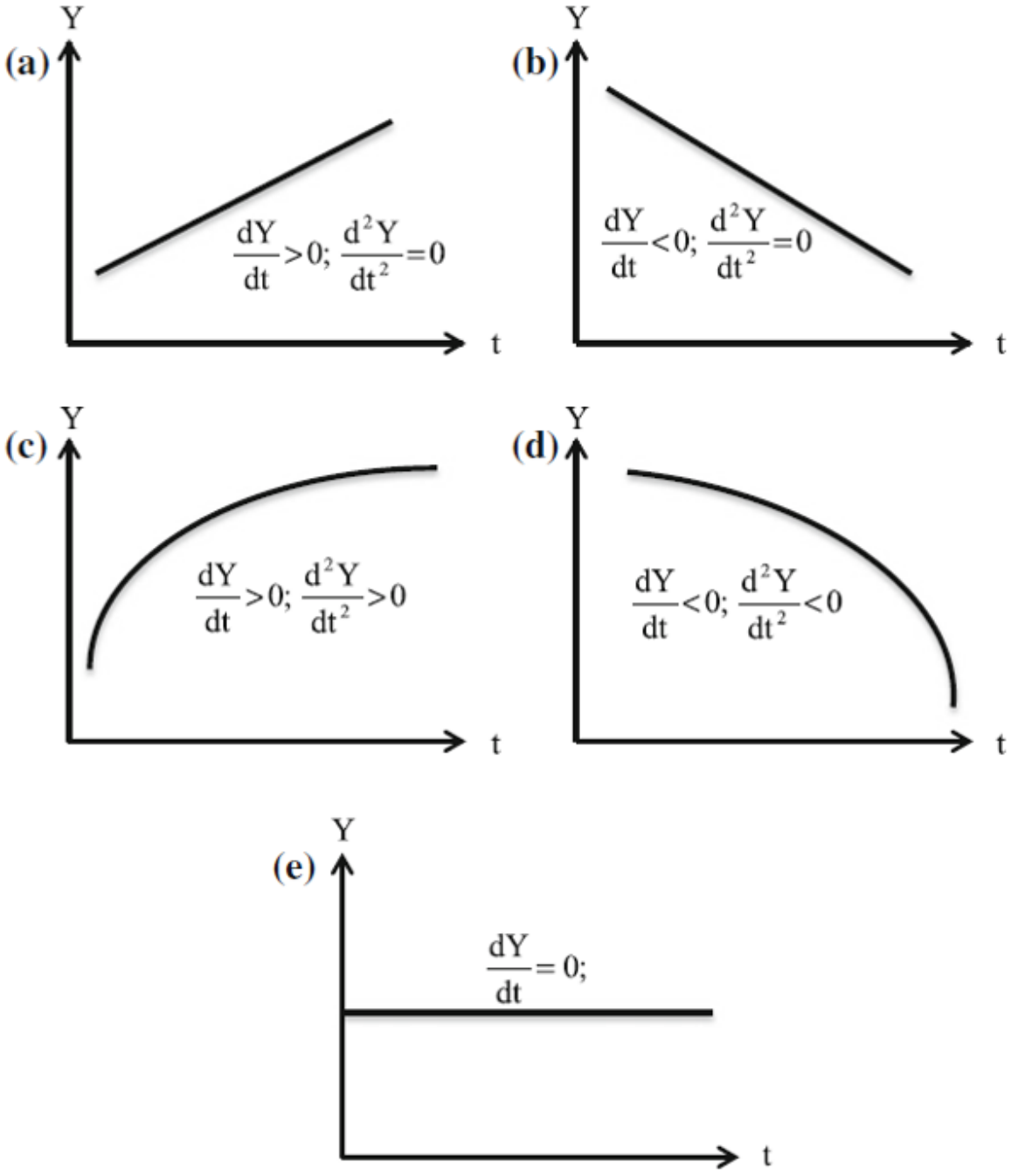

Figure 4-4:Partial differentials of trend

On the other hand, the first and second order differentials of Eq. (4.2) yield the following two differential equations (4.6) and (4.7).

$$\frac{dY}{dt} = \pm b \pm 2ct \qquad \textbf{(4.6)}$$

And

$$\frac{d^2Y}{dt} = \pm 2ct \qquad \textbf{(4.7)}$$

4.3.4 Statistical Trend

After the visual inspection of time series possible trend, sudden changes, outliers and random pattern around the trend component can be interpreted linguistically. Subsequently, data values can be converted to moving average value, which clarifies the background patters well because of smoothing. Finally, a regression model can be fitted to the final pattern.

In most contexts, trends are formed and interpreted from sets of data through probability, statistics and stochastic methodologies, which imply that there are random element embeds in the systematic deterministic components (trend, seasonality, step and shift-jump) in a time series. Natural and artificial time series measurements are not free of errors or inherent random components. In industrial machines, there are measurement errors but in natural, social and economic events additionally there are uncontrollable inherent random ingredients. As mentioned before, in section 4.3.2 time series in Figure 4-2 have random components, and therefore, deterministic equations cannot describe such time series completely. In order to represent them with trend component, an extra uncertainty component, u_i, is added to the mathematical expressions. The symbolic representation of a time series is Y1, Y2, …, Xn or Yi (i = 1, 2, …, n), where n is the number

of samples. For statistical expression of time series with a linear trend component, the mathematical formulation can be written in the most explicit form as equation (4.8),

$$\boldsymbol{Y_i = a \pm bt_i + u_i} \qquad \textbf{(4.8)}$$

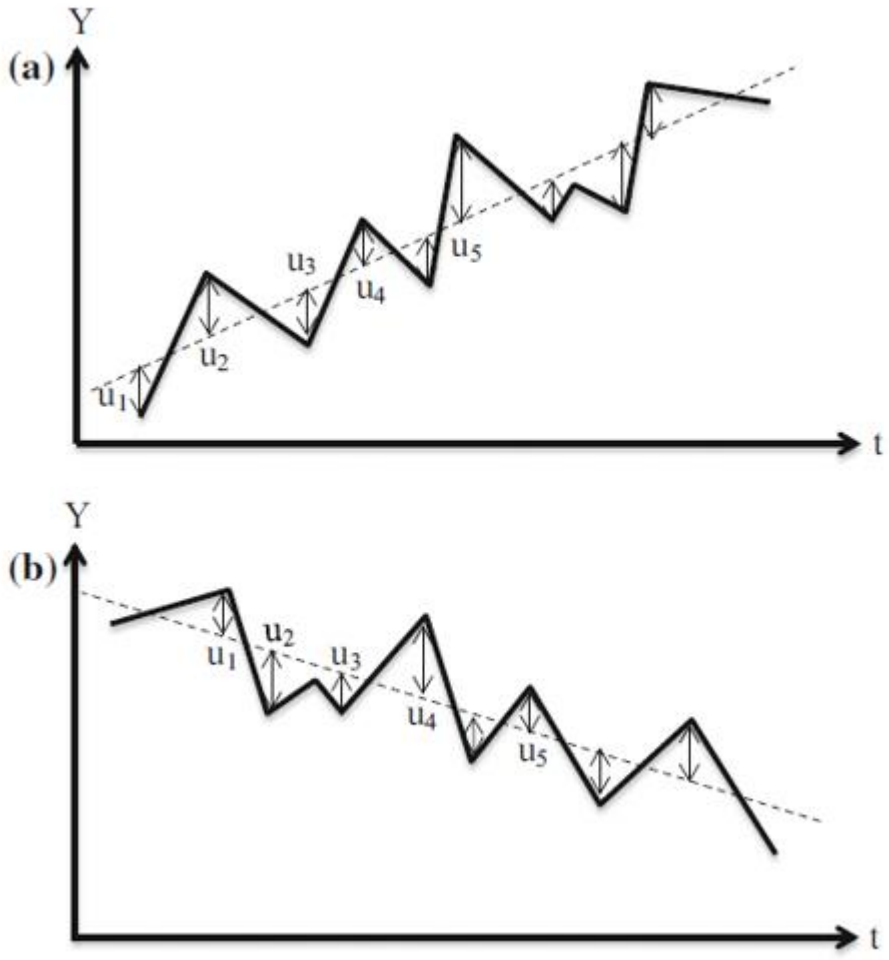

Figure 4-5: Uncertainty components a increasing trend, b decreasing trend

Figure 4-5 indicates the graphical representation of the time series with uncertainty terms that are represented by vertical deviations from the trend line. This figure indicates that the uncertainty components with respect to the trend line has + and – values. It brings to the mind logically as the first condition, for the best trend representation, the summation of the uncertainty terms must be equal to zero as the equation (4.9).

$$\sum_{i=i}^{n} u_i = 0 \qquad (4.9)$$

This is a necessary condition but not sufficient, because the + and – deviations may be far away from the trend line, but still their summation may appear as zero. In the case of complete determinism, satisfaction of this condition is possible only when each one of the uncertainty amounts is equal to zero, which is never the case in natural or artificial time series. Completely deterministic case can be represented by taking the absolute value of each uncertainty term and see whether their summation is equal to zero, see equation (4.10).

$$\sum_{i=1}^{n} |u_i| = 0 \qquad (4.10)$$

However, in practice there is never a completely deterministic case, but there are uncertainties, and therefore, the logic deducts that the summation of absolute errors must be as small as possible (minimum). In practical calculations, instead of the absolute value, the square of each term is adapted for calculation convenience and the second and most significant condition for trend identification is the equation (4.11).

$$\sum_{i=1}^{n} u_i^2 = \text{minimum} \qquad (4.11)$$

Equations (4.9) and (4.11) are the basic requirements in the classical statistical regression analysis, which is one of the trend identification techniques in the literature (Şen, 2012). Where:

Y, t = the coordinates of any point on the line.

b = the slope of the line.

a = is the y-intercept (where the line crosses the y-axis).

Y, t = the coordinates of any point on the line.

b = the slope of the line.

a = is the y-intercept (where the line crosses the y-axis).

u = random elemant.

c = constant.

4.4 PURPOSE OF THIS CHAPTER

During the last 50 years, time series analyses methodologies have been applied in a variety of fields including hydrology, meteorology, climatology, geology, oceanography, seismology, economics, health, space research, earth, marine and agricultural sciences, etc.

This chapter provides innovative methodology for the most effective ways of trend identification, determination, assessment and interpretation. Although there are numerous applications of the well-known time series and trend analyses in different domains, unfortunately a smaller number of studies is developed on innovative approaches/methodologies or even modification of existing approaches for trend analysis.

Hence, the main goal of this chapter, is to present up to date modernly developed innovative trend analyses of different types, which provide simple, effective, rational and logical linguistically interpretations and quantitative theoretical developments with almost no assumption. In the past, most researchers have employed the applications of the classical trend analyses without significant improvements except few modifications that could not avoid the drawbacks and assumptions.

In the applications, such trend analyses have been applied so frequently and consequently that other time series features (stationarity, homogeneity, periodicity and persistence) have been overlooked by depending on unchecked assumptions. It is hoped that in the future studies in addition to trend methodological developments, the basic features and assumptions are also taken into consideration. Future researches are expected to deal with the applications of time series analysis techniques in different disciplines toward more robust and widely acceptable interpretation and implementation possibilities. The most important and preliminary requirement is to have reliable measurement records for providing better and useful methodologies.

4.5 TREND IDENTIFICATION TESTS

There are various classically established trend identification tests in the literature and their preliminary explanations are useful for further and innovative trend proposal understandings. In general, these methodologies are divided into two groups as parametric and non-parametric approaches.

Statistics can be categorized into parametric and non-parametric statistics. The selection of statistical tests purely depends on the hypothesis needs to be proved, if there is no hypothesis there is no need of statistical tests. All statistical tests are derived based on some assumptions about the data. We are all conducting research with an aim of a goal that is to discover some truth about the population and what is the effect of an intervention on that population. It is usually impossible to collect data from all individuals of interest in a population, so our only solution is to collect data from the subset of population that is called the sample.

From this sample we can find some quantities of population that is (mean, standard deviation, …etc) or we can say some proportions on the base of some attributes, these are all very important in case of a population as general. So, these quantities are called “parameters”, so the parameters about the population is derived from the population for

finding the parameters of population. All these parameters are just an estimation, so using sample we are estimating the parameters about the population. Find parameters from the sample is called statistic “Statistic estimates parameters”.

Parametric statistical procedures assume that the sample distributions are about the same shape and has the same parameters as the general population distribution.
A parameter is the characteristic of the population or aspect of the population, parametric assumes data is normally distributed.

If the information about the population from which the sample has been drawn is completely known through its parameters, then the test is called parametric test. Non-parametric means no assumption about the population, they are also called distribution free-tests. Non-parametric are not based on the parameters of normal curve, that means the distribution is skewed (Şen, 2017).

4.5.1 Assumption of parametric test.

Usually, parametric tests are known to be associated with strict assumption about the underlying population distribution, but one thing is very important that different parametric tests have different assumptions.

4.5.2 Common assumption of parametric tests

4.5.2.1 Normality:

Most of parametric test require the data roughly fits a bell curve sample. To test the assumption of normality we can use Kolmogorov–Smirnov test, D'Agostino's K-squared test …etc

4.5.2.2 Homogeneity of variances:

Mean data from multiple groups have the same variance, that is the population variance of two or more samples are considered equal, for testing the homogeneity of variance one can use Levene’s test.

4.5.2.3 Interval or ratio level measurement:

In a parametric test the data should be in the interval or ratio scale, but in the case of non-parametric test the data may be in nominal or ordinal scale, that means you can apply quantitative data in parametric test and apply qualitative data in non- parametric test, nominal and ordinal scale data normally considered as qualitative data for example gender, department, religion, demographic region …etc, for resuming, parametric tests are for quantitative data and non-parametric tests for qualitative data.

4.5.2.4 Independence

Data point values for variables for different groups should be independent of each other.

4.5.2.5 Nature of analysis

If the aim is to compare the parameters of the data that is mean or standard deviation than the application of parametric test is preferred, however, if it is for comparing proportions or percentages derived from nominal or ranked data then non-parametric test is more suitable.

4.5.3 Innovative Trend Significance Test

Time series might embed characteristics of past changes concerning climate variability in terms of shifts, cyclic fluctuations, and more significantly in the form of trends. Identification of such features from the available records is one of the prime tasks of hydrologists, climatologists, applied statisticians, or experts in related topics. Although there are different trend identification and significance tests in the literature, they require restrictive assumptions, which may not be existent in the structure of time series. In this chapter, a method is suggested with statistical significance test for trend identification in an innovative manner. This method has nonparametric basis without any restrictive assumption and its application is rather simple with the concept of subseries comparisons that are extracted from the main time series. The method provides privilege for selection of sub-temporal half periods for the comparison, and finally, generates trend on objective and quantitative manners (Şen, 2012).

4.6 AN OVERVIEW OF THE ITA METHODOLOGY

Professor Zekai Şen the one who developed this method replied on the question about how he thought of the idea of the ITA:
When he was a child, he used to be a grazer, the winter was very cold with a lot of rain and snow, after 40 years when he returned back to his home town, he noticed that there is less rain and snow than it used to be, he decided to compare the precipitation behavior of the old time with the current time, so he took the two time series and plot them against each other, the resulting graph was unclear and hard to read, so he decided to rearrange the two time series from lower to higher, in that way he can compare each category separately, low values of old series with low values of recent series …etc, and yet his idea came to the light and decided to go farther in this study.

4.6.1 Brief explanation of the basics of the ITA method

A trendless time series: it is a time series that shows the same behavior along the time series, mathematically if we divide this time series into two halves and plot them against each other, the resulting scatter point should fall on the 45°straight line.

Example 1:

4.6.1.1 Case of trendless time series

Let us consider time series perfectly trendless like Table *4-1*.

Table 4-1: Trendless time series

Months	Old time series (Example: precipitation mm)	Sorted Old time series (lower to higher)	Recent time series (Example: precipitation mm)	Sorted Recent time series (lower to higher)
Sep	100	30	100	30
Oct	150	40	150	40
Nov	200	50	200	50
Dec	250	80	250	80
Jan	300	100	300	100
Feb	270	110	270	110
Mar	180	150	180	150
Apr	110	180	110	180
May	80	200	80	200
Jun	50	250	50	250
Jul	40	270	40	270
Aug	30	300	30	300

If we plot the two halves against each other we get the graph shown in Figure 4-6:

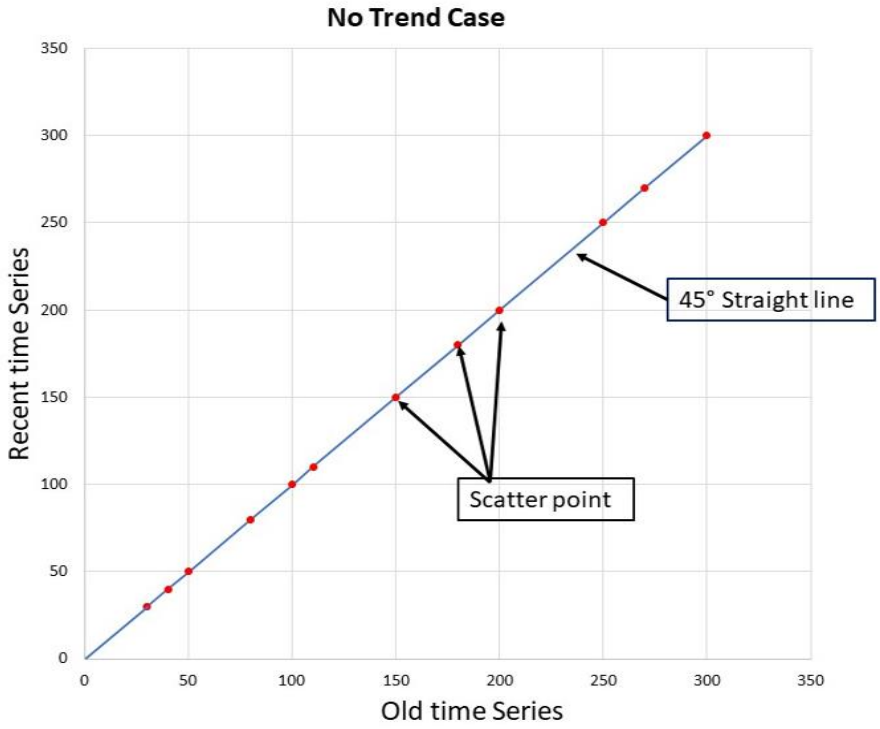

Figure 4-6: No trend plot

Since the time series has the same behavior all along the time, so the old years would have the same values as the recent years, and their plot against each other would be in the middle following the 45°straight line, see Figure 4-6.

From here came the idea of ITA, where the professor Zekai Sen suggests to dividing the time series into two halves, then plotting them against each other where the old half will be the X-axis and the recent will be Y-axis

4.6.1.2 Case of decreasing trend

Let's make some changes to our time series, the first half remain the same but the second half takes lower values than the first, in other word the recent half decreases, like presented in Table *4-2*.

Note: each half should be sorted from lower to higher before plotting.

Table 4-2: Decreasing time series

Months	Old time series (Example: precipitation mm)	Sorted Old Half (Lower to higher)	Recent time series (Example: precipitation mm)	Sorted Recent Half (lower to higher)
Sep	100	30	40	12
Oct	150	40	75	19
Nov	200	50	80	20
Dec	250	80	110	30
Jan	300	100	160	40
Feb	270	110	150	58
Mar	180	150	90	75
Apr	110	180	58	80
May	80	200	30	90
Jun	50	250	20	110
Jul	40	270	19	150
Aug	30	300	12	160

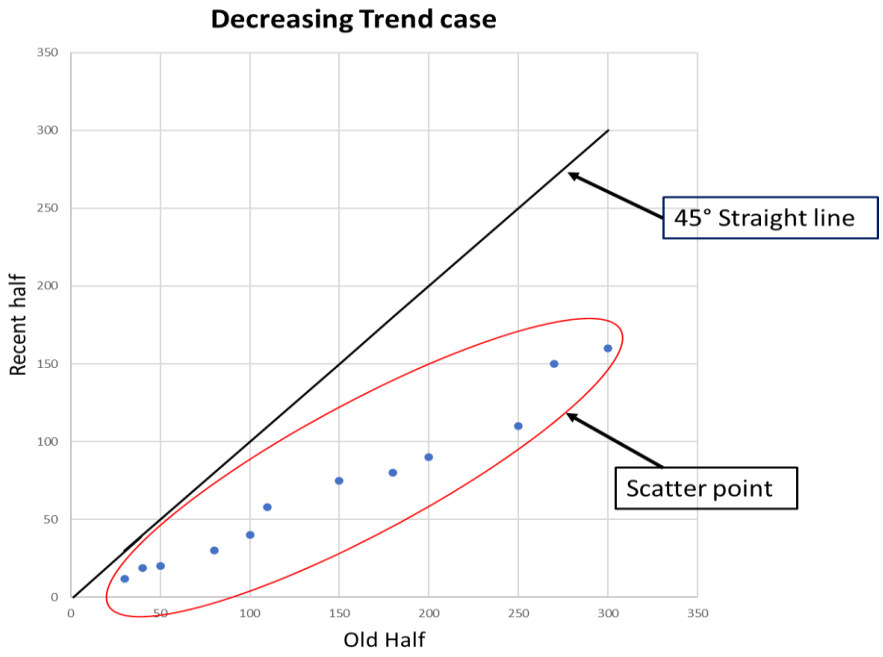

Figure 4-7: Decreasing time series plot

The Figure 4-7 is the plot of Table *4-2*, it shows that the scatter point moves toward beneath the 45°straight line, the more the value increases the more distance from the trendless zone get wider.

4.6.1.3 Case of Increasing trend

This time the first half remain the same, however, the second half will take higher values instead of lowers, as in the Table *4-3* :

Table 4-3: Increasing time series

Month	Old half (Example: precipitation mm)	Sorted Old Half (Lower to higher)	Resent half (Example: precipitation mm)	Sorted Second Half (Lower to higher)
Sep	100	30	145	50
Oct	150	40	220	90
Nov	200	50	270	110
Dec	250	80	310	145
Jan	300	100	340	160
Feb	270	110	300	200
Mar	180	150	260	220
Apr	110	180	200	260
May	80	200	160	270
Jun	50	250	110	300
Jul	40	270	90	310
Aug	30	300	50	340

The plot of the Table *4-3* give the Figure 4-8.

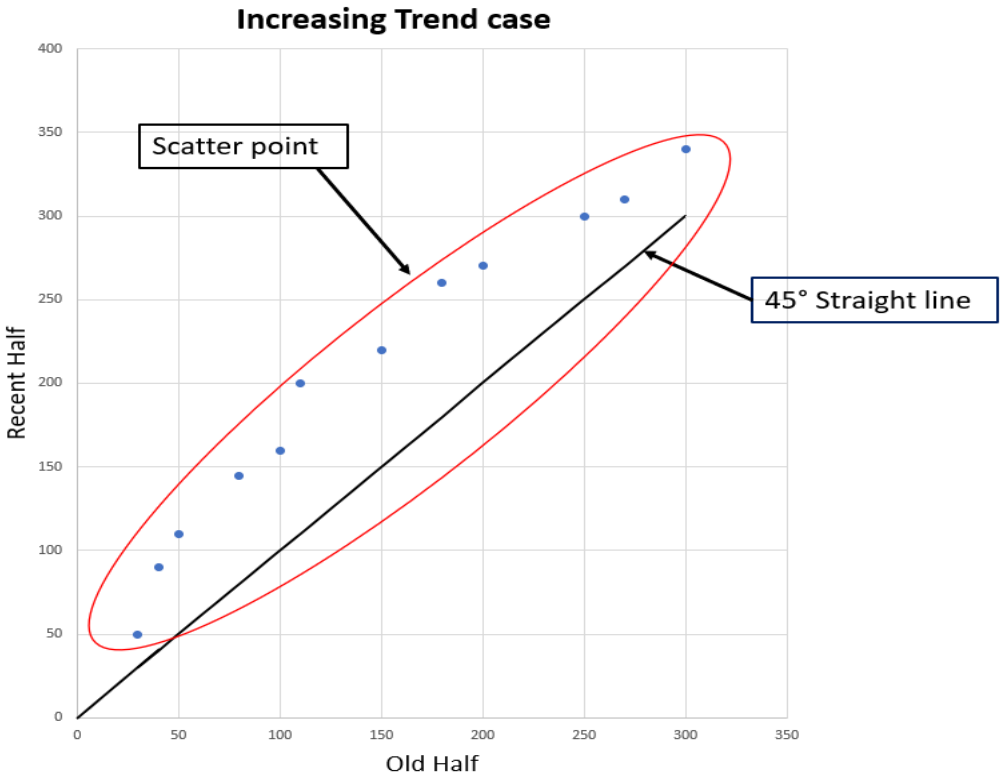

Figure 4-8: Increasing time series plot

Here in Figure 4-8, the scatter point moves towards the upper triangle above the 45°straight line, also, the more the values deviate from each other the more the scatter point diverge from the trendless zone.

4.7 INNOVATIVE TREND IDENTIFICATION METHODOLOGY

There are commonly used trend identification techniques such as Mann–Kendall (MK) and Spearman's Rho (SR) tests, but their validity is possible under a set of restrictive assumptions such as independent structure of the time series, normality of the distribution and length of data. It is also not possible to calculate trend magnitude (slope) except through regression approach, which brings additional assumptions for the theoretical validation in practical applications.

Recent hydrologic regime changes due to potential climate variability impacts brought into focus the search for effective trend identification analysis. Numerous works in different parts of the world showed quasi-periodic natural behavior and systematic trends of key climate variables due to climate change and/or climate variability. It is well known that changing climate is expected to have notable impacts on the rainfall–runoff processes due to increasing or decreasing trends in hydro-meteorological time series (floods, droughts, heat waves, etc.).

These impacts can no longer be assumed to be stationary, which means that future replicates are no more statistically indistinguishable from the historical counterparts. If climate change is not taken into account, then such changes or variability can lead to underestimation/overestimation of parameters for the design and operation of water infrastructures, water shortages, water stresses, and agricultural failures. Although some test procedures are presented for trend identification, there are restrictive assumptions with respect to serial structure (ignorance of correlation coefficient), normal probability distribution function (PDF) of the variables and rather lengthy datasets.

In the past, time series were often assumed as stationary or weakly stationary stochastic processes for simulation purposes. Due to anthropogenic (human disturbance) effects on climate, environment, drainage basin and atmosphere, such an assumption is not valid anymore.

This chapter presents preliminary results and applications of an effective and potential innovative trend identification methodology that do not require many of the restrictive assumptions. This method is concerned with the plot of a set of subseries from the original time series on a cartesian coordinate system, where 45° straight-line implies no trend but any plot appearance above (below) this line implies increasing (decreasing) trends. The same methodology is capable to provide trend magnitude (slope) calculation.

Many time series records have serial dependence, and therefore, it is very helpful to provide a methodology, which is not affected by such restriction. In order to avoid such restrictive assumption innovative trend analysis (ITA) methodology Şen (2012) is used in this chapter. Herein, partial form of ITA is considered for finer application studies within the three categories of "Low", "Medium", and "High" data values trend classifications.

In the ITA methodology upper and lower triangular areas correspond to trend existence as in Figure 4-9, where sorted half time series are plotted against each other. In the Figure 4-9, 1:1 (45°) straight-line implies trendless case. Along the main diagonal the area between the boundaries at ±5% is for no trend domain. The scatter points that fall within this area do not contribute to trend, and therefore is referred to as a "no trend area". This area appears around the main diagonal with slope equal to 1:1 (45°). The upper (lower) triangular area implies increasing (decreasing) trend existence. Additionally, on the same figure the scatter points can be grouped into "low", "medium" and "high" classes (Şen, 2017; Boudiaf et al., 2021).

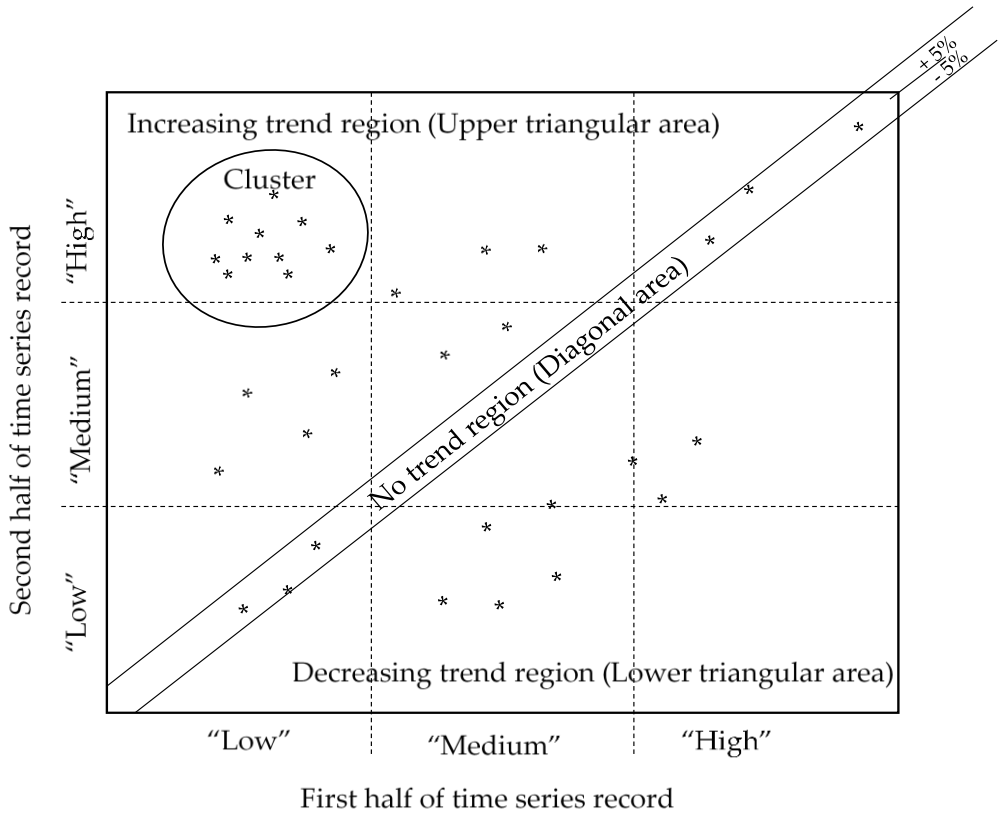

Figure 4-9: ITA template

The scatter points on this template come about after partition of the time series into two halves and then sorting each half in ascending order, and then plotting, first (early) part versus second (late) part. As explained in the ITA template, there are three areas for trend identifications. Such templates, as the ITA, provide the following important interpretation prior to any quantitative analysis.

1) Visual trend inspections under the light of above explanations.
2) Identification of "Low", "Medium" and "High" data group trend behaviors.
3) Comparison of groups with each other for further interpretations.
4) Identification of dry or drought cases from the "Low" data group and whether there is an increase or decrease in small data records.
5) Similarly, identification of wet and even flood possibility from the "High" data group trend.

6) Apart from the existing trends one may also identify clusters without any trend as shown at the upper left-hand side in figure 4-9.
7) "Medium" trend data values are important for water resources management studies.

Figure 4-10 provides explanations about different alternatives that may appear on the ITA template. In this figure rather than a group of points, two points are considered as representative of any data group with trend.

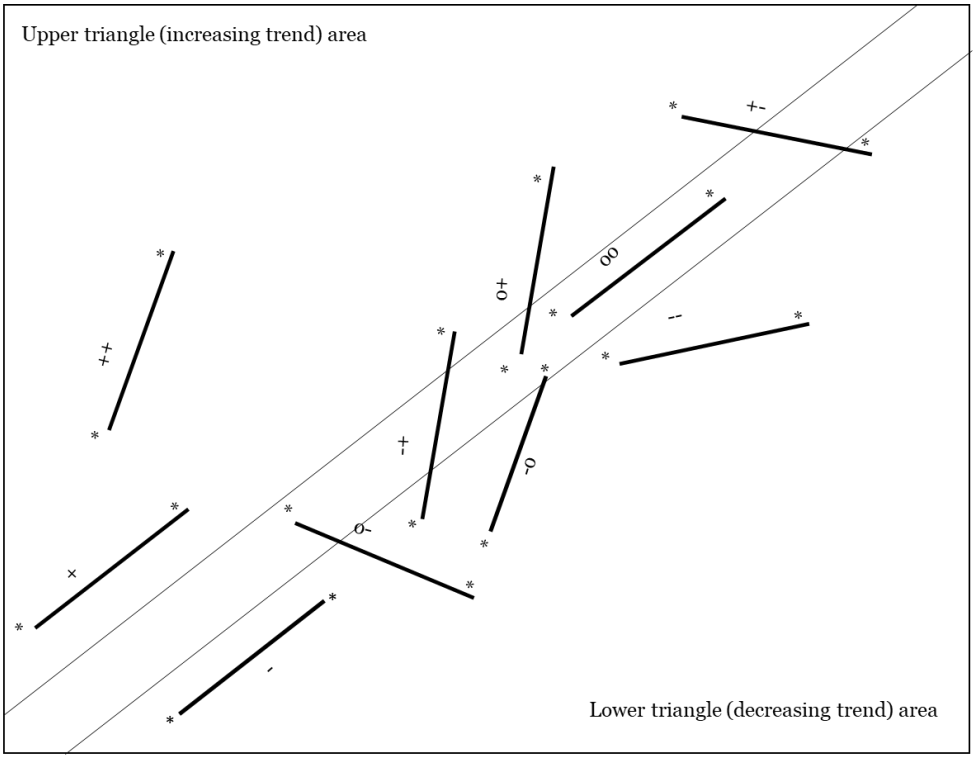

Figure 4-10: Trend Possibilities

1) **+:** implies always an increasing trend in the upper triangular area, which may not be very far away from 1:1 line;
2) ++: implies increasing trend similar to the previous step, but far away from the no trend line;

3) **+-**: implies initially increasing (upper triangular area) then onwards decreasing (lower triangular area);
4) **-**: implies always a decreasing trend in the lower triangular area, which is not very far away from the no trend area;
5) **-+**: implies initially decreasing (lower triangular area) then onwards increasing (upper triangular area);
6) **oo**: implies existing only always without trend;
7) **o+**: implies initially no-trend, but onwards with increasing trend (upper triangular area);
8) **–o**: implies initially decreasing trend starting from the lower triangular area then onwards without trend area;
9) **o-**: implies initially no trend then moving toward decreasing trend (from no trend zone to the lower triangular;
10) **--**: implies decreasing trend far away from the no trend line implying more significance.

4.8 APPLICATION

MATLAB software used to generate the appropriate results and the program is demonstrated in the appendix, see section 8.2.1.

4.9 RESULTS AND DISCUSSION

The ITA methodology is applied for each rainfall record series in the study area. 16 graphs have been obtained as a result, the elaboration of each single graph would be so long and it may be confusing, based on this, three different “in terms of scatter point distribution” obtained graphs Figure 4-11, Figure 4-12 and Figure 4-13 will be discussed in details and should shed light on the subsequent explanations.

The three chosen graphs are:

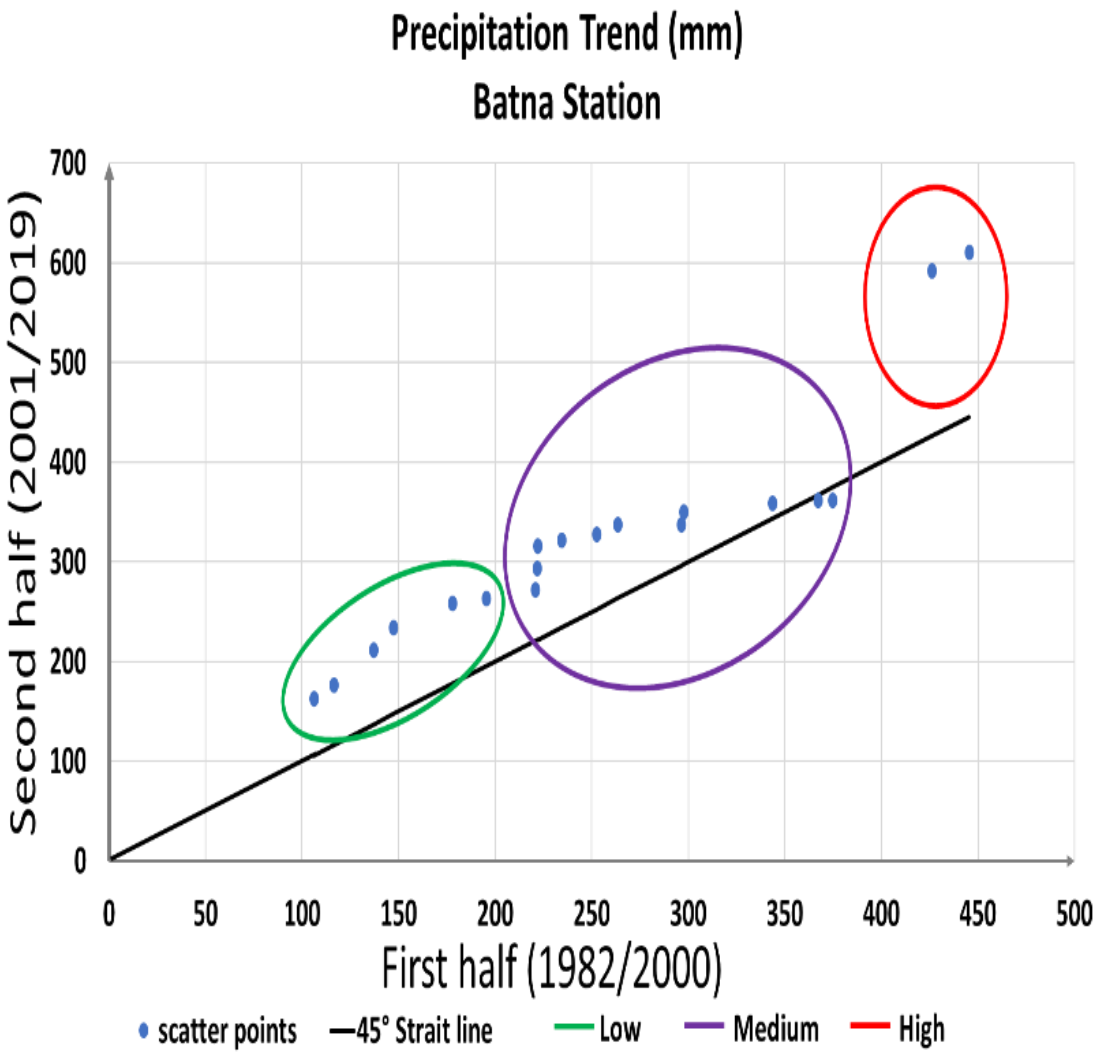

Figure 4-11: Batna station precipitation trend

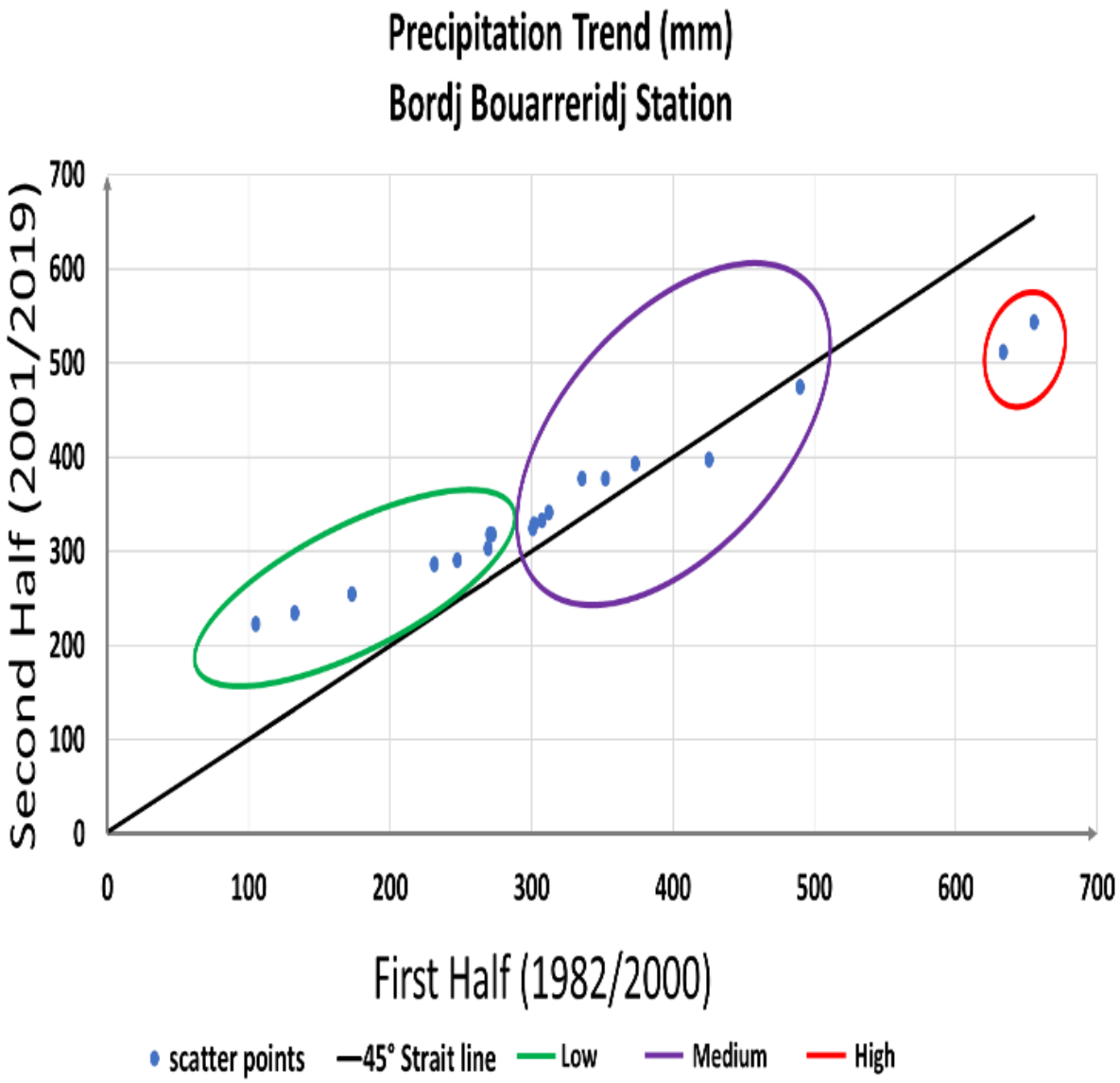

Figure 4-12: Bordj-Bouarreridj station precipitation trend

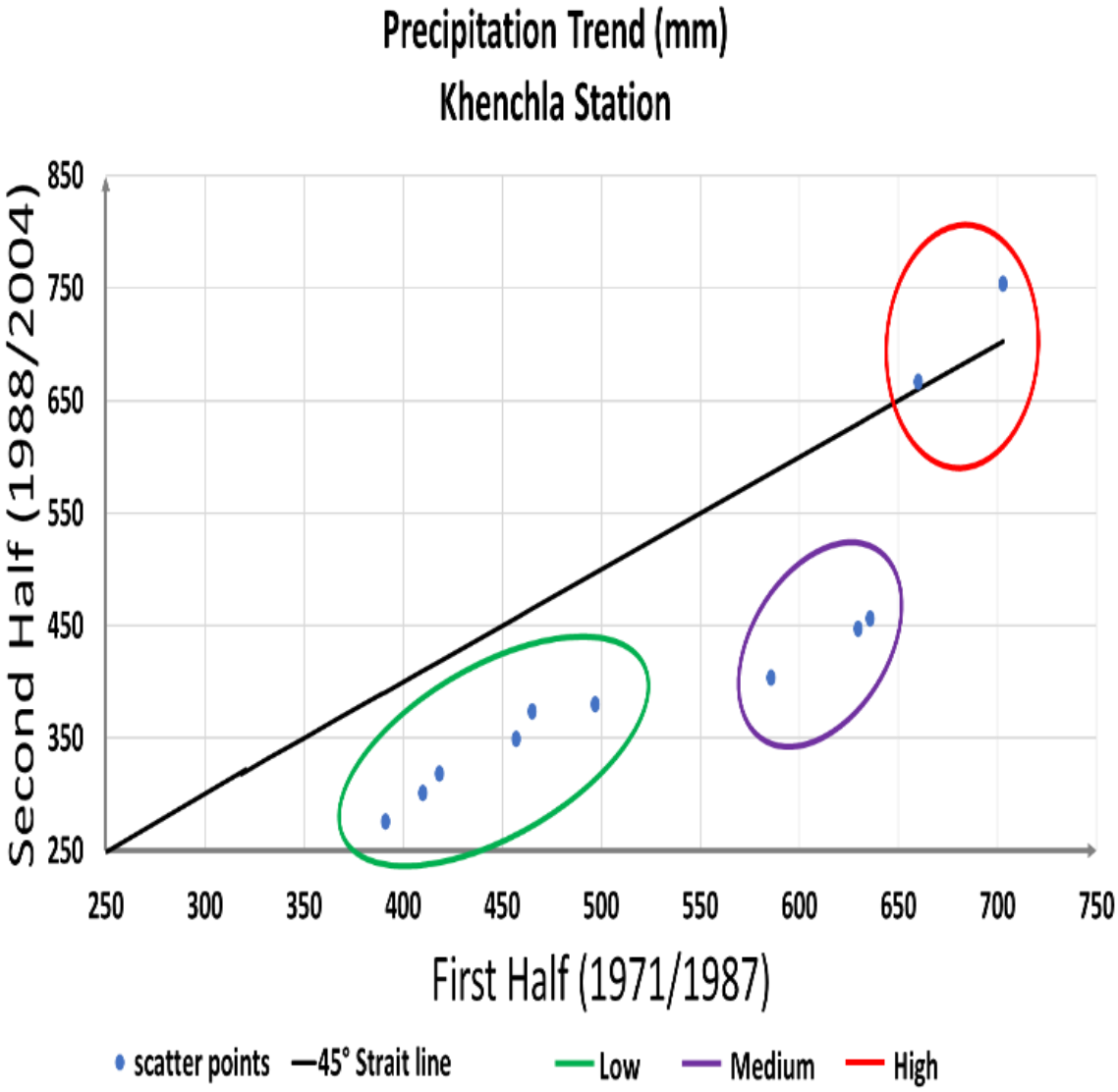

Figure 4-13: Khenchla station precipitation trend

Each graph will be classified into three groups, “Low” for lower rainfall amounts, “Medium” for the medium and “High” for the extremes.

Later, via the layout of the scatter point, the trend for each category will be determined. If it is located above the line the trend would be considered as increasing. although, if it is below, the trend is decreasing, while the area very close to the line is categorized as the no-trend zone.

- **Batna**

Low: represents 32 % of the entire data series, the scatter point is located above the line indicating an increasing trend.

Medium: represents 58% of the whole data series, the onset is above the line then it gradually approaches closer to it, revealing an increasing trend toward no trend.

High: it represents 10% of the data, the scatter point here is well above the line indicating an increasing trend.

Overall, the trend at the Batna station is increasing, indicating that the region is safe from dry spells and drought impacts, however there is still the possibility of floods occurring.

- **Bordj-Bouarreridj:**

Low: represents 42 % of the entire data series, the scatter point is located above the line indicating an increasing trend.

Medium: represents 47% of the entire data series, the layout spreading along the no-trend zone.

High: represents 11% of the entire data series, the points being located below the line revealing a decreasing trend.

Overall, Bordj station is receiving more rainfall in the range between 100 and 300 mm and it tends to be more frequent, while rainfall amounts in the range between 300

and 500 mm remain regular, in contrast the days with extreme rainfall tend to decrease which put Bordj station in the safe zone relative to the frequency of floods.

- **Khenchla**:

Low: represents 55 % of the entire data series, the scatter point is located below the line indicating a decreasing trend.

Medium: represents 27% of the entire data series, the layout situated well below the line indicating a decreasing trend.

High: represents 18% of the whole data series, the points onset is in the no-trend zone then approaching the increasing trend area.

Overall, there is a decreasing trend in Khanchla's rainfall with the probability of extreme rainfall occurring.

The obtained figures from the application of the ITA methodology to the remaining rainfall time series records will be added as an appendix, see section 8.2.2, where their interpretation will be summarized in Table 4-4. According to the aforementioned signs in columns 2-4 and in the last three columns the percentages are given for data scatter points that fall within the "Low", "Medium" and "High" sub areas in the ITA template.

Table 4-4: Partial groups of data trend types and percentages

Station name	Trend types			Trend percentage		
	"Low"	"Medium"	"High"	"Low"	"Medium"	"High"
El Taref	+	-+	++	12	38	50
Annaba	+0	0	0-	21	58	21
Skikda	0	0+	0+	11	42	47
Jijel	++	++	++	11	42	47
Bejaia	+	+0	++	26	53	21
Souk Ahras	+	0+	0+	25	44	31
Guelma	0	+-	-	25	62	13
Constantine	0	0+	--	42	47	11
Setif	+-	0	+	16	74	10
Bordj Bouarreridj	+0	0	-	42	47	11
Oum Bouaghi	+0	0+	+	9	73	18
Tebessa	0	0+	0+	26	48	26
Khenchla	-	-	0+	55	27	18
Batna	+	+0	+	32	58	10
M'Sila	+	0	-	9	73	18
Mila	++	+	++	50	33	17
Arithmetic average				24	52	24
Standard deviation				14	14	14

For the study area, the following useful interpretations can be deduced from table 4-4 by consideration of the signs and percentages.

A: "Low" data values group

1) In the "Low" group of trends, there is only Khenchla station where there is a continuous decrease (-) in the low data points, and therefore, this station can be considered as a potential location for dry spell and drought effectiveness in the future.
2) Setif station has a decreasing trend (+-) with significant reduction in the low data values.
3) In five stations (El Taref, Bejaia, Souk Ahras, Batna, and M'Sila) increasing trends (+) are present, which implies an increase in the low data values. This further implies these five regions are safe against dry spells and drought impacts.
4) Four of the stations (Skikda, Guelma, Constantine and Tebessa) are without trend (o) component and they all have more or less similar positions within the no trend band.
5) Jijel and Mila stations have extremely significant trends (++) in an increasing manner, where there is no expectation for drought events.

Overall, the stations have no-trend or increasing trend over the study area where the "Low" rainfall occurrences exist.

B: "Medium" data values group

1) Khenchla station has continuous decrease (-) in the "Medium" rainfall records. This point supports the interpretation in the "Low" data group that there is drought expectation in the future.
2) In the Guelma station there is a decreasing trend (+-) that starts from the increasing trend area on the ITA template, but ends in the decreasing area, hence there is a continuous decrease in the "Medium" rainfall value groups.

3) The opposite situation (-+) is valid in El Taref station, where the trend increase is from the decreasing area towards the increasing area on the ITA template.
4) The trendless (o) cases exist in four stations, namely, Annaba, Bejaia, Setif and Bordi Bouarreridj).
5) The case of increasing trend starting from the no trend area (o+) occurs at stations Skikda, Souk Ahras, Constantine, Oum Bouaghi and Tebessa stations.
6) Just the opposite (+o) case appears at Batna station, where decreasing trend ends up inside the no trend area.
7) Mila station show continuous increase (+).

The overall trend picture at the study area rainfall stations reflects either stable (no trend) or increasing trend in the "Medium" data value range.

C: "High" data values group

1) In the "High" data group, there are three cases with continuous trend decrease (-) Guelma, Bordj Bouarreridj and M'Sila stations;
2) Rather mild trend increments (+) appear at stations Setif and Oum Bouaghi, which imply the possibility of some floods at these locations;
3) Extremely high rainfall trends (++) are dominant at El Taref , Mila, Jijel and Bejaia stations;
4) Constantine station "High" rainfall amounts are in continuously decreasing trend with no flood danger.
5) No trend area origin trend increases (o+) are available at stations, Skikda, Souk Ahras, Tebessa and Khenchla, which also support the idea of flood;
6) At Annaba station the trend starts in the no trend area (o-) and continue towards the decreasing trend area (lower triangular area).

The overall interpretation for this “High” rainfall amounts group is that there are flood occurrence possibilities at many stations.

In the last three columns in Table *4-4*, data percentages in each group are given for further analysis on the basis of frequencies. In the “Low” class the three stations whose data appear most frequently are in order: Khenchla, Mila, Bordj Bouarreridj , Constantine and Batna. In the “Medium” class: Setif, M’Sila, Oum Bouaghi and Guelma stations. In the “High” group, top ranking percentages are at: El Taref; Skikda and Jijel stations. The arithmetic averages of the percentages show the most frequent data values are confined within the “Medium” group in equal percentages for the “Low” and “High” classes. The standard deviation percentages are equal to each other in each class. These points lead to the understanding, for the study area being considered, that “Medium” rainfall amounts are the key group for water resources management studies.

In light of everything discussed above, it is determined there are rainfall increments recorded at many stations, especially at stations within “Medium” and “High” data groups. Apparently, after all trend analyses and interpretations, it becomes obvious that about 63 % of the study area is bound to become wetter in the near future as shown in Figure 4-14.

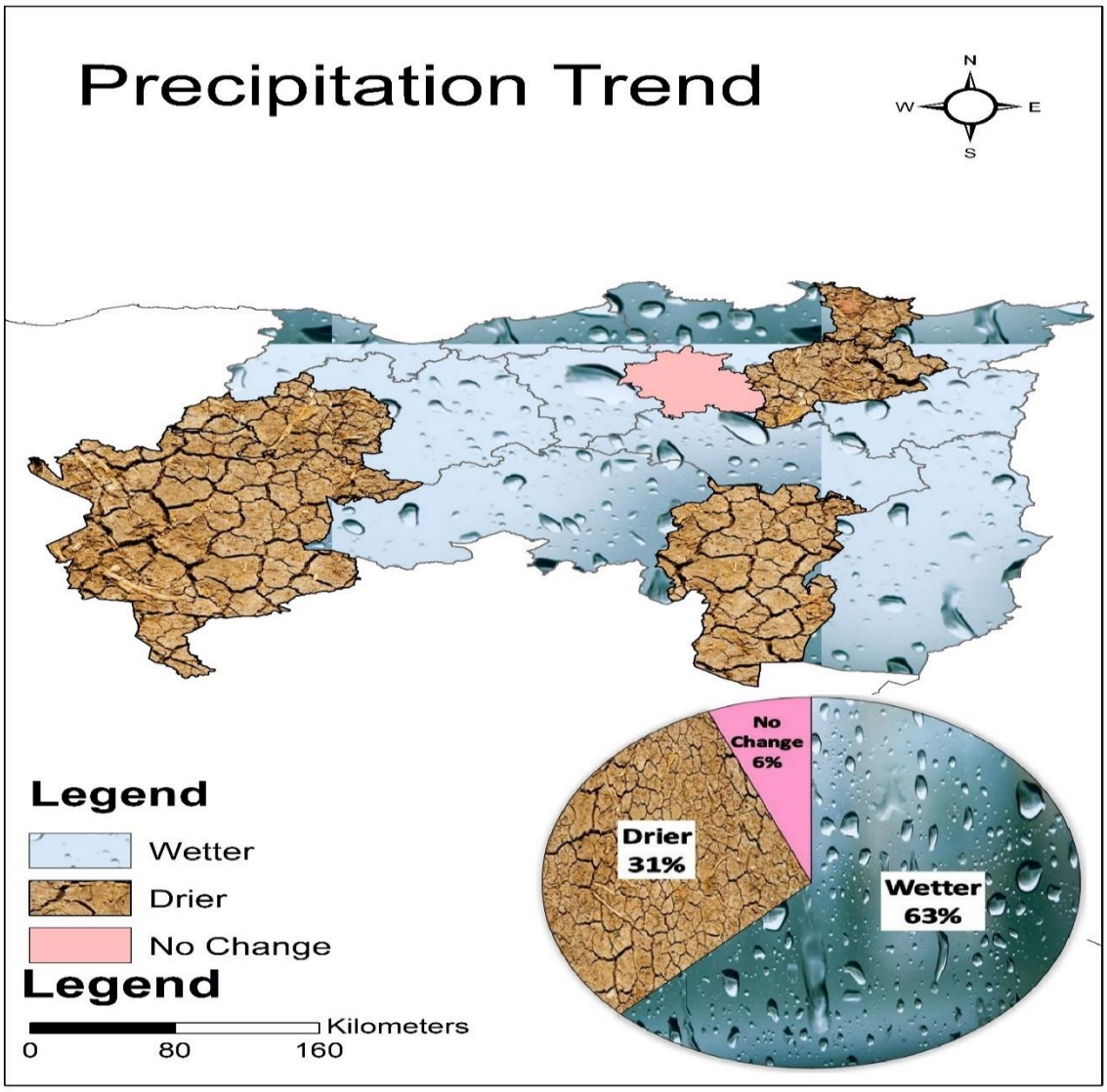

Figure 4-14: Precipitation spatial designation according to the obtained results

It is also obvious from this figure that the drier precipitation stations share only 31% of the cases, whereas Constantine meteorology station precipitation performance shows no change during the time series, which implies that at this location there is no significant impact of climate change on precipitation amounts, and hence, the same is expected in the future.

Finally, the map in Figure 4-15 indicates the sub-regions of trend tendencies over the study region. It is obvious from the pie diagram that although 62% of the area is subject to trend increase, only 25% of it is covered by the locations of decreasing trend.

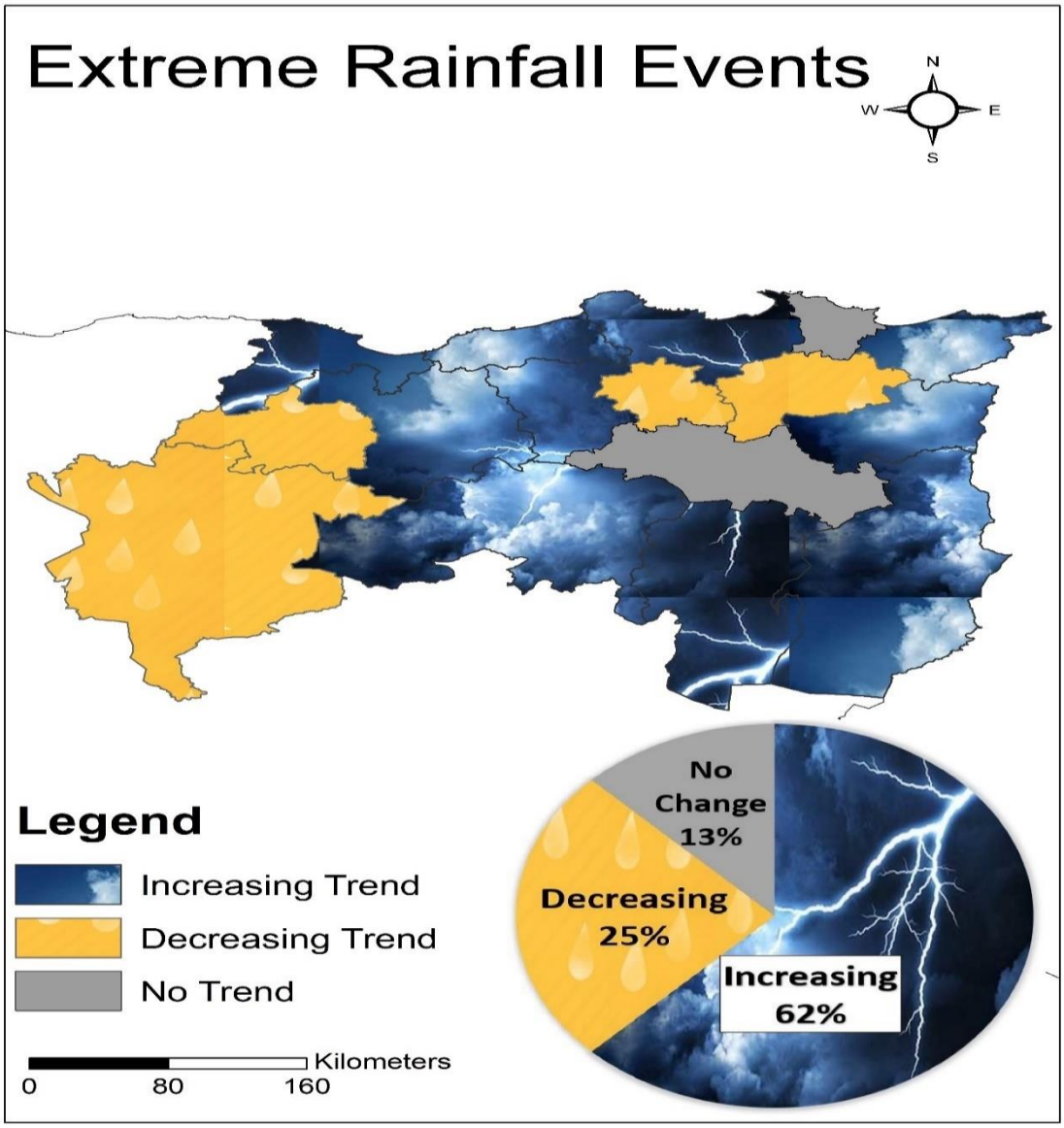

Figure 4-15: Extreme rainfall obtained spatial map

Upholding the previous studies, mentioned earlier in the literature review, the north eastern part of Algeria is understood to be experiencing a significant increasing trend in

its precipitation patterns, subsequently it will be subject to recurring floods and it will be necessary to reconsider the existing infrastructure and take into account the impact of climate change in all calculations.

4.10 CONCLUSION

The objective of this chapter is to detect partial trends in precipitation records for sixteen stations spread across the North East part of Algeria over a period 38 years (1982-2019) which are experiencing impacts from climate change, using the innovative trend analysis (ITA) methodology in partial manner with “low”, “medium” and “high” precipitation groups.

The study made in this chapter led to the following inferences. On the subject of possible droughts, Khenchla station can be considered as a potential location for dry spell and drought conditions in the future. El Taref, Bejaia, Souk Ahras, Batna and M’Sila present an increasing trend in their low data values which should alternatively mean that they are safe against dry spell and drought impacts, Finaly Jijel and Mila show no expectation for drought events. The overall interpretation at “High” rainfall amounts occurrence possibilities at many stations: Extremely high rainfall trends dominate at El Taref, Jijel, Mila and Bejaia stations. Constantine station “high” rainfall amounts are in continuously decreasing trend form with no flood danger. Skikda, Souk Ahras, Tebessa and Khenchla support the idea of flood.

Snaping back to the previous chapter where Mila, Jijel and Bejaia were found most prone to floods, with superposing the results it is confirmed that these three stations are experiencing extreme increasing trend in rainfall which need an immediate solution against flash flood. whereas for Guelma station, both chapters 3 and 4 were due to ratify the drought presence which may get aggravated in future.
In general, 16 meteorology stations are used for ITA templates. According to the results about 63% of the study area is bound to get wetter, which implies that dry spell and

drought impacts are not expected in the near future. In addition, it has been considered, that “Medium” rainfall amounts are the key group for water resources management studies.

Clearly climate change is having an impact over the North East part of Algeria. The majority of provinces will experience an increase in the amount of precipitation, in addition to the appearance of extreme rainfall episodes which can cause serious floods and serious damage considering that the urban system is not in line with the such circumstances. The ITA partial trend identification methodology can be applied objectively in any area provided that precipitation records are available.

Chapter V
Polygon Innovative Trend Analysis (IPTA)

5 CHAPTER V: INNOVATIVE POLYGON TREND ANALYSIS (IPTA)

5.1 ABSTRACT

Any hydro-meteorology variable includes various component, in general, as periodicity, trend, possibly jump and the uncertain stochastic parts. Among these the trend analysis gained importance in the last three decades due to the global warming and climate change effects. The literature is full of monotonic trend applications by taking into consideration trend analyses methodologies such as Mann-Kendall trend identification, Sen trend slope calculation, and Şen Innovative Trend Analysis (ITA). It is more important in the practical studies to deal with less than one-year durations so as to assess the possible trend pieces for better practical uses such as agricultural productivity purposes. In this chapter a new concept is applied known as the innovative trend polygon methodology (IPTA) to assess the trend components transitions between two successive months. The application of the methodology is presented for the North-Eastern region of Algerian precipitation records. El Taref station has the most unstable precipitation behavior among all the meteorology stations in the study area, moving from a month to another rather very unsystematically; whereas the rest of the study area has systematic movement from a month to another.

5.2 INTRODUCTION

The world meteorological and climatological variables started to take a new direction since almost three decades due to the global warming and climate change impacts. Intergovernmental Panel on Climate Change IPCC (2014) reports confirmed that there is a steady, but creeping temperature increments as a result of anthropogenic greenhouse gas (GHG) emissions. The temperature is estimated to increase by 2°C to 6°C until 2100, which is a tremendous increase from our current average temperature of 1.7°C (IPCC,

2014). there may be much more bad implications due to climate change globally and humanity will be at high risk, developments will get shattered and rescue efforts will gain higher priorities.

The global warming, climate change and global energy imbalance are considered as the main consequences of the dramatic increase in the concentration of GHG due to human activities, especially industrialization, the burning of fossil fuel, and land use/land cover changes (Chu et al., 2010). From the various studies and reports, it is evident that with the current rate of carbon dioxide release in the atmosphere, there would not only be increase in the global temperature, but it will also cause rise in sea level and increase in the frequency of disasters (Meehl et al., 2012, Domingues et al., 2018, Walsh et al., 2012, Mann and Emanuel, 2006). Emissions from human activities are causing increase in the frequency of extreme weather events. In particular, there are likely to be many more heatwaves, droughts and changes in rainfall patterns and hydrological regimes, which in turn will affect other human systems such as residential, industrial and agricultural water supply, hydro-power energy exploitation, and human health (Huang et al., 2011).

Global warming and consequent climate change will nevertheless place additional stresses on water resources, whether or not future rainfall is significantly altered Mike et al. (2001). They have significant impact on regional rainfall patterns, which may not only alter rainfall amount, but rainfall temporal and spatial distributions and patterns (Adefisan, 2018). Broadly, the spatiotemporal variability of climatic variables such as rainfall and temperature will be affected by climate change (Held and Soden, 2006, Wu et al., 2013, Collados-Lara et al., 2020).

A study made by Hendrix and Salehyan (2012), resulted that rainfall variability has a significant effect on both large and smaller scale instances of political conflict, where rainfall correlates with civil war and insurgency, although wetter years are more likely to suffer from violent events.

Rainfall is of vital importance for mankind, and therefore, all over the world scientists are doing their best to understand the physical processes and, based on this come up with plausible scenarios for the future years up to 2100.

Recently, south coast regions of western Mediterranean basin have been subjected to strong climate disturbances, where the signs of change are extremely eloquent for the latest years in all this region and North Africa (Nouaceur and Murărescu, 2016).

Observed rainfall trends are less homogeneous and significant with strong declines over the Mediterranean parts of Algeria and Morocco, and parts of Libya, and a slight increase over Mediterranean Egypt. Most of the African continent is semi-arid, and hence, prone to extreme variations in rainfall from year to year (Nicholson et al., 2018).

The projected precipitation decreases in North Africa will affect water resources, in particular surface water that supplies the largest dams and reservoirs in North Africa (Tramblay et al., 2018). This decline in water supply is likely to occur in a region, where water demand is expected to increase due to population growth and economic development indicating higher water stress in the future (Schilling et al., 2020).

Algeria has received exceptional rainfall amounts, which led to an unprecedented dam filling up reaching 72% in 2010 and 81% in April 2013 for 65 dams in operation and to 80.4% in March 2014. The effects of climate change are also manifested in Algeria by extreme events (a succession of hot episodes in 2015) with exceedance over the threshold temperature of 50°C at Ouargla on 2nd August 2015 and of snowfall in the Assekrem mountains in Hoggar massif located in the southern Algeria as a very rare fact never observed since 1945 (Nouaceur and Murărescu, 2016).

In addition, Taïbi et al. (2013) analyzed more than 100 rainfall series over northern Algeria and demonstrated a significant decrease in the annual rainfall in northwestern Algeria since the 1970s and 1980s, while rainfall variability in the eastern region did not

change. Many studies have shown significant decrease in the temporal variability of rainfall in northwest Algeria (Medjerab and Henia (2005); Meddi and Meddi (2007);Meddi and Talia (2008); Bekkoussa et al. (2008); Meddi et al. (2010a). Taïbi et al. (2019)) found that rainfall variability in northern Algeria is correlated to a variation in the number of wet days ranging from 10 mm to 50 mm, leading to a negative/positive rainfall trend in the West/East direction since the 1970s.

In order to better deal with the climate evolution, scientists paid more attention towards future estimations and probabilities. Trend analysis is one of the most effective methods to have a closer look on climate changes and variabilities. The large range of possibilities observed by trend analysis makes it key for developing robust scenarios that meet essential criteria as plausible (logical, consistent and believable), relevant (highlighting key challenges and dynamics of the future), divergent (different from each other in strategically significant ways), and challenging (questioning fundamental beliefs and assumptions).

Trend analysis is, fundamentally, a method for understanding how and why things have changed – or will change – over time. It can be defined here as an approach which collates data and then attempts to discover patterns, or trends, within that data for the purposes of understanding or predicting behaviors (Rae, 2014). In this chapter, Innovative Polygon Trend Analysis (IPTA) methodology is used for monthly trend analysis (Şen, 2012; Şen et al., 2019).

In this chapter, a new method developed by IPTA meant to detect the trend within the year (from month to the next) for the North-eastern region of Algeria during (1982-2019). The application subject to the study region is the North-Eastern part of Algeria, which is in sub-humid Mediterranean climate characterized by a dry season from May to September followed by a wet season from October to April.

5.3 METHODOLOGY

The literature is full of linearly (monotonic) increasing or decreasing trend analyses on temperature and rainfall records such as: Asfaw et al. (2018), Addisu et al. (2015), Gebrechorkos et al. (2019), Seleshi and Zanke (2004), Feng et al. (2016), but they do not indicate the sub-temporal variations or possible hidden trend components along small time periods like days or months. Most of the methodologies are developed for monotonic trend identification as mentioned in the introduction section of this chapter.

IPTA proposed by Şen et al. (2019) can be applied on several time scales (i.e. daily, monthly, annual, etc.). In case of monthly statistical parameters, basically arithmetic average is taken as template construction between 12 set from the first half of the original time series versus to the second part 12 monthly values.

The time series should be organized in a matrix form composed of [$x_{i,j}$], where x is the parameter to be studied (in this case it is precipitation records), " i " is the year number goes from 1 to n as the length of the time series, and " j " is the month number which goes from 1 to 12. This sequence can be arranged into a monthly matrix as follows:

$$\begin{bmatrix} x_{1,1}, & x_{1,2}, & \dots & , x_{1,12} \\ x_{2,1}, & x_{2,2}, & \dots & , x_{2,12} \\ \dots & \dots & \dots & \dots \\ x_{i,1}, & x_{i,2}, & \dots & , x_{i,12} \\ \dots & \dots & \dots & \dots \\ x_{n,1}, & x_{n,2}, & \dots & , x_{n,12} \end{bmatrix}$$

↑ Upper half (the first half, (i=1, 2,.., (n/2)))

↓ Lower half (the second half, (i= (n/2)+1, (n/2)+2,.., n))

First this matrix is divided into two halves, then the arithmetic average is calculated afterward for each halve, and finally, the matrix will shrink into two lines as follow.

[a_1, a_2, a_3, a_4, a_1, a_5, a_6, a_7, a_8, a_9, a_{10}, a_{11}, a_{12}]

[b_1, b_2, b_3, b_4, b_5, b_6, b_7, b_8, b_9, b_{10}, b_{11}, b_{12}]

The a and b lines correspond to the arithmetic average of the first and second half of the matrix respectively.

Graphically, the two lines are plotted against each other, then the scatter of points is represented by a straight line that extends from month 1 to month 2 until month 12 and back to month 1 forming a closed polygon as in Figure 5-1.

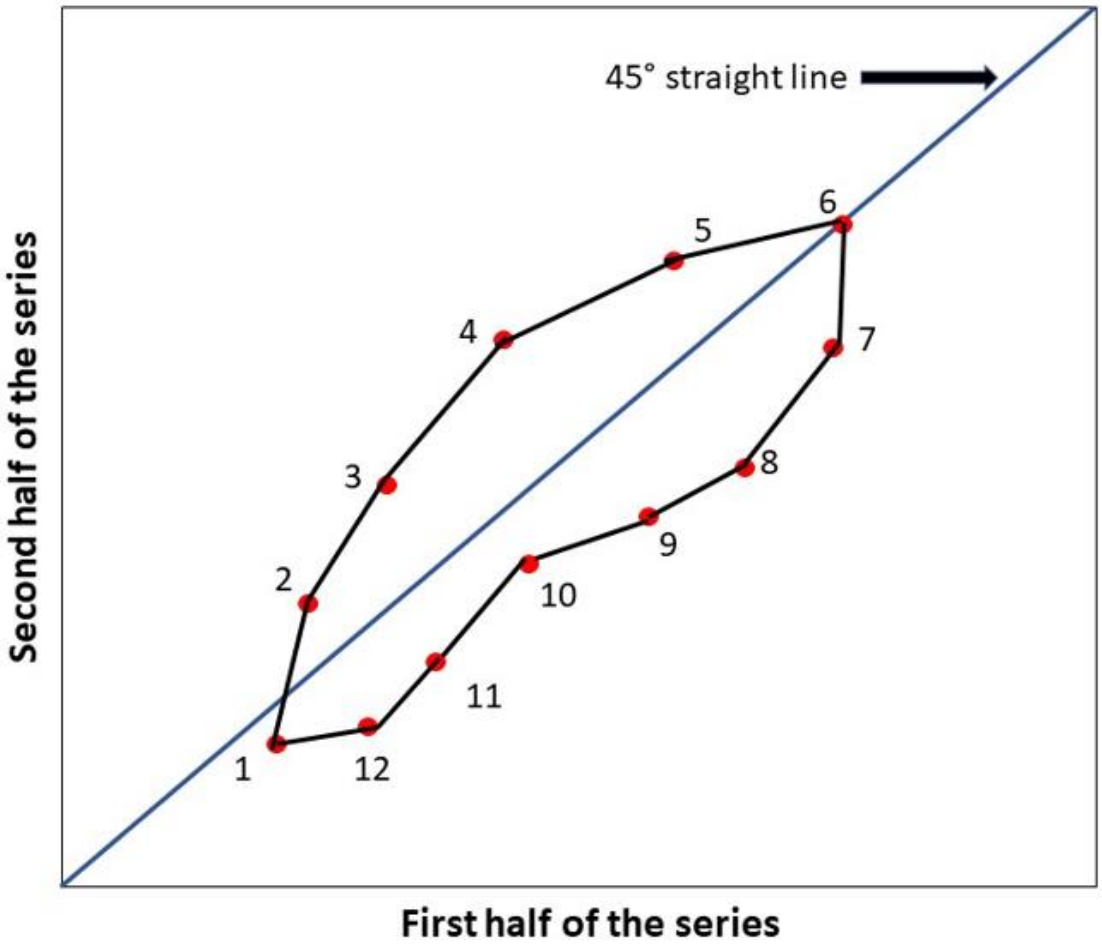

Figure 5-1: Trend polygon

The polygonal template figure provides a general idea about the monthly trend behaviors during the whole record duration like the innovative trend analysis by comparison of two

record duration halves. The wider the polygons the more unstable the monthly trend features, but the narrower it is the more is the climatological stabilization like the annual trend. In the following, some specific features are given concerning the IPTA graphs in general.

5.3.1 The trend-length, L

It indicates the distance between two successive months on the polygons, which implies the weak or strong trend transition existence from one month to the next. The longer is this length the more is the climatological distinction between the months. In order to make it more feasible, the lengths are considered in four possible categories as follows.

1) Weak for $0 < L < 30$ mm.
2) Medium for $30 \text{ mm} < L < 50$ mm.
3) Strong for $50 \text{ mm} < L < 75$ mm.
4) Very strong for $L > 75$ mm.

5.3.2 The slope, S, of the trend-length

It illustrates the rate of change from one month to the next with the comparison between the first half and the last halves of the time series record duration. In general, consideration of the two consecutive months leads to the following interpretations.

1) If the slope is positive, the trend moves from one month to another in the same direction on both axes of the polygonal pattern, which means that there is a decrease or increase during the two halves of the available hydro-meteorological record.
2) If the slope is negative then the trend of one month moves inversely between the first and second record duration halves.
3) If the slope is less than 1 then the variation of the parameter (monthly average precipitation) between the two months in the first half of the time series is wider than the second half. In the case of slope exceeding 1, the variation is greater in the second half compared to the first half of the time series.

5.3.3 The trend mid-distance, D

It represents the projection of the mid distance point of the two consecutive months on the trendless line, which gives an idea about the intensity of the trend change, and the more it is far from the trendless zone the more is the trend significance.

5.4 APPLICATIONS AND DISCUSSION

The application of monthly trend polygon methodology is applied on a set of rainfall records from Algerian eastern provinces. A MATLAB program used in order to get the figures with tables below (result section). Afterwards, the obtained upshots should be interpreted as follows. The inspection of corresponding tables to each meteorology station IPTA template graph provides information about the wideness or narrowness of the polygons in addition to the single or double or more polygonal patterns, each one of them provides a treasure of interpretations about the climatological behavior of each meteorology station.
The corresponding program added as appendix, see section 8.3.1.

5.4.1 Annaba meteorology station

Annaba meteorology station IPTA graph is given in Figure 5-2. In general, the polygon has a descending form from December to July then it switches to an ascending form from July to December, which means that this hydro-meteorological time series has pretty much balanced behavior, also it contains two loops, where the perfect regime appears in one loop, but most of the months lay in the increasing trend branch. For example, May is the only month that presents a significantly decreasing trend, February has the most significant increasing trend among all the other months, whereas December, November, October, August and July remain trendless as it is clear in the figure that they lay in the trendless zone.

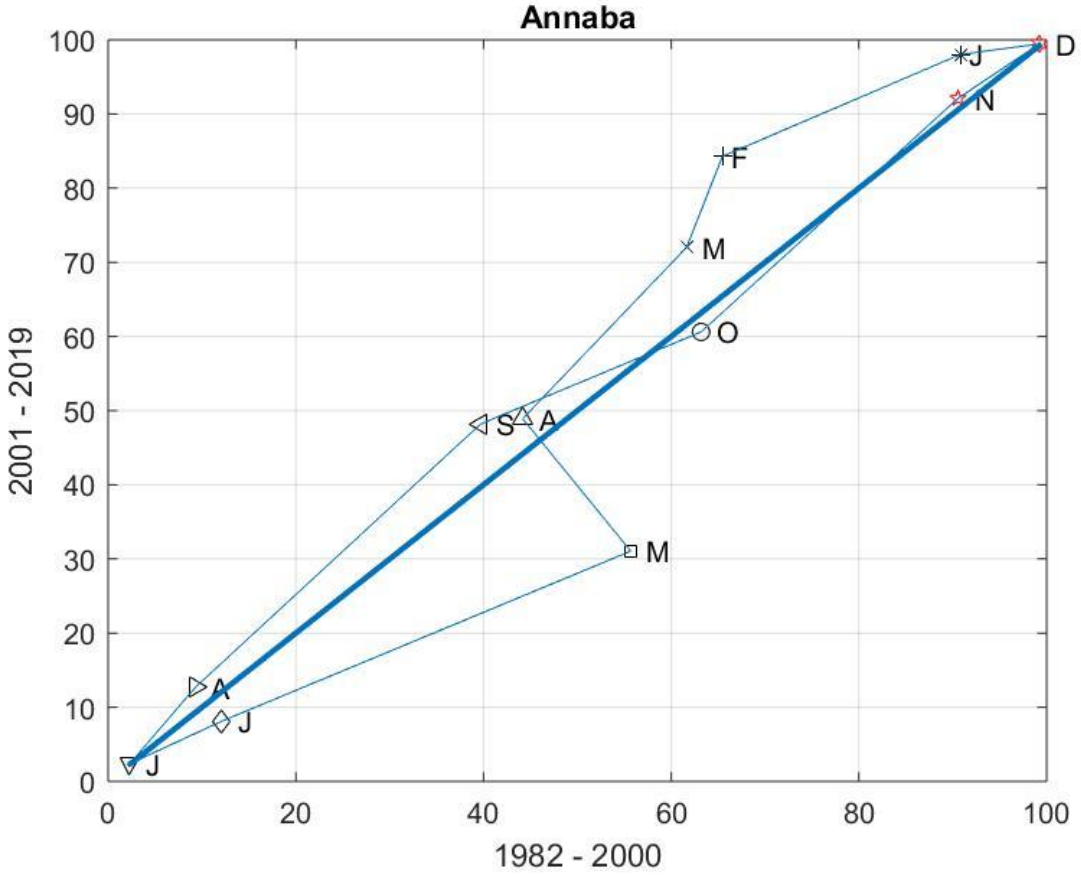

Figure 5-2: IPTA template for Annaba meteorology station

By inspecting the Table *5-1*, the length of most lines is under 30, which means that the change between these months is considered as weak; (May-Jun), (Aug-Sep) and (Oct-Nov) show a medium change, whereas May-Jun is the strongest in the record length duration.

The slope of all the trend-lines is positive, which means that the change from month to another is in the same direction during the whole time series, except (Apr-May) is negative, where the change is contrary from Apr toward May during the 1982/2000 as moving to 2001/2019, and May was rainier in the past then April, but with time precipitation tends to increase in April and decrease in May.

By looking at the mid distances, it is clear that the trend during the period Feb-Mar is the most significant with positive sign followed by Jan-Feb, while Apr-May represents a significantly decreasing trend comparatively to other months.

Table 5-1: IPTA monthly statistical values of arithmetic mean deviation of Annaba station

Annaba						
Month	**Jan_Feb**	**Feb_Mar**	**Mar_Apr**	**Apr_May**	**May_Jun**	**Jun_Jul**
TrendLength	28.8	12.9	29.0	21.2	49.2	11.4
TrendSlope	0.5	3.2	1.3	-1.6	0.5	0.6
MidDistance	13.0	14.6	7.6	-9.9	0.0	-2.0
Month	**Jul_Aug**	**Aug_Sep**	**Sep_Oct**	**Oct_Nov**	**Nov_Dec**	**Dec_Jan**
TrendLength	12.5	46.7	26.6	41.7	11.3	8.6
TrendSlope	1.5	1.2	0.5	1.2	0.8	0.2
MidDistance	1.7	6.0	3.0	-0.5	0.9	3.7

5.4.2 El-Taref meteorology station

The IPTA template of this station is presented in Figure 5-3, which presents a polygon with five loops reflecting the non-stability of the precipitation during this hydro-meteorological time series, three of them appear during periods of Feb-Mar, Mar-Apr and Sep-Oct, which shows an abnormal behavior. Oct, Dec, Mar and Apr are lying far from the trendless zone (45° straight line), where October has a deceasing precipitation and the others are having increases. November is the rainiest month during 1992/2000 and December took that place during 2001/2019, whereas July is the scarce month during the whole period.

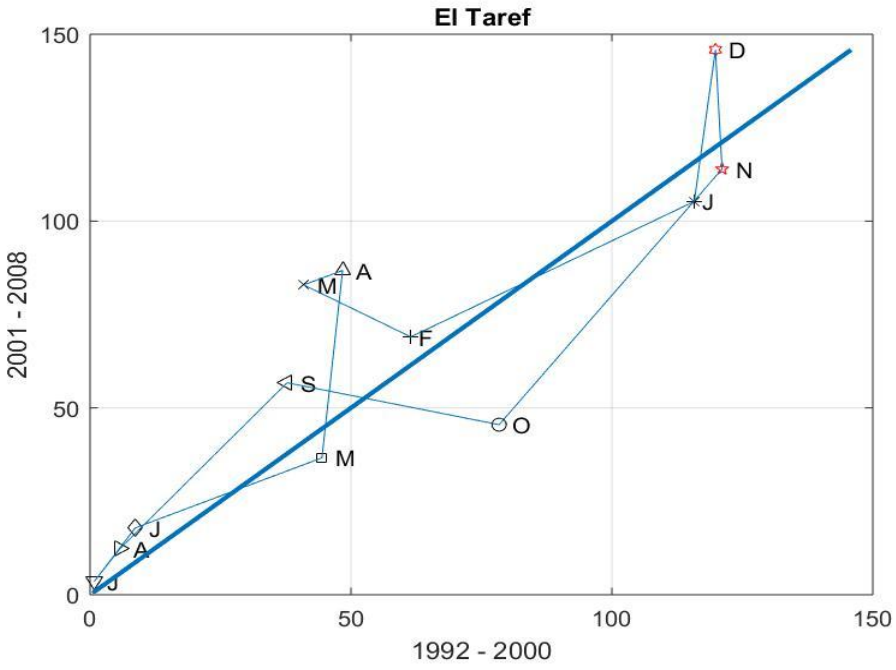

Figure 5-3: IPTA template for El Taref meteorology station

Table *5-2* shows that the period Oct-Nov has the longest line with a category of very strong change, and then it is followed by Jan-Feb, Aug-Sep and Apr-May with a strong change respectively, the others are considered as in the medium and weak categories.

Table 5-2: IPTA monthly statistical values of arithmetic mean deviation of El Taref station

El Taref						
Month	**Jan_Feb**	**Feb_Mar**	**Mar_Apr**	**Apr_May**	**May_Jun**	**Jun_Jul**
TRendLength	65.3194	24.7925	8.4086	50.3188	40.4018	16.3907
TrendSlope	0.6671	-0.6789	0.5193	12.6593	0.5239	1.8254
MidDistance	-1.4938	24.7688	40.1938	15.3	0	5.9875
Month	**Jul_Aug**	**Aug_Sep**	**Sep_Oct**	**Oct_Nov**	**Nov_Dec**	**Dec_Jan**
TRendLength	10.1383	54.7135	42.156	80.6685	31.9125	40.7779
TrendSlope	1.7788	1.3864	-0.2759	1.6015	-25.2574	9.9877
MidDistance	4.6721	12.7908	-6.95	-20.025	9.4	7.7188

There are three periods that show negative slopes due to the reversible change between the successive months from the first half of the time series to the second half. Nov-Dec has the most elevated slope with negative sing (-25.2564), the average precipitation from Nov to Dec decreases in the period 1992/2000 and increases during 2001/2008. Apr-May has a significant slope with (12.6593) value followed by (9.9877) for Dec-Jan, which reflects the huge decreasing jump between the months and since it exceeds 1 the decreasing is higher in the second half.

The mid-distance of Mar-Apr has the higher value among all the others, and hence, it is positive with an increasing trend between these two months, which is the most significant, while Oct-Nov presents the most decreasing trend during this time series.

5.4.3 Skikda meteorology station

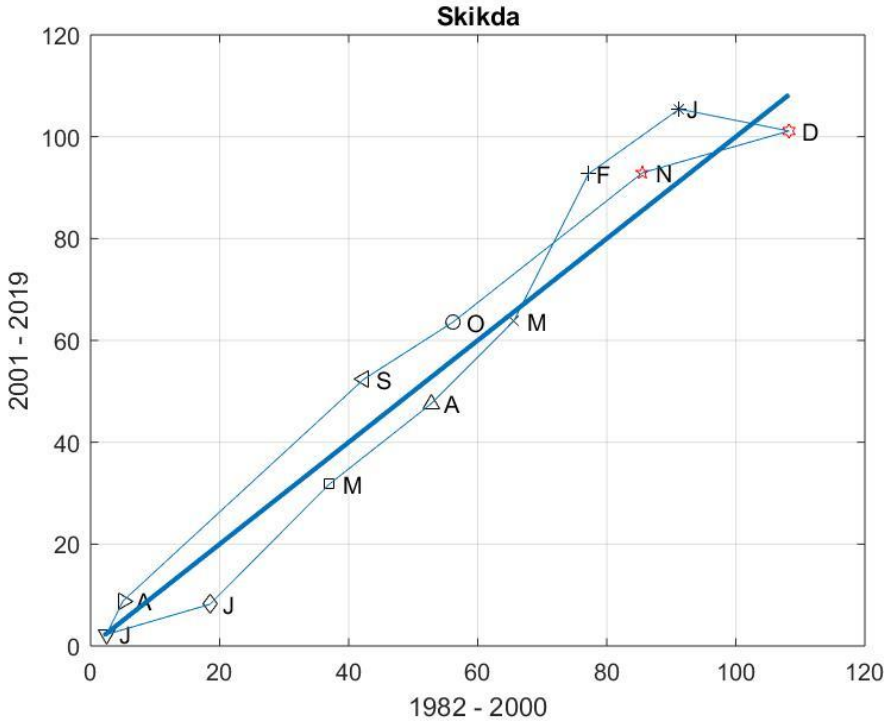

Figure 5-4: IPTA template of Skikda meteorology station

Figure 5-4 reveals that during 1982/2000 December was the rainiest month, which tends to decrease, and January took the place in 2001/2019, whereas July is the scarce month with no trend. The polygon has only two loops and all the months lay close to the trendless zone. January and February show a tinny increasing trend. In general, the precipitation in this station remains stable during the time series.

Table 5-3: IPTA monthly statistical values of arithmetic mean deviation of Skikda station

Skikda						
Month	**Jan_Feb**	**Feb_Mar**	**Mar_Apr**	**Apr_May**	**May_Jun**	**Jun_Jul**
TRendLength	18.9	31.2	20.7	22.3	30.0	17.1
TrendSlope	0.9	2.5	1.3	1.0	1.3	0.4
MidDistance	14.9	6.9	-3.5	-5.2	0.0	-5.3
Month	**Jul_Aug**	**Aug_Sep**	**Sep_Oct**	**Oct_Nov**	**Nov_Dec**	**Dec_Jan**
TRendLength	7.1	57.3	17.9	41.5	24.2	17.6
TrendSlope	2.6	1.2	0.8	1.0	0.4	-0.3
MidDistance	1.8	6.9	8.7	7.4	0.1	3.5

By moving from a season to another, a remarkable change happens in the average precipitation, where the strongest one is between August to September (summer to autumn), and the less change happens between July to August, which means that they behave pretty much similarly.

Table *5-3* indicate that the slope is very close to 1, which means that there is no difference in the change during the time series, only two periods, namely, Jun-Jul and Nov-Dec has changes in the precipitation as wider in the past, because the slope is 0.3, also all the slopes are positive meaning that there is a balance in the precipitation behavior during the whole time series. January to December shows a decreasing trend in the first half, which shift to increasing case in the second half concluding that the rainy season lately has been postponed.

5.4.4 Jijel meteorology station

Jijel IPTA plot is represented in Figure 5-5. All the months are situated in the increasing trend zone revealing the significant increase in the precipitation in Jijel station, where December is the rainiest month during 1982-2000, but in recent time, November took the place with an average of 160 mm. Month-to-month movement seems logical since there is a respectful descending from January to July then an ascending from July to December. However, in the second half of the time series there exists a break in November, which records a significant increase that exceeded in December. The polygon has only 3 loops, which reveals a pretty stable behavior in precipitation in this station.

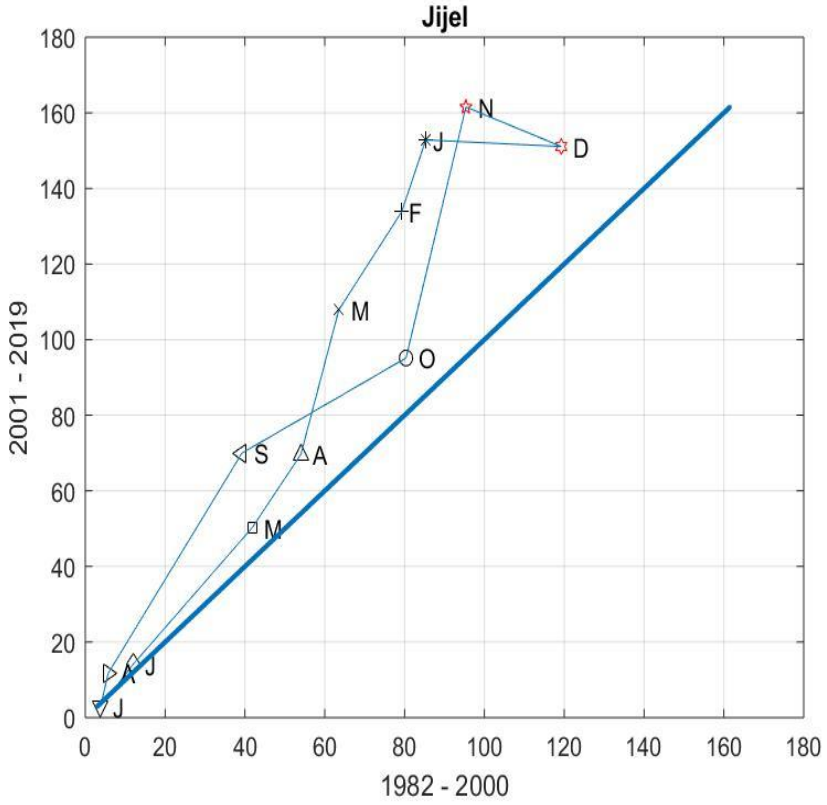

Figure 5-5: IPTA template of Jijel meteorology station

Table 5-4: IPTA monthly statistical values of arithmetic mean deviation of Jijel station

Jijel						
Month	**Jan_Feb**	**Feb_Mar**	**Mar_Apr**	**Apr_May**	**May_Jun**	**Jun_Jul**
TRendLength	19.9	30.3	39.4	23.0	46.8	13.8
TrendSlope	3.1	1.6	4.0	1.6	1.2	1.4
MidDistance	61.0	49.4	30.0	12.0	0.0	0.6
Month	**Jul_Aug**	**Aug_Sep**	**Sep_Oct**	**Oct_Nov**	**Nov_Dec**	**Dec_Jan**
TRendLength	9.0	67.2	48.2	68.1	26.1	34.0
TrendSlope	4.6	1.7	0.6	4.4	-0.4	-0.1
MidDistance	2.6	18.4	22.8	40.5	49.0	49.7

Table *5-4* provide extra details as follow:

The significant change between two successive months happened in Oct-Nov, which is clear in the table with a strong value more than 68, Aug-Sep come after with 67, 5 others present a medium change.

Dec-Jan presents a very flat negative slope (-0.05), in the recent years the behavior of precipitation in January becomes very similar to December's contrary in the past, because December was rainier than January with 40 mm of received precipitation in average.

The obtained mid-distance values are quite high, which could be explained by saying that the changes are far from the trendless area and since they are all positive with increasing trends.

5.4.5 Bejaia meteorology station

The polygon in Figure 5-6 is systematic from January to September, then a perturbation happens between September to December. There are periodic acts alike, Dec-Jan with Feb-Mar and Oct-Nov, where these couples used to be close to each other in the precipitation behavior; in contrast Sep-Oct and Nov-Dec have same behavior in the recent time. A high part of the polygon is situated in the increasing trend area, which gives a general idea that Bejaia station is acquiring more rain during last years.

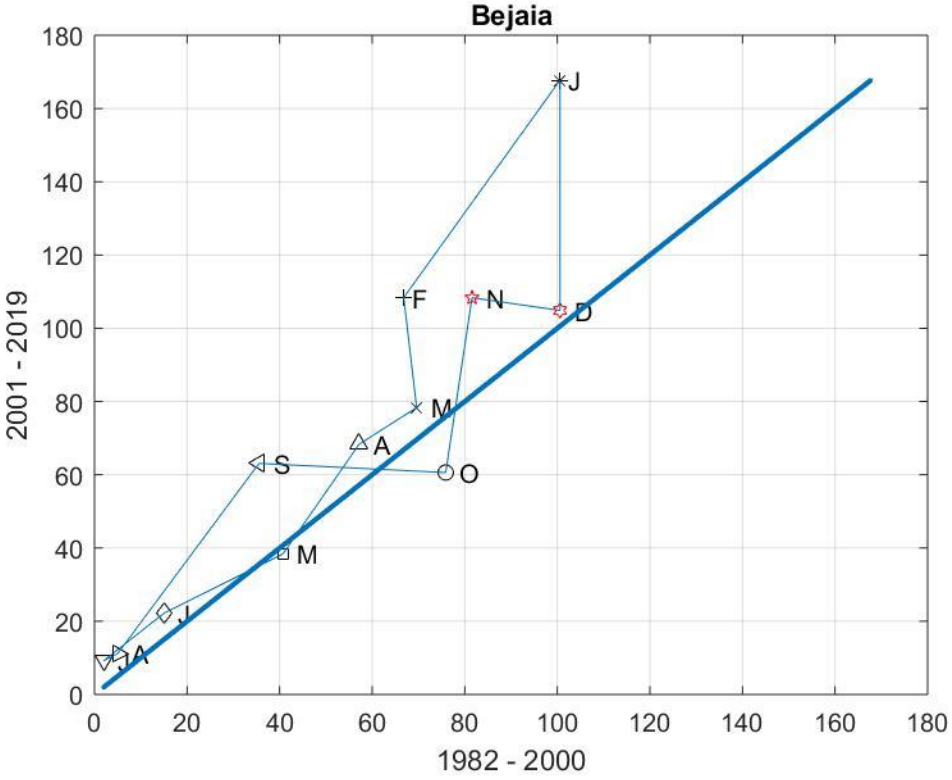

Figure 5-6: IPTA template of Bejaia meteorology station

Table 5-5:IPTA monthly statistical values of arithmetic mean deviation of Bejaia station

Bejaia						
Month	**Jan_Feb**	**Feb_Mar**	**Mar_Apr**	**Apr_May**	**May_Jun**	**Jun_Jul**
TRendLength	68.3	30.2	15.9	34.2	30.4	18.4
TrendSlope	1.8	-10.8	0.8	1.8	0.6	1
MidDistance	54.4	25.2	10	4.4	0	7.2
Month	**Jul_Aug**	**Aug_Sep**	**Sep_Oct**	**Oct_Nov**	**Nov_Dec**	**Dec_Jan**
TRendLength	3.7	60.2	40.4	48.1	19.3	62.9
TrendSlope	0.7	1.7	-0.1	8.4	-0.2	-9.1
MidDistance	6.7	16.9	6.1	5.7	15.5	35.7

In Table *5-5*, Jan-Feb, Aug-Sep and Dec-Jan present a strong jump in the average precipitation as shown in the figure, also the slopes clearly reveal a remarkable shift in the behavior during the last years in the couples (Feb-Mar, Oct-Nov, Dec-Jan, Sep-Oct,

and Nov-Dec). Jun-Jul behaves the same manner during the whole time series, where the slope is 1.
Mid distances are all positive, which confirms that Bejaia station presents an increasing trend concerning its precipitation.
The results of the remaining stations will be demonstrated in the appendix, see section 8.3.2.

5.5 CONCLUSION

This chapter presents the application of monthly innovative polygonal trend analysis methodology (IPTA) for sixteen precipitation records covering the north eastern region of Algeria. In this manner one can identify detailed information besides the monotonic linear trend component. Hence, it is possible to compare the relative position of each monthly trend component situation, position and detailed interpretations with respect to the traditional monotonic trend component. This comparison distinguishes months with more (less) than the monotonic trend component contribution.

The emanated results from this study provided information that most stations present generally increasing trend. Only three stations pursue inversely, namely Khenchla, Guelma and M'Sila where Khenchla shows the most significant decreasing trend.
Six stations perform almost systematically, namely: Annaba, Bejaia, Constantine, Jijel, Skikda and Souk Ahras. However, the remaining stations show unsystematic pursue.
Furthermore, most stations witnessed a delay in the wet season, which generally runs from January until April. While April in particular shows a remarkable increasing trend during the recent part of the time series.

The dry season from Jun to August remain stable for the whole region with no significant change.

General Conclusion and Perspective

6 GENERAL CONCLUSION AND PERSPECTIVE

The most immediate impact of climate change is the perturbation of the precipitation regime which can implicate multiple risks such of floods and droughts, those risks could be at least handled if they are inevitable.
Analyzing the trend of the precipitation is important tool to make predictions. Through this thesis we wanted to contribute modestly to make available to the institutions concerned with this aspect of an analysis of the precipitation time series in order to detect the impact of climate change in the North Eastern part of Algeria using new and Innovative methods such as; including the Slope in the risk probability calculations instead of the classical approach. In addition, application of an Innovative Trend Analysis (ITA) method originated by Şen (2017) was used which does not require many restrictive assumptions. Finally, Innovative Polygon Trend Analysis meant to detect the trend within the year (from one month to the next) was applied.

The risk assessment study along with dry and wet spells examination revealed climate change will aggravate situations in the study area, and that the top three locations needing quick rehabilitation against floods are Bejaia, Mila and Jijel, coming in second position are : Constantine, Bordj Bouarreridj, Skikda, Annaba, Oum Bouaghi, and Tebessa, with Khenchla is already under flood risk but it tends to get less rainfall while Guelma station will need solutions for droughts because they tend to be more frequent. Furthermore, it has been determined that 81% of the study area is experiencing an increasing trend in rainfall, with certain regions experiencing speedier return periods, with some of them seeing return periods as much as 95% sooner.

The ITA methodology application supported the previous outcomes, El Taref, Bejaia, Souk Ahras, Batna and M'Sila present an increasing trend in their low data values which should alternatively mean that they are safe against dry spell and drought impacts, with the overall possibility of "High" amounts of rainfall occurring at many stations: Extremely

high rainfall trends dominate at El Taref, Jijel, Mila and Bejaia stations. Constantine station “high” rainfall amounts are in continuously decreasing trend form with no flood danger. Stations in Skikda, Souk Ahras, Tebessa and Khenchla support the possibility of flood. In addition, it has been considered, that “Medium” rainfall amounts are the key group for water resources management studies.

The IPTA methodology conclusions match what mentioned above, besides, six stations follow almost systematic order passing from a month to another, namely: Annaba, Bejaia, Constantine, Jijel, Skikda and Souk Ahras. However, the remaining stations show unsystematic pursue.
Moreover, most stations witnessed a delay in the wet season, which generally runs from January until April. While April in particular shows a remarkable increasing trend during the recent part of the time series.

In conclusion, climate change has significantly disturbed the precipitation regime in the northeastern part of Algeria, the assessment of the general trend found that thirteen stations out of 16 sixteen represent an increasing trend, and this result was not sufficient to make a decision on which stations are in direct danger , it was necessary to carry out partial directional investigations along with a drought check, and in the end, if two stations are presenting an increasing trend but one of them already has rainfall redundancy, then this station is clearly the most threatened one.

In perspective view, building resilience against climate threats is essential, rehabilitation of infrastructures will be necessary in order to avoid floods impact in the study region, with priority given to Jijel, Mila and Bejaia. In contrast Guelma and Khenchla in second position will need strategies to contain the drought effect.

References

7 REFERENCES

ACS. 2015. *The Keeling Curve* [Online]. Available: American Chemical Society National Historic Chemical Landmarks. The Keeling Curve. http://www.acs.org/content/acs/en/education/whatischemistry/landmarks/keeling-curve.html (accessed Month Day, Year).

ADDISU, S., SELASSIE, Y. G., FISSHA, G. & GEDIF, B. 2015. Time series trend analysis of temperature and rainfall in lake Tana Sub-basin, Ethiopia. *Environmental Systems Research,* 4**,** 25.

ADEFISAN, E. 2018. Climate Change Impact on Rainfall and Temperature Distributions Over West Africa from Three IPCC Scenarios. *Journal of Earth Science & Climatic Change,* 09.

ALDA, E. 2014. *RISING TEMPERS, RISING TEMPERATURES: A Look at Climate Change, Migration and Conflict and the Implications for Youth in the Sahel Region*.

ASFAW, A., SIMANE, B., HASSEN, A. & BANTIDER, A. 2018. Variability and time series trend analysis of rainfall and temperature in northcentral Ethiopia: A case study in Woleka sub-basin. *Weather and Climate Extremes,* 19**,** 29-41.

BAKER, D. 2000. Effects of the Sun on the Earth's environment. *Journal of Atmospheric and Solar-Terrestrial Physics,* 62**,** 1669-1681.

BANHOLZER, S., KOSSIN, J. & DONNER, S. 2014. The Impact of Climate Change on Natural Disasters. *In:* SINGH, A. & ZOMMERS, Z. (eds.) *Reducing Disaster: Early Warning Systems For Climate Change.* Dordrecht: Springer Netherlands.

BANKOFF, G. & CHRISTENSEN, J. 2016. Bordering on Danger: An Introduction. *In:* BANKOFF, G. & CHRISTENSEN, J. (eds.) *Natural Hazards and Peoples in the Indian Ocean World: Bordering on Danger.* New York: Palgrave Macmillan US.

BEKKOUSSA, B., MEDDI, M. & JOURDE, H. 2008. Forçage climatique et anthropique sur la ressource en eau souterraine d'une région semi-aride : cas de la plaine de Ghriss (Nord-Ouest algérien). *Science et changements planétaires secheresse,* Volume 19.

BELDJAZIA AMINA, A. D. 2016. Precipitation Variability on the Massif Forest of Mahouna (North Eastern-Algeria) from 1986 to 2010. *International Journal of Management Sciences and Business Research,* Vol. 5, Issue 3**,** 21-28.

BELLINGHAM, P. J., KAPOS, V., VARTY, N., HEALEY, J. R., TANNER, E. V. J., KELLY, D. L., DALLING, J. W., BURNS, L. S., LEE, D. & SIDRAK, G. 1992. Hurricanes need not cause high mortality: the effects of Hurricane Gilbert on forests in Jamaica. *Journal of Tropical Ecology,* 8**,** 217-223.

BENJAMIN, J. & CORNELL, C. 1970. Probability, decision, and statistics for civil engineers. McGraw-Hill, New York.

BERNICE DE JONG, B. 1995. Mount Tambora in 1815: A Volcanic Eruption in Indonesia and Its Aftermath. *Indonesia*, 37-60.

BESSAKLIA, H., GHENIM, A., MEGNOUNIF, A. & MARTIN-VIDE, J. 2018. Spatial variability of concentration and aggressiveness of precipitation in North-East of Algeria. *Journal of Water and Land Development,* 36, 3-15.

BOUCHAMA, A. 2004. The 2003 European heat wave. *Intensive Care Medicine,* 30, 1-3.

BOUDIAF, B., DABANLI, I., BOUTAGHANE, H. & ŞEN, Z. 2020. Temperature and Precipitation Risk Assessment Under Climate Change Effect in Northeast Algeria. *Earth Systems and Environment,* 4, 1-14.

BOUDIAF, B., ŞEN, Z. & BOUTAGHANE, H. 2021. Climate change impact on rainfall in north-eastern Algeria using innovative trend analyses (ITA). *Arabian Journal of Geosciences,* 14, 511.

BRADE, I., HERFERT, G. & WIEST, K. 2009. Recent trends and future prospects of socio-spatial differentiation in urban regions of Central and Eastern Europe: A lull before the storm? *Cities,* 26, 233-244.

BRÁZDIL, R., ŘEZNÍČKOVÁ, L., VALÁŠEK, H., DOLÁK, L. & KOTYZA, O. 2016. Climatic effects and impacts of the 1815 eruption of Mount Tambora in the Czech Lands. *Clim. Past,* 12, 1361-1374.

BUFFONI, L., MAUGERI, M. & NANNI, T. 1999. Precipitation in Italy from 1833 to 1996. *Theoretical and Applied Climatology,* 63, 33-40.

BURT, S. D. & MANSFIELD, D. A. 1988. THE GREAT STORM OF 15–16 OCTOBER 1987. *Weather,* 43, 90-110.

CAESAR, L., RAHMSTORF, S., ROBINSON, A., FEULNER, G. & SABA, V. 2018. Observed fingerprint of a weakening Atlantic Ocean overturning circulation. *Nature,* 556, 191-196.

CALOIERO, T., COSCARELLI, R., FERRARI, E. & MANCINI, M. 2011. Trend detection of annual and seasonal rainfall in Calabria (Southern Italy). *International Journal of Climatology,* 31, 44-56.

CARTER, J. G., CAVAN, G., CONNELLY, A., GUY, S., HANDLEY, J. & KAZMIERCZAK, A. 2015. Climate change and the city: Building capacity for urban adaptation. *Progress in Planning,* 95, 1-66.

CHAOUCHE, K., NEPPEL, L., DIEULIN, C., PUJOL, N., LADOUCHE, B., MARTIN, E., SALAS, D. & CABALLERO, Y. 2010. Analyses of precipitation, temperature and evapotranspiration in a French Mediterranean region in the context of climate change. *Comptes Rendus Geoscience,* 342, 234-243.

CHOWDHURY, R. 2021. Climate Change Impact and Disaster Vulnerabilities in the Coastal Areas of Bangladesh.

CHU, J. T., XIA, J., XU, C. Y. & SINGH, V. P. 2010. Statistical downscaling of daily mean temperature, pan evaporation and precipitation for climate change scenarios in Haihe River, China. *Theoretical and Applied Climatology,* 99**,** 149-161.

COLLADOS-LARA, A.-J., PULIDO-VELAZQUEZ, D. & PARDO-IGUZQUIZA, E. 2020. A Statistical Tool to Generate Potential Future Climate Scenarios for Hydrology Applications. *Scientific Programming,* 2020.

COWAN, N. B., VOIGT, A. & ABBOT, D. S. 2012. THERMAL PHASES OF EARTH-LIKE PLANETS: ESTIMATING THERMAL INERTIA FROM ECCENTRICITY, OBLIQUITY, AND DIURNAL FORCING. *The Astrophysical Journal,* 757**,** 80.

D'ALEO, J. S. & KHANDEKAR, M. 2016. Chapter 6 - Weather Extremes. *In:* EASTERBROOK, D. J. (ed.) *Evidence-Based Climate Science (Second Edition).* Elsevier.

DE KRAKER, A. M. J. 2015. Flooding in river mouths: human caused or natural events? Five centuries of flooding events in the SW Netherlands, 1500–2000. *Hydrol. Earth Syst. Sci.,* 19**,** 2673-2684.

DI LORENZO, E., COBB, K. M., FURTADO, J. C., SCHNEIDER, N., ANDERSON, B. T., BRACCO, A., ALEXANDER, M. A. & VIMONT, D. J. 2010. Central Pacific El Niño and decadal climate change in the North Pacific Ocean. *Nature Geoscience,* 3**,** 762-765.

DINAN, T. 2017. Projected Increases in Hurricane Damage in the United States: The Role of Climate Change and Coastal Development. *Ecological Economics,* 138**,** 186-198.

DOMINGUES, R., GONI, G., BARINGER, M. & VOLKOV, D. 2018. What Caused the Accelerated Sea Level Changes Along the U.S. East Coast During 2010–2015? *Geophysical Research Letters,* 45**,** 13,367-13,376.

DONG, S., BARINGER, M. O. & GONI, G. J. 2019. Slow Down of the Gulf Stream during 1993–2016. *Scientific reports,* 9**,** 6672.

DULL, R. A., SOUTHON, J. R. & SHEETS, P. 2001. Volcanism, Ecology and Culture: A Reassessment of the Volcán Ilopango TBJ Eruption in the Southern Maya Realm. *Latin American Antiquity,* 12**,** 25-44.

ELMEDDAHI, Y., MAHMOUDI, H., ISSAADI, A., GOOSEN, M. & RAGAB, R. 2016. Evaluating the Effects of Climate Change and Variability on Water Resources: A Case Study of the Cheliff Basin in Algeria. *American Journal of Engineering and Applied Sciences,* 9.

EMEIS, K.-C., ANDERSON, D. M., DOOSE, H., KROON, D. & SCHULZ-BULL, D. 1995. Sea-Surface Temperatures and the History of Monsoon Upwelling in the

Northwest Arabian Sea during the Last 500,000 Years. *Quaternary Research,* 43**,** 355-361.

ENGELBRECHT, F., ADEGOKE, J., BOPAPE, M.-J., NAIDOO, M., GARLAND, R., THATCHER, M., MCGREGOR, J., KATZFEY, J., WERNER, M., ICHOKU, C. & GATEBE, C. 2015. Projections of rapidly rising surface temperatures over Africa under low mitigation. *Environmental Research Letters,* 10**,** 085004.

ERLANDSON, J. M. 2008. Racing a Rising Tide: Global Warming, Rising Seas, and the Erosion of Human History. *The Journal of Island and Coastal Archaeology,* 3**,** 167-169.

FENG, G., COBB, S., ABDO, Z., FISHER, D. K., OUYANG, Y., ADELI, A. & JENKINS, J. N. 2016. Trend Analysis and Forecast of Precipitation, Reference Evapotranspiration, and Rainfall Deficit in the Blackland Prairie of Eastern Mississippi. *Journal of Applied Meteorology and Climatology,* 55**,** 1425-1439.

FRIERSON, D. M. W., LU, J. & CHEN, G. 2007. Width of the Hadley cell in simple and comprehensive general circulation models. *Geophysical Research Letters,* 34.

FRISKEN, W. R. 1971. Extended industrial revolution and climate change. *Eos, Transactions American Geophysical Union,* 52**,** 500-508.

FUNK, C., PETERSON, P., LANDSFELD, M., PEDREROS, D., VERDIN, J., SHUKLA, S., HUSAK, G., ROWLAND, J., HARRISON, L., HOELL, A. & MICHAELSEN, J. 2015. The climate hazards infrared precipitation with stations—a new environmental record for monitoring extremes. *Scientific Data,* 2**,** 150066.

GAFFNEY, O. & STEFFEN, W. 2017. The Anthropocene equation. *The Anthropocene Review,* 4**,** 53-61.

GARDNER-OUTLAW, T. & ENGLEMAN, R. 1997. Sustaining water, easing scarcity: a second update. Washington, DC: Population Action International.

GEBRECHORKOS, S. H., HÜLSMANN, S. & BERNHOFER, C. 2019. Long-term trends in rainfall and temperature using high-resolution climate datasets in East Africa. *Scientific reports,* 9**,** 11376.

GLEN, W. 1994. *The mass-extinction debates: How science works in a crisis*, Stanford University Press.

GORNEY, D. J. 1990. Solar cycle effects on the near-Earth space environment. *Reviews of Geophysics,* 28**,** 315-336.

HADOUR, A., MAHE, G. & MEDDI, M. 2020. Watershed based hydrological evolution under climate change effect: An example from North Western Algeria. *Journal of Hydrology: Regional Studies,* 28**,** 100671.

HALLEGATTE, S. 2007. The Use of Synthetic Hurricane Tracks in Risk Analysis and Climate Change Damage Assessment. *Journal of Applied Meteorology and Climatology - J APPL METEOROL CLIMATOL,* 46**,** 1956-1966.

HALLOUZ, F., MEDDI, M., MAHÉ, G., ALI RAHMANI, S., KARAHACANE, H. & BRAHIMI, S. 2020. Analysis of meteorological drought sequences at various timescales in semi-arid climate: case of the Cheliff watershed (northwest of Algeria). *Arabian Journal of Geosciences,* 13**,** 280.

HALLOUZ, F., MEDDI, M., MAHE, G., TOUMI, S. & SALAH EDDINE, A. R. 2018. Erosion, suspended sediment transport and sedimentation on the Wadi Mina at the Sidi M'Hamed Ben Aouda Dam, Algeria. *Water (Switzerland),* 10.

HAMLAOUI-MOULAI, L., MESBAH, M., SOUAG-GAMANE, D. & MEDJERAB, A. 2013. Detecting hydro-climatic change using spatiotemporal analysis of rainfall time series in Western Algeria. *Natural Hazards,* 65**,** 1293-1311.

HARRIS, D. 2010. Charles David Keeling and the Story of Atmospheric CO2 Measurements. *Analytical chemistry,* 82**,** 7865-70.

HARRIS, P. T. 2020. Frozen Ocean: Ice Ages and Climate Change. *In:* HARRIS, P. T. (ed.) *Mysterious Ocean: Physical Processes and Geological Evolution.* Cham: Springer International Publishing.

HASSINI, N., BELAID, A. & ABDELMADJID, D. 2011. Trends of Precipitation and Drought on the Algerian Litoral: Impact on the Water Reserves. *International Journal of Water Resources and Arid Environments,* 1**,** 271-276.

HELD, I. & SODEN, B. 2006. Robust Responses of the Hydrological Cycle to Global Warming. *Journal of Climate,* 19**,** 5686-5699.

HELLIN, J., HAIGH, M. & MARKS, F. 1999. Rainfall characteristics of hurricane Mitch. *Nature,* 399**,** 316-316.

HENDRIX, C. S. & SALEHYAN, I. 2012. Climate change, rainfall, and social conflict in Africa. *Journal of Peace Research,* 49**,** 35-50.

HERGET, J., KAPALA, A., KRELL, M., RUSTEMEIER, E., SIMMER, C. & WYSS, A. 2015. The millennium flood of July 1342 revisited. *CATENA,* 130**,** 82-94.

HOEGH-GULDBERG, JACOB, O., D. , TAYLOR, M., BINDI, M., BROWN, S., CAMILLONI, I., DIEDHIOU, A., DJALANTE, R., EBI, K. L., ENGELBRECHT, F., GUIOT, J., HIJIOKA, Y., MEHROTRA, S., PAYNE, A., SENEVIRATNE, S. I., THOMAS, A., WARREN, R. & ZHOU, G. 2018. Impacts of 1.5ºC Global Warming on Natural and Human Systems. In: Global Warming of 1.5°C. An IPCC Special Report on the impacts of global warming of 1.5°C above pre-industrial levels and related global greenhouse gas emission pathways, in the context of strengthening the global response to the threat of climate change, sustainable development, and efforts to eradicate poverty [Masson-Delmotte, V., P. Zhai, H.-O. Pörtner, D. Roberts, J. Skea, P.R. Shukla, A. Pirani, W. Moufouma-Okia, C. Péan, R. Pidcock,

S. Connors, J.B.R. Matthews, Y. Chen, X. Zhou, M.I.Gomis, E. Lonnoy, T.Maycock, M.Tignor, and T. Waterfield (eds.)]. In Press.
HOLLAND, G. & BRUYÈRE, C. L. 2014. Recent intense hurricane response to global climate change. *Climate Dynamics,* 42**,** 617-627.
HOMAR, V., RAMIS, C., ROMERO, R. & ALONSO, S. 2009. Recent trends in temperature and precipitation over the Balearic Islands (Spain). *Climatic Change,* 98**,** 199.
HUANG, J., ZHANG, J., ZHANG, Z., XU, C., WANG, B. & YAO, J. 2011. Estimation of future precipitation change in the Yangtze River basin by using statistical downscaling method. *Stochastic Environmental Research and Risk Assessment,* 25**,** 781-792.
IPCC 2014. *Climate Change 2014 – Impacts, Adaptation and Vulnerability: Part A: Global and Sectoral Aspects: Working Group II Contribution to the IPCC Fifth Assessment Report: Volume 1: Global and Sectoral Aspects,* Cambridge, Cambridge University Press.
ISHIDA, K., GORGUNER, M., ERCAN, A., TRINH, T. & KAVVAS, M. L. 2017. Trend analysis of watershed-scale precipitation over Northern California by means of dynamically-downscaled CMIP5 future climate projections. *Science of The Total Environment,* 592**,** 12-24.
Karla Panchuk (2017) CC BY 4.0
KELSEY, A. M., MENK, F. W. & MOSS, P. T. 2015. An astronomical correspondence to the 1470 year cycle of abrupt climate change. *Clim. Past Discuss.,* 2015**,** 4895-4915.
KENDALL, M. G. 1975. *Rank correlation methods,* London, Griffin.
KHEDIMALLAH, A., MEDDI, M. & MAHE, G. 2020. Characterization of the interannual variability of precipitation and runoff in the Cheliff and Medjerda basins (Algeria). *Journal of Earth System Science,* 129.
KIM, J.-H., MEGGERS, H., RIMBU, N., LOHMANN, G., FREUDENTHAL, T., MÜLLER, P. J. & SCHNEIDER, R. R. 2007. Impacts of the North Atlantic gyre circulation on Holocene climate off northwest Africa. *Geology,* 35**,** 387-390.
KNUTSON, T. R., MCBRIDE, J. L., CHAN, J., EMANUEL, K., HOLLAND, G., LANDSEA, C., HELD, I., KOSSIN, J. P., SRIVASTAVA, A. K. & SUGI, M. 2010. Tropical cyclones and climate change. *Nature Geoscience,* 3**,** 157-163.
LAMBECK, K., ESAT, T. M. & POTTER, E.-K. 2002. Links between climate and sea levels for the past three million years. *Nature,* 419**,** 199-206.
LIU, L., WAN, W., CHEN, Y. & LE, H. 2011. Solar activity effects of the ionosphere: A brief review. *Chinese Science Bulletin,* 56**,** 1202-1211.
LOUADI, K., TERZO, M., BENACHOUR, K., BERCHI, S., SIHEM, A., MAGHNI, N. & BENARFA, N. 2008. Les Hyménoptères Apoidea de l'Algérie orientale avec une

liste d'espèces et comparaison avec les faunes ouest-paléarctiques. *Bulletin de la Société entomologique de France,* 113**,** 459-472.

LU, J., VECCHI, G. A. & REICHLER, T. 2007. Expansion of the Hadley cell under global warming. *Geophysical Research Letters,* 34.

MADSEN, H., LAWRENCE, D., LANG, M., MARTINKOVA, M. & KJELDSEN, T. R. 2014. Review of trend analysis and climate change projections of extreme precipitation and floods in Europe. *Journal of Hydrology,* 519**,** 3634-3650.

MAHE, G., LIENOU, G., DESCROIX, L., BAMBA, F., PATUREL, J. E., LARAQUE, A., MEDDI, M., HABAIEB, H., ADEAGA, O., DIEULIN, C., CHAHNEZ KOTTI, F. & KHOMSI, K. 2013. The rivers of Africa: witness of climate change and human impact on the environment. *Hydrological Processes,* 27**,** 2105-2114.

MANN, H. B. 1945. Nonparametric Tests Against Trend. *Econometrica,* 13**,** 245-259.

MANN, M. E. & EMANUEL, K. A. 2006. Atlantic hurricane trends linked to climate change. *Eos, Transactions American Geophysical Union,* 87**,** 233-241.

MARSOOLI, R., LIN, N., EMANUEL, K. & FENG, K. 2019. Climate change exacerbates hurricane flood hazards along US Atlantic and Gulf Coasts in spatially varying patterns. *Nature Communications,* 10**,** 3785.

MARTINEZ, L. H. 2005. POST INDUSTRIAL REVOLUTION HUMAN ACTIVITY AND CLIMATE CHANGE: WHY THE UNITED STATES MUST IMPLEMENT MANDATORY LIMITS ON INDUSTRIAL GREENHOUSE GAS EMMISSIONS. *Journal of Land Use & Environmental Law,* 20**,** 403-421.

MEDDI, M., ASSANI, A. & MEDDI, H. 2010a. Temporal Variability of Annual Rainfall in the Macta and Tafna Catchments, Northwestern Algeria. *Water Resources Management,* 24**,** 3817-3833.

MEDDI, M. & MEDDI, H. 2007. VARIABILITE SPATIALE ET TEMPORELLE DES PRECIPITATIONS DU NORD-OUEST DE L'ALGERIE. *Geographia Technica,* 2**,** 49-55.

MEDDI, M. & TALIA, A. 2008. Pluviometric Regime Evolution in the North of Algeria. *Arab Gulf Journal of Scientific Research,* 26**,** 152-162.

MEDDI, M. M., ASSANI, A. A. & MEDDI, H. 2010b. Temporal Variability of Annual Rainfall in the Macta and Tafna Catchments, Northwestern Algeria. *Water Resources Management,* 24**,** 3817-3833.

MEDJERAB, A. & HENIA, L. 2005. Régionalisation des pluies annuelles dans l'Algérie nord-occidentaleRegionalisation of annual rainfall in the north-western parts of Algeria.Regionalisierung des Jahresniederschlags im Nordwesten Algerien. *Revue Géographique de l'Est,* 45.

MEEHL, G. A., HU, A., TEBALDI, C., ARBLASTER, J. M., WASHINGTON, W. M., TENG, H., SANDERSON, B. M., AULT, T., STRAND, W. G. & WHITE, J. B. 2012. Relative outcomes of climate change mitigation related to global temperature versus sea-level rise. *Nature Climate Change,* 2**,** 576-580.

MERABTI, A., MEDDI, M., MARTINS, D. S. & PEREIRA, L. S. 2018. Comparing SPI and RDI Applied at Local Scale as Influenced by Climate. *Water Resources Management,* 32**,** 1071-1085.

MIKE, H., RUTH, D., TODD, N., MARK, N. & DAVID, L. 2001. African climate change: 1900-2100. *Climate Research,* 17**,** 145-168.

MILLAR, C. I. & WOOLFENDEN, W. B. 1999. The role of climate change in interpreting historical variability. *Ecological Applications,* 9**,** 1207-1216.

MIMURA, N. 2013. Sea-level rise caused by climate change and its implications for society. *Proceedings of the Japan Academy. Series B, Physical and biological sciences,* 89**,** 281-301.

MORRIS, S. S., NEIDECKER-GONZALES, O., CARLETTO, C., MUNGUíA, M., MEDINA, J. M. & WODON, Q. 2002. Hurricane Mitch and the Livelihoods of the Rural Poor in Honduras. *World Development,* 30**,** 49-60.

NASA. 2020. *Global Temperature* [Online]. Available: https://climate.nasa.gov/vital-signs/global-temperature/

NEW, M., TODD, M., HULME, M. & JONES, P. 2001. Precipitation measurements and trends in the twentieth century. *International Journal of Climatology,* 21**,** 1889-1922.

NICHOLLS, R. J. 2011. Planning for the Impacts of Sea Level Rise. *Oceanography,* 24**,** 144-157.

NICHOLSON, S. E., FUNK, C. & FINK, A. H. 2018. Rainfall over the African continent from the 19th through the 21st century. *Global and Planetary Change,* 165**,** 114-127.

NOAA.

NOUACEUR, Z. & MURĂRESCU, O. 2016. Rainfall Variability and Trend Analysis of Annual Rainfall in North Africa. *International Journal of Atmospheric Sciences,* 2016**,** 7230450.

OGILVIE, A. E. J. & JÓNSSON, T. 2001. "Little Ice Age" Research: A Perspective from Iceland. *Climatic Change,* 48**,** 9-52.

OLI BROWN, C. S. E. N. 2019. CLIMATE-FRAGILITY RISK BRIEF NORTH AFRICA & SAHEL. Available: https://climate-security-expert-network.org/sites/climate-security-expert-network.com/files/documents/csen_climate_fragility_risk_brief_-_north_africa_sahel_.pdf.

PAILLARD, D. 2010. Climate and the orbital parameters of the Earth. *Comptes Rendus Geoscience,* 342**,** 273-285.

PHILANDER, S. G. 2018. 9. El Niño, La Niña, and the Southern Oscillation
Is the Temperature Rising? : Princeton University Press.
PINAULT, J.-L. 2012. Global warming and rainfall oscillation in the 5–10 yr band in Western Europe and Eastern North America. *Climatic Change,* 114**,** 621-650.
QUINN, T. R., TREMAINE, S. & DUNCAN, M. 1991. A three million year integration of the Earth's orbit. *The Astronomical Journal,* 101**,** 2287-2305.
RADABAUGH, K. R., MOYER, R. P., CHAPPEL, A. R., DONTIS, E. E., RUSSO, C. E., JOYSE, K. M., BOWNIK, M. W., GOECKNER, A. H. & KHAN, N. S. 2020. Mangrove Damage, Delayed Mortality, and Early Recovery Following Hurricane Irma at Two Landfall Sites in Southwest Florida, USA. *Estuaries and Coasts,* 43**,** 1104-1118.
RAE, A. 2014. Trend Analysis. *In:* MICHALOS, A. C. (ed.) *Encyclopedia of Quality of Life and Well-Being Research.* Dordrecht: Springer Netherlands.
REN, L., ARKIN, P., SMITH, T. & SHEN, S. 2013. Global precipitation trends in 1900–2005 from a reconstruction and coupled model simulations. *Journal of Geophysical Research: Atmospheres,* 118.
SAHNOUNE, F., BELHAMEL, M., ZELMAT, M. & KERBACHI, R. 2013. Climate Change in Algeria: Vulnerability and Strategy of Mitigation and Adaptation. *Energy Procedia,* 36**,** 1286-1294.
SATTLER, D. N., WHIPPY, A., GRAHAM, J. M. & JOHNSON, J. 2018. A Psychological Model of Climate Change Adaptation: Influence of Resource Loss, Posttraumatic Growth, Norms, and Risk Perception Following Cyclone Winston in Fiji. *In:* LEAL FILHO, W. (ed.) *Climate Change Impacts and Adaptation Strategies for Coastal Communities.* Cham: Springer International Publishing.
SCHILLING, J., HERTIG, E., TRAMBLAY, Y. & SCHEFFRAN, J. 2020. Climate change vulnerability, water resources and social implications in North Africa. *Regional Environmental Change,* 20**,** 15.
SCHMIDT, G., RUEDY, R., HANSEN, J., ALEINOV, I., BELL, N., BAUER, M., BAUER, S., CAIRNS, B., CANUTO, V., CHENG, Y., DELGENIO, A., FALUVEGI, G., FRIEND, A., HALL, T., HU, Y., KELLEY, M., KIANG, N., KOCH, D., LACIS, A. & YAO, M.-S. 2006. Present-Day Atmospheric Simulations Using GISS ModelE: Comparison to In Situ, Satellite, and Reanalysis Data. *Journal of Climate,* 19**,** 153.
SELESHI, Y. & ZANKE, U. 2004. Recent changes in rainfall and rainy days in Ethiopia. *International Journal of Climatology,* 24**,** 973-983.
ŞEN 2017 <Zekâi-Şen-auth.-Innovative-Trend-Methodologies-in-Science-and-Engineering-Springer-International-Publishing-2017.pdf>.

SEN, P. K. 1968. Estimates of the Regression Coefficient Based on Kendall's Tau. *Journal of the American Statistical Association,* 63**,** 1379-1389.

ŞEN, Z. 2012. Innovative Trend Analysis Methodology. *Journal of Hydrologic Engineering,* 17**,** 1042-1046.

ŞEN, Z. 2015. Chapter Two - Basic Drought Indicators. *In:* ŞEN, Z. (ed.) *Applied Drought Modeling, Prediction, and Mitigation.* Boston: Elsevier.

ŞEN, Z. 2017. *Innovative Trend Methodologies in Science and Engineering*.

ŞEN, Z. 2019. *Earth Systems Data Processing and Visualization Using MATLAB*, Springer International Publishing.

ŞEN, Z., MOHORJI, A. M. & ALMAZROUI, M. 2017. Engineering risk assessment on water structures under climate change effects. *Arabian Journal of Geosciences,* 10**,** 517.

ŞEN, Z., ŞIŞMAN, E. & DABANLI, I. 2019. Innovative Polygon Trend Analysis (IPTA) and applications. *Journal of Hydrology,* 575**,** 202-210.

SHEA, J. J. 2008. Transitions or turnovers? Climatically-forced extinctions of Homo sapiens and Neanderthals in the east Mediterranean Levant. *Quaternary Science Reviews,* 27**,** 2253-2270.

SMITH, T., ARKIN, P., REN, L. & SHEN, S. 2012. Improved Reconstruction of Global Precipitation since 1900. *Journal of Atmospheric and Oceanic Technology,* 29**,** 1505-1517.

STAGL, J., MAYR, E., KOCH, H., HATTERMANN, F. F. & HUANG, S. 2014. Effects of Climate Change on the Hydrological Cycle in Central and Eastern Europe. *In:* RANNOW, S. & NEUBERT, M. (eds.) *Managing Protected Areas in Central and Eastern Europe Under Climate Change.* Dordrecht: Springer Netherlands.

STAUBWASSER, M., DRĂGUȘIN, V., ONAC, B. P., ASSONOV, S., ERSEK, V., HOFFMANN, D. L. & VERES, D. 2018. Impact of climate change on the transition of Neanderthals to modern humans in Europe. *Proceedings of the National Academy of Sciences,* 115**,** 9116.

STERN, N. & RYDGE, J. 2012. The New Energy-industrial Revolution and International Agreement on Climate Change. *Economics of Energy & Environmental Policy,* 1**,** 101-120.

Steven Earle (2015) CC BY 4.0

STOTHERS, R. B. 1984. The Great Tambora Eruption in 1815 and Its Aftermath. *Science,* 224**,** 1191.

TAÏBI, S., MEDDI, M., DOUDJA, S.-G. & MAHE, G. 2013. Evolution et régionalisation des précipitations au nord de l'Algérie (1936–2009). *IAHS Publ.,* 359**,** 191-197.

TAÏBI, S., MEDDI, M. & MAHE, G. 2018. Seasonal rainfall variability in the southern Mediterranean border: Observations, regional model simulations and future climate projections. *Atmosfera,* 32**,** 39-54.

TAÏBI, S., MEDDI, M. & MAHÉ, G. 2019. Seasonal rainfall variability in the southern Mediterranean border: Observations, regional model simulations and future climate projections. *Atmosfera,* 32**,** 39-54.

TAKEMI, T., ITO, R. & ARAKAWA, O. 2016. Effects of global warming on the impacts of Typhoon Mireille (1991) in the Kyushu and Tohoku regions. *Hydrological Research Letters,* 10**,** 81-87.

THORNE, P. W., LANZANTE, J. R., PETERSON, T. C., SEIDEL, D. J. & SHINE, K. P. 2011. Tropospheric temperature trends: history of an ongoing controversy. *WIREs Climate Change,* 2**,** 66-88.

TRAMBLAY, Y., JARLAN, L., HANICH, L. & SOMOT, S. 2018. Future Scenarios of Surface Water Resources Availability in North African Dams. *Water Resources Management,* 32**,** 1291-1306.

TRENBERTH, K. 2011. Changes in Precipitation with Climate Change. Climate Change Research. *Climate Research,* 47**,** 123-138.

TRENBERTH, K. E. 1998. Atmospheric Moisture Residence Times and Cycling: Implications for Rainfall Rates and Climate Change. *Climatic Change,* 39**,** 667-694.

VAN AALST, M. K. 2006. The impacts of climate change on the risk of natural disasters. *Disasters,* 30**,** 5-18.

WALSH, K. J. E., MCINNES, K. L. & MCBRIDE, J. L. 2012. Climate change impacts on tropical cyclones and extreme sea levels in the South Pacific — A regional assessment. *Global and Planetary Change,* 80-81**,** 149-164.

WANG, X., HUI, B., WAN, H., ZWIERS, F., SWAIL, V., COMPO, G., ROBERT, B., ALLAN, J., VOSE, R., SYLVIE, B., BULLET, J. & YIN, X. 2011. Trends and low-frequency variability of storminess over western Europe, 1878-2007. *Climate Dynamics,* 37**,** 2355-2371.

WILLOUGHBY, H. & BLACK, P. 1996. Hurricane Andrew in Florida: Dynamics of a Disaster. *Bulletin of The American Meteorological Society - BULL AMER METEOROL SOC,* 77**,** 543-652.

WU, P., CHRISTIDIS, N. & STOTT, P. 2013. Anthropogenic Impact on Earth's Hydrological Cycle. *Nature Climate Change,* 3**,** 807-810.

WUNDERLE, J. M., JR., LODGE, D. J. & WAIDE, R. B. 1992. Short-Term Effects of Hurricane Gilbert on Terrestrial Bird Populations on Jamaica. *The Auk,* 109**,** 148-166.

XIA, X., WU, Q., MOU, X. L. & LAI, Y. 2015. Potential Impacts of Climate Change on the Water Quality of Different Water Bodies. *Journal of Environmental Informatics,* 25**,** 85-98.

ZEROUAL, A., ASSANI, A. A., MEDDI, M. & ALKAMA, R. 2019. Assessment of climate change in Algeria from 1951 to 2098 using the Köppen–Geiger climate classification scheme. *Climate Dynamics,* 52**,** 227-243.

Appendix

8 APPENDIX

8.1 APPENDIX OF CHAPTER III

8.1.1 MATLAB program

```
function [V,I] = ProbabilityDistributionFunctionChoice(D,Xtitle,StName)
% Istanbul Technical University e-mail:zsen@itu.edu.tr
% This program produces Intensity-frequency curve for any given time
% duration
% D            : Time series data
% Xtitle        :Time series data variable name with unit
% R            : Risk levels
% StName         : Station name
% V            : It is the least sum of squares of probability deviations
%               from the theoretical probability distribution
% I            : The number of PDF
%               If I = 1 Gamma PDF
%               If I = 2 Log-Normal PDF
%               If I = 3 Extreme value (Gumbel)PDF
%               If I = 4 Generalized extreme value (Pearson III)PDF
%               If I = 5 Weibull PDF
Risk=0.001:0.001:0.999;
R=[1-Risk(500) 1-Risk(200) 1-Risk(100) 1-Risk(40) 1-Risk(20) 1-Risk(10) 1-Risk(4) 1-
Risk(2)];
n=length(D);
DM=1.1*max(D);
Dm=min(D);
x=Dm:0.1:DM;
pp=(1:1:n)/(n+1); % Data probability in ascending order
p=1-pp'; % Data probability in descending order
SD=sort(D); % Sorted time series in ascending order
pgam=gamfit(D); % Gamma PDF parameters
ygam=1-gamcdf(x,pgam(1),pgam(2));
ptgam=1-gamcdf(SD,pgam(1),pgam(2));
ppt2gam=(p-ptgam).^2;
GTest=mean(ppt2gam);
plon=lognfit(D); % Log-Normal PDF parameters
ylon=1-logncdf(x,plon(1),plon(2));
ptlon=1-logncdf(SD,plon(1),plon(2));
ppt2lon=(p-ptlon).^2;
```

```
LNTest=mean(ppt2lon);
pevd=evfit(D); % Extreme value PDF parameters
yevd=1-evcdf(x,pevd(1),pevd(2));
ptevd=1-evcdf(SD,pevd(1),pevd(2));
ppt2evd=(p-ptevd).^2;
EVTest=mean(ppt2evd);
pgev=gevfit(D); % Generalized extreme value PDF parameters
ygev=1-gevcdf(x,pgev(1),pgev(2),pgev(3));
ptgev=1-gevcdf(SD,pgev(1),pgev(2),pgev(3));
ppt2gev=(p-ptgev).^2;
GEVTest=mean(ppt2gev);
pwbl=wblfit(D); % Weibull PDF parameters
ywbl=1-wblcdf(x,pwbl(1),pwbl(2));
ptwbl=1-wblcdf(SD,pwbl(1),pwbl(2));
ppt2wbl=(p-ptwbl).^2;
WBLTest=mean(ppt2wbl);
rgam=gaminv(R,pgam(1),pgam(2));
rlon=logninv(R,plon(1),plon(2));
revd=evinv(R,pevd(1),pevd(2));
rgev=gevinv(R,pgev(1),pgev(2),pgev(3));
rwbl=wblinv(R,pwbl(1),pwbl(2));
[V I]=min([GTest LNTest EVTest GEVTest WBLTest]);
if I == 1
   yf=ygam;
   rf=rgam;
   pr=pgam;
   PR='Gamma PDF';
   elseif I ==2
      yf=ylon;
      rf=rlon;
      pr=plon;
      PR='Log-normal PDF';
      elseif I == 3
         yf=yevd;
         rf=revd;
         pr=pevd;
         PR='Gumbel';
elseif I == 4
   yf=ygev;
   rf=rgev;
   pr=pgev;
   PR='Pearson PD';
else
   yf=ywbl;
```

```
    rf=rwbl;
    pr=pwbl;
    PR='Weibull PDF';
end
figure
scatter(SD,p,'k*')
title(StName)
xlabel(Xtitle)
ylabel('Exceedence probability')
hold on
grid on
box on
plot(x,yf,'LineWidth',2,'Color','r') % Theoretical PDF plot
legend('Data values',PR,'Location','Northeast')
text(DM/2,0.80,['Location parameter = ' num2str(pr(1))])
text(DM/2,0.75,['Scale    parameter   = ' num2str(pr(2))])
text(0.60*DM,0.60,['  2-years = ' num2str(rf(1)),'  mm'])
text(0.60*DM,0.55,['  5-years = ' num2str(rf(2)),'  mm'])
text(0.60*DM,0.50,[' 10-years = ' num2str(rf(3)),'  mm'])
text(0.60*DM,0.45,[' 25-years = ' num2str(rf(4)),'  mm'])
text(0.60*DM,0.40,[' 50-years = ' num2str(rf(5)),'  mm'])
text(0.60*DM,0.35,['100-years = ' num2str(rf(6)),'  mm'])
text(0.60*DM,0.30,['250-years = ' num2str(rf(7)),'  mm'])
text(0.60*DM,0.25,['500-years = ' num2str(rf(8)),'  mm'])
if I == 4
    text(DM/2,0.70,['Shape parameter = ' num2str(pr(3))])
else
end
end
```

8.1.2 : Precipitation time series plots with CDF curves

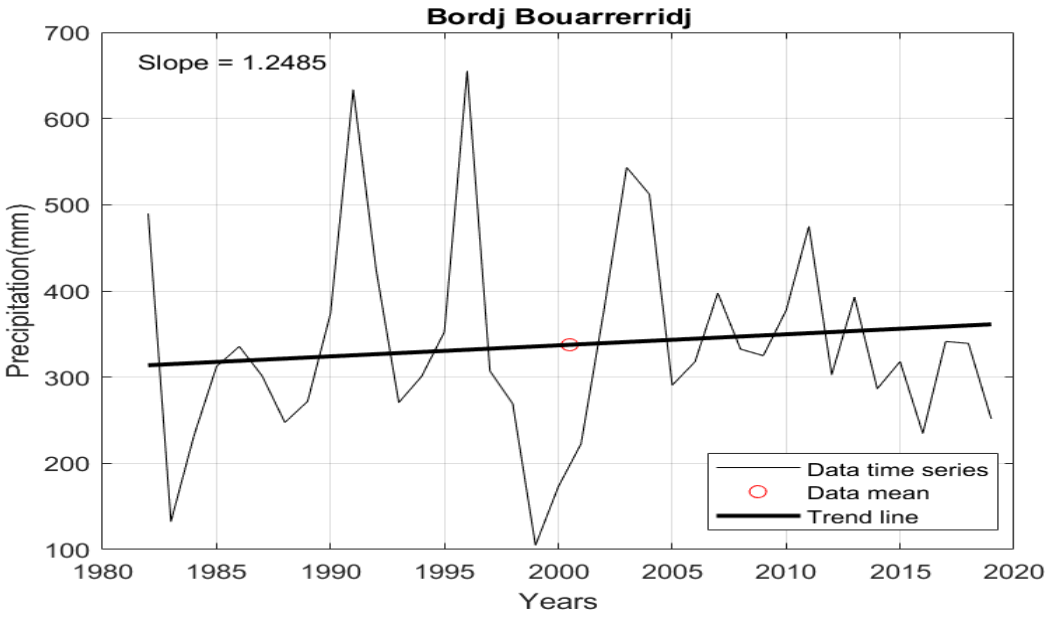

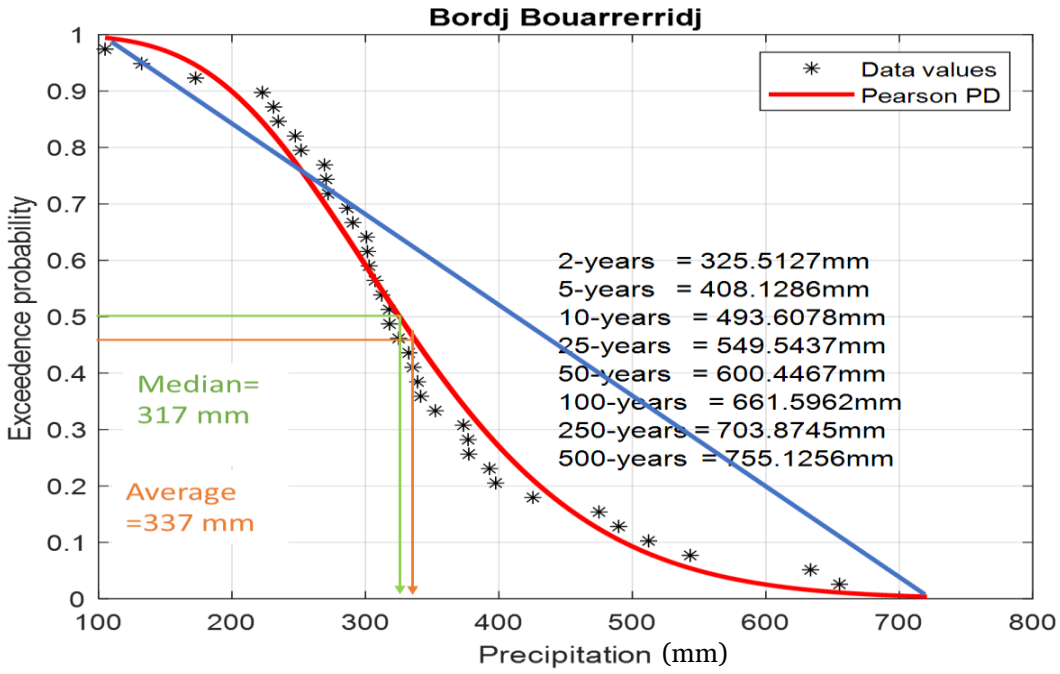

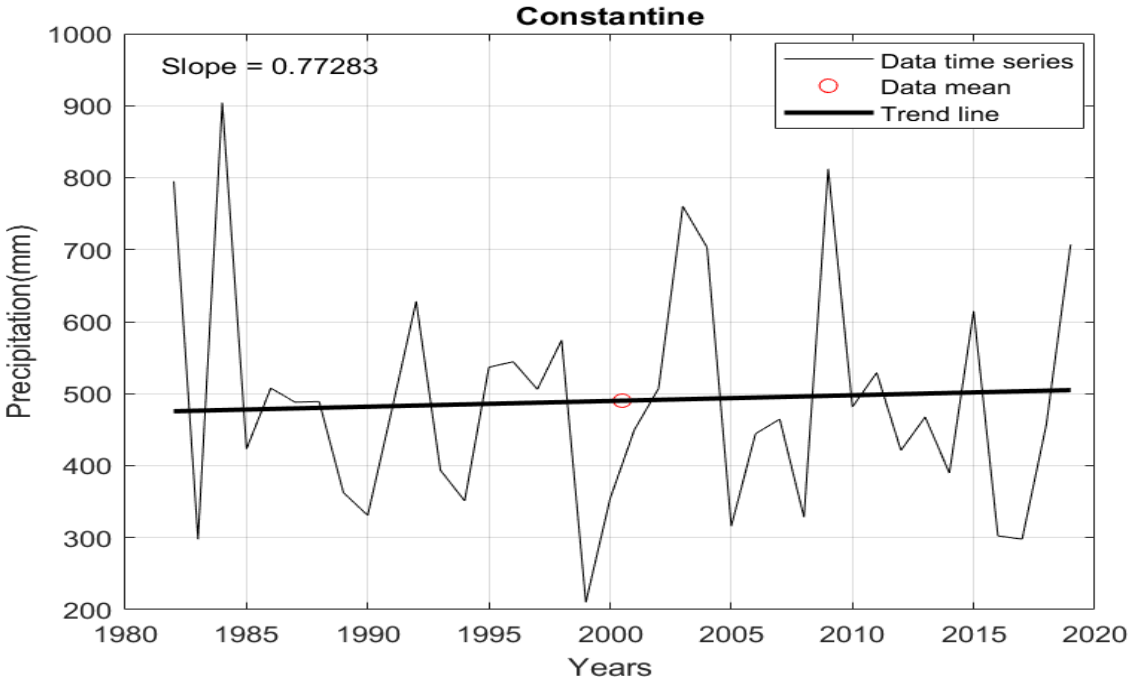
Constantine
Slope = 0.77283
Data time series
Data mean
Trend line
Precipitation(mm)
Years
1000
900
800
700
600
500
400
300
200
1980
1985
1990
1995
2000
2005
2010
2015
2020

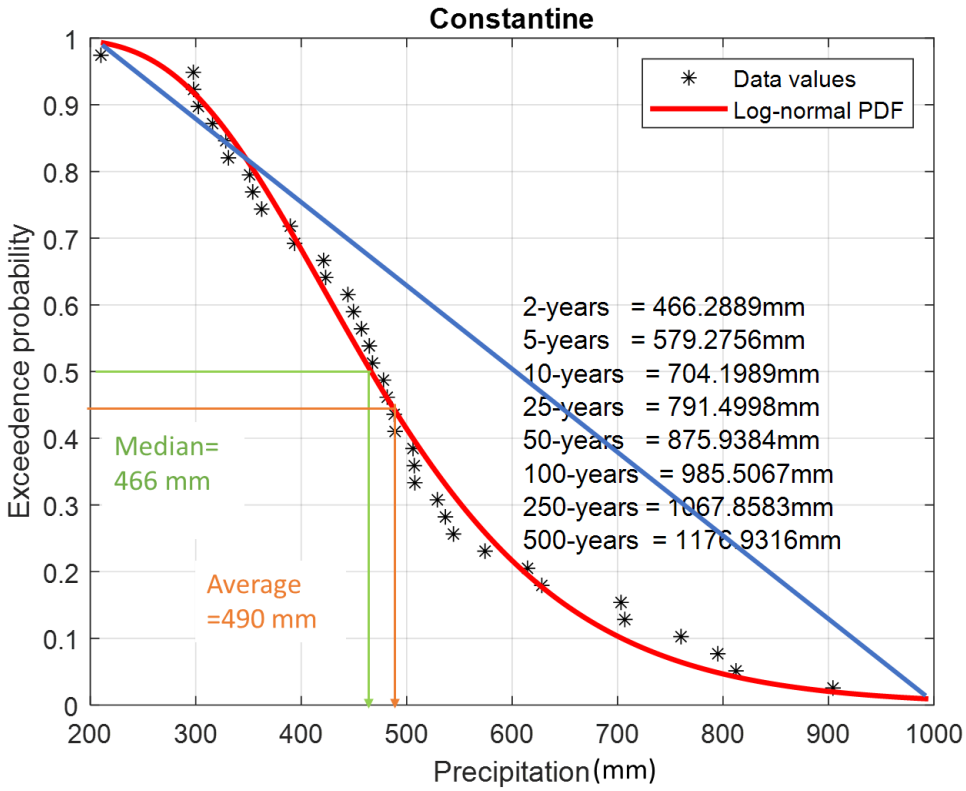
Constantine
Data values
Log-normal PDF
Exceedence probability
Precipitation(mm)
Median=
466 mm
Average
=490 mm
2-years = 466.2889mm
5-years = 579.2756mm
10-years = 704.1989mm
25-years = 791.4998mm
50-years = 875.9384mm
100-years = 985.5067mm
250-years = 1067.8583mm
500-years = 1176.9316mm
1
0.9
0.8
0.7
0.6
0.5
0.4
0.3
0.2
0.1
0
200
300
400
500
600
700
800
900
1000

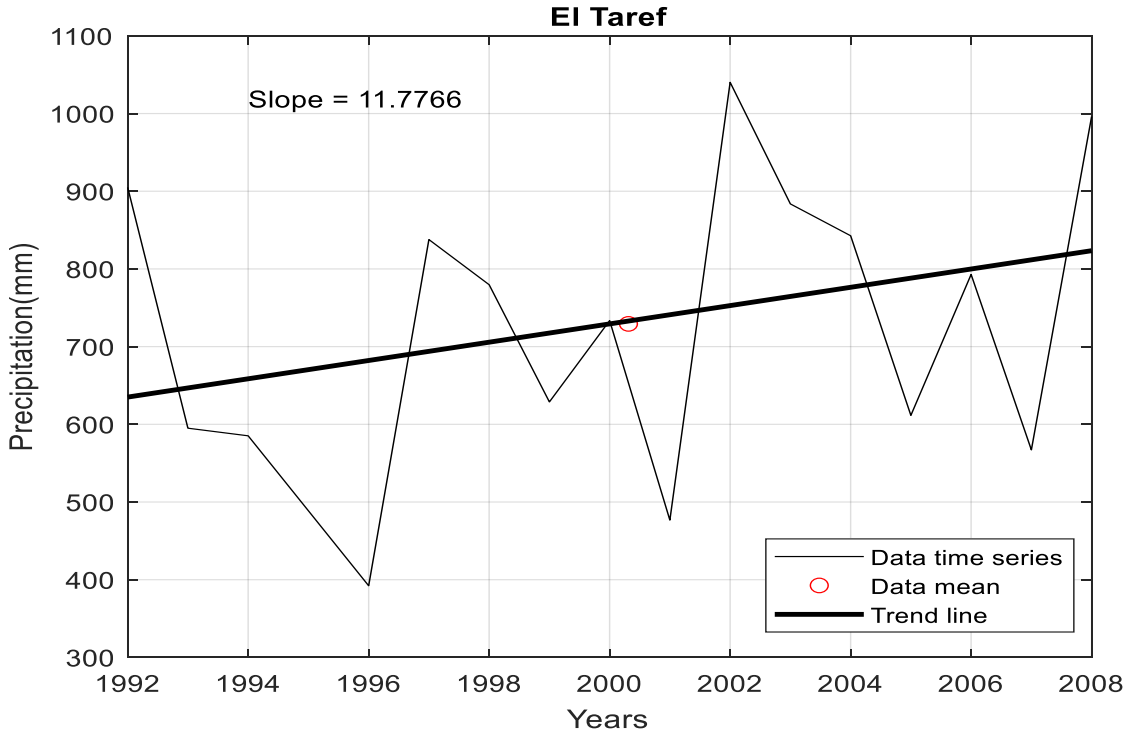
El Taref
Slope = 11.7766
Precipitation(mm)
Years
Data time series
Data mean
Trend line

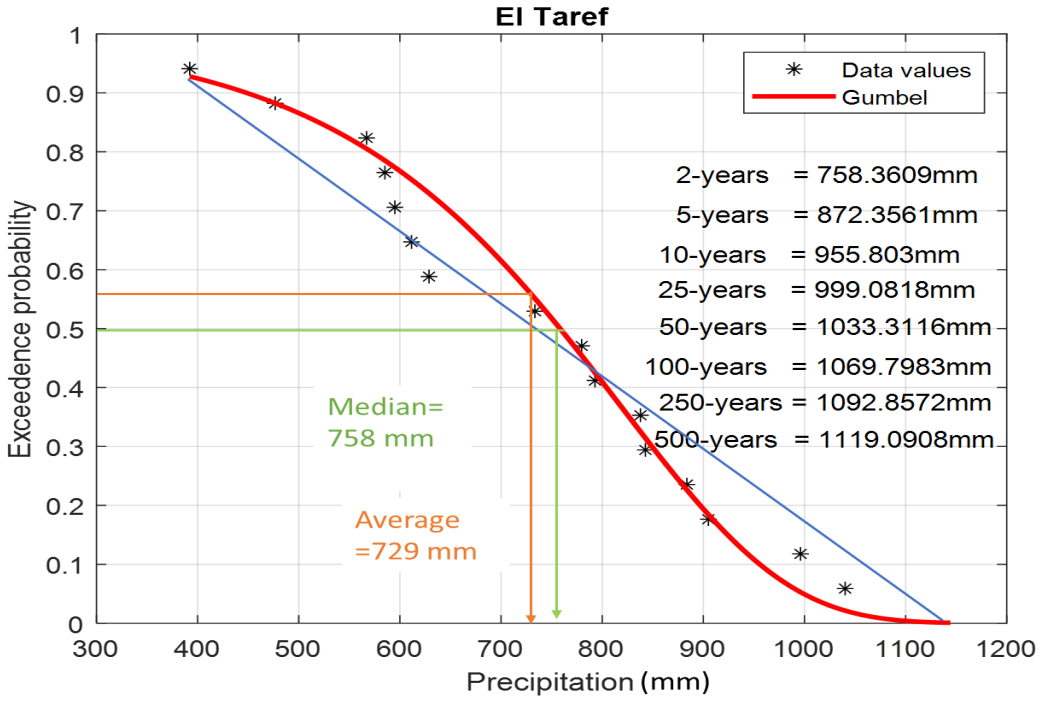
El Taref
Exceedence probability
Precipitation (mm)
Data values
Gumbel
2-years = 758.3609mm
5-years = 872.3561mm
10-years = 955.803mm
25-years = 999.0818mm
50-years = 1033.3116mm
100-years = 1069.7983mm
250-years = 1092.8572mm
500-years = 1119.0908mm
Median= 758 mm
Average =729 mm

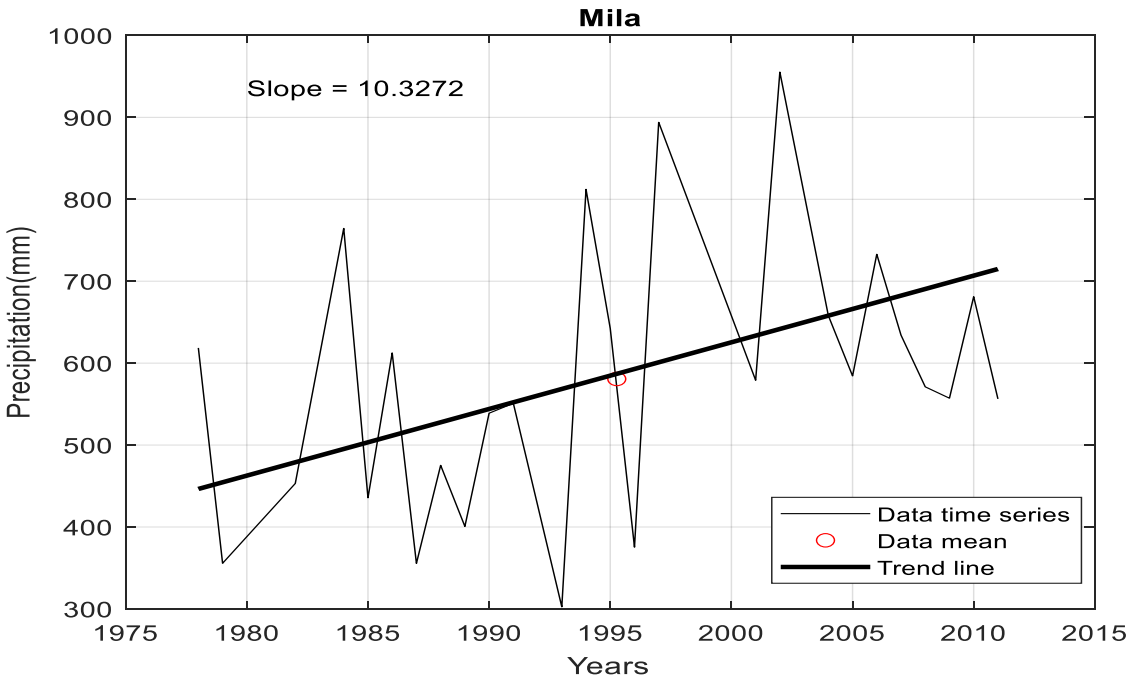
Mila
Slope = 10.3272
Precipitation(mm)
Years
Data time series
Data mean
Trend line

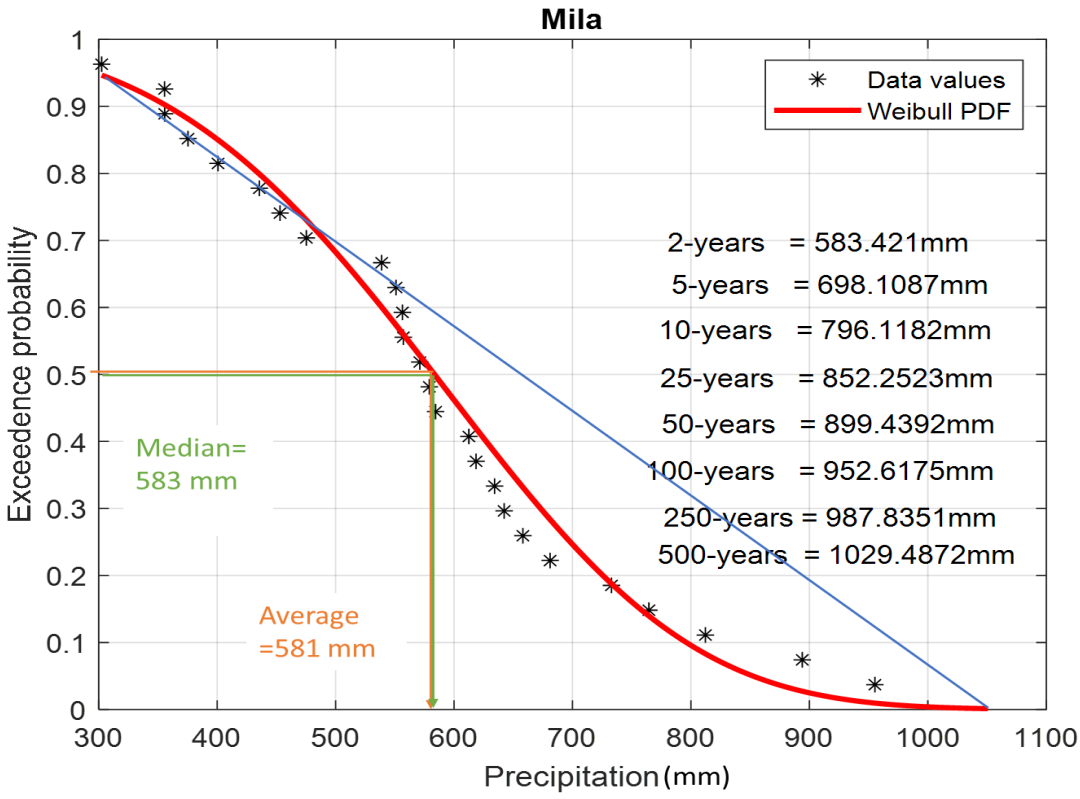
Mila
Data values
Weibull PDF
Exceedence probability
Precipitation (mm)
2-years = 583.421mm
5-years = 698.1087mm
10-years = 796.1182mm
25-years = 852.2523mm
50-years = 899.4392mm
100-years = 952.6175mm
250-years = 987.8351mm
500-years = 1029.4872mm
Median= 583 mm
Average =581 mm

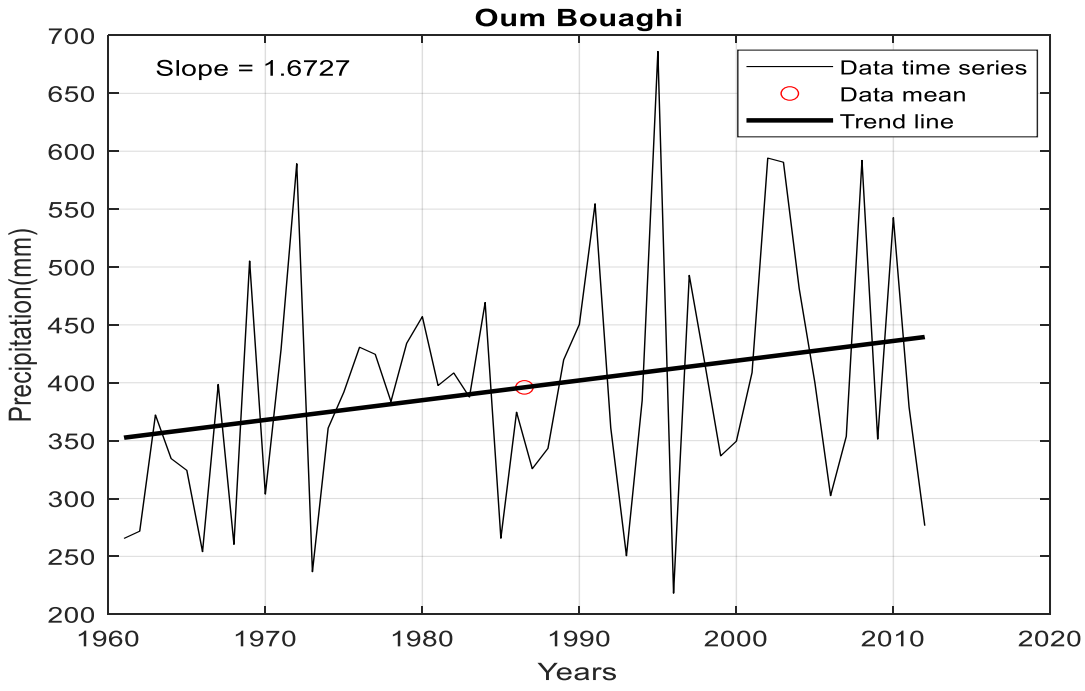
Oum Bouaghi
Slope = 1.6727
Data time series
Data mean
Trend line
Precipitation(mm)
Years
700
650
600
550
500
450
400
350
300
250
200
1960
1970
1980
1990
2000
2010
2020

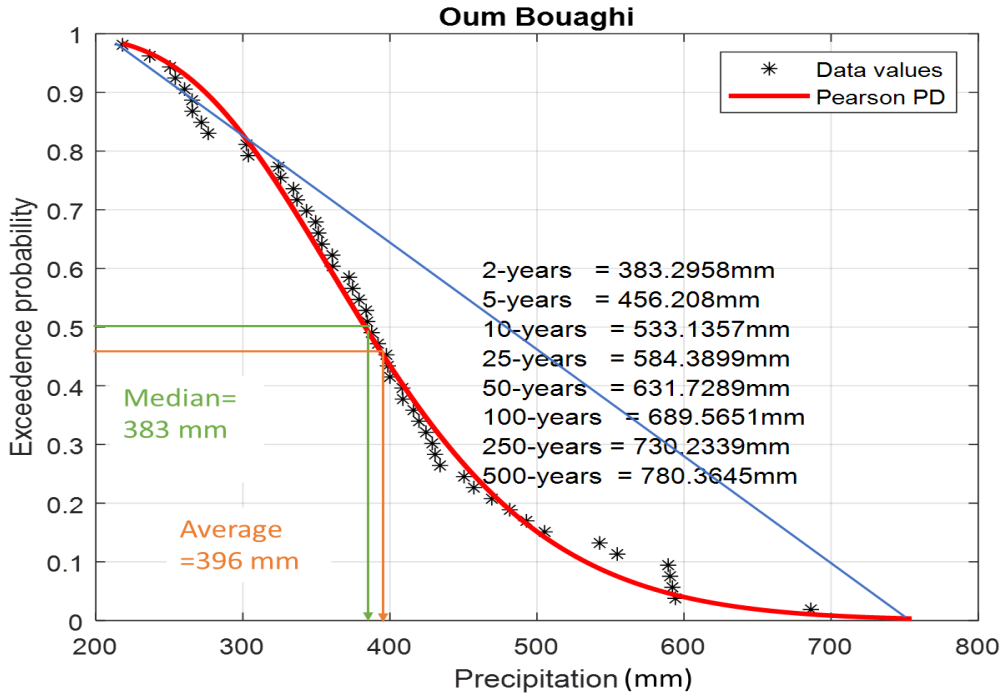
Oum Bouaghi
Data values
Pearson PD
Exceedence probability
Precipitation (mm)
2-years = 383.2958mm
5-years = 456.208mm
10-years = 533.1357mm
25-years = 584.3899mm
50-years = 631.7289mm
100-years = 689.5651mm
250-years = 730.2339mm
500-years = 780.3645mm
Median=
383 mm
Average
=396 mm
1
0.9
0.8
0.7
0.6
0.5
0.4
0.3
0.2
0.1
0
200
300
400
500
600
700
800

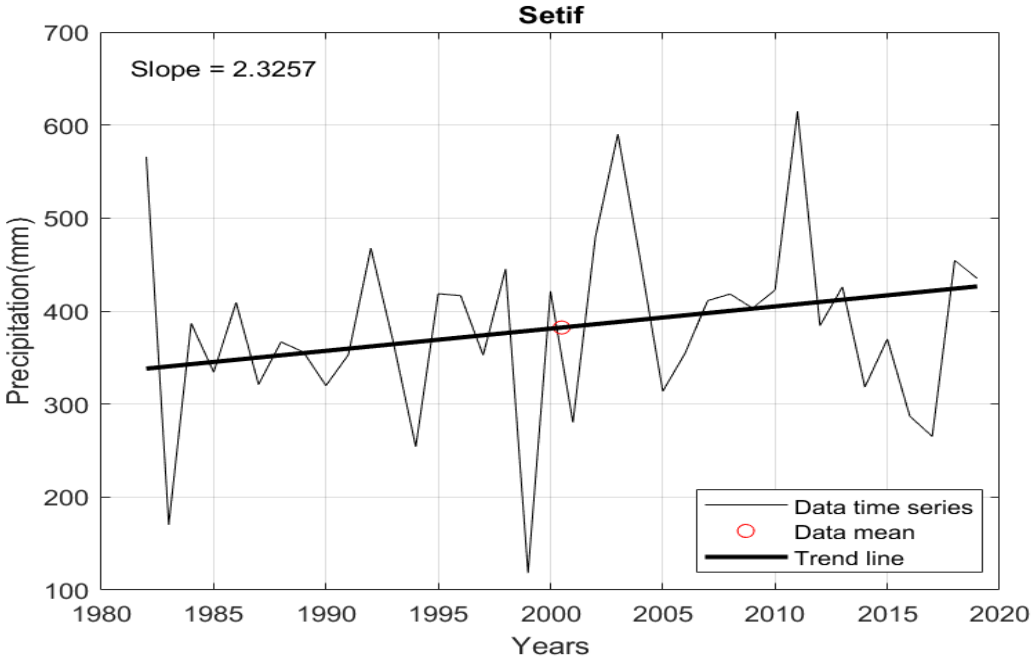
Setif
Slope = 2.3257
Precipitation(mm)
Years
Data time series
Data mean
Trend line

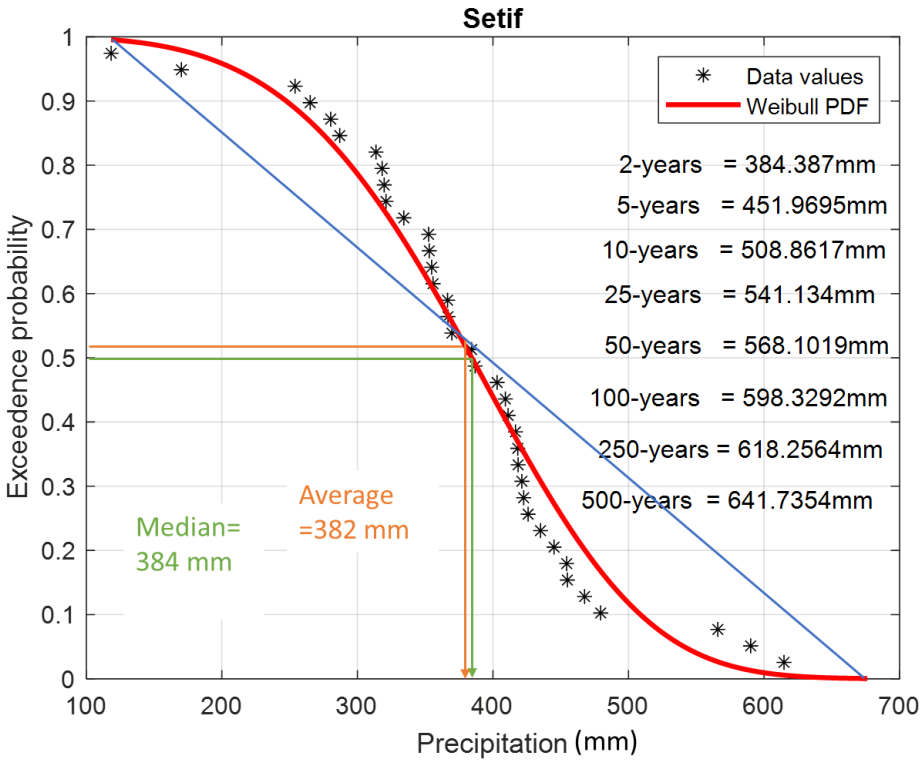
Setif
Exceedence probability
Precipitation (mm)
Data values
Weibull PDF
2-years = 384.387mm
5-years = 451.9695mm
10-years = 508.8617mm
25-years = 541.134mm
50-years = 568.1019mm
100-years = 598.3292mm
250-years = 618.2564mm
500-years = 641.7354mm
Median= 384 mm
Average =382 mm

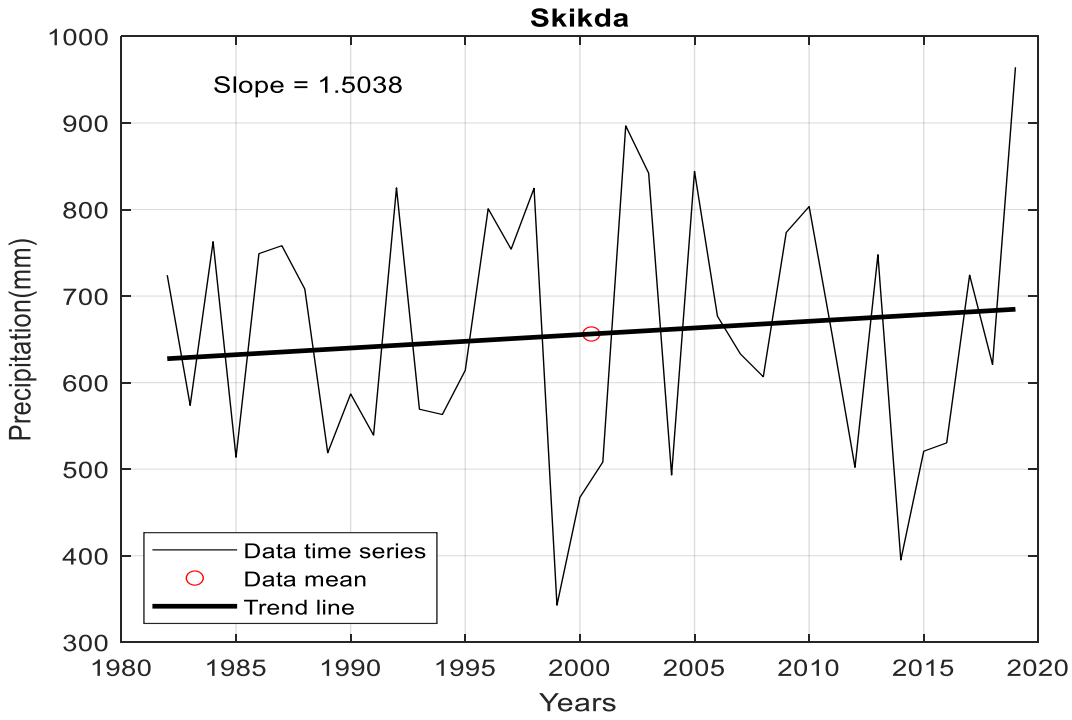
Skikda
Slope = 1.5038
Precipitation(mm)
Years
Data time series
Data mean
Trend line
1000
900
800
700
600
500
400
300
1980
1985
1990
1995
2000
2005
2010
2015
2020

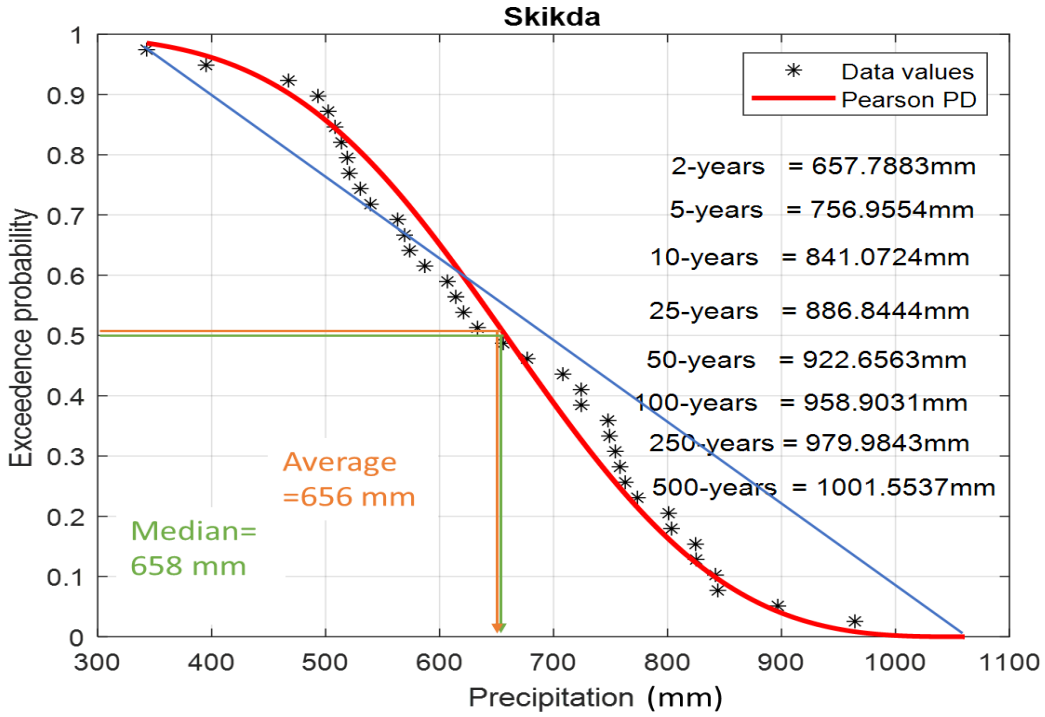
Skikda
Exceedence probability
Precipitation (mm)
Data values
Pearson PD
2-years = 657.7883mm
5-years = 756.9554mm
10-years = 841.0724mm
25-years = 886.8444mm
50-years = 922.6563mm
100-years = 958.9031mm
250-years = 979.9843mm
500-years = 1001.5537mm
Average
=656 mm
Median=
658 mm
1
0.9
0.8
0.7
0.6
0.5
0.4
0.3
0.2
0.1
0
300
400
500
600
700
800
900
1000
1100

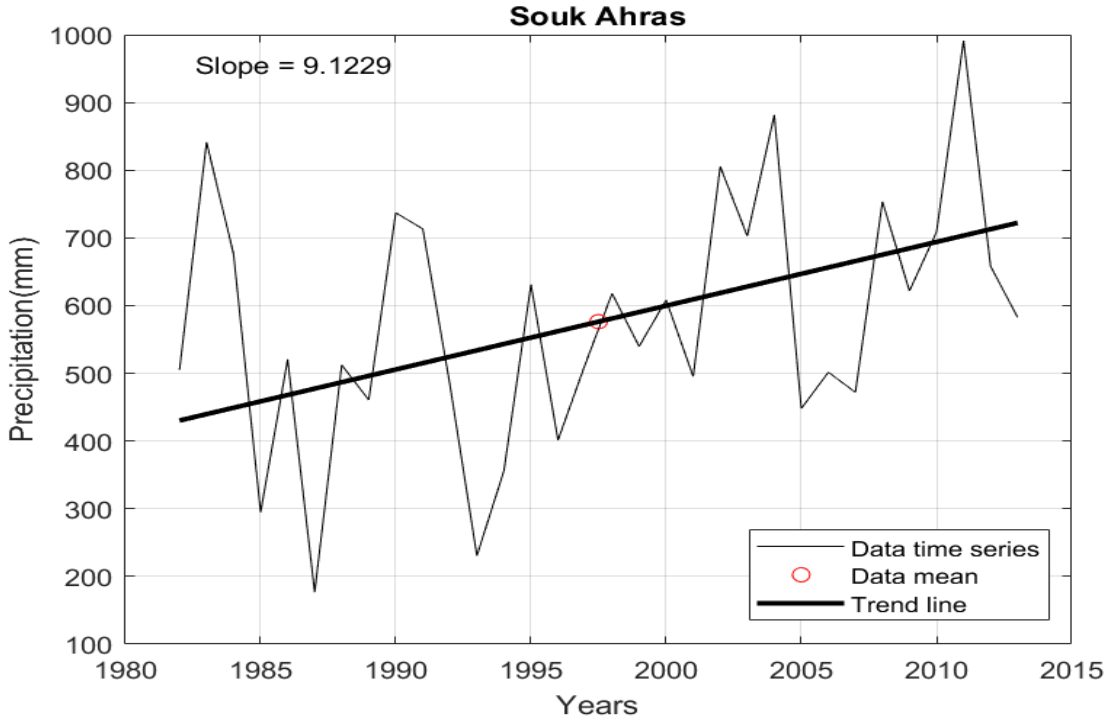
Souk Ahras
Slope = 9.1229
Precipitation(mm)
Years
Data time series
Data mean
Trend line

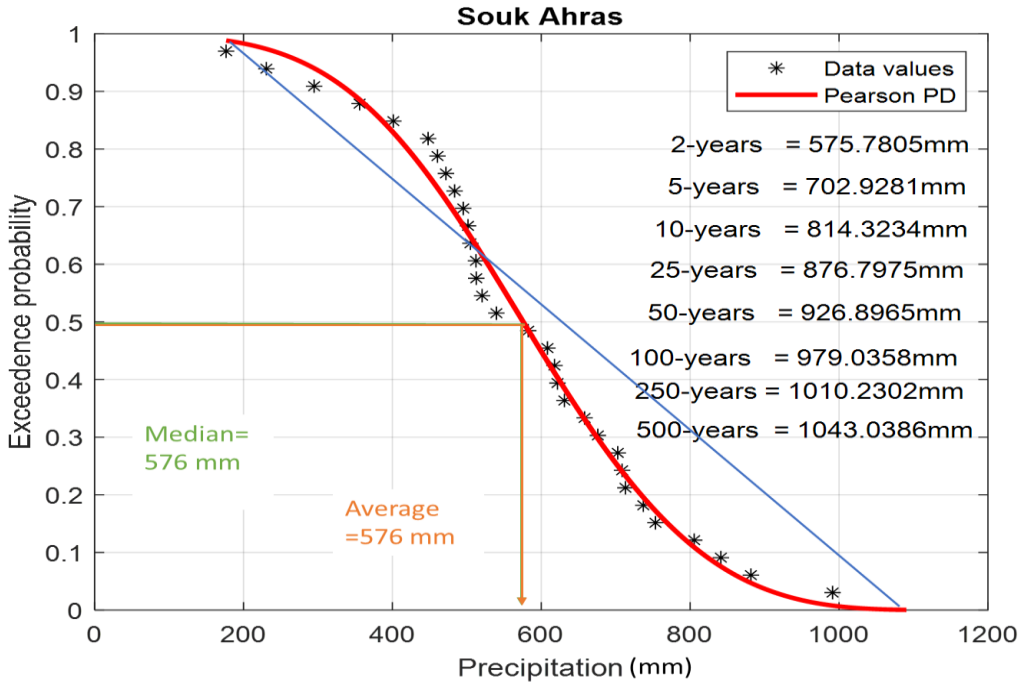
Souk Ahras
Exceedence probability
Precipitation (mm)
Data values
Pearson PD
2-years = 575.7805mm
5-years = 702.9281mm
10-years = 814.3234mm
25-years = 876.7975mm
50-years = 926.8965mm
100-years = 979.0358mm
250-years = 1010.2302mm
500-years = 1043.0386mm
Median= 576 mm
Average =576 mm

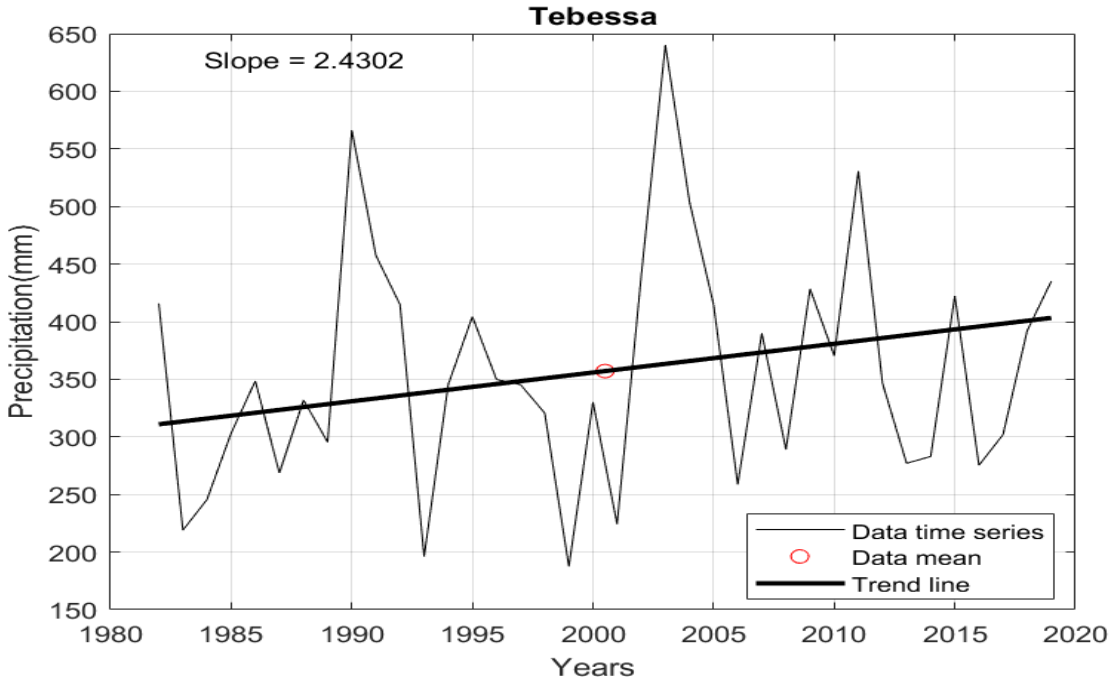
Tebessa
Slope = 2.4302
Precipitation(mm)
Years
Data time series
Data mean
Trend line

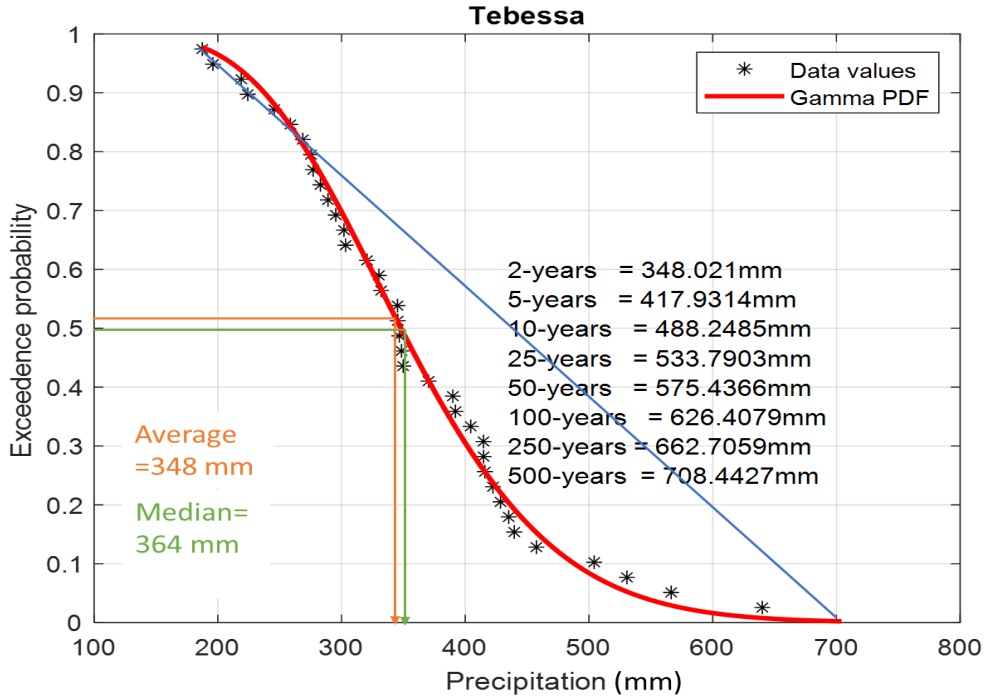
Tebessa
Exceedence probability
Precipitation (mm)
Data values
Gamma PDF
2-years = 348.021mm
5-years = 417.9314mm
10-years = 488.2485mm
25-years = 533.7903mm
50-years = 575.4366mm
100-years = 626.4079mm
250-years = 662.7059mm
500-years = 708.4427mm
Average =348 mm
Median= 364 mm

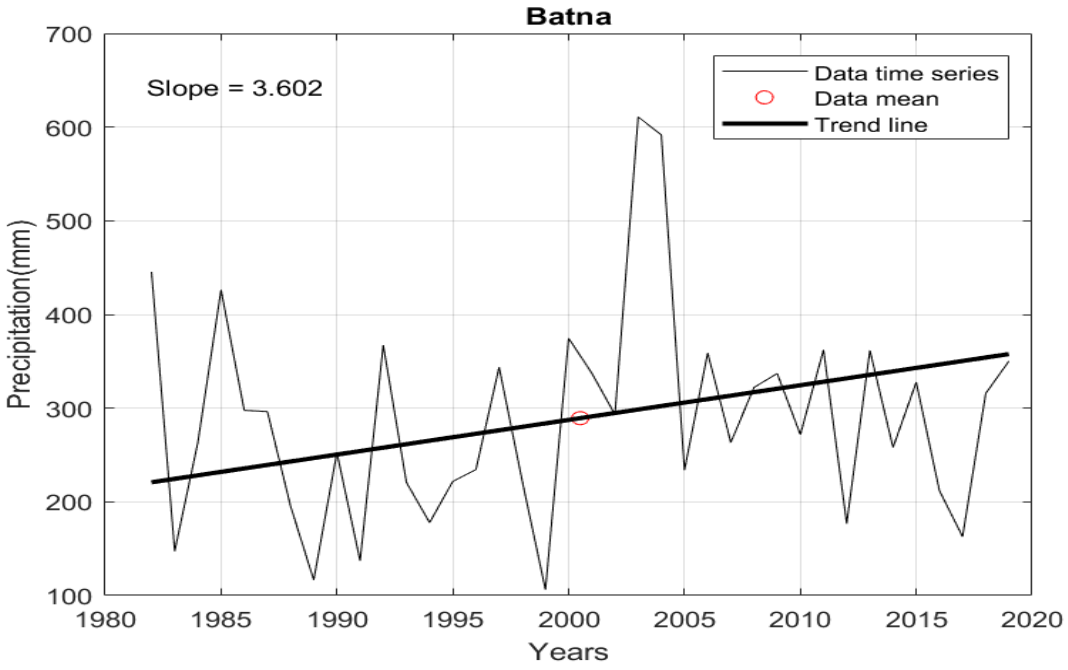
Batna
Slope = 3.602
Data time series
Data mean
Trend line
Precipitation(mm)
Years
700
600
500
400
300
200
100
1980
1985
1990
1995
2000
2005
2010
2015
2020

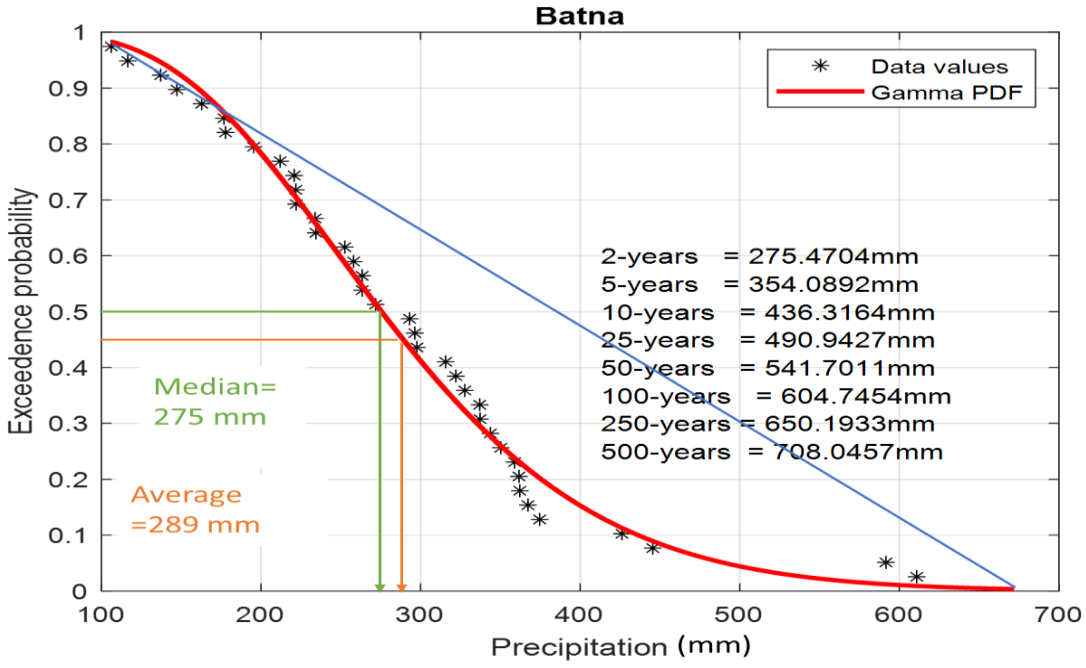
Batna
Data values
Gamma PDF
2-years = 275.4704mm
5-years = 354.0892mm
10-years = 436.3164mm
25-years = 490.9427mm
50-years = 541.7011mm
100-years = 604.7454mm
250-years = 650.1933mm
500-years = 708.0457mm
Median=
275 mm
Average
=289 mm
Exceedence probability
Precipitation (mm)
1
0.9
0.8
0.7
0.6
0.5
0.4
0.3
0.2
0.1
0
100
200
300
400
500
600
700

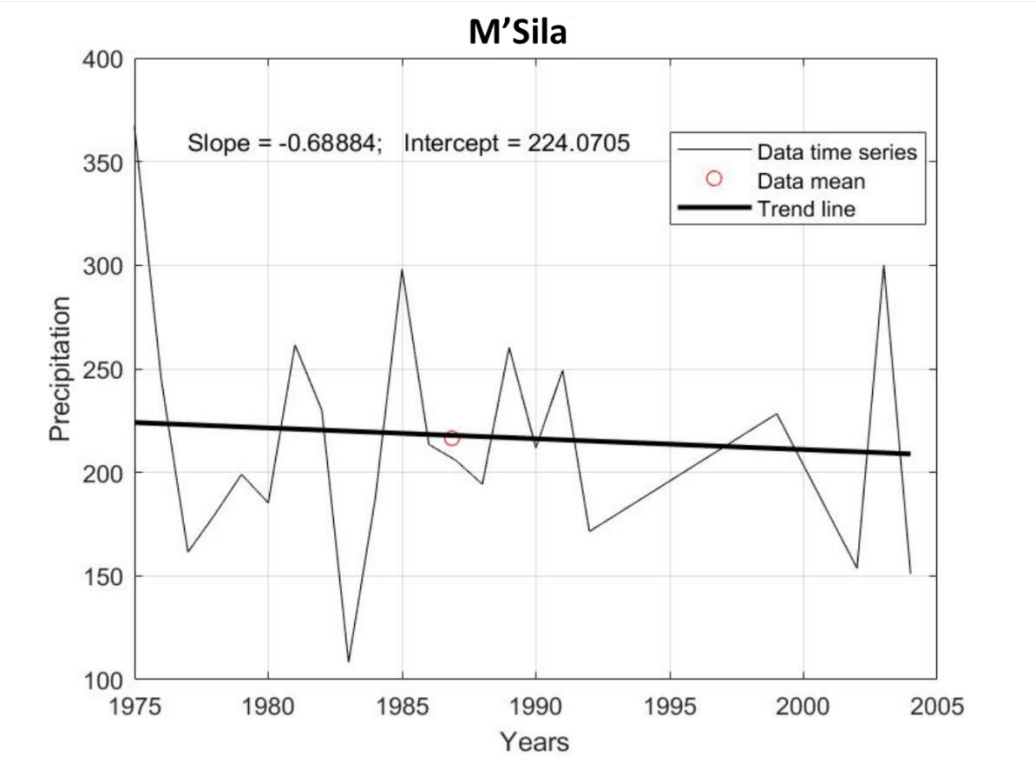
M'Sila
Slope = -0.68884; Intercept = 224.0705
Data time series
Data mean
Trend line
Precipitation
Years
400
350
300
250
200
150
100
1975
1980
1985
1990
1995
2000
2005

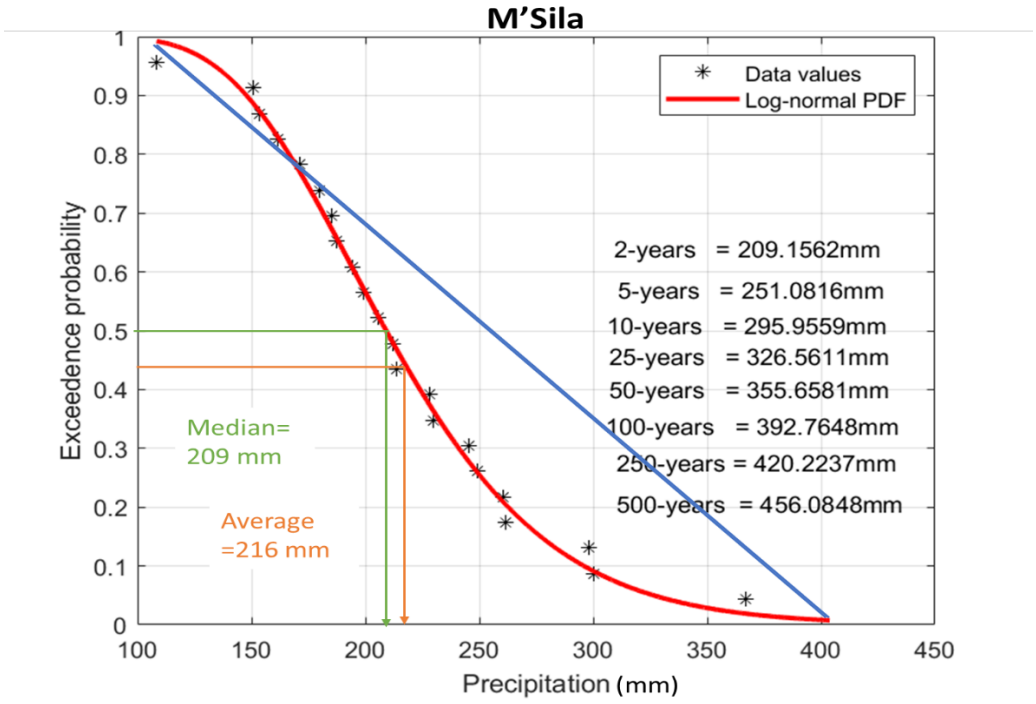
M'Sila
Data values
Log-normal PDF
2-years = 209.1562mm
5-years = 251.0816mm
10-years = 295.9559mm
25-years = 326.5611mm
50-years = 355.6581mm
100-years = 392.7648mm
250-years = 420.2237mm
500-years = 456.0848mm
Median= 209 mm
Average =216 mm
Exceedence probability
Precipitation (mm)
1
0.9
0.8
0.7
0.6
0.5
0.4
0.3
0.2
0.1
0
100
150
200
250
300
350
400
450

8.1.3 Drought MATLAB program

```
function [C,S,SL,SM,SI,D,DL,DM,DI]=BESME_DROUGHT(T,X,Title,Xtitle,Ytitle)
Xo=mean(X);
FY=T(1); % First year
LY=T(end); % Last year
XM=mean(X); % Arithmetic average
figure
plot(T,X,'k','LineWidth',2)
title(Title)
xlabel(Xtitle)
ylabel(Ytitle)
grid on
box on
line([FY LY], [XM XM])
SF=({'Crossing number','Surplus amounts', 'Surplus length','Surplus magnitude','Surplus
intensity'}); % Surplus names
DF=({'Deficit amounts','Deficit length','Deficit magnitude','Deficit intensity'}); % Deficit
names
n=length(X);
X(1)=Xo+0.1;
j=0;
for i=2:n
   sign =(X(i-1)-Xo)*(X(i)-Xo);
   if sign < 0
      j=j+1;
      C(j)=i-1;
   else
   end
end
j1=j-1;
if X(1) > 0
   for i=1:C(1)
      surplus(i)=(X(i)-Xo);
   end
   S(1)=sum(surplus(1:C(1)));
   SM(1)=max(surplus(1:C(1)));
   SL(1)=C(1);
   SI(1)=S(1)/SL(1);
   m=1;
   for i=2:2:j1
      m=m+1;
      for k=(C(i)+1):C(i+1)
         surplus(k)=(X(k)-Xo);
```

```
      end
      S(m)=sum(surplus(C(i):C(i+1)));
      SM(m)=max(surplus(C(i):C(i+1)));
      SL(m)=C(i+1)-C(i);
      SI(m)=S(m)/SL(m);
   end
      m=0;
   for i=1:2:j1
      m=m+1;
      for k=(C(i)+1):C(i+1)
         deficit(k)=(Xo-X(k));
      end
      D(m)=sum(deficit(C(i):C(i+1)));
      DM(m)=max(deficit(C(i):C(i+1)));
      DL(m)=C(i+1)-C(i);
      DI(m)=D(m)/DL(m);
   end
       for i=(C(end)+1):n
          deficit(i)= (Xo-X(i));
       end
      D(m+1)=sum(deficit(C(end)+1:n));
      DM(m+1)=max(deficit(C(end)+1:n));
      DL(m+1)=n-C(end);
      DI(m+1)=D(m)/DL(m);
else
  for i=1:C(1)
     deficit(i)=(Xo-X(i));
   end
   D(1)=sum(deficit(1:C(1)));
   DM(1)=max(deficit(1:C(1)));
   DL(1)=C(1);
   DI(1)=D(1)/DL(1);
   m=1 ;
   for i=2:2:j1
      m=m+1;
      for k=(C(i)+1):C(i+1)
         deficit(k)=(Xo-X(k));
      end
      D(m)=sum(deficit(C(i):C(i+1)));
      DM(m)=max(deficit(C(i):C(i+1)));
      DL(m)=C(i+1)-C(i);
      DI(m)=D(m)/DL(m);
   end
      for i=(C(end)+1):n
```

```
    deficit(i)= (Xo-X(i));
    end
    D(m+1)=sum(deficit((C(end)+1):n));
    DM(m+1)=max(deficit((C(end)+1):n));
    DL(m+1)=n-C(end)+1;
    DI(m+1)=D(m)/DL(m);
    m=0;
  for i=1:2:j1
    m=m+1;
    for k=(C(i)+1):C(i+1)
       surplus(k)=(X(k)-Xo);
    end
    S(m)=sum(surplus(C(i):C(i+1)));
    SM(m)=max(surplus(C(i):C(i+1)));
    SL(m)=C(i+1)-C(i);
    SI(m)=S(m)/SL(m);
  end
   for i=1:C(1)
    surplus(i)=(X(i)-Xo);
  end
  S(1)=sum(surplus(1:C(1)));
  SM(1)=max(surplus(1:C(1)));
  SL(1)=C(1);
  SI(1)=S(1)/SL(1);
  m=1;
  for i=2:2:j1
    m=m+1;
    for k=(C(i)+1):C(i+1)
       surplus(k)=(X(k)-Xo);
    end
    S(m)=sum(surplus(C(i):C(i+1)));
    SM(m)=max(surplus(C(i):C(i+1)));
    SL(m)=C(i+1)-C(i);
    SI(m)=S(m)/SL(m);
  end
    m=0;
  for i=1:2:j1
    m=m+1;
    for k=(C(i)+1):C(i+1)
       deficit(k)=(Xo-X(k));
    end
    D(m)=sum(deficit(C(i):C(i+1)));
    DM(m)=max(deficit(C(i):C(i+1)));
    DL(m)=C(i+1)-C(i);
```

```
      DI(m)=D(m)/DL(m);
   end
      for i=(C(end)+1):n
         deficit(i)= (Xo-X(i));
      end
      D(m+1)=sum(deficit(C(end)+1:n));
      DM(m+1)=max(deficit(C(end)+1:n));
      DL(m+1)=n-C(end);
      DI(m+1)=D(m)/DL(m);
end
[V,I] = ProbabilityDistributionFunctionChoice(C',SF(1),Title);
[V,I] = ProbabilityDistributionFunctionChoice(S',SF(2),Title);
[V,I] = ProbabilityDistributionFunctionChoice(SL',SF(3),Title);
[V,I] = ProbabilityDistributionFunctionChoice(SM',SF(4),Title);
[V,I] = ProbabilityDistributionFunctionChoice(SI',SF(5),Title);
[V,I] = ProbabilityDistributionFunctionChoice(abs(D'),DF(1),Title);
[V,I] = ProbabilityDistributionFunctionChoice(abs(DL'),DF(2),Title);
[V,I] = ProbabilityDistributionFunctionChoice(abs(DM'),DF(3),Title);
[V,I] = ProbabilityDistributionFunctionChoice(abs(DI'),DF(4),Title);
end
```

8.1.4 Wet and dry spells figures and tables

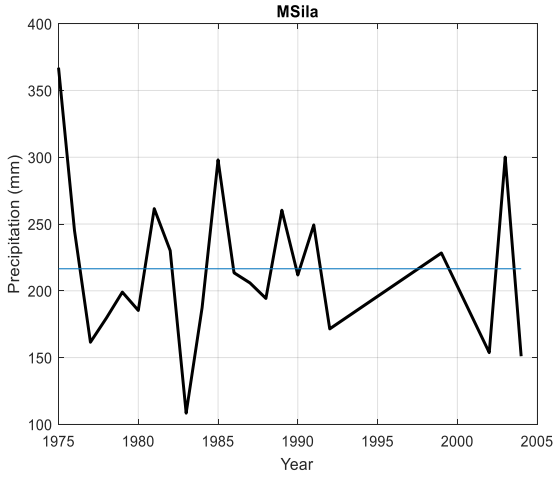

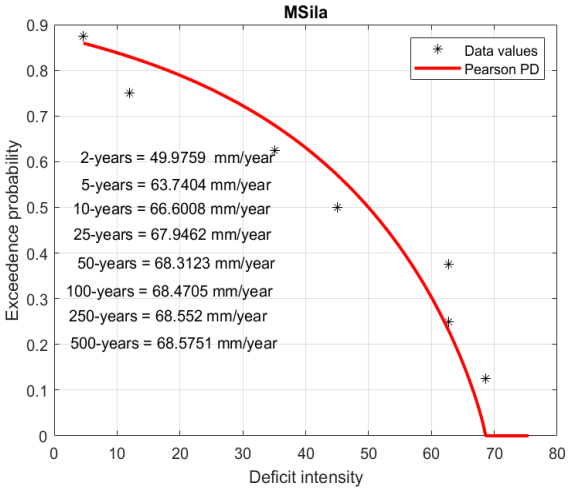

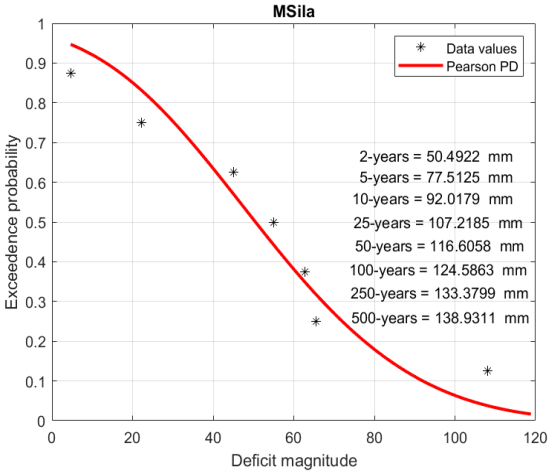

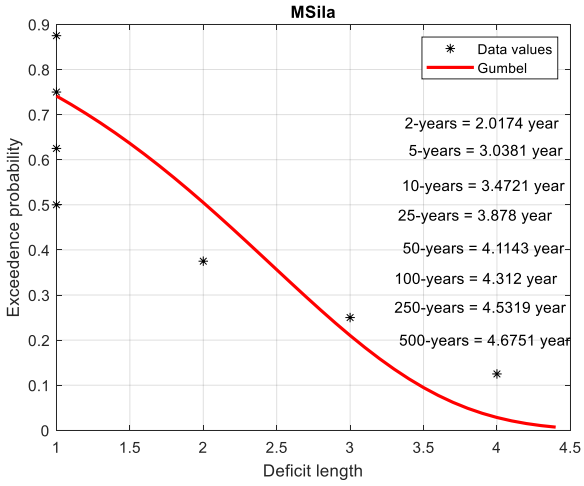

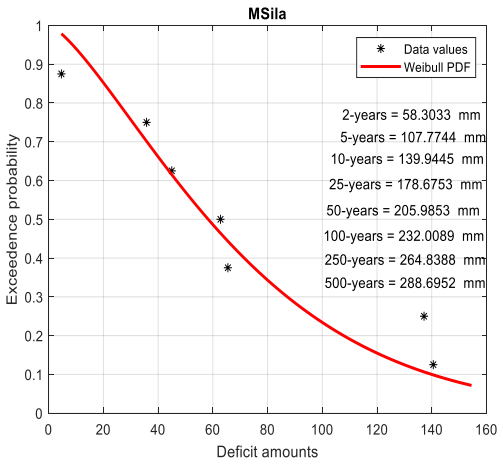
MSila
Data values
Weibull PDF
2-years = 58.3033 mm
5-years = 107.7744 mm
10-years = 139.9445 mm
25-years = 178.6753 mm
50-years = 205.9853 mm
100-years = 232.0089 mm
250-years = 264.8388 mm
500-years = 288.6952 mm
Exceedence probability
Deficit amounts

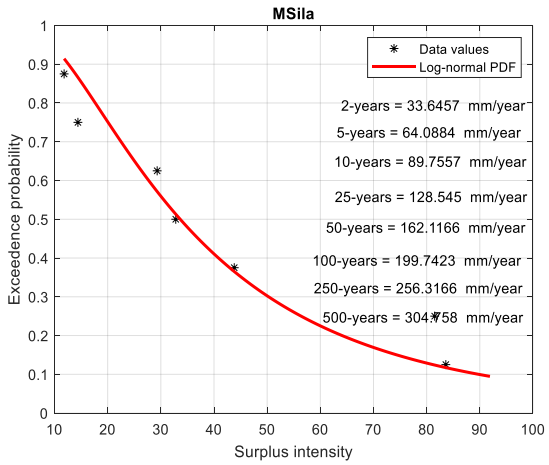
MSila
Data values
Log-normal PDF
2-years = 33.6457 mm/year
5-years = 64.0884 mm/year
10-years = 89.7557 mm/year
25-years = 128.545 mm/year
50-years = 162.1166 mm/year
100-years = 199.7423 mm/year
250-years = 256.3166 mm/year
500-years = 304.758 mm/year
Exceedence probability
Surplus intensity

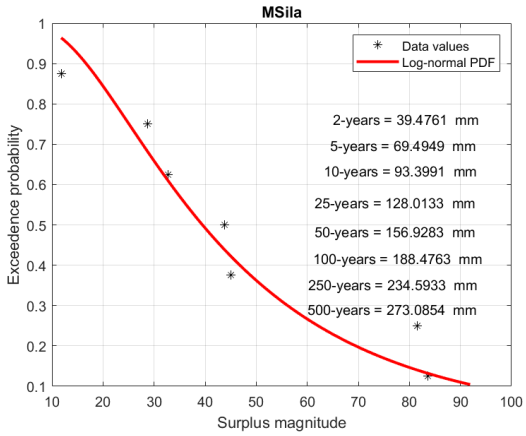
MSila
Data values
Log-normal PDF
2-years = 39.4761 mm
5-years = 69.4949 mm
10-years = 93.3991 mm
25-years = 128.0133 mm
50-years = 156.9283 mm
100-years = 188.4763 mm
250-years = 234.5933 mm
500-years = 273.0854 mm
Exceedence probability
Surplus magnitude

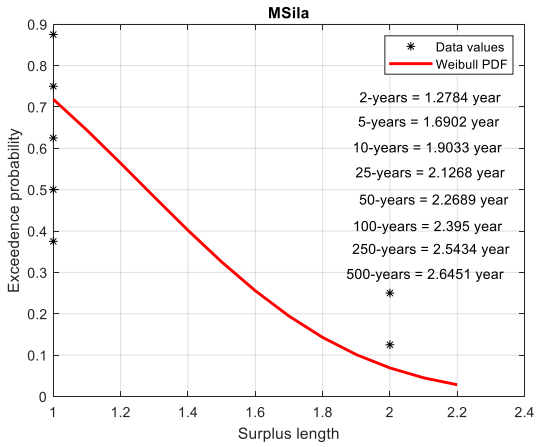
MSila
Data values
Weibull PDF
2-years = 1.2784 year
5-years = 1.6902 year
10-years = 1.9033 year
25-years = 2.1268 year
50-years = 2.2689 year
100-years = 2.395 year
250-years = 2.5434 year
500-years = 2.6451 year
Exceedence probability
Surplus length

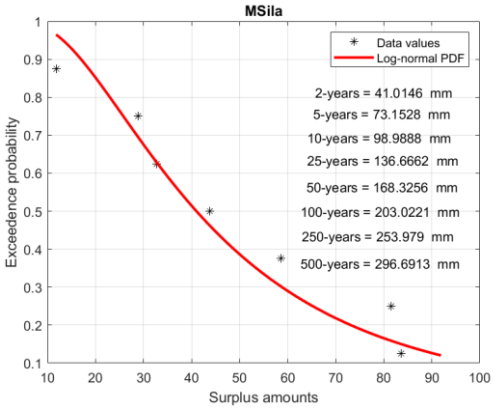
MSila
Data values
Log-normal PDF
2-years = 41.0146 mm
5-years = 73.1528 mm
10-years = 98.9888 mm
25-years = 136.6662 mm
50-years = 168.3256 mm
100-years = 203.0221 mm
250-years = 253.979 mm
500-years = 296.6913 mm
Exceedence probability
Surplus amounts

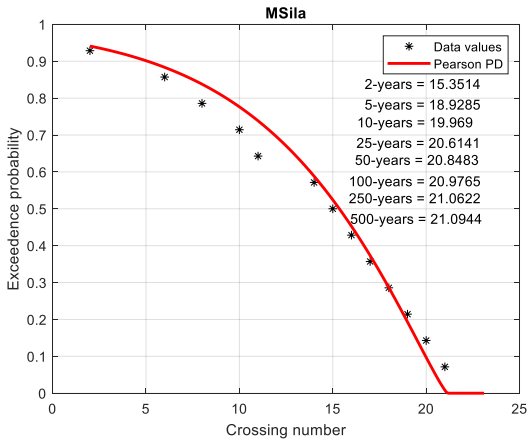
MSila
Data values
Pearson PD
2-years = 15.3514
5-years = 18.9285
10-years = 19.969
25-years = 20.6141
50-years = 20.8483
100-years = 20.9765
250-years = 21.0622
500-years = 21.0944
Exceedence probability
Crossing number

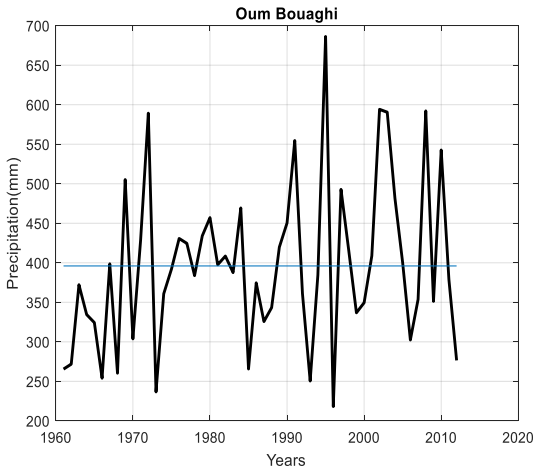
Oum Bouaghi
Precipitation(mm)
Years

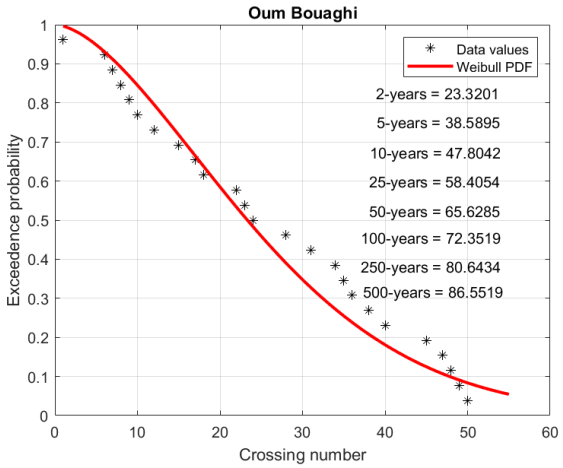
Oum Bouaghi
Data values
Weibull PDF
2-years = 23.3201
5-years = 38.5895
10-years = 47.8042
25-years = 58.4054
50-years = 65.6285
100-years = 72.3519
250-years = 80.6434
500-years = 86.5519
Exceedence probability
Crossing number

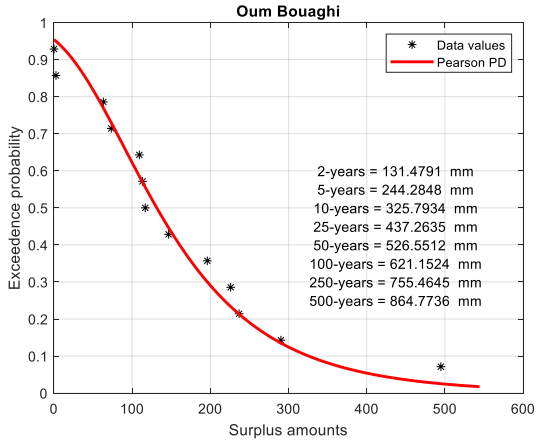
Oum Bouaghi
Data values
Pearson PD
2-years = 131.4791 mm
5-years = 244.2848 mm
10-years = 325.7934 mm
25-years = 437.2635 mm
50-years = 526.5512 mm
100-years = 621.1524 mm
250-years = 755.4645 mm
500-years = 864.7736 mm
Exceedence probability
Surplus amounts

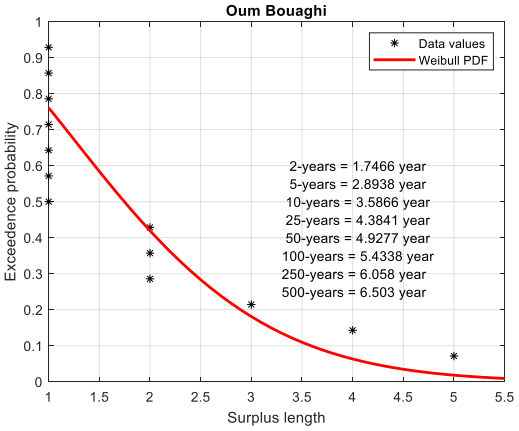
Oum Bouaghi
Data values
Weibull PDF
2-years = 1.7466 year
5-years = 2.8938 year
10-years = 3.5866 year
25-years = 4.3841 year
50-years = 4.9277 year
100-years = 5.4338 year
250-years = 6.058 year
500-years = 6.503 year
Exceedence probability
Surplus length

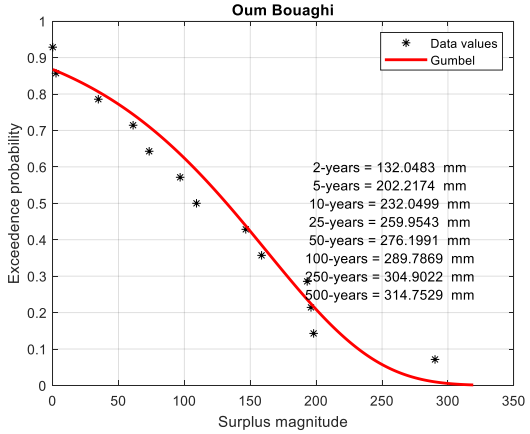
Oum Bouaghi
Data values
Gumbel
2-years = 132.0483 mm
5-years = 202.2174 mm
10-years = 232.0499 mm
25-years = 259.9543 mm
50-years = 276.1991 mm
100-years = 289.7869 mm
250-years = 304.9022 mm
500-years = 314.7529 mm
Exceedence probability
Surplus magnitude

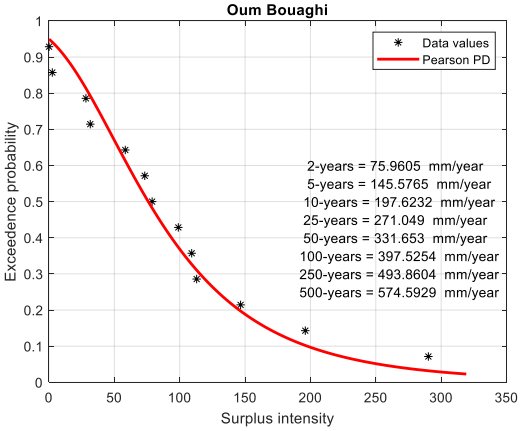
Oum Bouaghi
Data values
Pearson PD
2-years = 75.9605 mm/year
5-years = 145.5765 mm/year
10-years = 197.6232 mm/year
25-years = 271.049 mm/year
50-years = 331.653 mm/year
100-years = 397.5254 mm/year
250-years = 493.8604 mm/year
500-years = 574.5929 mm/year
Exceedence probability
Surplus intensity

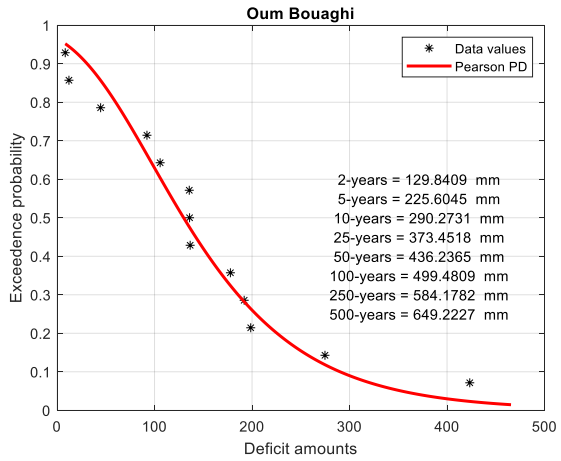
Oum Bouaghi
Data values
Pearson PD
2-years = 129.8409 mm
5-years = 225.6045 mm
10-years = 290.2731 mm
25-years = 373.4518 mm
50-years = 436.2365 mm
100-years = 499.4809 mm
250-years = 584.1782 mm
500-years = 649.2227 mm
Exceedence probability
Deficit amounts

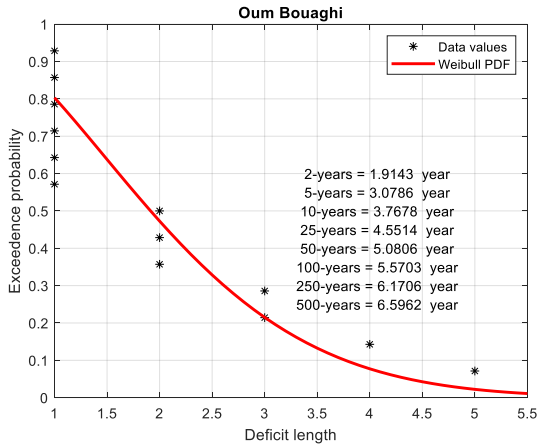
Oum Bouaghi
Data values
Weibull PDF
2-years = 1.9143 year
5-years = 3.0786 year
10-years = 3.7678 year
25-years = 4.5514 year
50-years = 5.0806 year
100-years = 5.5703 year
250-years = 6.1706 year
500-years = 6.5962 year
Exceedence probability
Deficit length

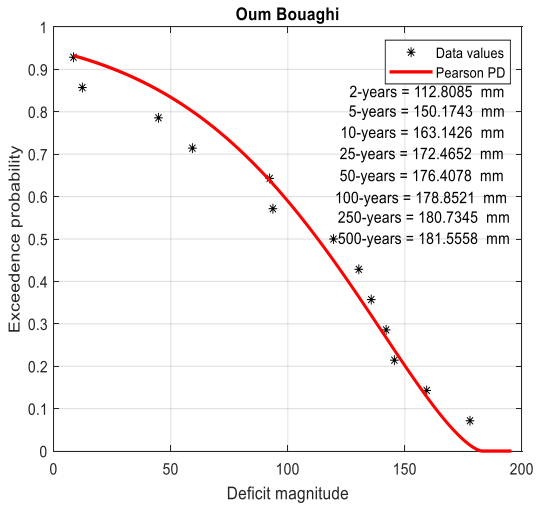
Oum Bouaghi
Data values
Pearson PD
2-years = 112.8085 mm
5-years = 150.1743 mm
10-years = 163.1426 mm
25-years = 172.4652 mm
50-years = 176.4078 mm
100-years = 178.8521 mm
250-years = 180.7345 mm
500-years = 181.5558 mm
Exceedence probability
Deficit magnitude

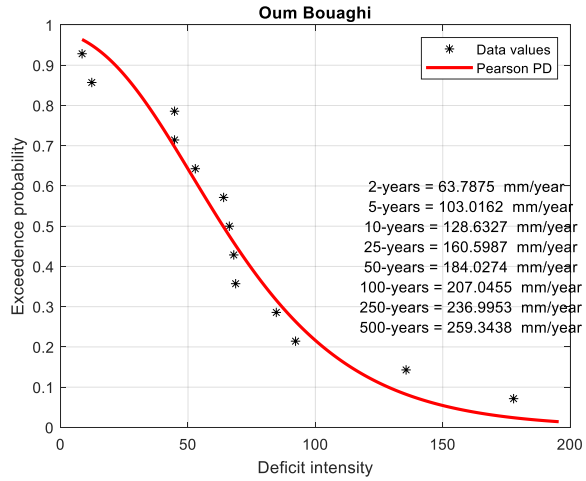
Oum Bouaghi
Data values
Pearson PD
2-years = 63.7875 mm/year
5-years = 103.0162 mm/year
10-years = 128.6327 mm/year
25-years = 160.5987 mm/year
50-years = 184.0274 mm/year
100-years = 207.0455 mm/year
250-years = 236.9953 mm/year
500-years = 259.3438 mm/year
Exceedence probability
Deficit intensity

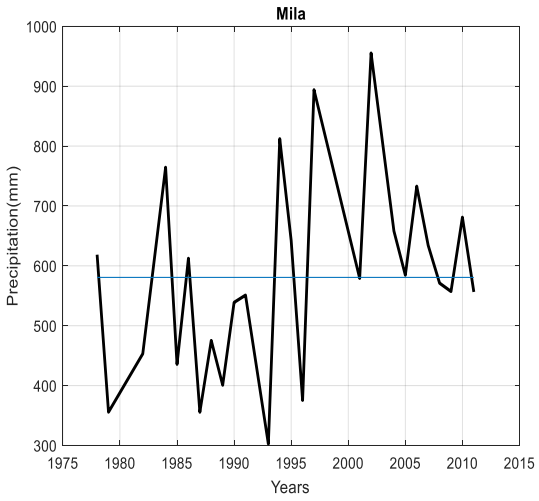
Mila
Precipitation(mm)
Years

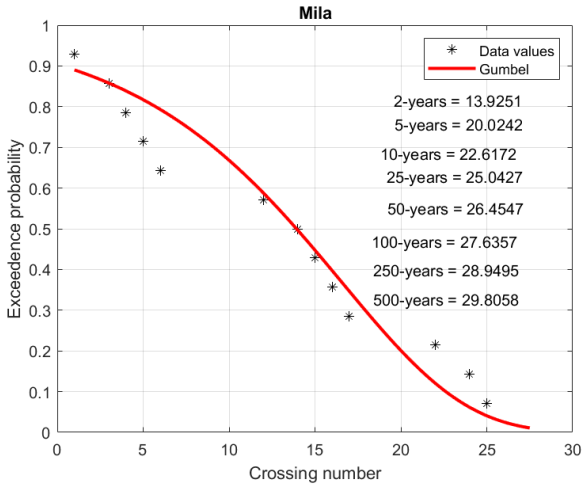
Mila
Data values
Gumbel
2-years = 13.9251
5-years = 20.0242
10-years = 22.6172
25-years = 25.0427
50-years = 26.4547
100-years = 27.6357
250-years = 28.9495
500-years = 29.8058
Exceedence probability
Crossing number

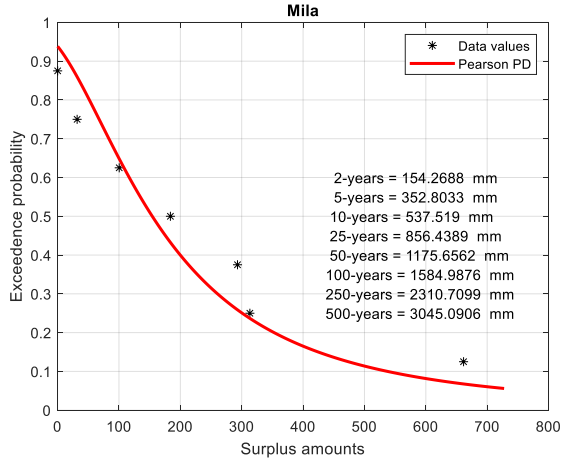
Mila
Data values
Pearson PD
2-years = 154.2688 mm
5-years = 352.8033 mm
10-years = 537.519 mm
25-years = 856.4389 mm
50-years = 1175.6562 mm
100-years = 1584.9876 mm
250-years = 2310.7099 mm
500-years = 3045.0906 mm
Exceedence probability
Surplus amounts

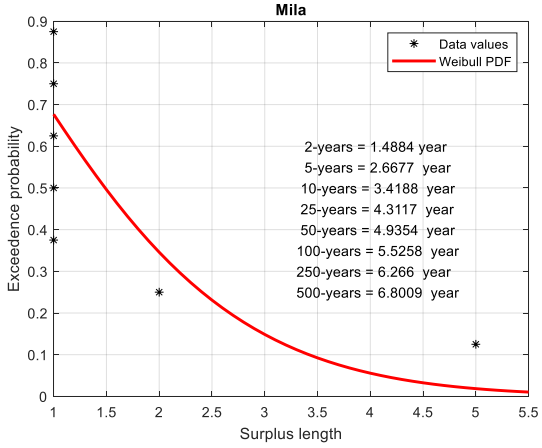
Mila
Data values
Weibull PDF
2-years = 1.4884 year
5-years = 2.6677 year
10-years = 3.4188 year
25-years = 4.3117 year
50-years = 4.9354 year
100-years = 5.5258 year
250-years = 6.266 year
500-years = 6.8009 year
Exceedence probability
Surplus length

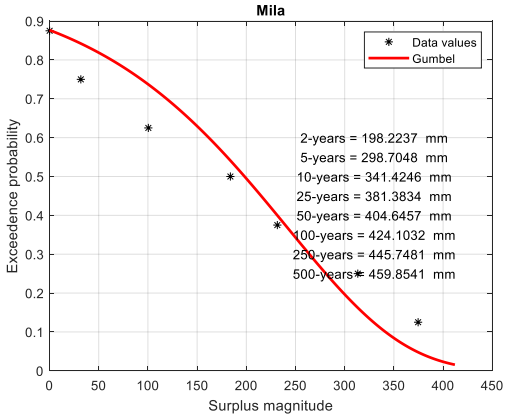
Mila
Data values
Gumbel
2-years = 198.2237 mm
5-years = 298.7048 mm
10-years = 341.4246 mm
25-years = 381.3834 mm
50-years = 404.6457 mm
100-years = 424.1032 mm
250-years = 445.7481 mm
500-years = 459.8541 mm
Exceedence probability
Surplus magnitude

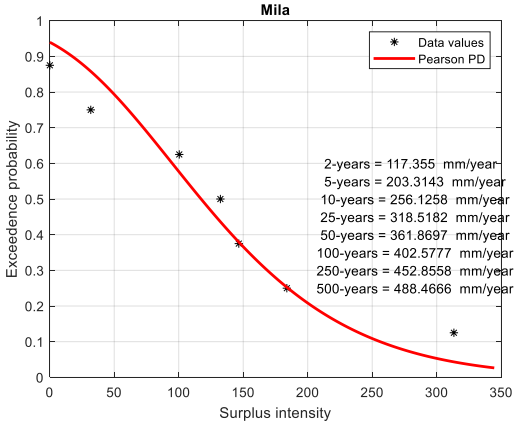
Mila
Data values
Pearson PD
2-years = 117.355 mm/year
5-years = 203.3143 mm/year
10-years = 256.1258 mm/year
25-years = 318.5182 mm/year
50-years = 361.8697 mm/year
100-years = 402.5777 mm/year
250-years = 452.8558 mm/year
500-years = 488.4666 mm/year
Exceedence probability
Surplus intensity

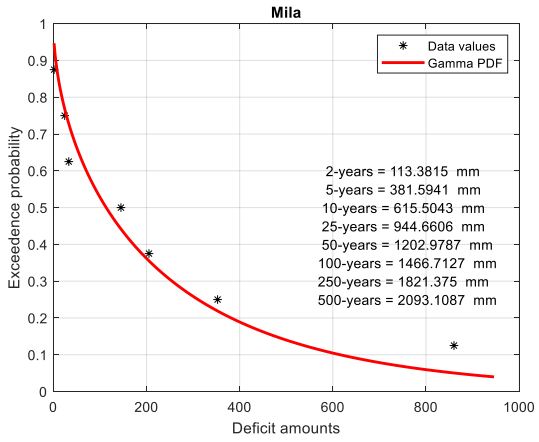
Mila
Data values
Gamma PDF
2-years = 113.3815 mm
5-years = 381.5941 mm
10-years = 615.5043 mm
25-years = 944.6606 mm
50-years = 1202.9787 mm
100-years = 1466.7127 mm
250-years = 1821.375 mm
500-years = 2093.1087 mm
Exceedence probability
Deficit amounts

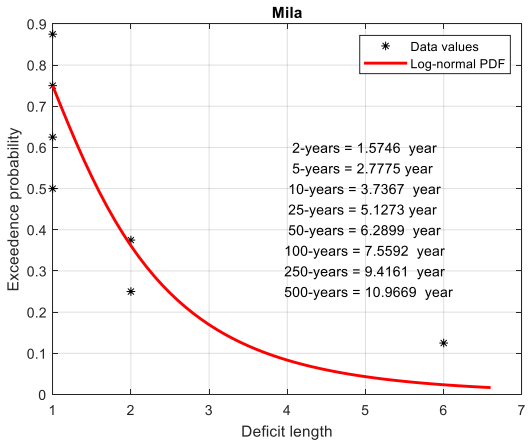
Mila
Data values
Log-normal PDF
2-years = 1.5746 year
5-years = 2.7775 year
10-years = 3.7367 year
25-years = 5.1273 year
50-years = 6.2899 year
100-years = 7.5592 year
250-years = 9.4161 year
500-years = 10.9669 year
Exceedence probability
Deficit length

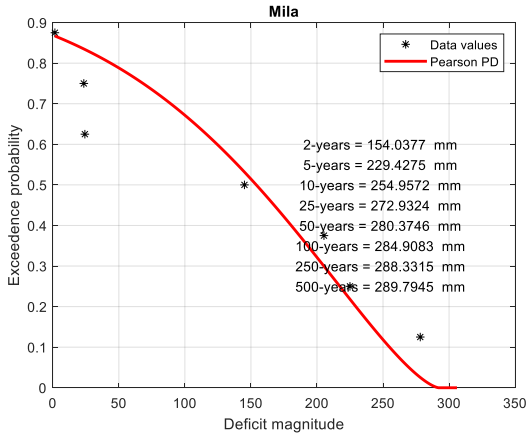
Mila
Data values
Pearson PD
2-years = 154.0377 mm
5-years = 229.4275 mm
10-years = 254.9572 mm
25-years = 272.9324 mm
50-years = 280.3746 mm
100-years = 284.9083 mm
250-years = 288.3315 mm
500-years = 289.7945 mm
Exceedence probability
Deficit magnitude

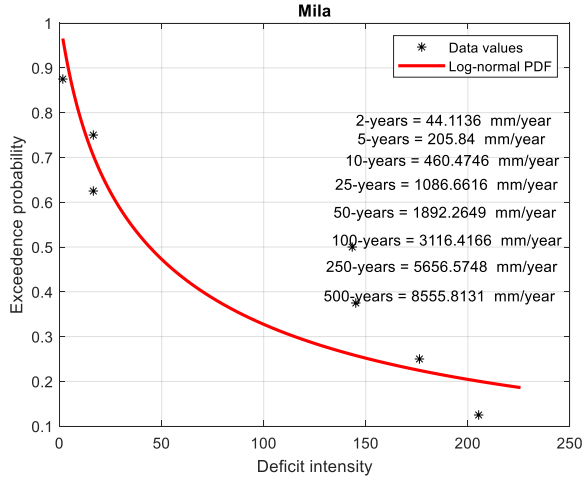
Mila
Data values
Log-normal PDF
2-years = 44.1136 mm/year
5-years = 205.84 mm/year
10-years = 460.4746 mm/year
25-years = 1086.6616 mm/year
50-years = 1892.2649 mm/year
100-years = 3116.4166 mm/year
250-years = 5656.5748 mm/year
500-years = 8555.8131 mm/year
Exceedence probability
Deficit intensity

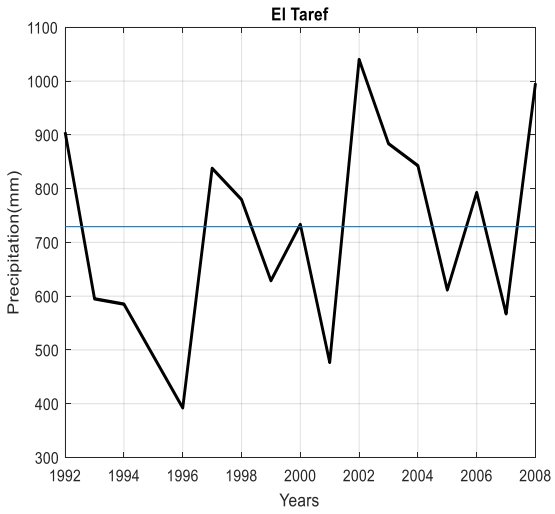
El Taref
Precipitation(mm)
Years

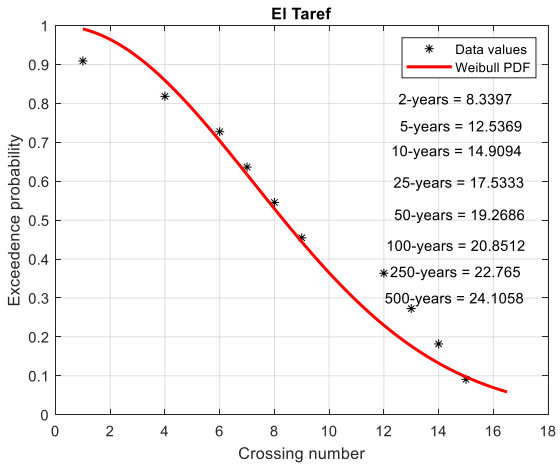
El Taref
Data values
Weibull PDF
2-years = 8.3397
5-years = 12.5369
10-years = 14.9094
25-years = 17.5333
50-years = 19.2686
100-years = 20.8512
250-years = 22.765
500-years = 24.1058
Exceedence probability
Crossing number

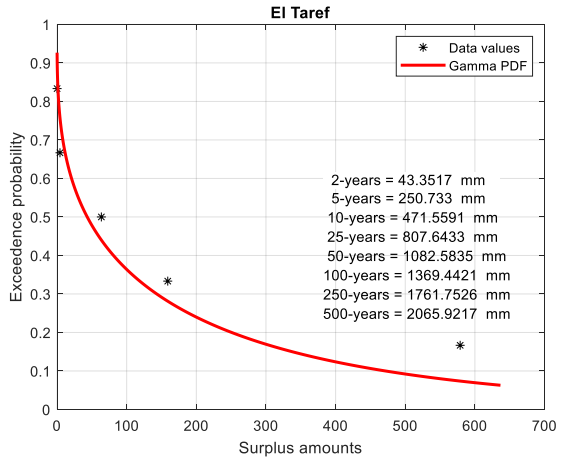
El Taref
Data values
Gamma PDF
2-years = 43.3517 mm
5-years = 250.733 mm
10-years = 471.5591 mm
25-years = 807.6433 mm
50-years = 1082.5835 mm
100-years = 1369.4421 mm
250-years = 1761.7526 mm
500-years = 2065.9217 mm
Exceedence probability
Surplus amounts

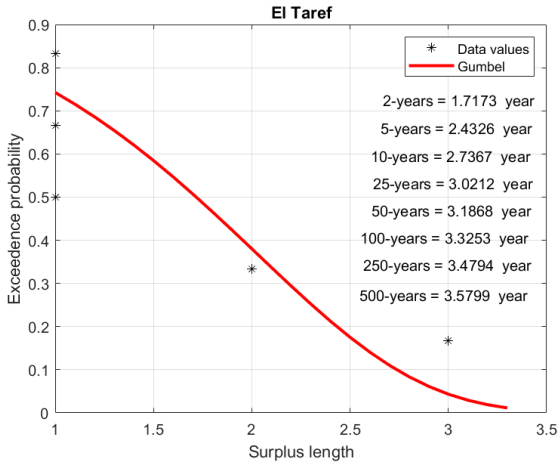
El Taref
Data values
Gumbel
2-years = 1.7173 year
5-years = 2.4326 year
10-years = 2.7367 year
25-years = 3.0212 year
50-years = 3.1868 year
100-years = 3.3253 year
250-years = 3.4794 year
500-years = 3.5799 year
Exceedence probability
Surplus length

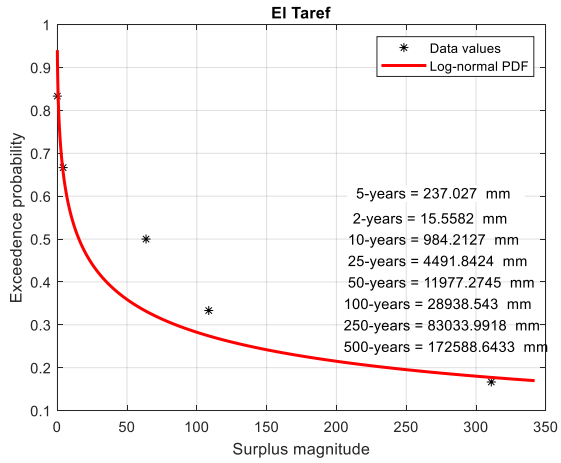
El Taref
Data values
Log-normal PDF
5-years = 237.027 mm
2-years = 15.5582 mm
10-years = 984.2127 mm
25-years = 4491.8424 mm
50-years = 11977.2745 mm
100-years = 28938.543 mm
250-years = 83033.9918 mm
500-years = 172588.6433 mm
Exceedence probability
Surplus magnitude

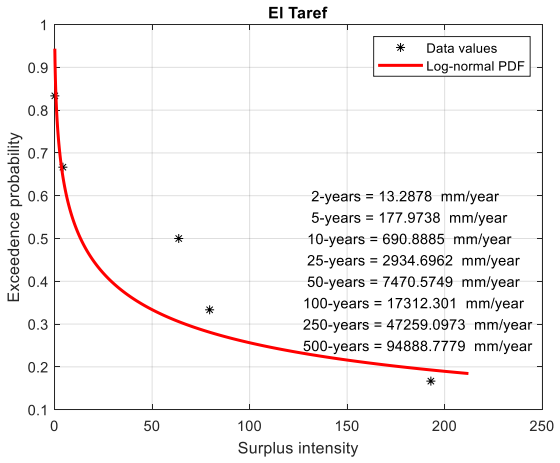
El Taref
Data values
Log-normal PDF
2-years = 13.2878 mm/year
5-years = 177.9738 mm/year
10-years = 690.8885 mm/year
25-years = 2934.6962 mm/year
50-years = 7470.5749 mm/year
100-years = 17312.301 mm/year
250-years = 47259.0973 mm/year
500-years = 94888.7779 mm/year
Exceedence probability
Surplus intensity

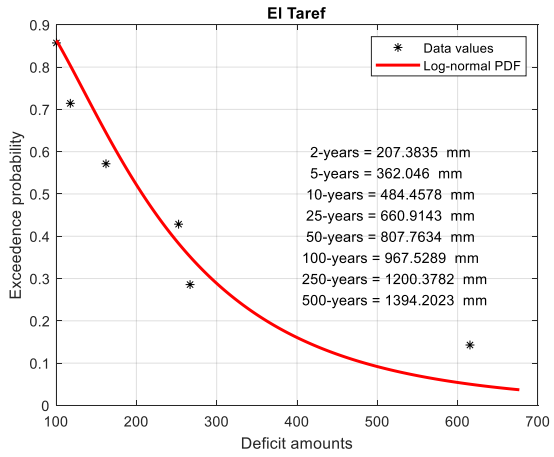
El Taref
Data values
Log-normal PDF
2-years = 207.3835 mm
5-years = 362.046 mm
10-years = 484.4578 mm
25-years = 660.9143 mm
50-years = 807.7634 mm
100-years = 967.5289 mm
250-years = 1200.3782 mm
500-years = 1394.2023 mm
Exceedence probability
Deficit amounts

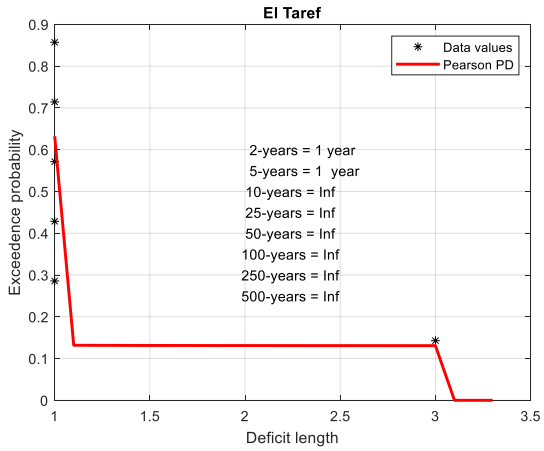
El Taref
Data values
Pearson PD
2-years = 1 year
5-years = 1 year
10-years = Inf
25-years = Inf
50-years = Inf
100-years = Inf
250-years = Inf
500-years = Inf
Exceedence probability
Deficit length

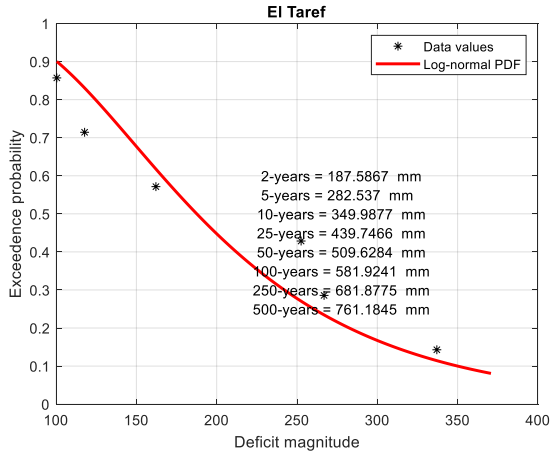
El Taref
Data values
Log-normal PDF
2-years = 187.5867 mm
5-years = 282.537 mm
10-years = 349.9877 mm
25-years = 439.7466 mm
50-years = 509.6284 mm
100-years = 581.9241 mm
250-years = 681.8775 mm
500-years = 761.1845 mm
Exceedence probability
Deficit magnitude

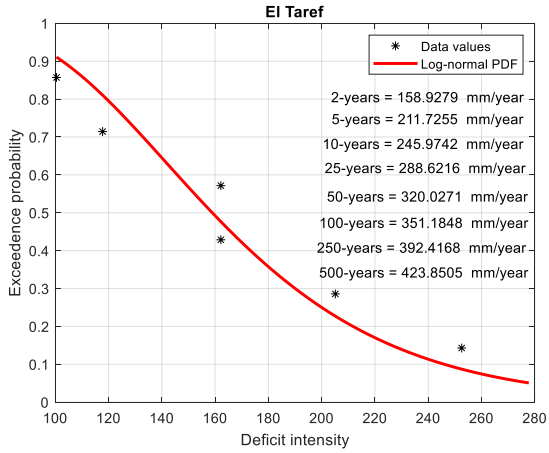
El Taref
Data values
Log-normal PDF
2-years = 158.9279 mm/year
5-years = 211.7255 mm/year
10-years = 245.9742 mm/year
25-years = 288.6216 mm/year
50-years = 320.0271 mm/year
100-years = 351.1848 mm/year
250-years = 392.4168 mm/year
500-years = 423.8505 mm/year
Exceedence probability
Deficit intensity

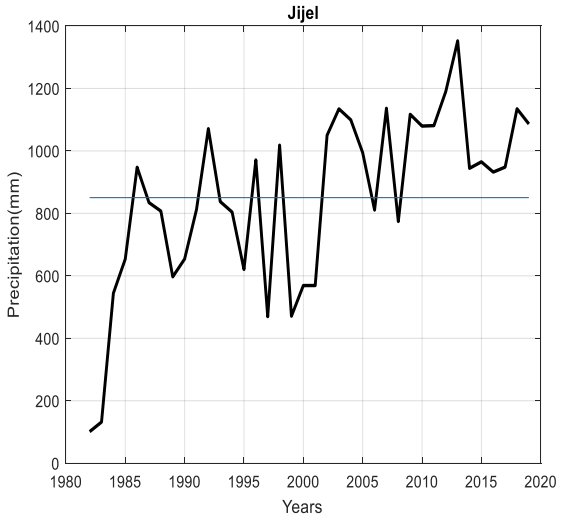
Jijel
Precipitation(mm)
Years

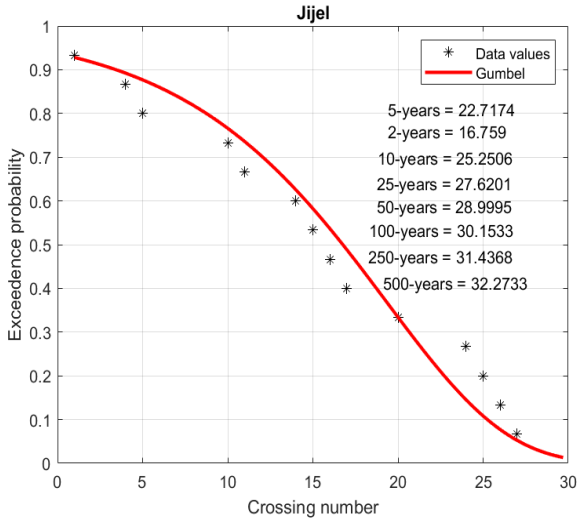
Jijel
Data values
Gumbel
5-years = 22.7174
2-years = 16.759
10-years = 25.2506
25-years = 27.6201
50-years = 28.9995
100-years = 30.1533
250-years = 31.4368
500-years = 32.2733
Exceedence probability
Crossing number

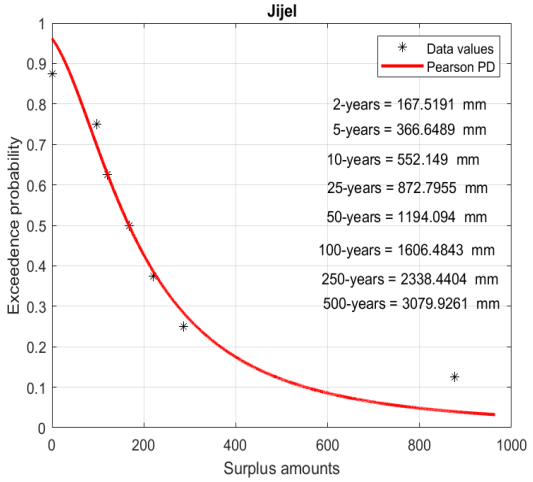
Jijel
Data values
Pearson PD
2-years = 167.5191 mm
5-years = 366.6489 mm
10-years = 552.149 mm
25-years = 872.7955 mm
50-years = 1194.094 mm
100-years = 1606.4843 mm
250-years = 2338.4404 mm
500-years = 3079.9261 mm
Exceedence probability
Surplus amounts

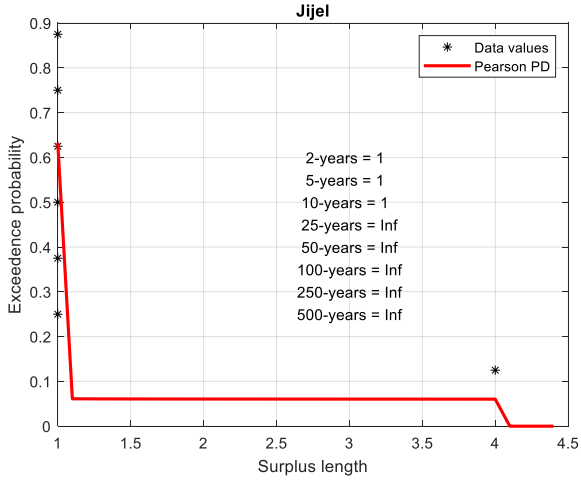
Jijel
Data values
Pearson PD
2-years = 1
5-years = 1
10-years = 1
25-years = Inf
50-years = Inf
100-years = Inf
250-years = Inf
500-years = Inf
Exceedence probability
Surplus length

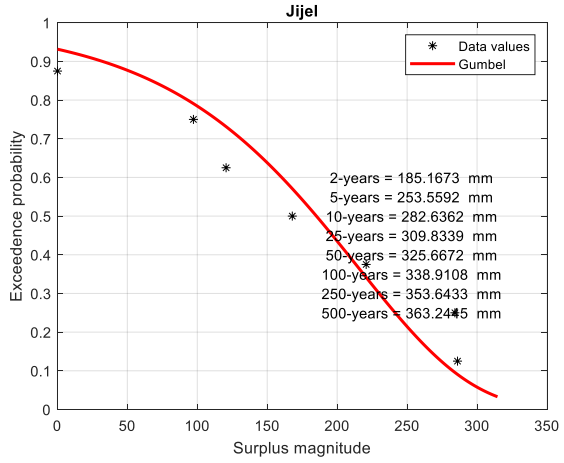
Jijel
Data values
Gumbel
2-years = 185.1673 mm
5-years = 253.5592 mm
10-years = 282.6362 mm
25-years = 309.8339 mm
50-years = 325.6672 mm
100-years = 338.9108 mm
250-years = 353.6433 mm
500-years = 363.2445 mm
Exceedence probability
Surplus magnitude

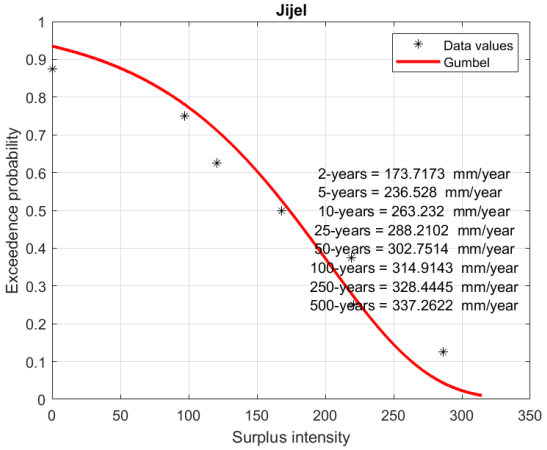
Jijel
Data values
Gumbel
2-years = 173.7173 mm/year
5-years = 236.528 mm/year
10-years = 263.232 mm/year
25-years = 288.2102 mm/year
50-years = 302.7514 mm/year
100-years = 314.9143 mm/year
250-years = 328.4445 mm/year
500-years = 337.2622 mm/year
Exceedence probability
Surplus intensity

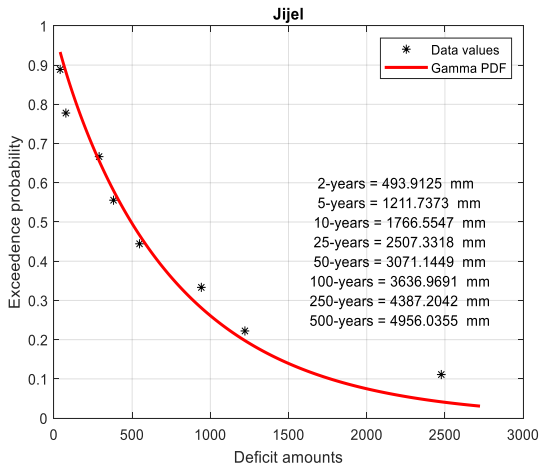
Jijel
Data values
Gamma PDF
2-years = 493.9125 mm
5-years = 1211.7373 mm
10-years = 1766.5547 mm
25-years = 2507.3318 mm
50-years = 3071.1449 mm
100-years = 3636.9691 mm
250-years = 4387.2042 mm
500-years = 4956.0355 mm
Exceedence probability
Deficit amounts

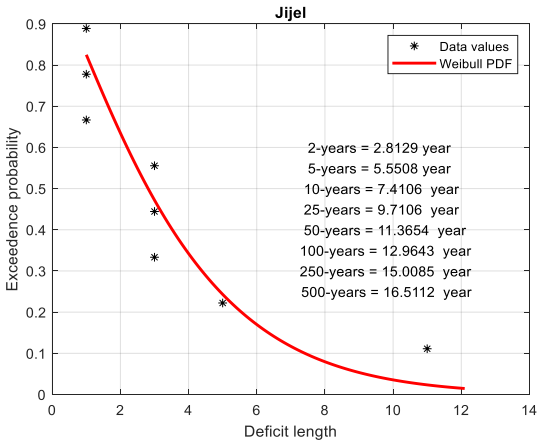
Jijel
Data values
Weibull PDF
2-years = 2.8129 year
5-years = 5.5508 year
10-years = 7.4106 year
25-years = 9.7106 year
50-years = 11.3654 year
100-years = 12.9643 year
250-years = 15.0085 year
500-years = 16.5112 year
Exceedence probability
Deficit length

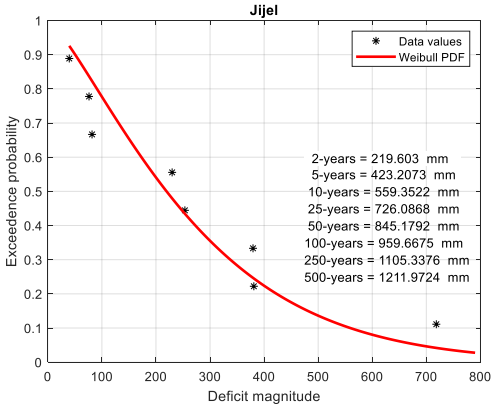
Jijel
Data values
Weibull PDF
2-years = 219.603 mm
5-years = 423.2073 mm
10-years = 559.3522 mm
25-years = 726.0868 mm
50-years = 845.1792 mm
100-years = 959.6675 mm
250-years = 1105.3376 mm
500-years = 1211.9724 mm
Exceedence probability
Deficit magnitude

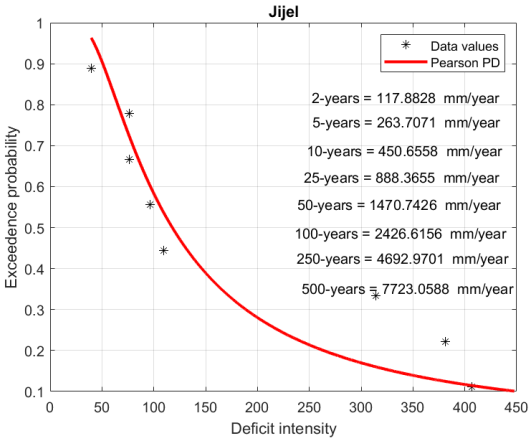
Jijel
Data values
Pearson PD
2-years = 117.8828 mm/year
5-years = 263.7071 mm/year
10-years = 450.6558 mm/year
25-years = 888.3655 mm/year
50-years = 1470.7426 mm/year
100-years = 2426.6156 mm/year
250-years = 4692.9701 mm/year
500-years = 7723.0588 mm/year
Exceedence probability
Deficit intensity

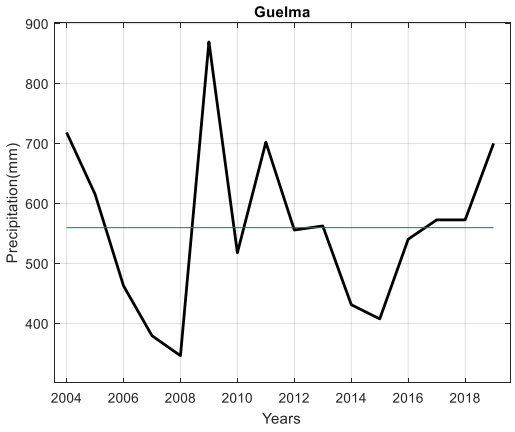
Guelma
Precipitation(mm)
Years

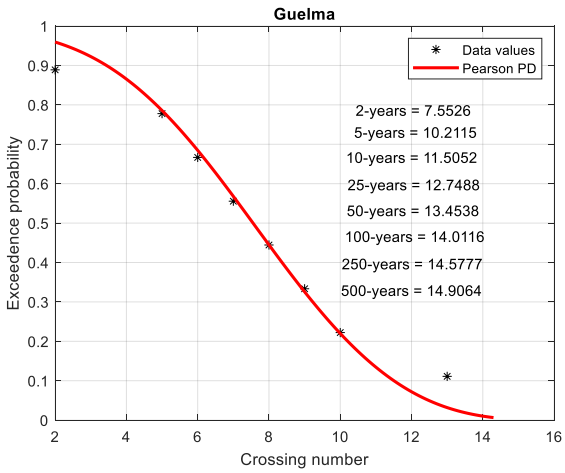
Guelma
Data values
Pearson PD
2-years = 7.5526
5-years = 10.2115
10-years = 11.5052
25-years = 12.7488
50-years = 13.4538
100-years = 14.0116
250-years = 14.5777
500-years = 14.9064
Exceedence probability
Crossing number

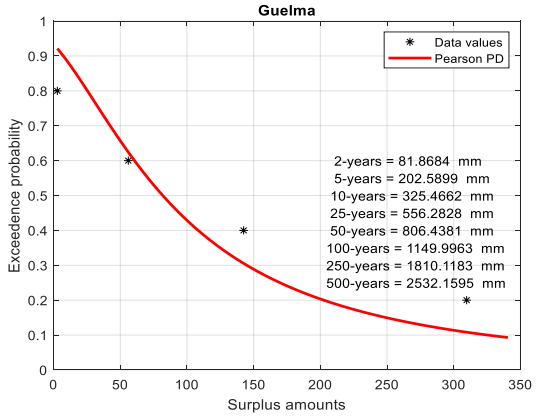
Guelma
Data values
Pearson PD
2-years = 81.8684 mm
5-years = 202.5899 mm
10-years = 325.4662 mm
25-years = 556.2828 mm
50-years = 806.4381 mm
100-years = 1149.9963 mm
250-years = 1810.1183 mm
500-years = 2532.1595 mm
Exceedence probability
Surplus amounts

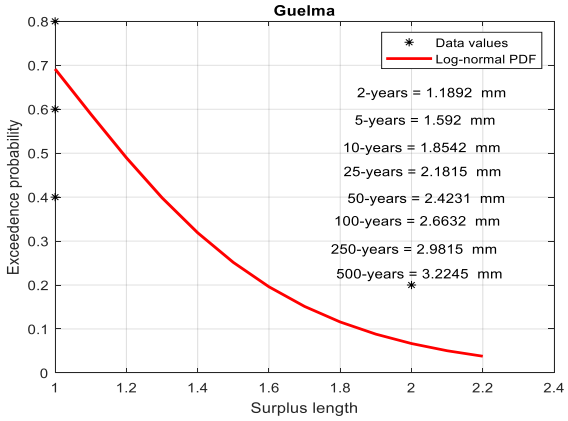
Guelma
Data values
Log-normal PDF
2-years = 1.1892 mm
5-years = 1.592 mm
10-years = 1.8542 mm
25-years = 2.1815 mm
50-years = 2.4231 mm
100-years = 2.6632 mm
250-years = 2.9815 mm
500-years = 3.2245 mm
Exceedence probability
Surplus length

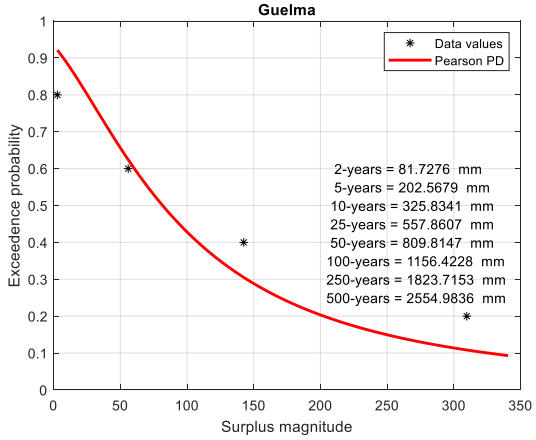
Guelma
Data values
Pearson PD
2-years = 81.7276 mm
5-years = 202.5679 mm
10-years = 325.8341 mm
25-years = 557.8607 mm
50-years = 809.8147 mm
100-years = 1156.4228 mm
250-years = 1823.7153 mm
500-years = 2554.9836 mm
Exceedence probability
Surplus magnitude

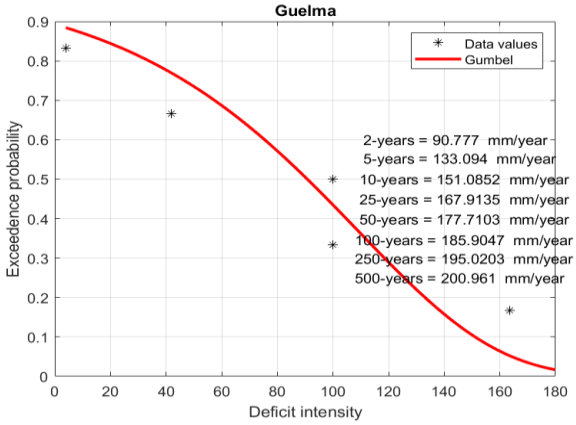
Guelma
Data values
Gumbel
2-years = 90.777 mm/year
5-years = 133.094 mm/year
10-years = 151.0852 mm/year
25-years = 167.9135 mm/year
50-years = 177.7103 mm/year
100-years = 185.9047 mm/year
250-years = 195.0203 mm/year
500-years = 200.961 mm/year
Exceedence probability
Deficit intensity

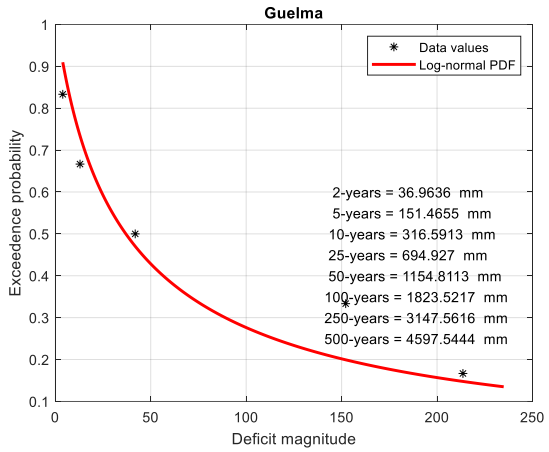
Guelma
Data values
Log-normal PDF
2-years = 36.9636 mm
5-years = 151.4655 mm
10-years = 316.5913 mm
25-years = 694.927 mm
50-years = 1154.8113 mm
100-years = 1823.5217 mm
250-years = 3147.5616 mm
500-years = 4597.5444 mm
Exceedence probability
Deficit magnitude

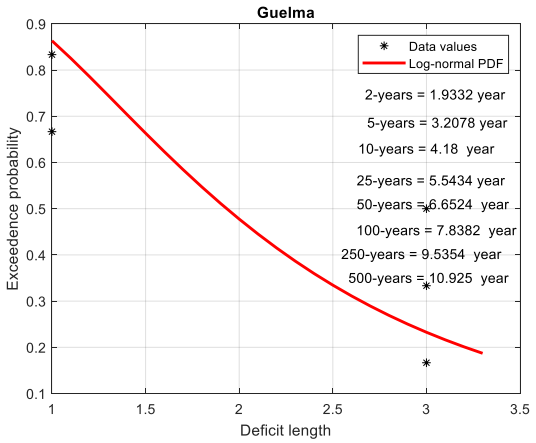
Guelma
Data values
Log-normal PDF
2-years = 1.9332 year
5-years = 3.2078 year
10-years = 4.18 year
25-years = 5.5434 year
50-years = 6.6524 year
100-years = 7.8382 year
250-years = 9.5354 year
500-years = 10.925 year
Exceedence probability
Deficit length

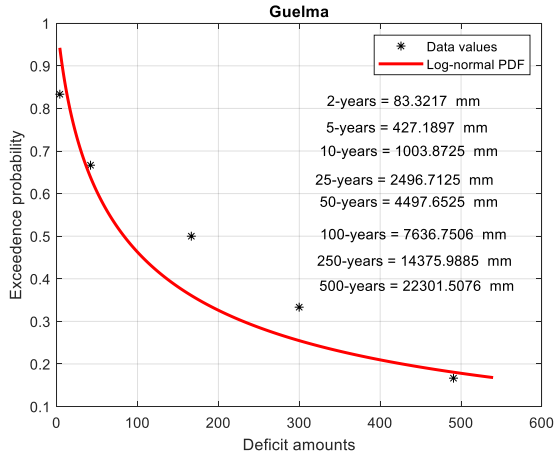
Guelma
Data values
Log-normal PDF
2-years = 83.3217 mm
5-years = 427.1897 mm
10-years = 1003.8725 mm
25-years = 2496.7125 mm
50-years = 4497.6525 mm
100-years = 7636.7506 mm
250-years = 14375.9885 mm
500-years = 22301.5076 mm
Exceedence probability
Deficit amounts

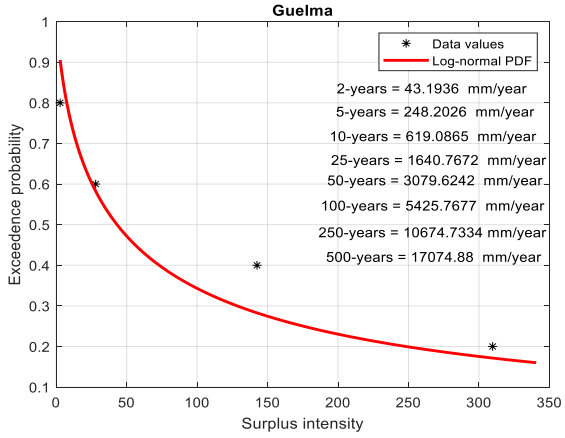
Guelma
Data values
Log-normal PDF
2-years = 43.1936 mm/year
5-years = 248.2026 mm/year
10-years = 619.0865 mm/year
25-years = 1640.7672 mm/year
50-years = 3079.6242 mm/year
100-years = 5425.7677 mm/year
250-years = 10674.7334 mm/year
500-years = 17074.88 mm/year
Exceedence probability
Surplus intensity

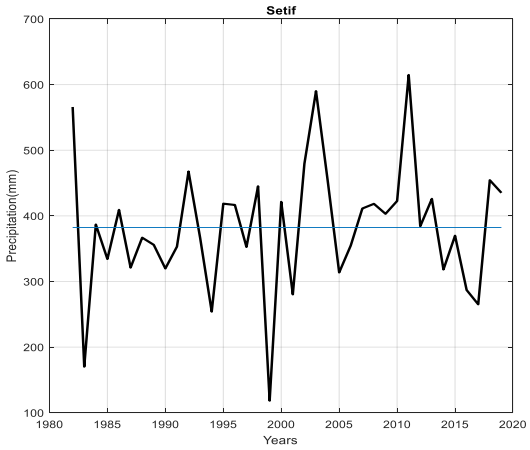
Setif
Precipitation(mm)
Years

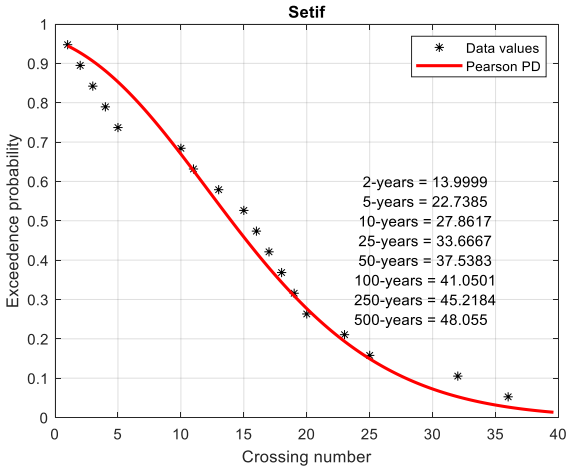
Setif
Data values
Pearson PD
Exceedence probability
Crossing number
2-years = 13.9999
5-years = 22.7385
10-years = 27.8617
25-years = 33.6667
50-years = 37.5383
100-years = 41.0501
250-years = 45.2184
500-years = 48.055

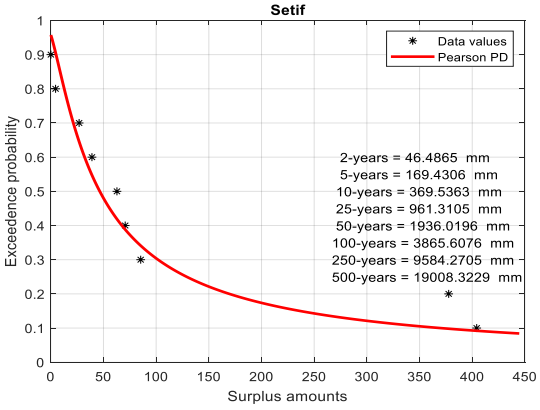
Setif
Data values
Pearson PD
Exceedence probability
Surplus amounts
2-years = 46.4865 mm
5-years = 169.4306 mm
10-years = 369.5363 mm
25-years = 961.3105 mm
50-years = 1936.0196 mm
100-years = 3865.6076 mm
250-years = 9584.2705 mm
500-years = 19008.3229 mm

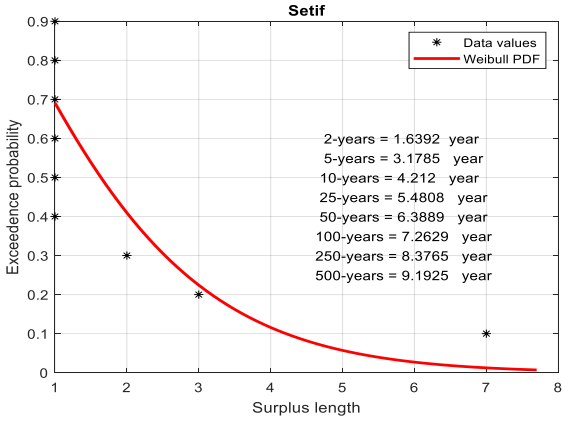
Setif
Data values
Weibull PDF
Exceedence probability
Surplus length
2-years = 1.6392 year
5-years = 3.1785 year
10-years = 4.212 year
25-years = 5.4808 year
50-years = 6.3889 year
100-years = 7.2629 year
250-years = 8.3765 year
500-years = 9.1925 year

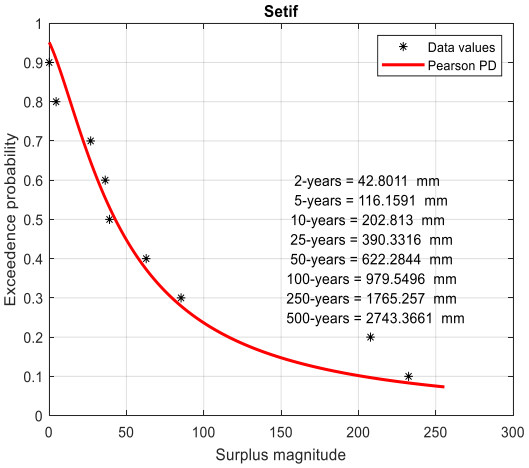
Setif
Data values
Pearson PD
Exceedence probability
Surplus magnitude
2-years = 42.8011 mm
5-years = 116.1591 mm
10-years = 202.813 mm
25-years = 390.3316 mm
50-years = 622.2844 mm
100-years = 979.5496 mm
250-years = 1765.257 mm
500-years = 2743.3661 mm

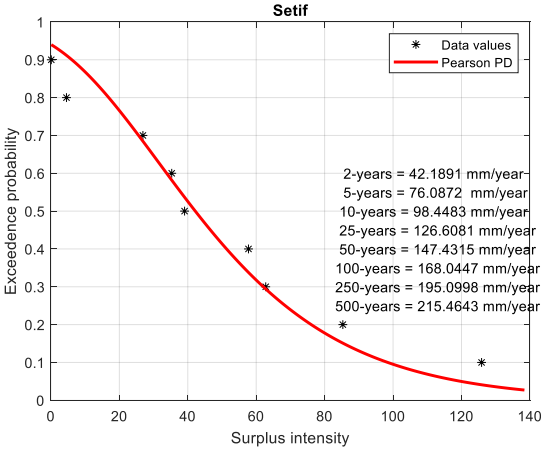
Setif
Data values
Pearson PD
Exceedence probability
Surplus intensity
2-years = 42.1891 mm/year
5-years = 76.0872 mm/year
10-years = 98.4483 mm/year
25-years = 126.6081 mm/year
50-years = 147.4315 mm/year
100-years = 168.0447 mm/year
250-years = 195.0998 mm/year
500-years = 215.4643 mm/year

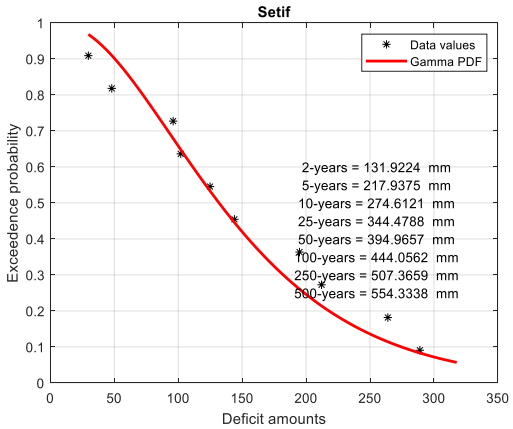
Setif
Data values
Gamma PDF
2-years = 131.9224 mm
5-years = 217.9375 mm
10-years = 274.6121 mm
25-years = 344.4788 mm
50-years = 394.9657 mm
100-years = 444.0562 mm
250-years = 507.3659 mm
500-years = 554.3338 mm
Exceedence probability
Deficit amounts

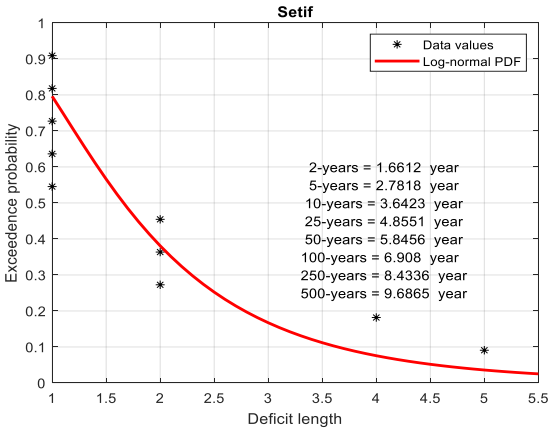
Setif
Data values
Log-normal PDF
2-years = 1.6612 year
5-years = 2.7818 year
10-years = 3.6423 year
25-years = 4.8551 year
50-years = 5.8456 year
100-years = 6.908 year
250-years = 8.4336 year
500-years = 9.6865 year
Exceedence probability
Deficit length

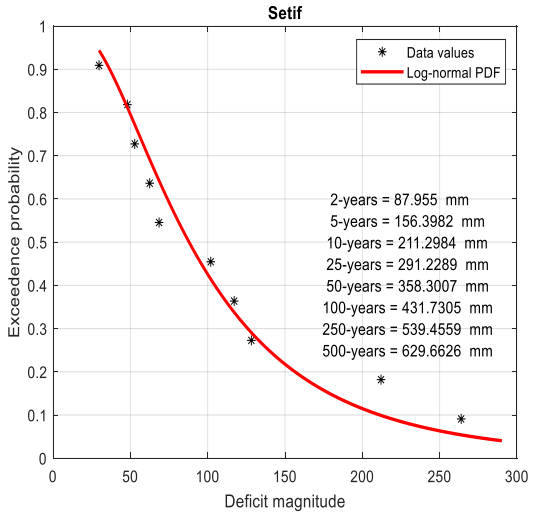
Setif
Data values
Log-normal PDF
2-years = 87.955 mm
5-years = 156.3982 mm
10-years = 211.2984 mm
25-years = 291.2289 mm
50-years = 358.3007 mm
100-years = 431.7305 mm
250-years = 539.4559 mm
500-years = 629.6626 mm
Exceedence probability
Deficit magnitude

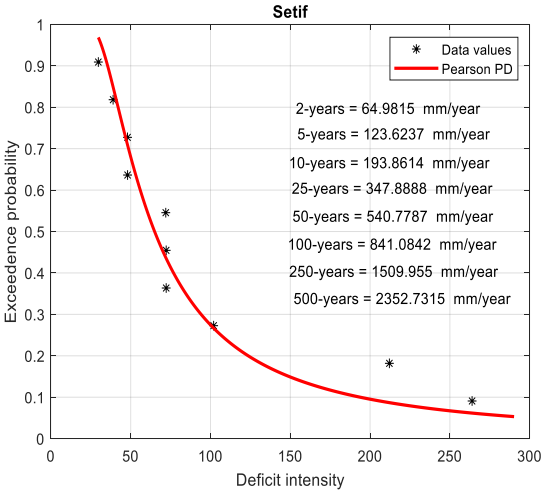
Setif
Data values
Pearson PD
2-years = 64.9815 mm/year
5-years = 123.6237 mm/year
10-years = 193.8614 mm/year
25-years = 347.8888 mm/year
50-years = 540.7787 mm/year
100-years = 841.0842 mm/year
250-years = 1509.955 mm/year
500-years = 2352.7315 mm/year
Exceedence probability
Deficit intensity

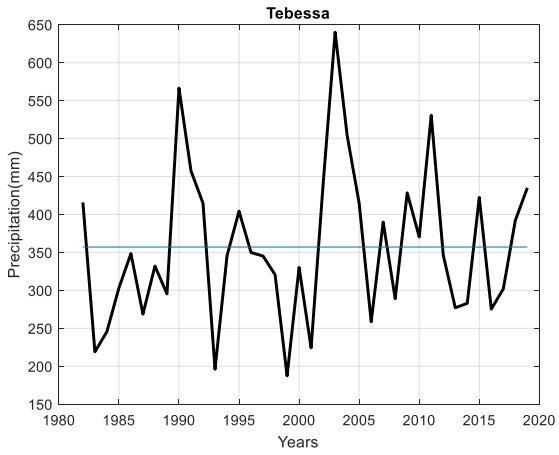
Tebessa
Precipitation (mm)
Years

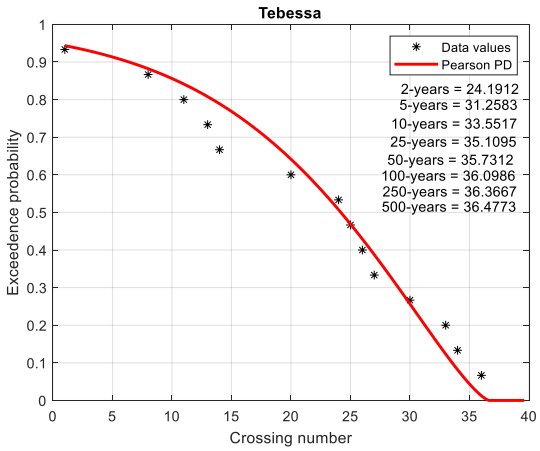
Tebessa
Data values
Pearson PD
2-years = 24.1912
5-years = 31.2583
10-years = 33.5517
25-years = 35.1095
50-years = 35.7312
100-years = 36.0986
250-years = 36.3667
500-years = 36.4773
Exceedence probability
Crossing number

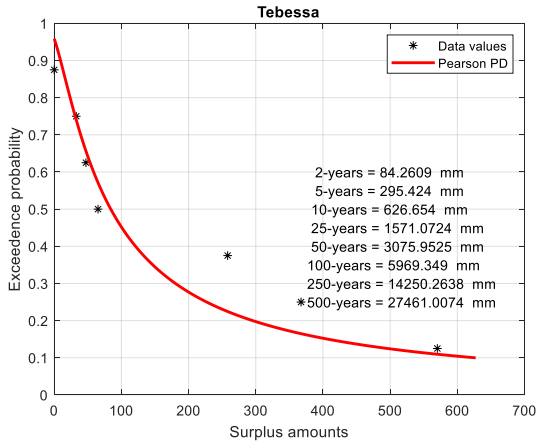
Tebessa
Data values
Pearson PD
2-years = 84.2609 mm
5-years = 295.424 mm
10-years = 626.654 mm
25-years = 1571.0724 mm
50-years = 3075.9525 mm
100-years = 5969.349 mm
250-years = 14250.2638 mm
500-years = 27461.0074 mm
Exceedence probability
Surplus amounts

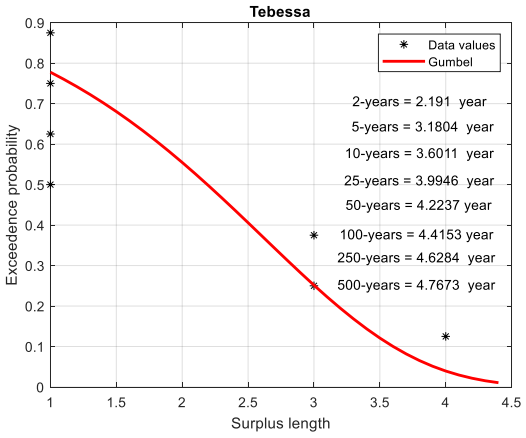
Tebessa
Data values
Gumbel
2-years = 2.191 year
5-years = 3.1804 year
10-years = 3.6011 year
25-years = 3.9946 year
50-years = 4.2237 year
100-years = 4.4153 year
250-years = 4.6284 year
500-years = 4.7673 year
Exceedence probability
Surplus length

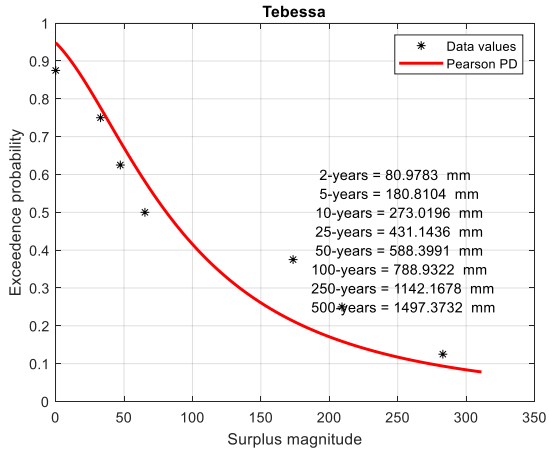
Tebessa
Data values
Pearson PD
2-years = 80.9783 mm
5-years = 180.8104 mm
10-years = 273.0196 mm
25-years = 431.1436 mm
50-years = 588.3991 mm
100-years = 788.9322 mm
250-years = 1142.1678 mm
500-years = 1497.3732 mm
Exceedence probability
Surplus magnitude

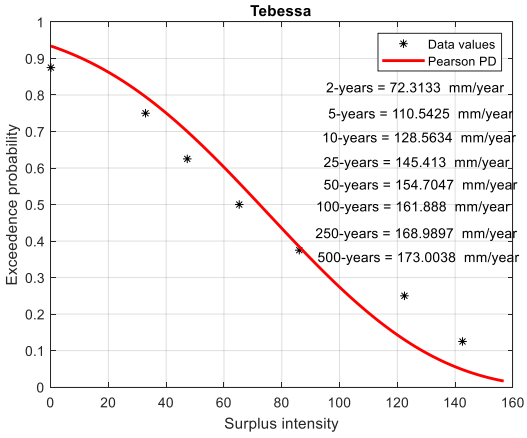
Tebessa
Data values
Pearson PD
2-years = 72.3133 mm/year
5-years = 110.5425 mm/year
10-years = 128.5634 mm/year
25-years = 145.413 mm/year
50-years = 154.7047 mm/year
100-years = 161.888 mm/year
250-years = 168.9897 mm/year
500-years = 173.0038 mm/year
Exceedence probability
Surplus intensity

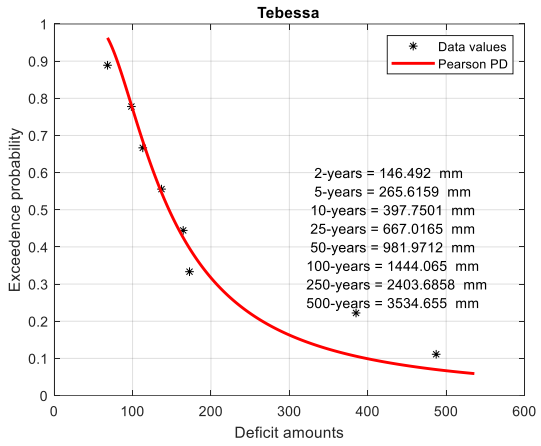
Tebessa
Data values
Pearson PD
2-years = 146.492 mm
5-years = 265.6159 mm
10-years = 397.7501 mm
25-years = 667.0165 mm
50-years = 981.9712 mm
100-years = 1444.065 mm
250-years = 2403.6858 mm
500-years = 3534.655 mm
Exceedence probability
Deficit amounts

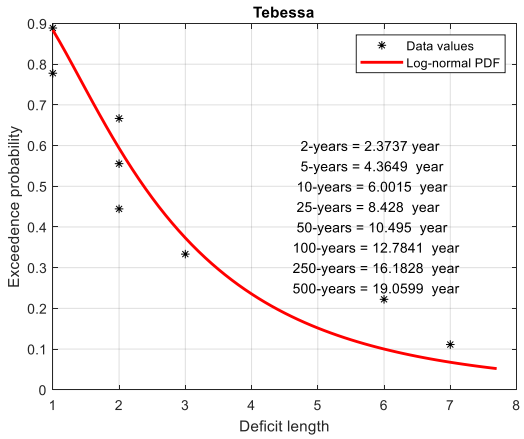
Tebessa
Data values
Log-normal PDF
2-years = 2.3737 year
5-years = 4.3649 year
10-years = 6.0015 year
25-years = 8.428 year
50-years = 10.495 year
100-years = 12.7841 year
250-years = 16.1828 year
500-years = 19.0599 year
Exceedence probability
Deficit length

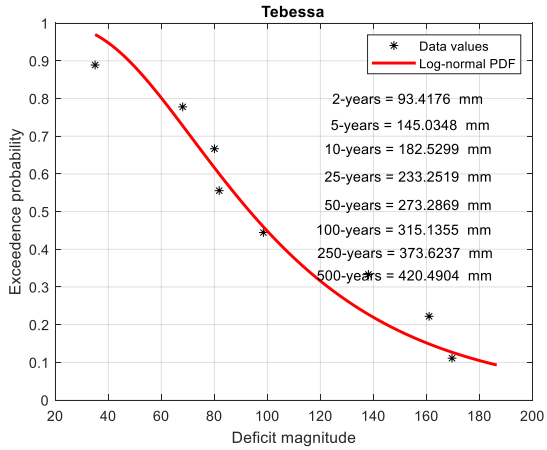
Tebessa
Data values
Log-normal PDF
2-years = 93.4176 mm
5-years = 145.0348 mm
10-years = 182.5299 mm
25-years = 233.2519 mm
50-years = 273.2869 mm
100-years = 315.1355 mm
250-years = 373.6237 mm
500-years = 420.4904 mm
Exceedence probability
Deficit magnitude

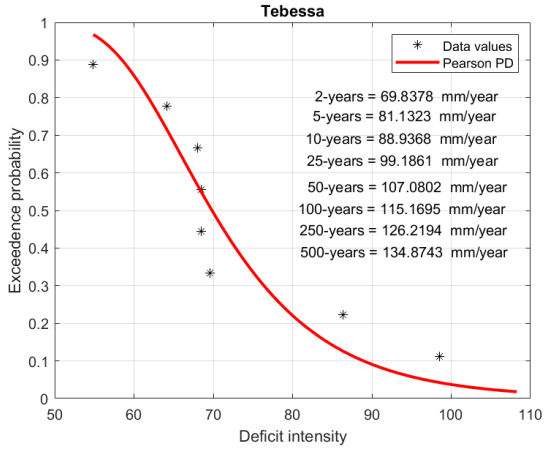
Tebessa
Data values
Pearson PD
2-years = 69.8378 mm/year
5-years = 81.1323 mm/year
10-years = 88.9368 mm/year
25-years = 99.1861 mm/year
50-years = 107.0802 mm/year
100-years = 115.1695 mm/year
250-years = 126.2194 mm/year
500-years = 134.8743 mm/year
Exceedence probability
Deficit intensity

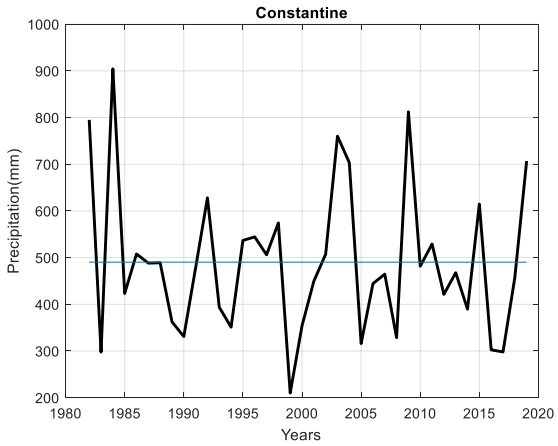
Constantine
Precipitation(mm)
Years

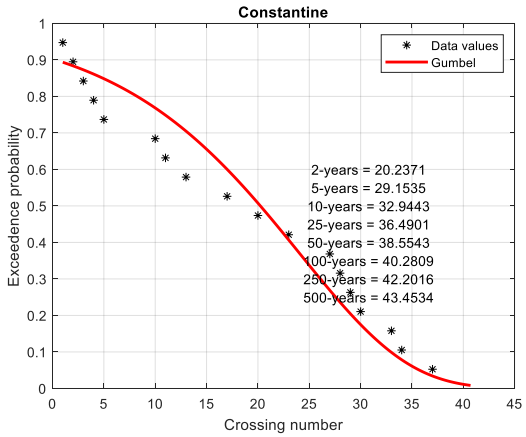
Constantine
Data values
Gumbel
Exceedence probability
Crossing number
2-years = 20.2371
5-years = 29.1535
10-years = 32.9443
25-years = 36.4901
50-years = 38.5543
100-years = 40.2809
250-years = 42.2016
500-years = 43.4534

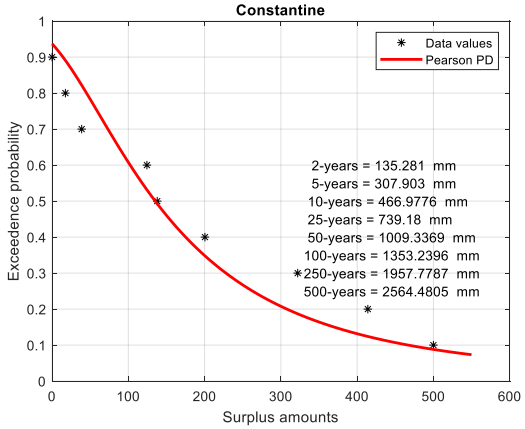
Constantine
Data values
Pearson PD
Exceedence probability
Surplus amounts
2-years = 135.281 mm
5-years = 307.903 mm
10-years = 466.9776 mm
25-years = 739.18 mm
50-years = 1009.3369 mm
100-years = 1353.2396 mm
250-years = 1957.7787 mm
500-years = 2564.4805 mm

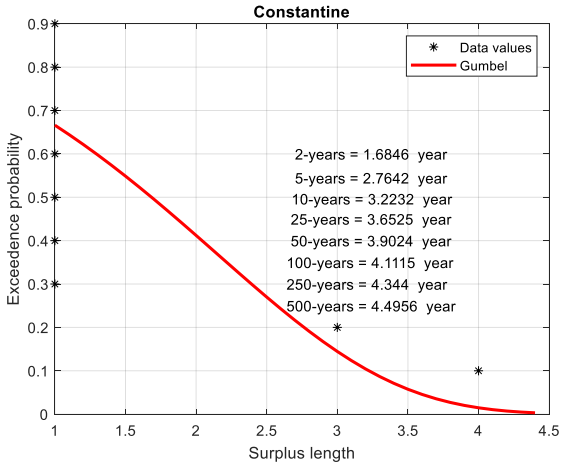
Constantine
Data values
Gumbel
Exceedence probability
Surplus length
2-years = 1.6846 year
5-years = 2.7642 year
10-years = 3.2232 year
25-years = 3.6525 year
50-years = 3.9024 year
100-years = 4.1115 year
250-years = 4.344 year
500-years = 4.4956 year

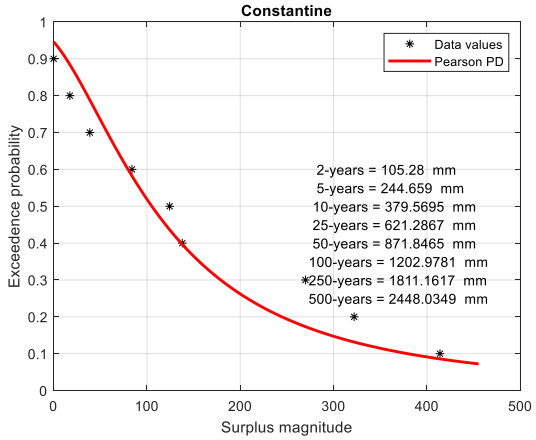
Constantine
Data values
Pearson PD
Exceedence probability
Surplus magnitude
2-years = 105.28 mm
5-years = 244.659 mm
10-years = 379.5695 mm
25-years = 621.2867 mm
50-years = 871.8465 mm
100-years = 1202.9781 mm
250-years = 1811.1617 mm
500-years = 2448.0349 mm

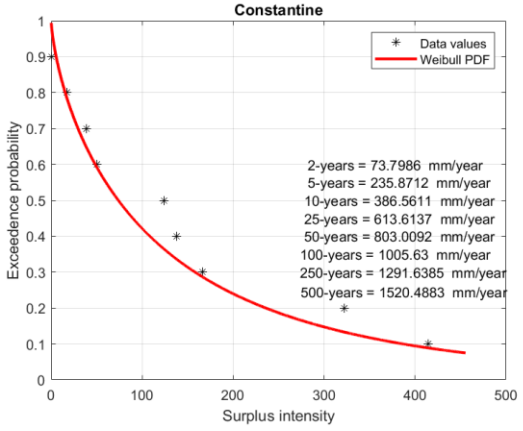
Constantine
Data values
Weibull PDF
Exceedence probability
Surplus intensity
2-years = 73.7986 mm/year
5-years = 235.8712 mm/year
10-years = 386.5611 mm/year
25-years = 613.6137 mm/year
50-years = 803.0092 mm/year
100-years = 1005.63 mm/year
250-years = 1291.6385 mm/year
500-years = 1520.4883 mm/year

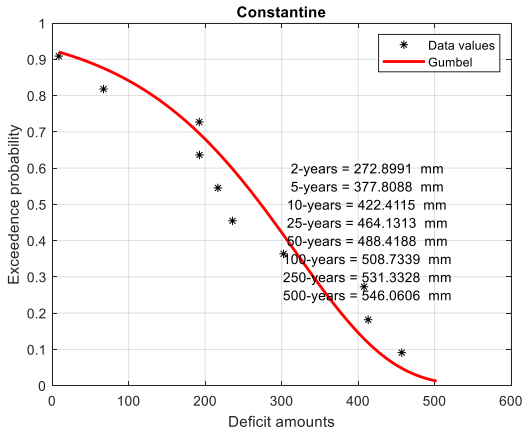
Constantine
Data values
Gumbel
2-years = 272.8991 mm
5-years = 377.8088 mm
10-years = 422.4115 mm
25-years = 464.1313 mm
50-years = 488.4188 mm
100-years = 508.7339 mm
250-years = 531.3328 mm
500-years = 546.0606 mm
Exceedence probability
Deficit amounts

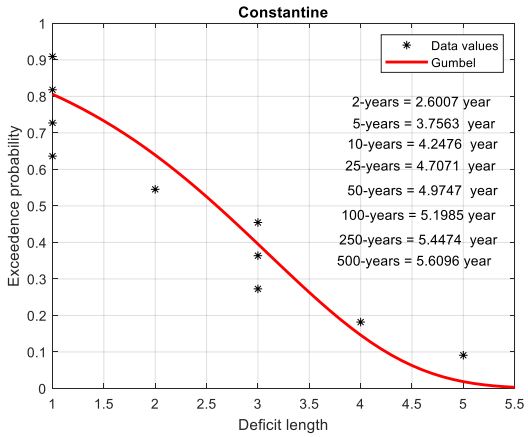
Constantine
Data values
Gumbel
2-years = 2.6007 year
5-years = 3.7563 year
10-years = 4.2476 year
25-years = 4.7071 year
50-years = 4.9747 year
100-years = 5.1985 year
250-years = 5.4474 year
500-years = 5.6096 year
Exceedence probability
Deficit length

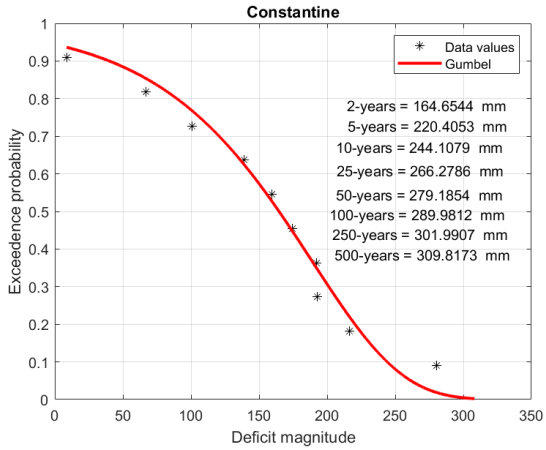
Constantine
Data values
Gumbel
2-years = 164.6544 mm
5-years = 220.4053 mm
10-years = 244.1079 mm
25-years = 266.2786 mm
50-years = 279.1854 mm
100-years = 289.9812 mm
250-years = 301.9907 mm
500-years = 309.8173 mm
Exceedence probability
Deficit magnitude

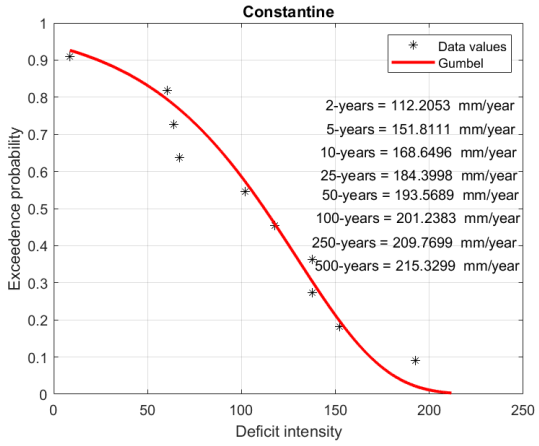
Constantine
Data values
Gumbel
2-years = 112.2053 mm/year
5-years = 151.8111 mm/year
10-years = 168.6496 mm/year
25-years = 184.3998 mm/year
50-years = 193.5689 mm/year
100-years = 201.2383 mm/year
250-years = 209.7699 mm/year
500-years = 215.3299 mm/year
Exceedence probability
Deficit intensity

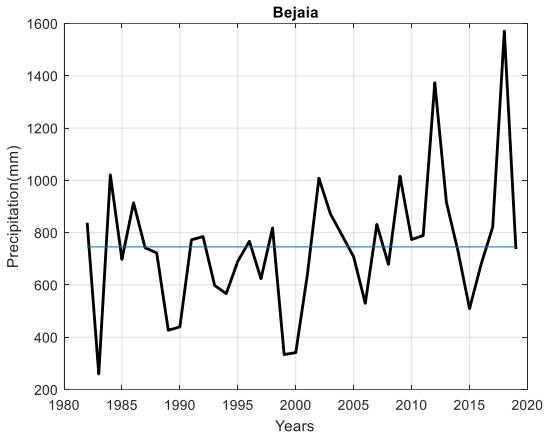
Bejaia
Precipitation(mm)
Years

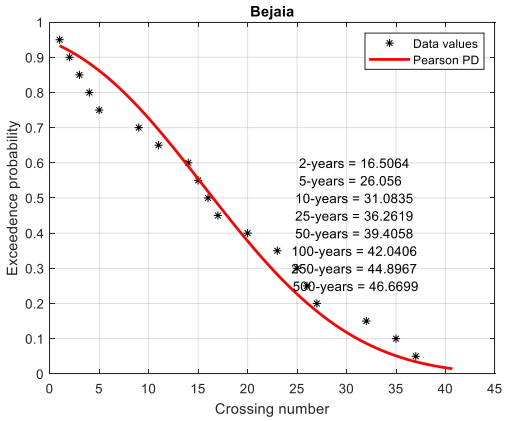
Bejaia
Data values
Pearson PD
Exceedence probability
Crossing number
2-years = 16.5064
5-years = 26.056
10-years = 31.0835
25-years = 36.2619
50-years = 39.4058
100-years = 42.0406
250-years = 44.8967
500-years = 46.6699

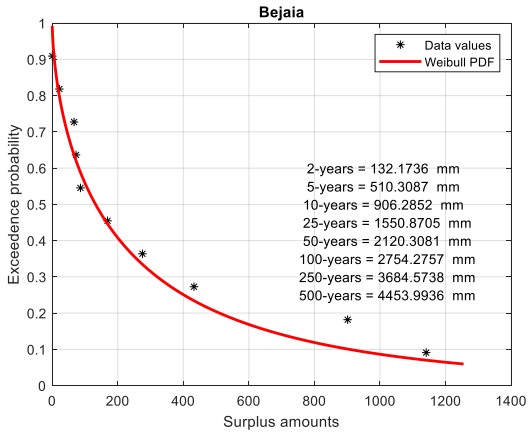
Bejaia
Data values
Weibull PDF
Exceedence probability
Surplus amounts
2-years = 132.1736 mm
5-years = 510.3087 mm
10-years = 906.2852 mm
25-years = 1550.8705 mm
50-years = 2120.3081 mm
100-years = 2754.2757 mm
250-years = 3684.5738 mm
500-years = 4453.9936 mm

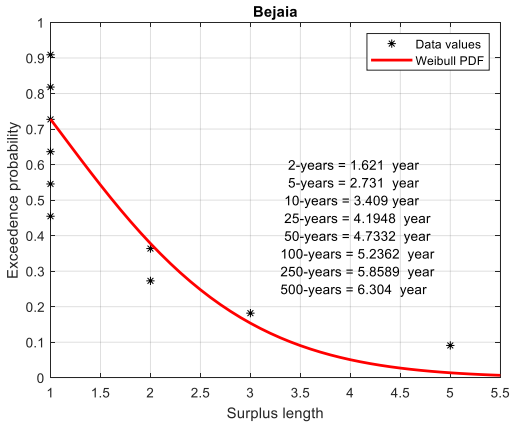
Bejaia
Data values
Weibull PDF
Exceedence probability
Surplus length
2-years = 1.621 year
5-years = 2.731 year
10-years = 3.409 year
25-years = 4.1948 year
50-years = 4.7332 year
100-years = 5.2362 year
250-years = 5.8589 year
500-years = 6.304 year

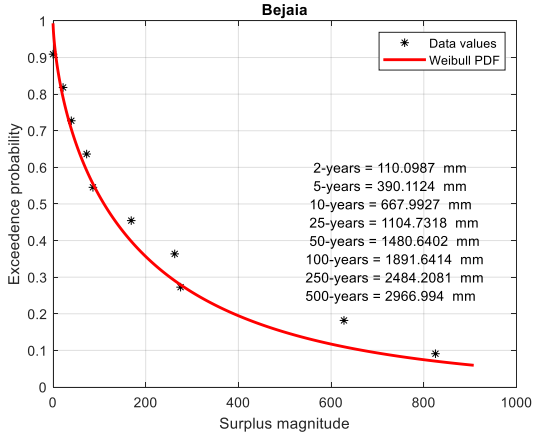
Bejaia
Data values
Weibull PDF
Exceedence probability
Surplus magnitude
2-years = 110.0987 mm
5-years = 390.1124 mm
10-years = 667.9927 mm
25-years = 1104.7318 mm
50-years = 1480.6402 mm
100-years = 1891.6414 mm
250-years = 2484.2081 mm
500-years = 2966.994 mm

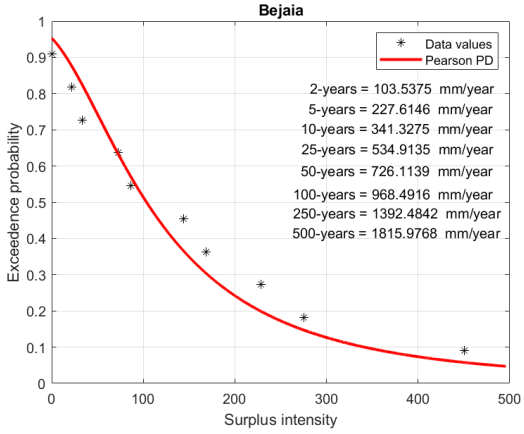
Bejaia
Data values
Pearson PD
Exceedence probability
Surplus intensity
2-years = 103.5375 mm/year
5-years = 227.6146 mm/year
10-years = 341.3275 mm/year
25-years = 534.9135 mm/year
50-years = 726.1139 mm/year
100-years = 968.4916 mm/year
250-years = 1392.4842 mm/year
500-years = 1815.9768 mm/year

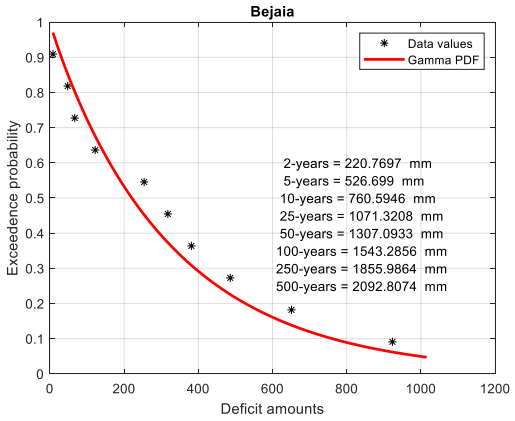
Bejaia
Data values
Gamma PDF
2-years = 220.7697 mm
5-years = 526.699 mm
10-years = 760.5946 mm
25-years = 1071.3208 mm
50-years = 1307.0933 mm
100-years = 1543.2856 mm
250-years = 1855.9864 mm
500-years = 2092.8074 mm
Exceedence probability
Deficit amounts

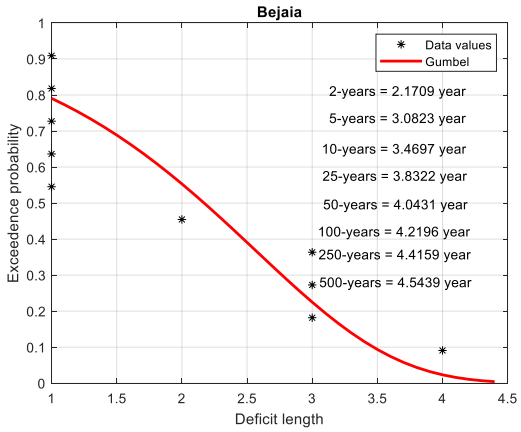
Bejaia
Data values
Gumbel
2-years = 2.1709 year
5-years = 3.0823 year
10-years = 3.4697 year
25-years = 3.8322 year
50-years = 4.0431 year
100-years = 4.2196 year
250-years = 4.4159 year
500-years = 4.5439 year
Exceedence probability
Deficit length

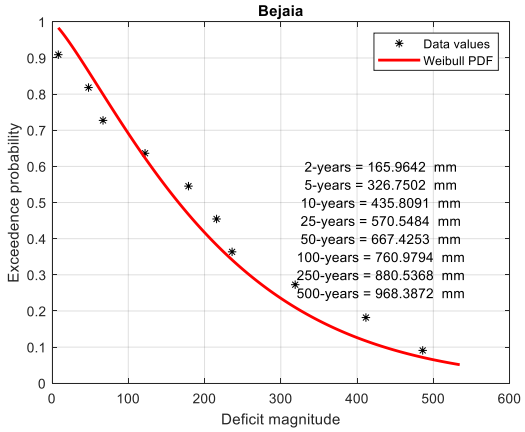
Bejaia
Data values
Weibull PDF
2-years = 165.9642 mm
5-years = 326.7502 mm
10-years = 435.8091 mm
25-years = 570.5484 mm
50-years = 667.4253 mm
100-years = 760.9794 mm
250-years = 880.5368 mm
500-years = 968.3872 mm
Exceedence probability
Deficit magnitude

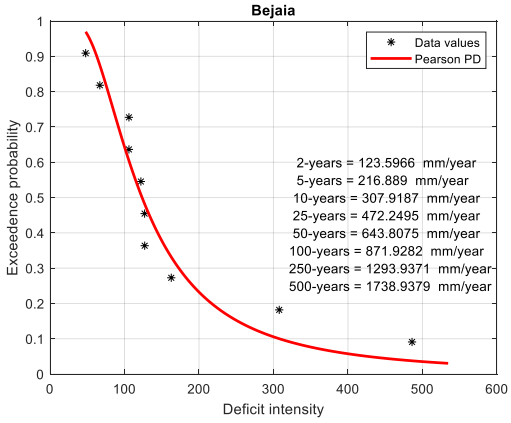
Bejaia
Data values
Pearson PD
2-years = 123.5966 mm/year
5-years = 216.889 mm/year
10-years = 307.9187 mm/year
25-years = 472.2495 mm/year
50-years = 643.8075 mm/year
100-years = 871.9282 mm/year
250-years = 1293.9371 mm/year
500-years = 1738.9379 mm/year
Exceedence probability
Deficit intensity

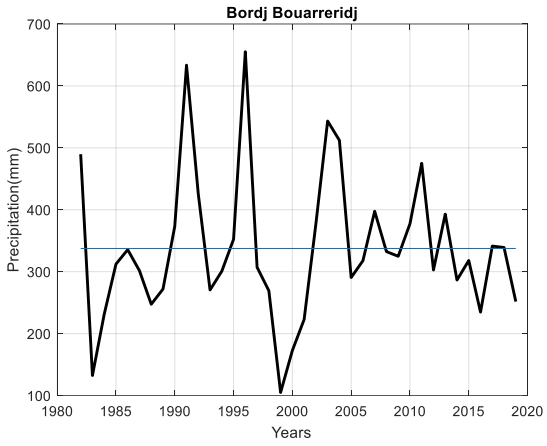
Bordj Bouarreridj
Precipitation(mm)
Years

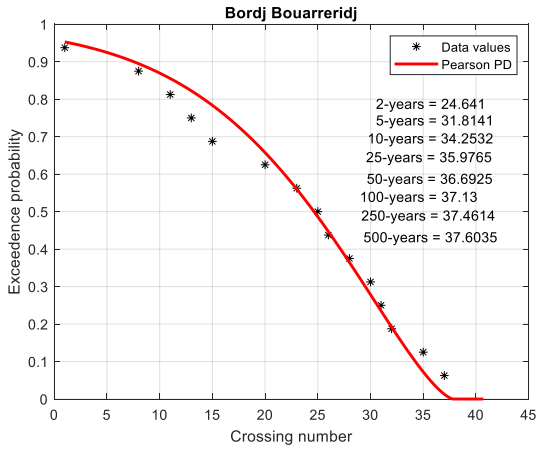
Bordj Bouarreridj
Data values
Pearson PD
2-years = 24.641
5-years = 31.8141
10-years = 34.2532
25-years = 35.9765
50-years = 36.6925
100-years = 37.13
250-years = 37.4614
500-years = 37.6035
Exceedence probability
Crossing number

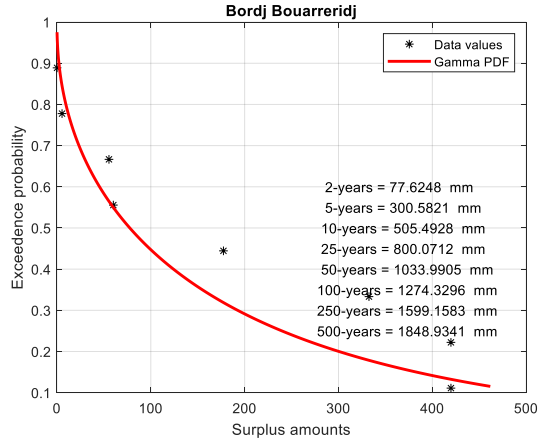
Bordj Bouarreridj
Data values
Gamma PDF
2-years = 77.6248 mm
5-years = 300.5821 mm
10-years = 505.4928 mm
25-years = 800.0712 mm
50-years = 1033.9905 mm
100-years = 1274.3296 mm
250-years = 1599.1583 mm
500-years = 1848.9341 mm
Exceedence probability
Surplus amounts

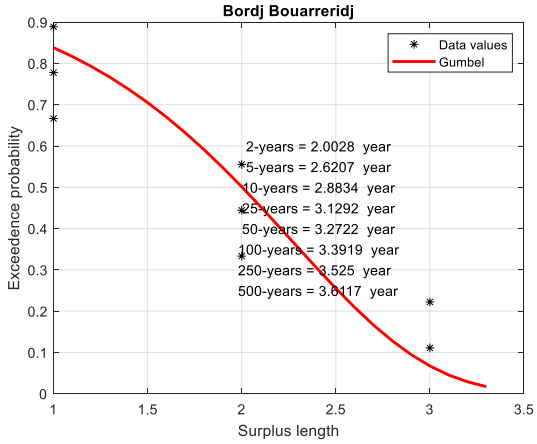
Bordj Bouarreridj
Data values
Gumbel
2-years = 2.0028 year
5-years = 2.6207 year
10-years = 2.8834 year
25-years = 3.1292 year
50-years = 3.2722 year
100-years = 3.3919 year
250-years = 3.525 year
500-years = 3.6417 year
Exceedence probability
Surplus length

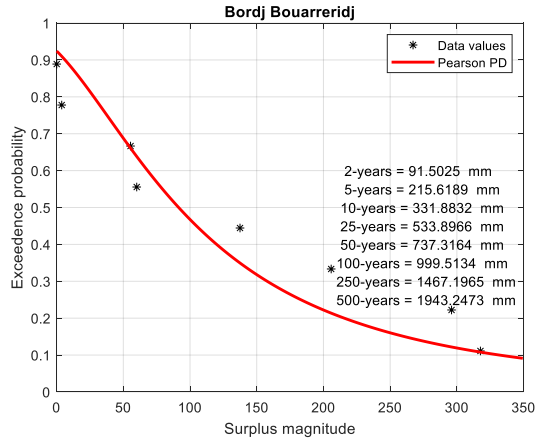
Bordj Bouarreridj
Data values
Pearson PD
2-years = 91.5025 mm
5-years = 215.6189 mm
10-years = 331.8832 mm
25-years = 533.8966 mm
50-years = 737.3164 mm
100-years = 999.5134 mm
250-years = 1467.1965 mm
500-years = 1943.2473 mm
Exceedence probability
Surplus magnitude

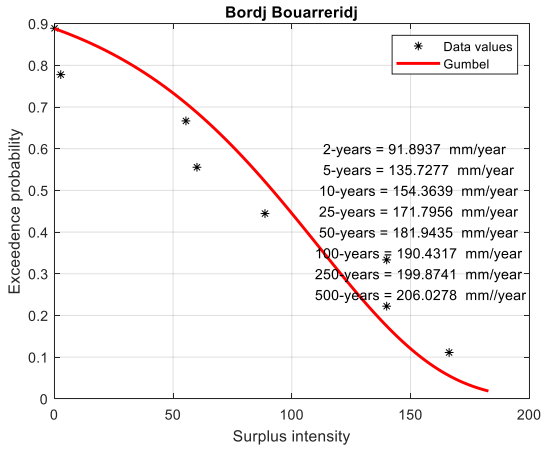
Bordj Bouarreridj
Data values
Gumbel
2-years = 91.8937 mm/year
5-years = 135.7277 mm/year
10-years = 154.3639 mm/year
25-years = 171.7956 mm/year
50-years = 181.9435 mm/year
100-years = 190.4317 mm/year
250-years = 199.8741 mm/year
500-years = 206.0278 mm//year
Exceedence probability
Surplus intensity

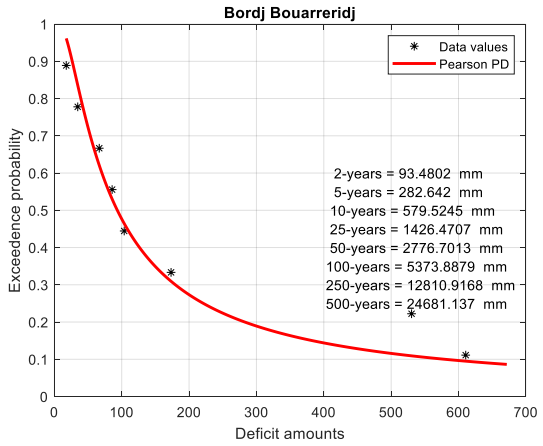
Bordj Bouarreridj
Data values
Pearson PD
2-years = 93.4802 mm
5-years = 282.642 mm
10-years = 579.5245 mm
25-years = 1426.4707 mm
50-years = 2776.7013 mm
100-years = 5373.8879 mm
250-years = 12810.9168 mm
500-years = 24681.137 mm
Exceedence probability
Deficit amounts

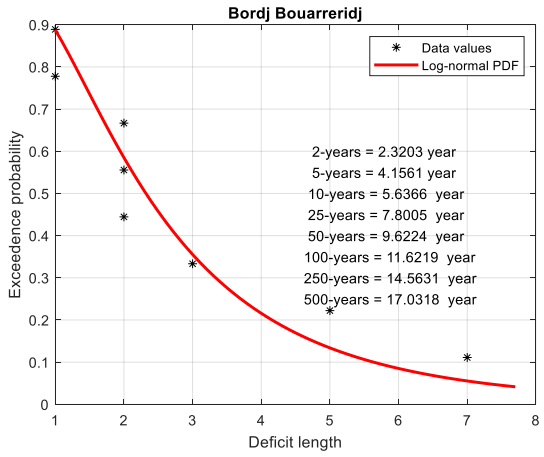
Bordj Bouarreridj
Data values
Log-normal PDF
2-years = 2.3203 year
5-years = 4.1561 year
10-years = 5.6366 year
25-years = 7.8005 year
50-years = 9.6224 year
100-years = 11.6219 year
250-years = 14.5631 year
500-years = 17.0318 year
Exceedence probability
Deficit length

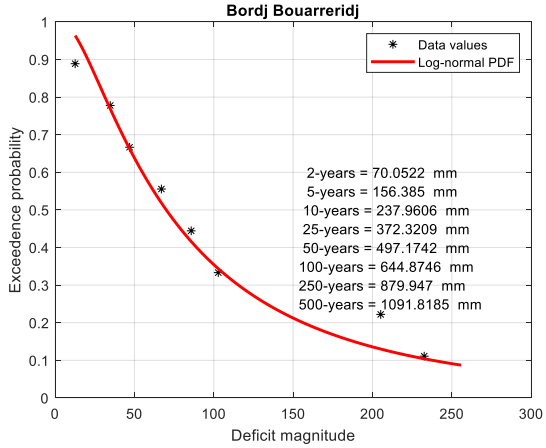
Bordj Bouarreridj
Data values
Log-normal PDF
2-years = 70.0522 mm
5-years = 156.385 mm
10-years = 237.9606 mm
25-years = 372.3209 mm
50-years = 497.1742 mm
100-years = 644.8746 mm
250-years = 879.947 mm
500-years = 1091.8185 mm
Exceedence probability
Deficit magnitude

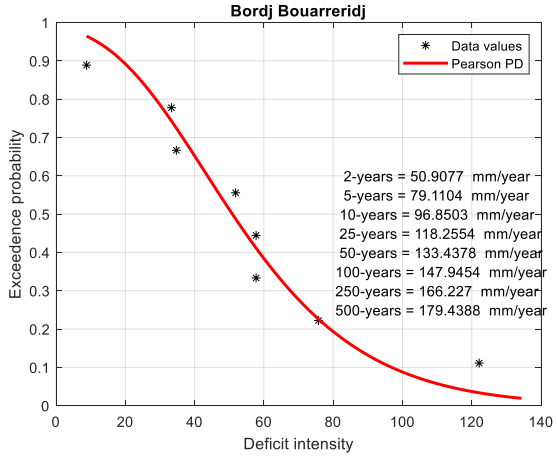
Bordj Bouarreridj
Data values
Pearson PD
2-years = 50.9077 mm/year
5-years = 79.1104 mm/year
10-years = 96.8503 mm/year
25-years = 118.2554 mm/year
50-years = 133.4378 mm/year
100-years = 147.9454 mm/year
250-years = 166.227 mm/year
500-years = 179.4388 mm/year
Exceedence probability
Deficit intensity

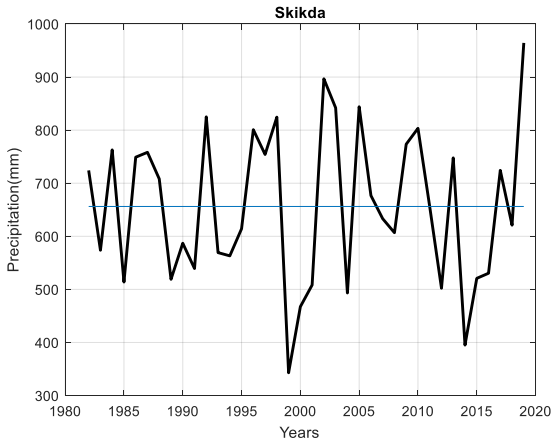
Skikda
Precipitation(mm)
Years

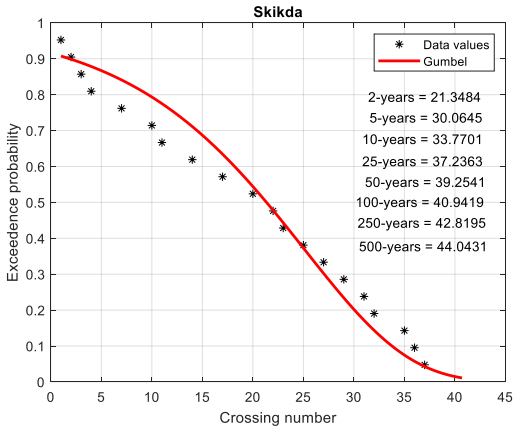
Skikda
Data values
Gumbel
2-years = 21.3484
5-years = 30.0645
10-years = 33.7701
25-years = 37.2363
50-years = 39.2541
100-years = 40.9419
250-years = 42.8195
500-years = 44.0431
Exceedence probability
Crossing number

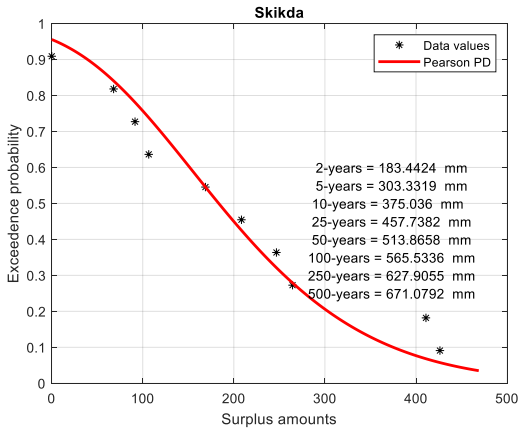
Skikda
Data values
Pearson PD
2-years = 183.4424 mm
5-years = 303.3319 mm
10-years = 375.036 mm
25-years = 457.7382 mm
50-years = 513.8658 mm
100-years = 565.5336 mm
250-years = 627.9055 mm
500-years = 671.0792 mm
Exceedence probability
Surplus amounts

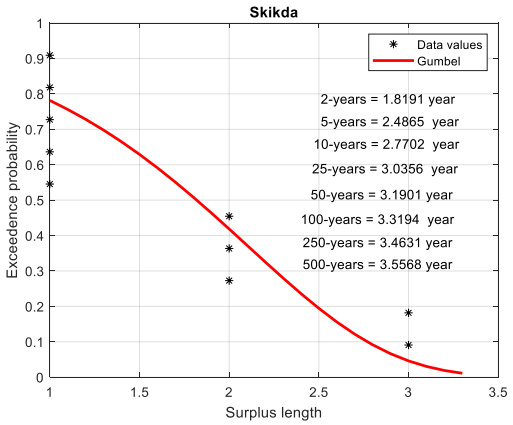
Skikda
Data values
Gumbel
2-years = 1.8191 year
5-years = 2.4865 year
10-years = 2.7702 year
25-years = 3.0356 year
50-years = 3.1901 year
100-years = 3.3194 year
250-years = 3.4631 year
500-years = 3.5568 year
Exceedence probability
Surplus length

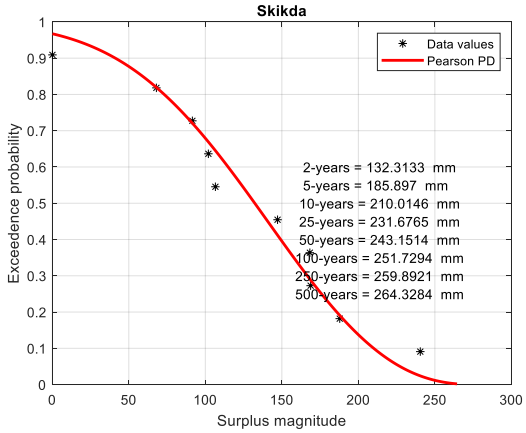
Skikda
Data values
Pearson PD
2-years = 132.3133 mm
5-years = 185.897 mm
10-years = 210.0146 mm
25-years = 231.6765 mm
50-years = 243.1514 mm
100-years = 251.7294 mm
250-years = 259.8921 mm
500-years = 264.3284 mm
Exceedence probability
Surplus magnitude

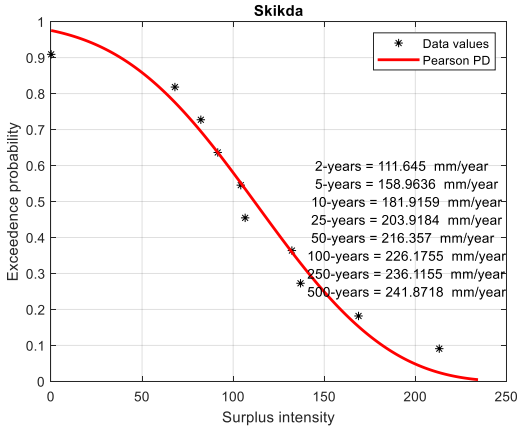
Skikda
Data values
Pearson PD
2-years = 111.645 mm/year
5-years = 158.9636 mm/year
10-years = 181.9159 mm/year
25-years = 203.9184 mm/year
50-years = 216.357 mm/year
100-years = 226.1755 mm/year
250-years = 236.1155 mm/year
500-years = 241.8718 mm/year
Exceedence probability
Surplus intensity

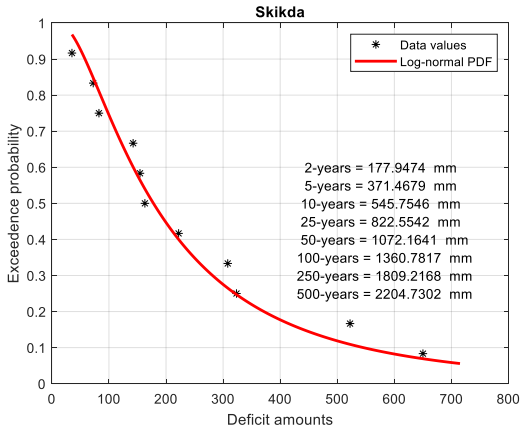
Skikda
Data values
Log-normal PDF
2-years = 177.9474 mm
5-years = 371.4679 mm
10-years = 545.7546 mm
25-years = 822.5542 mm
50-years = 1072.1641 mm
100-years = 1360.7817 mm
250-years = 1809.2168 mm
500-years = 2204.7302 mm
Exceedence probability
Deficit amounts

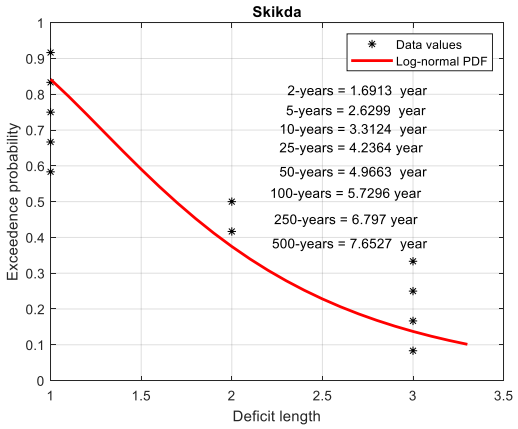
Skikda
Data values
Log-normal PDF
2-years = 1.6913 year
5-years = 2.6299 year
10-years = 3.3124 year
25-years = 4.2364 year
50-years = 4.9663 year
100-years = 5.7296 year
250-years = 6.797 year
500-years = 7.6527 year
Exceedence probability
Deficit length

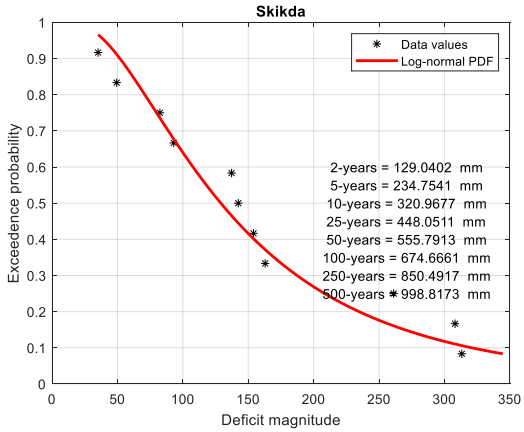
Skikda
Data values
Log-normal PDF
2-years = 129.0402 mm
5-years = 234.7541 mm
10-years = 320.9677 mm
25-years = 448.0511 mm
50-years = 555.7913 mm
100-years = 674.6661 mm
250-years = 850.4917 mm
500-years = 998.8173 mm
Exceedence probability
Deficit magnitude

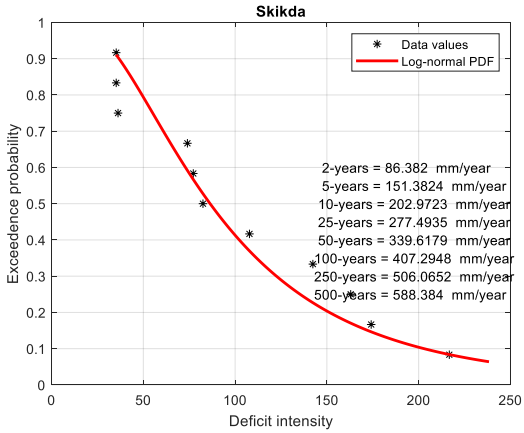
Skikda
Data values
Log-normal PDF
2-years = 86.382 mm/year
5-years = 151.3824 mm/year
10-years = 202.9723 mm/year
25-years = 277.4935 mm/year
50-years = 339.6179 mm/year
100-years = 407.2948 mm/year
250-years = 506.0652 mm/year
500-years = 588.384 mm/year
Exceedence probability
Deficit intensity

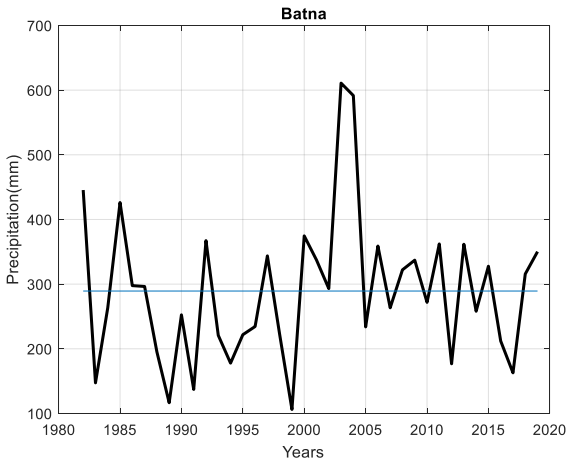
Batna
Precipitation(mm)
Years

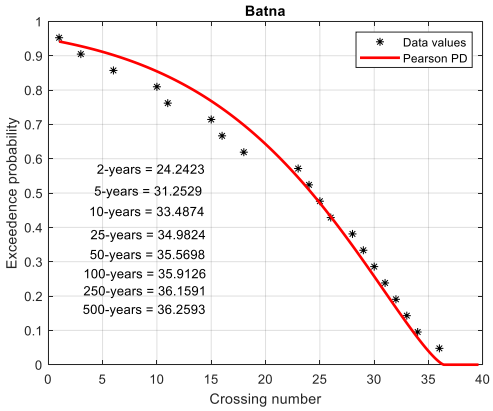
Batna
Data values
Pearson PD
Exceedence probability
2-years = 24.2423
5-years = 31.2529
10-years = 33.4874
25-years = 34.9824
50-years = 35.5698
100-years = 35.9126
250-years = 36.1591
500-years = 36.2593
Crossing number

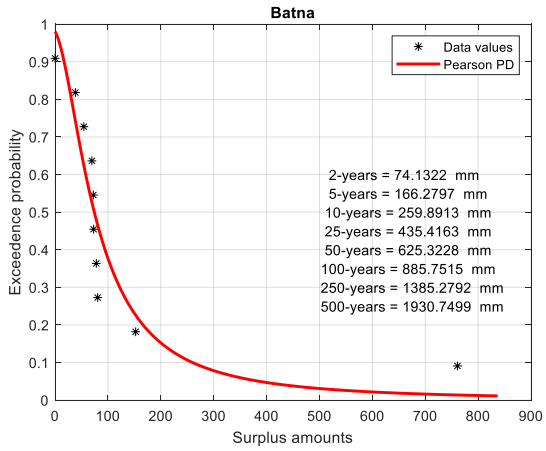
Batna
Data values
Pearson PD
Exceedence probability
2-years = 74.1322 mm
5-years = 166.2797 mm
10-years = 259.8913 mm
25-years = 435.4163 mm
50-years = 625.3228 mm
100-years = 885.7515 mm
250-years = 1385.2792 mm
500-years = 1930.7499 mm
Surplus amounts

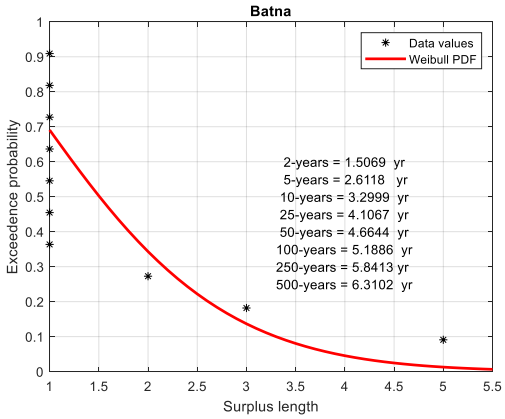
Batna
Data values
Weibull PDF
Exceedence probability
2-years = 1.5069 yr
5-years = 2.6118 yr
10-years = 3.2999 yr
25-years = 4.1067 yr
50-years = 4.6644 yr
100-years = 5.1886 yr
250-years = 5.8413 yr
500-years = 6.3102 yr
Surplus length

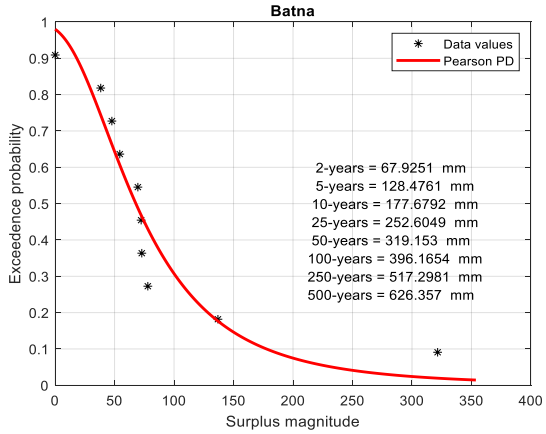
Batna
Data values
Pearson PD
Exceedence probability
2-years = 67.9251 mm
5-years = 128.4761 mm
10-years = 177.6792 mm
25-years = 252.6049 mm
50-years = 319.153 mm
100-years = 396.1654 mm
250-years = 517.2981 mm
500-years = 626.357 mm
Surplus magnitude

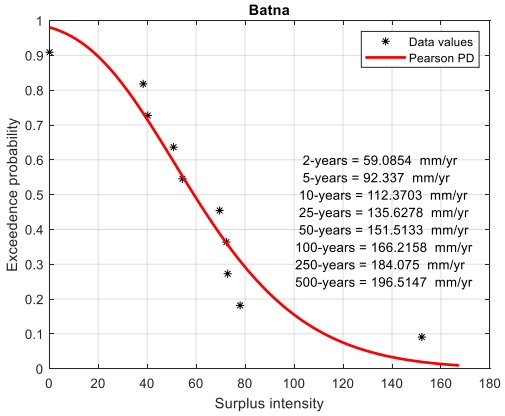
Batna
Data values
Pearson PD
Exceedence probability
2-years = 59.0854 mm/yr
5-years = 92.337 mm/yr
10-years = 112.3703 mm/yr
25-years = 135.6278 mm/yr
50-years = 151.5133 mm/yr
100-years = 166.2158 mm/yr
250-years = 184.075 mm/yr
500-years = 196.5147 mm/yr
Surplus intensity

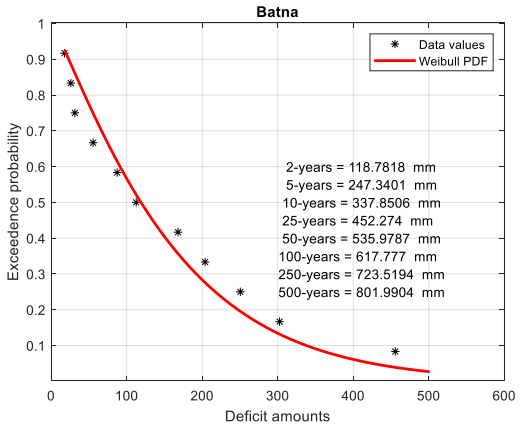
Batna
Data values
Weibull PDF
2-years = 118.7818 mm
5-years = 247.3401 mm
10-years = 337.8506 mm
25-years = 452.274 mm
50-years = 535.9787 mm
100-years = 617.777 mm
250-years = 723.5194 mm
500-years = 801.9904 mm
Exceedence probability
Deficit amounts

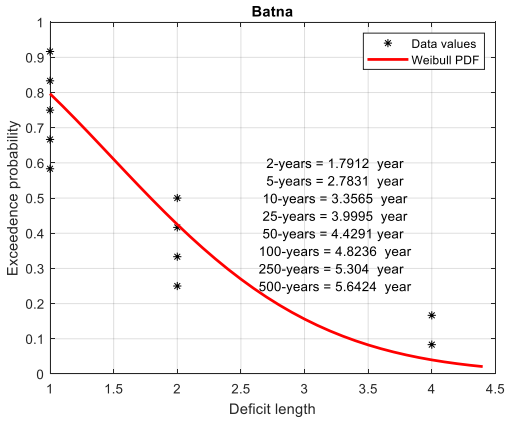
Batna
Data values
Weibull PDF
2-years = 1.7912 year
5-years = 2.7831 year
10-years = 3.3565 year
25-years = 3.9995 year
50-years = 4.4291 year
100-years = 4.8236 year
250-years = 5.304 year
500-years = 5.6424 year
Exceedence probability
Deficit length

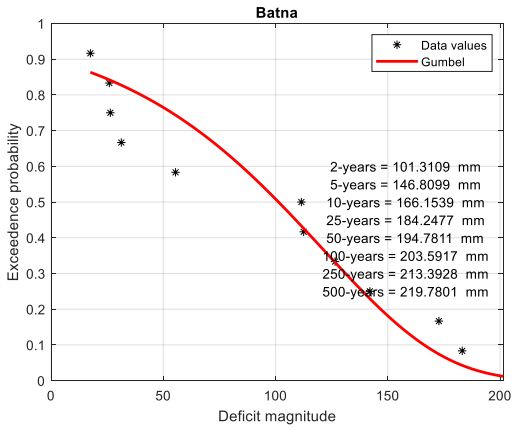
Batna
Data values
Gumbel
2-years = 101.3109 mm
5-years = 146.8099 mm
10-years = 166.1539 mm
25-years = 184.2477 mm
50-years = 194.7811 mm
100-years = 203.5917 mm
250-years = 213.3928 mm
500-years = 219.7801 mm
Exceedence probability
Deficit magnitude

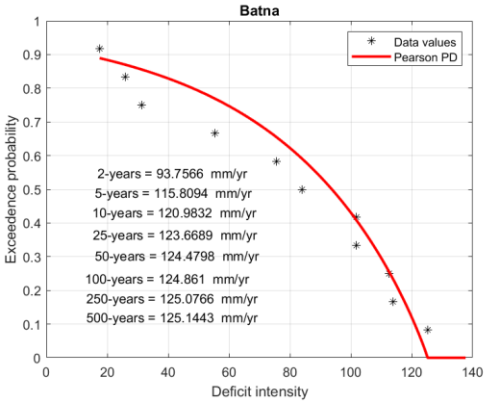
Batna
Data values
Pearson PD
2-years = 93.7566 mm/yr
5-years = 115.8094 mm/yr
10-years = 120.9832 mm/yr
25-years = 123.6689 mm/yr
50-years = 124.4798 mm/yr
100-years = 124.861 mm/yr
250-years = 125.0766 mm/yr
500-years = 125.1443 mm/yr
Exceedence probability
Deficit intensity

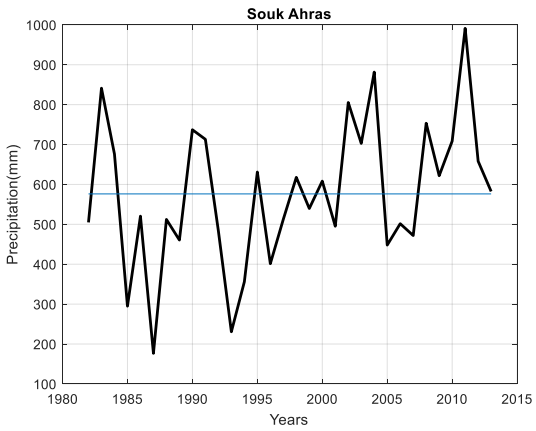
Souk Ahras
Precipitation(mm)
Years

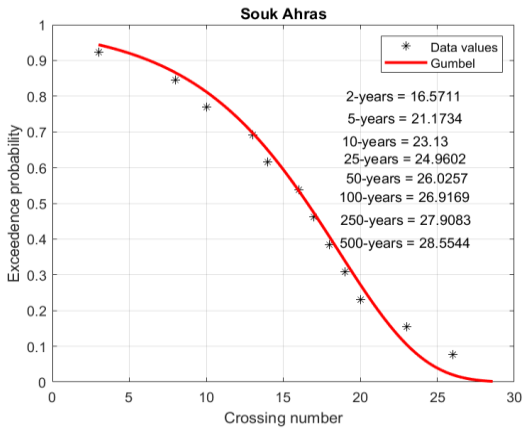
Souk Ahras
Data values
Gumbel
2-years = 16.5711
5-years = 21.1734
10-years = 23.13
25-years = 24.9602
50-years = 26.0257
100-years = 26.9169
250-years = 27.9083
500-years = 28.5544
Exceedence probability
Crossing number

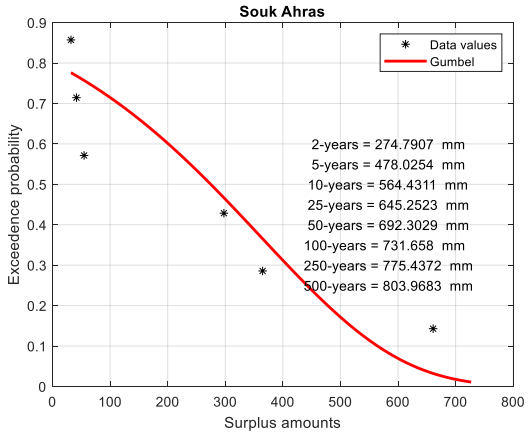
Souk Ahras
Data values
Gumbel
2-years = 274.7907 mm
5-years = 478.0254 mm
10-years = 564.4311 mm
25-years = 645.2523 mm
50-years = 692.3029 mm
100-years = 731.658 mm
250-years = 775.4372 mm
500-years = 803.9683 mm
Exceedence probability
Surplus amounts

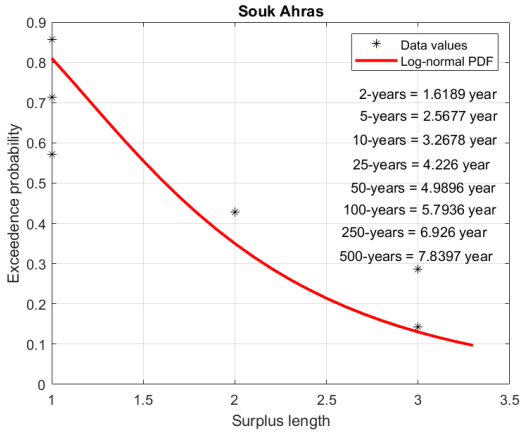
Souk Ahras
Data values
Log-normal PDF
2-years = 1.6189 year
5-years = 2.5677 year
10-years = 3.2678 year
25-years = 4.226 year
50-years = 4.9896 year
100-years = 5.7936 year
250-years = 6.926 year
500-years = 7.8397 year
Exceedence probability
Surplus length

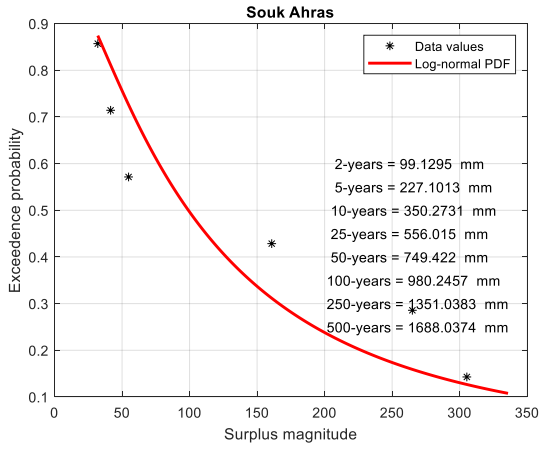
Souk Ahras
Data values
Log-normal PDF
2-years = 99.1295 mm
5-years = 227.1013 mm
10-years = 350.2731 mm
25-years = 556.015 mm
50-years = 749.422 mm
100-years = 980.2457 mm
250-years = 1351.0383 mm
500-years = 1688.0374 mm
Exceedence probability
Surplus magnitude

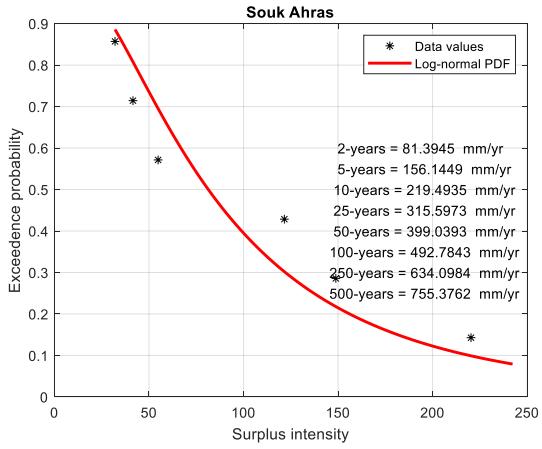
Souk Ahras
Data values
Log-normal PDF
2-years = 81.3945 mm/yr
5-years = 156.1449 mm/yr
10-years = 219.4935 mm/yr
25-years = 315.5973 mm/yr
50-years = 399.0393 mm/yr
100-years = 492.7843 mm/yr
250-years = 634.0984 mm/yr
500-years = 755.3762 mm/yr
Exceedence probability
Surplus intensity

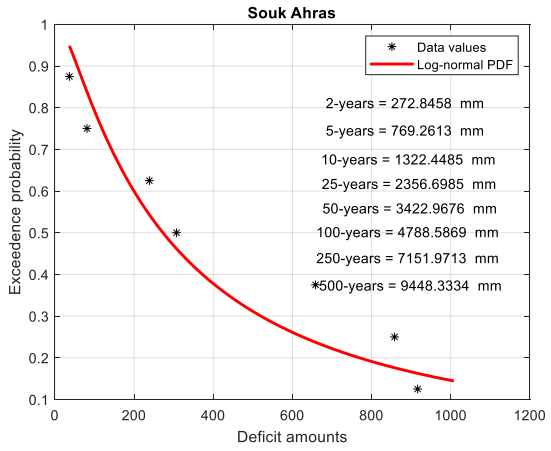
Souk Ahras
Data values
Log-normal PDF
2-years = 272.8458 mm
5-years = 769.2613 mm
10-years = 1322.4485 mm
25-years = 2356.6985 mm
50-years = 3422.9676 mm
100-years = 4788.5869 mm
250-years = 7151.9713 mm
500-years = 9448.3334 mm
Exceedence probability
Deficit amounts

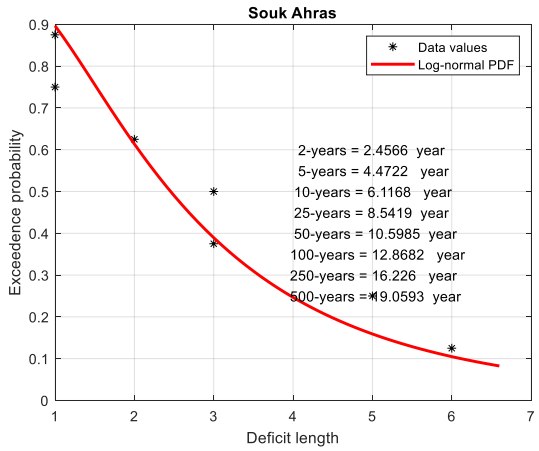
Souk Ahras
Data values
Log-normal PDF
2-years = 2.4566 year
5-years = 4.4722 year
10-years = 6.1168 year
25-years = 8.5419 year
50-years = 10.5985 year
100-years = 12.8682 year
250-years = 16.226 year
500-years = 19.0593 year
Exceedence probability
Deficit length

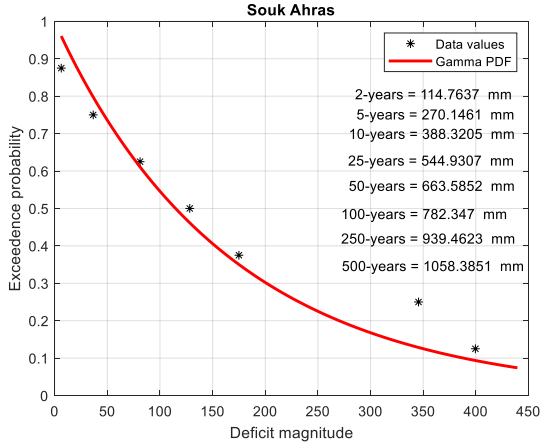
Souk Ahras
Data values
Gamma PDF
2-years = 114.7637 mm
5-years = 270.1461 mm
10-years = 388.3205 mm
25-years = 544.9307 mm
50-years = 663.5852 mm
100-years = 782.347 mm
250-years = 939.4623 mm
500-years = 1058.3851 mm
Exceedence probability
Deficit magnitude

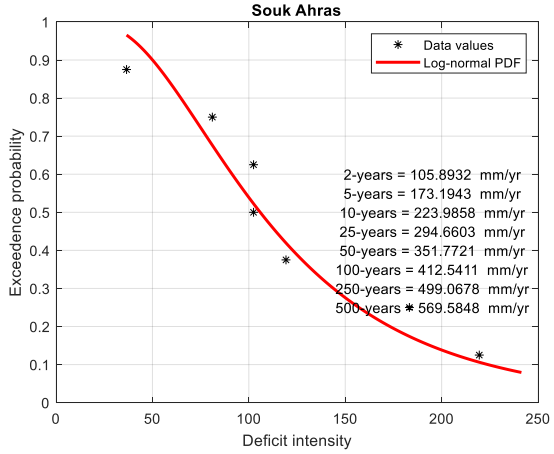
Souk Ahras
Data values
Log-normal PDF
2-years = 105.8932 mm/yr
5-years = 173.1943 mm/yr
10-years = 223.9858 mm/yr
25-years = 294.6603 mm/yr
50-years = 351.7721 mm/yr
100-years = 412.5411 mm/yr
250-years = 499.0678 mm/yr
500-years = 569.5848 mm/yr
Exceedence probability
Deficit intensity

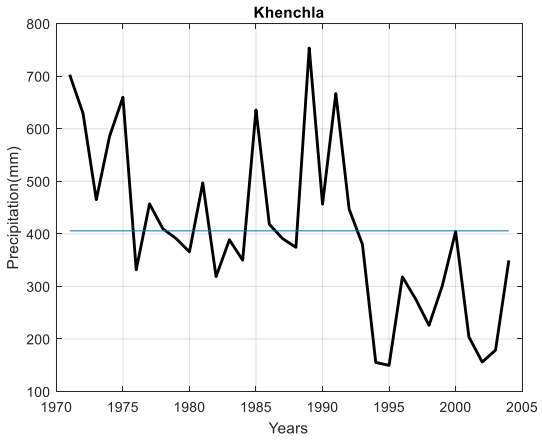
Khenchla
Precipitation(mm)
Years

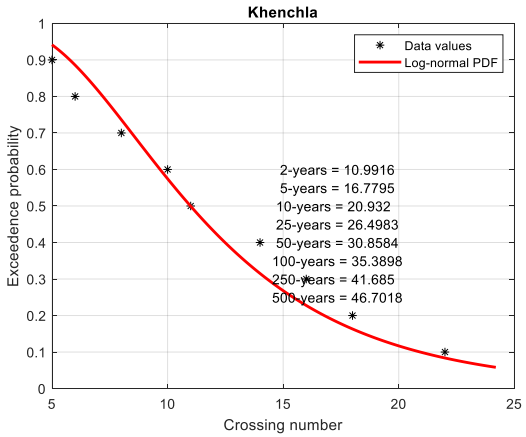
Khenchla
Data values
Log-normal PDF
Exceedence probability
Crossing number
2-years = 10.9916
5-years = 16.7795
10-years = 20.932
25-years = 26.4983
50-years = 30.8584
100-years = 35.3898
250-years = 41.685
500-years = 46.7018

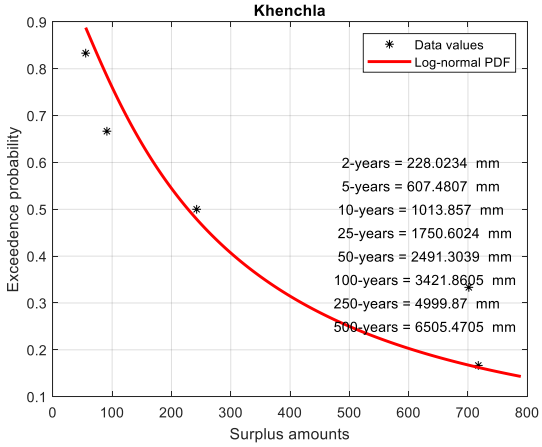
Khenchla
Data values
Log-normal PDF
Exceedence probability
Surplus amounts
2-years = 228.0234 mm
5-years = 607.4807 mm
10-years = 1013.857 mm
25-years = 1750.6024 mm
50-years = 2491.3039 mm
100-years = 3421.8605 mm
250-years = 4999.87 mm
500-years = 6505.4705 mm

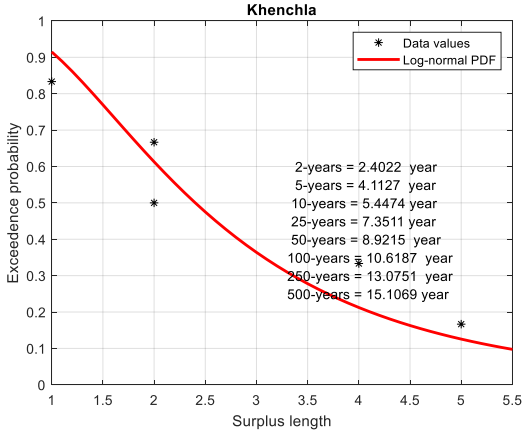
Khenchla
Data values
Log-normal PDF
Exceedence probability
Surplus length
2-years = 2.4022 year
5-years = 4.1127 year
10-years = 5.4474 year
25-years = 7.3511 year
50-years = 8.9215 year
100-years = 10.6187 year
250-years = 13.0751 year
500-years = 15.1069 year

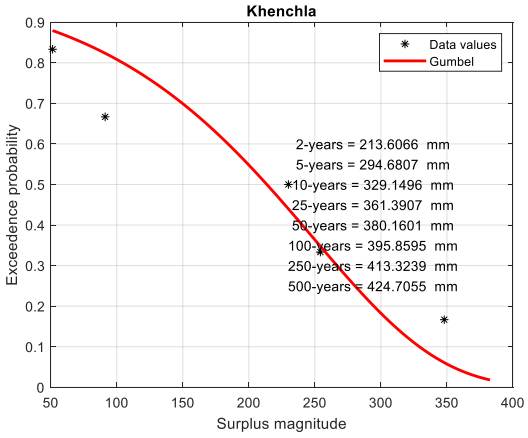
Khenchla
Data values
Gumbel
Exceedence probability
Surplus magnitude
2-years = 213.6066 mm
5-years = 294.6807 mm
10-years = 329.1496 mm
25-years = 361.3907 mm
50-years = 380.1601 mm
100-years = 395.8595 mm
250-years = 413.3239 mm
500-years = 424.7055 mm

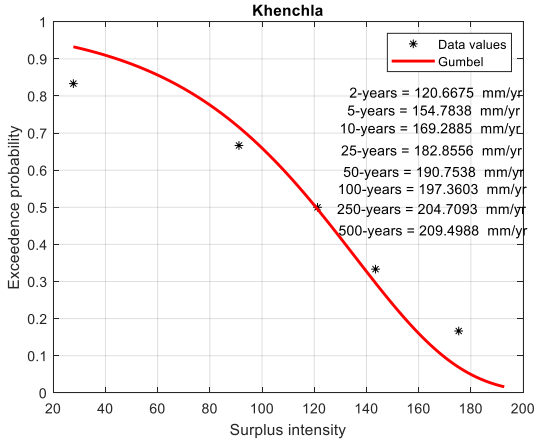
Khenchla
Data values
Gumbel
Exceedence probability
Surplus intensity
2-years = 120.6675 mm/yr
5-years = 154.7838 mm/yr
10-years = 169.2885 mm/yr
25-years = 182.8556 mm/yr
50-years = 190.7538 mm/yr
100-years = 197.3603 mm/yr
250-years = 204.7093 mm/yr
500-years = 209.4988 mm/yr

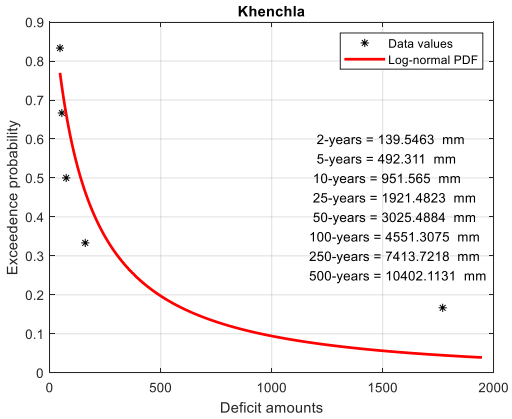
Khenchla
Data values
Log-normal PDF
2-years = 139.5463 mm
5-years = 492.311 mm
10-years = 951.565 mm
25-years = 1921.4823 mm
50-years = 3025.4884 mm
100-years = 4551.3075 mm
250-years = 7413.7218 mm
500-years = 10402.1131 mm
Exceedence probability
Deficit amounts

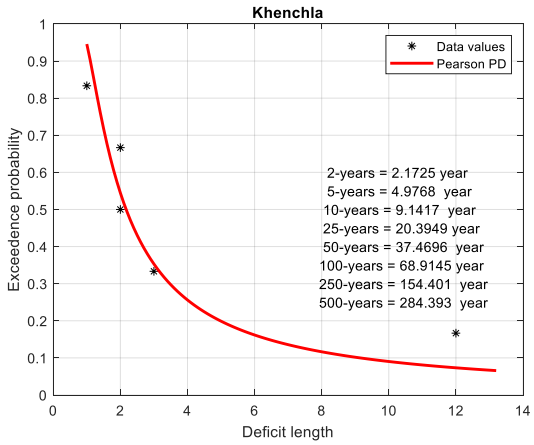
Khenchla
Data values
Pearson PD
2-years = 2.1725 year
5-years = 4.9768 year
10-years = 9.1417 year
25-years = 20.3949 year
50-years = 37.4696 year
100-years = 68.9145 year
250-years = 154.401 year
500-years = 284.393 year
Exceedence probability
Deficit length

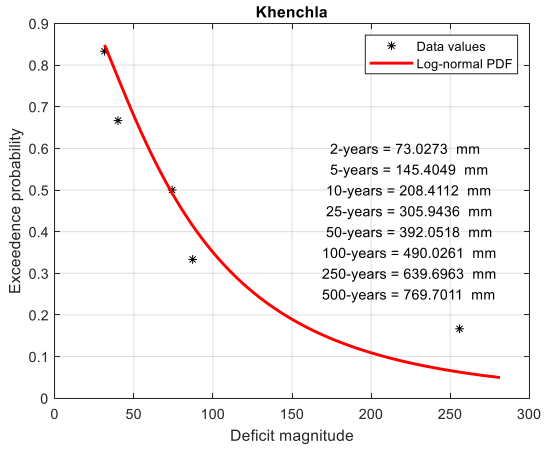
Khenchla
Data values
Log-normal PDF
2-years = 73.0273 mm
5-years = 145.4049 mm
10-years = 208.4112 mm
25-years = 305.9436 mm
50-years = 392.0518 mm
100-years = 490.0261 mm
250-years = 639.6963 mm
500-years = 769.7011 mm
Exceedence probability
Deficit magnitude

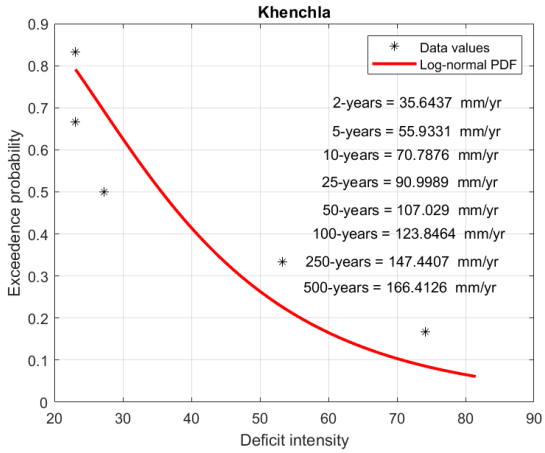
Khenchla
Data values
Log-normal PDF
2-years = 35.6437 mm/yr
5-years = 55.9331 mm/yr
10-years = 70.7876 mm/yr
25-years = 90.9989 mm/yr
50-years = 107.029 mm/yr
100-years = 123.8464 mm/yr
250-years = 147.4407 mm/yr
500-years = 166.4126 mm/yr
Exceedence probability
Deficit intensity

M'Sila Station								Total	gross
D magnitude (mm)	140.6	137.2	35.8	4.6	45.0	62.8	65.5	491.5	37
D intensity(mm/year)	35.1	68.6	11.9	4.6	45.0	62.8	62.8		
D length (year)	4.0	2.0	3.0	1.0	1.0	1.0	1.0	13.0	
D max (mm)	55.0	108.1	22.2	4.6	45.0	62.8	65.5		
S magnitude (mm)	28.8	58.6	81.5	43.8	32.8	11.8	83.6	341.0	37
S intensity (mm/year)	14.4	29.3	81.5	43.8	32.8	11.8	83.6		
S length (year)	2.0	2.0	1.0	1.0	1.0	1.0	1.0	9.0	
S max (mm)	28.7	45.0	81.5	43.8	32.8	11.8	83.6		

Oum Bouaghi														Total	Gross
D magnitude (mm)	423.3	135.6	92.2	198.7	12.2	8.4	274.8	191.9	177.8	105.7	135.9	44.7	136.5	1938	72
D intensity(mm/year)	84.7	135.6	92.2	66.2	12.2	8.4	68.7	64.0	177.8	52.9	68.0	44.7	44.7		
D length (year)	5	1	1	3	1	1	4	3	1	2	2	1	2	27	
D max (mm)	142.0	135.6	92.2	159.3	12.2	8.4	130.3	145.5	177.8	59.2	93.6	44.7	119.5		
S magnitude (mm)	0.1	2.6	109.2	226.0	63.2	113.1	73.3	236.7	290.2	116.8	494.8	196.1	146.6	2067	83
S intensity (mm/year)	0.1	2.6	109.2	113.0	31.6	28.3	73.3	78.9	290.2	58.4	99.0	196.1	146.6		
S length (year)	1	1	1	2	2	4	1	3	1	2	5	1	1	25	
S max (mm)	0.1	2.6	109.2	193.2	34.7	61.1	73.3	158.6	290.2	96.8	198.1	196.1	146.6		

Mila Station								Total	Gross
D magnitude (mm)	352.6	145.1	860.1	205.3	1.6	33.1	24.3	1622	116
D intensity (mm/year)	176.3	145.1	143.3	205.3	1.6	16.5	16.5		
D length (year)	2	1	6	1	1	2	1	14	
D max (mm)	225.0	145.1	278.2	205.3	1.6	23.5	24.3		
S magnitude (mm)	0.1	183.8	31.8	293.1	313.3	661.5	100.4	1584	132
S intensity (mm/year)	0.1	183.8	31.8	146.6	313.3	132.3	100.4		
S length (year)	1	1	1	2	1	5	1	12	
S max (mm)	0.1	183.8	31.8	231.5	313.3	374.6	100.4		

El Taref Station						Total	Gross
D magnitude (mm)	615.4	100.5	252.6	117.8	162.2	1248	178
D intensity (mm/year)	205.1	100.5	252.6	117.8	162.2		
D length (year)	3	1	1	1	1	7	
D max (mm)	337.1	100.5	252.6	117.8	162.2		
S magnitude (mm)	159.0	4.2	578.8	63.6	266.8	1072	119
S intensity (mm/year)	79.5	4.2	192.9	63.6	133.4		
S length (year)	2	1	3	1	2	9	
S max (mm)	108.5	4.2	310.9	63.6	266.8438		

Jijel Station								Total	Gross
D magnitude (mm)	1221.1	547.3	288.9	381.0	942.4	39.7	76.2	3496	207
D intensity (mm/year)	407.0	109.5	96.3	381.0	314.1	39.7	76.2		
D length (year)	3	5	3	1	3	1	1	17	
D max (mm)	718.5	253.5	229.9	381.0	379.5	39.7	76.2		
S magnitude (mm)	97.3	220.7	120.6	167.9	876.5	286.0	2476.7	4246	212
S intensity (mm/year)	97.3	220.7	120.6	167.9	219.1	286.0			
S length (year)	1	1	1	1	4	1	11	20	
S max (mm)	97.3	220.7	120.6	167.9	284.1	286.0			

Guelma Station						Total	Gross
D magnitude (mm)	490.6	41.9	3.9	299.9		836	104
D intensity (mm/year)	163.5	41.9	3.9	100.0			
D length (year)	3	1	1	3		8	
D max (mm)	213.6	41.9	3.9	152.1			
S magnitude (mm)	56.0	309.7	142.5	2.8	166.5	677	85
S intensity (mm/year)	28.0	309.7	142.5	2.8	100.0		
S length (year)	2	1	1	1	3	8	
S max (mm)	55.9	309.7	142.5	2.8	13.0		

Setif Station											Total	Gross
D magnitude (mm)	212.1	48.0	194.9	144.0	29.7	263.9	102.0	96.0	289.0		1380	77
D intensity (mm/year)	212.1	48.0	39.0	72.0	29.7	263.9	102.0	48.0	72.2			
D length (year)	1	1	5	2	1	1	1	2	4		18	
D max (mm)	212.1	48.0	62.5	128.2	29.7	263.9	102.0	68.6	117.1			
S magnitude (mm)	0.1	4.5	26.9	85.3	70.6	62.8	39.1	377.6	404.2	124.9	1196	60
S intensity (mm/year)	0.1	4.5	26.9	85.3	35.3	62.8	39.1	125.9	57.7	72.2		
S length (year)	1	1	1	1	2	1	1	3	7	2	20	
S max (mm)	0.1	4.5	26.9	85.3	36.3	62.8	39.1	207.8	232.4	52.8		

Tebessa Station									Total	Gross
D magnitude (mm)	487.3	172.6	385.1	98.5	68.1	164.6	136.9		1513	69
D intensity (mm/year)	69.6	86.3	64.2	98.5	68.1	54.9	68.5			
D length (year)	7	2	6	1	1	3	2		22	
D max (mm)	138.1	161.0	169.7	98.5	68.1	80.0	81.8			
S magnitude (mm)	0.1	367.4	47.3	570.2	32.9	258.2	65.3	113.0	1454	91
S intensity (mm/year)	0.1	122.5	47.3	142.6	32.9	86.1	65.3	68.5		
S length (year)	1	3	1	4	1	3	1	2	16	
S max (mm)	0.1	209.3	47.3	283.0	32.9	173.6	65.3	75.0		

Constantine Station											Total	Gross
D magnitude (mm)	192.5	67.1	302.5	235.7	457.0	407.7	8.6	192.3	413.1		2277	99
D intensity (mm/year)	192.5	67.1	60.5	117.8	152.3	101.9	8.6	64.1	137.7			
D length (year)	1	1	5	2	3	4	1	3	3		23	
D max (mm)	192.5	67.1	159.3	139.2	280.2	174.3	8.6	100.6	192.3			
S magnitude (mm)	0.1	414.0	17.5	137.9	200.5	499.9	322.0	38.9	124.4	216.6	1972	131
S intensity (mm/year)	0.1	414.0	17.5	137.9	50.1	166.6	322.0	38.9	124.4	137.7		
S length (year)	1	1	1	1	4	3	1	1	1	1	15	
S max (mm)	0.1	414.0	17.5	137.9	84.1	269.9	322.0	38.9	124.4	216.6		

Bejaia Station											Total	Gross
D magnitude (mm)	486.0	47.9	651.1	381.3	122.0	923.1	253.9	66.9	317.9	8.3	3258	163
D intensity(mm/year)	486.0	47.9	162.8	127.1	122.0	307.7	127.0	66.9	106.0	106.0		
D length (year)	1	1	4	3	1	3	2	1	3	1	20	
D max (mm)	486.0	47.9	318.9	178.9	122.0	411.6	215.8	66.9	236.1	8.3		
S magnitude (mm)	0.1	275.3	168.8	66.6	21.7	72.6	432.5	86.2	1140.9	901.3	3166	176
S intensity (mm/year)	0.1	275.3	168.8	33.3	21.7	72.6	144.2	86.2	228.2	450.7		
S length (year)	1	1	1	2	1	1	3	1	5	2	18	
S max (mm)	0.1	275.3	168.8	39.5	21.7	72.6	262.6	86.2	627.8	825.2		

Bordj Bouarreridj Station									Total	Gross
D magnitude (mm)	530.3	103.7	610.7	66.7	17.7	34.7	173.3	85.8	1623	71
D intensity (mm/year)	75.8	51.9	122.1	33.3	8.8	34.7	57.8	57.8		
D length (year)	7	2	5	2	2	1	3	1	23	
D max (mm)	205.2	67.0	232.6	46.9	12.6	34.7	102.8	85.8		
S magnitude (mm)	0.1	419.9	332.5	419.8	60.1	177.4	55.4	5.4	1471	98
S intensity (mm/year)	0.1	140.0	166.2	139.9	60.1	88.7	55.4	2.7		
S length (year)	1	3	2	3	1	2	1	2	15	
S max (mm)	0.1	296.0	317.7	205.8	60.1	137.5	55.4	3.8		

Skikda Station												Total	Gross
D magnitude (mm)	82.5	142.4	323.4	222.0	650.1	163.0	72.4	154.4	522.4	35.2		2368	118
D intensity (mm/year)	82.5	142.4	107.8	74.0	216.7	163.0	36.2	77.2	174.1	35.2			
D length (year)	1	1	3	3	3	1	2	2	3	1		20	
D max (mm)	82.5	142.4	137.3	93.1	313.3	163.0	49.4	154.0	261.1	35.2			
S magnitude (mm)	0.1	106.6	246.8	168.8	410.9	426.3	208.4	264.5	91.5	68.0	308.1	2300	128
S intensity (mm/year)	0.1	106.6	82.3	168.8	137.0	213.1	104.2	132.2	91.5	68.0	35.2		
S length (year)	1	1	3	1	3	2	2	2	1	1	1	18	
S max (mm)	0.1	106.6	102.0	168.8	168.3	240.5	187.8	147.2	91.5	68.0	308.1		

Batna Station												Total	Gross
D magnitude (mm)	167.9	455.7	302.4	250.4	55.4	25.9	17.5	112.5	31.3	203.8		1623	85
D intensity (mm/year)	83.9	113.9	75.6	125.2	55.4	25.9	17.5	112.5	31.3	101.9			
D length (year)	2	4	4	2	1	1	1	1	1	2		19	
D max (mm)	142.0	172.8	111.5	183.1	55.4	25.9	17.5	112.5	31.3	126.5			
S magnitude (mm)	0.1	152.3	78.0	54.4	760.9	69.6	80.5	72.9	72.3	38.4	87.3	1467	77
S intensity (mm/year)	0.1	50.8	78.0	54.4	152.2	69.6	40.3	72.9	72.3	38.4	101.9		
S length (year)	1.0	3.0	1.0	1.0	5.0	1.0	2.0	1.0	1.0	1.0	2	19	
S max (mm)	0.1	136.9	78.0	54.4	321.5	69.6	47.7	72.9	72.3	38.4	26.4		

Souk Ahras Station								Total	Gross
D magnitude (mm)	916.4	658.5	238.5	36.6	81.1	307.3		2238	149
D intensity(mm/year)	183.3	219.5	119.3	36.6	81.1	102.4			
D length (year)	5	3	2	1	1	3		15	
D max (mm)	399.6	345.6	175.0	36.6	81.1	128.3			
S magnitude (mm)	364.8	297.7	54.8	41.5	32.0	661.0	858.2	2310	136
S intensity (mm/year)	121.6	148.8	54.8	41.5	32.0	220.3	102.4		
S length (year)	3	2	1	1	1	3	6	17	
S max (mm)	265.0	160.8	54.8	41.5	32.0	305.3	420.0		

Khenchla Station						Total	Gross
D magnitude (mm)	74.1	54.6	159.9	46.2	1770.0	2105	105
D intensity(mm/year)	74.1	27.3	53.3	23.1	23.1		
D length (year)	1	2	3	2	12	20	
D max (mm)	74.1	39.9	87.1	31.4	255.9		
S magnitude (mm)	717.4	55.4	91.2	242.5	701.4	1808	129
S intensity (mm/year)	143.5	27.7	91.2	121.3	175.4		
S length (year)	5	2	1	2	4	14	
S max (mm)	300.0	51.4	91.2	230.0	348.0		

8.2 APPENDIX OF CHAPTER IV

8.2.1 MATLAB program

```
function [Intercept,Slope] = BESME_TREND(X,Y,Title,XTitle,YTitle)
% X = Given time series
% Y = Time sequence for the time series
% m = average
% s = standard deviation
% N = number of data
% MSlope = Mean trend Slope
% SSlope = Standard deviation slope
n=floor(length(X)); % Number of data
n2=floor(n/2);  % Half number of data
my=floor((Y(1,1)+Y(end,1))/2);   % Middle year
I=min(Y(:,1));  % Initial year
FY=my;  % First half last year
SY=my+1;    % Second half fisrt year
L=max(Y(:,1));  % Last year
nm=mean(Y); % Time duration mean value
m=mean(X);  % Variable mean value
FH=sort(X(1:n2,1)); % First half variables
SH=sort(X(n2+1:2*n2,1));% Second half variables
FHM=mean(FH);   % First half mean
SHM=mean(SH);   % Second half mean
figure
scatter(FH,SH,'k*');    % Scatter diagram between first and second halves
hold on
scatter(mean(FH),mean(SH),'rv');    % First and second half means
Xmin=min([min(FH),min(SH)]);
Xmax=max([max(FH),max(SH)]);
axis([Xmin Xmax Xmin Xmax]);
box on
grid on
title(Title)
line([Xmin Xmax],[Xmin Xmax],'Color','k','LineWidth',3);
Slope=(SHM-FHM)/n2;
Intercept=mean(X)-Slope*n2;
xlabel(['First half   (',num2str(I),' - ',num2str(FY),')'])
ylabel(['Second half    (',num2str(SY),' - ',num2str(L),')'])
legend('Data values','First and second halves mean','45^o (1:1) no trend
line','Location','Northwest')
```

```
figure
plot(Y,X,'k')
grid on
title(Title)
xlabel(XTitle)
ylabel(YTitle)
hold on
scatter(nm,m,'r')
MSlope=2*(mean(SH)-mean(FH))/n;
Mfin=m+MSlope*n2;
Mini=m-MSlope*n2;
May=max(Y);
Miy=min(Y);
Xmin=I+2;
Ymax=0.98*max(X(:,1));
text(Xmin,Ymax,['Slope = ',num2str(Slope),';   ','Intercept = ',num2str(Intercept)])
line([Miy May],[Mini Mfin],'LineWidth',2,'Color','k','LineStyle','-')
legend('Data time series','Data mean','Trend line','Location','Southwest')
end
```

8.2.2 Figures

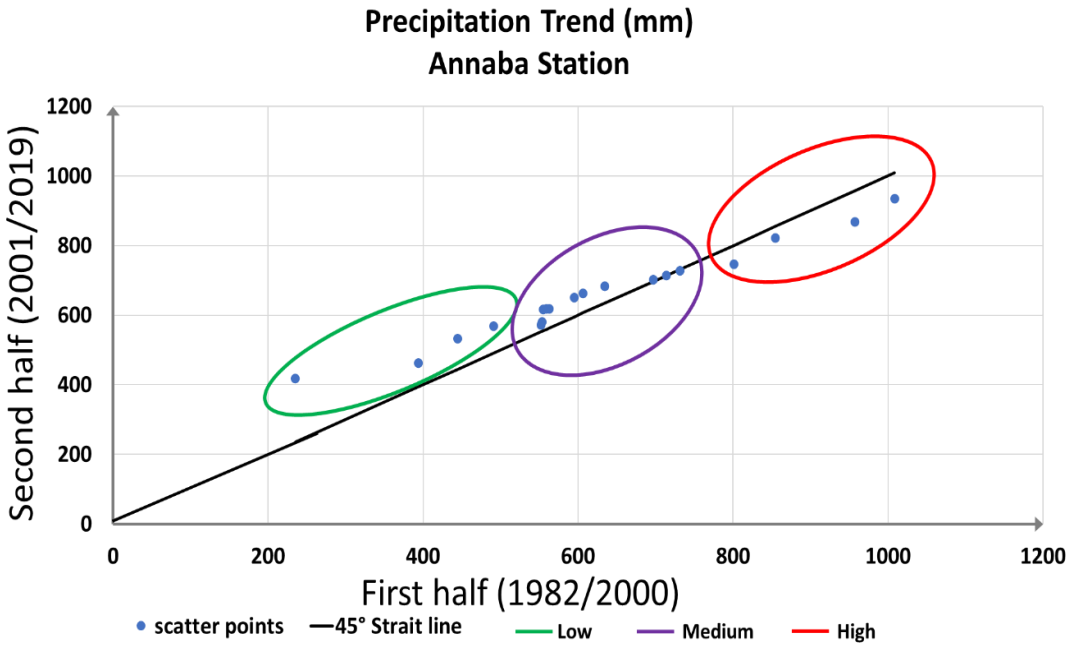

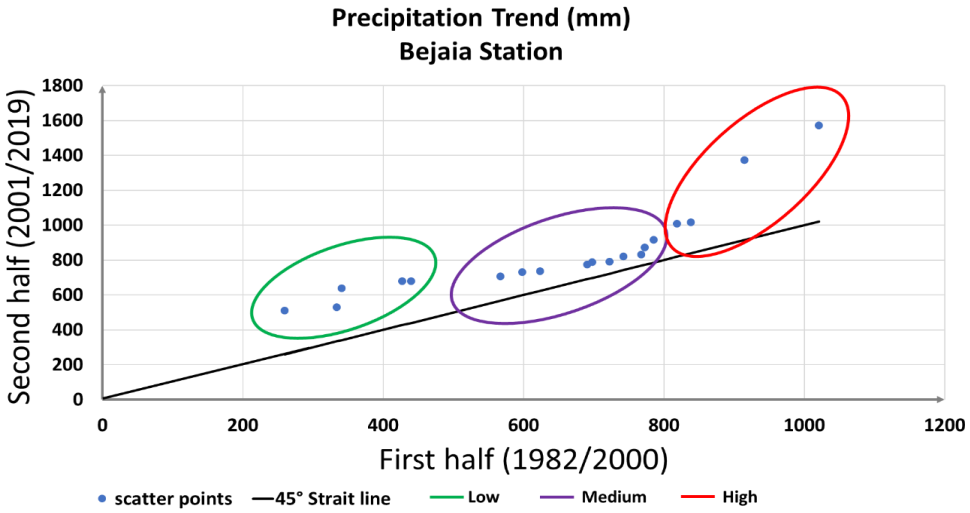
Precipitation Trend (mm)
Bejaia Station
Second half (2001/2019)
First half (1982/2000)
scatter points
45° Strait line
Low
Medium
High

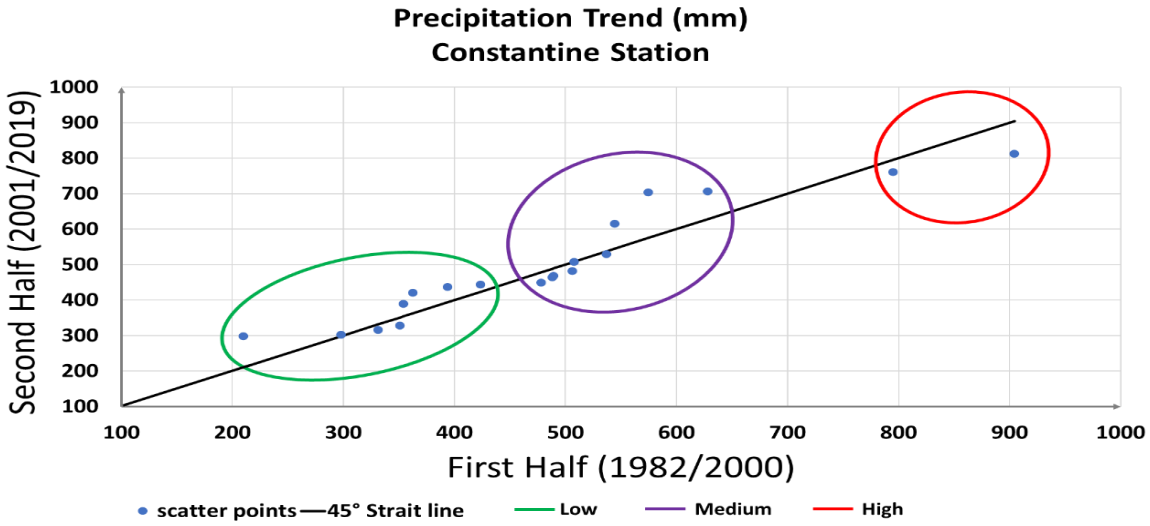
Precipitation Trend (mm)
Constantine Station
Second Half (2001/2019)
First Half (1982/2000)
scatter points
45° Strait line
Low
Medium
High

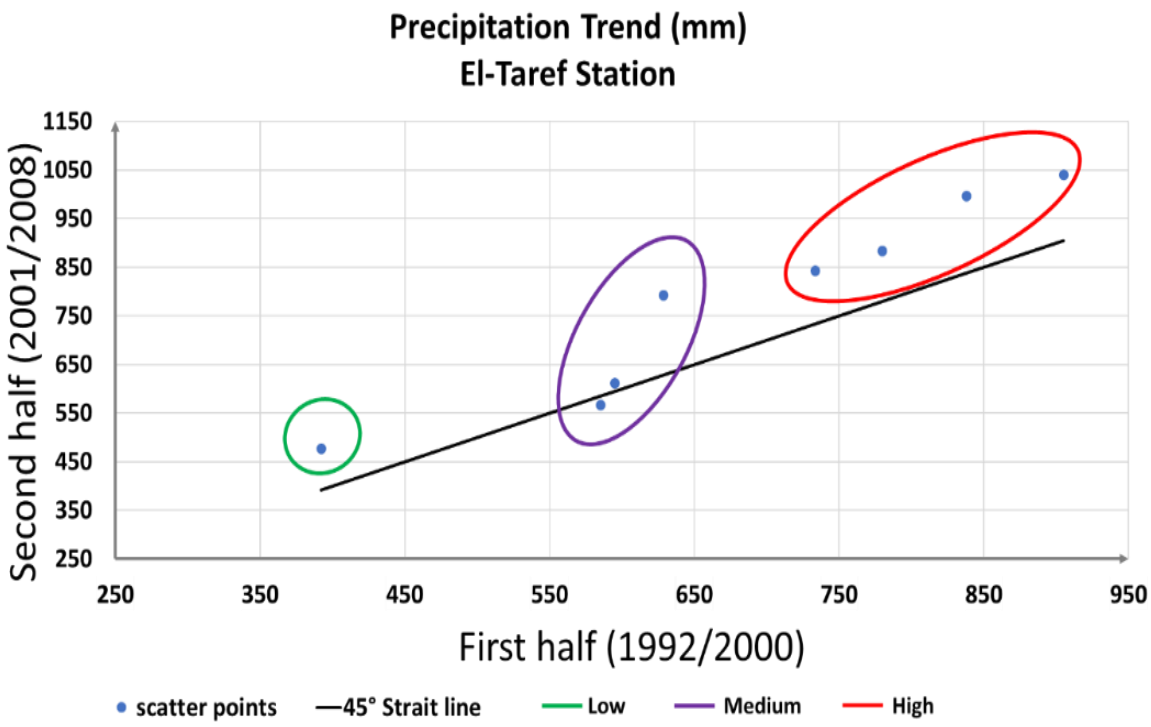
Precipitation Trend (mm)
El-Taref Station
Second half (2001/2008)
1150
1050
950
850
750
650
550
450
350
250
250
350
450
550
650
750
850
950
First half (1992/2000)
scatter points
45° Strait line
Low
Medium
High

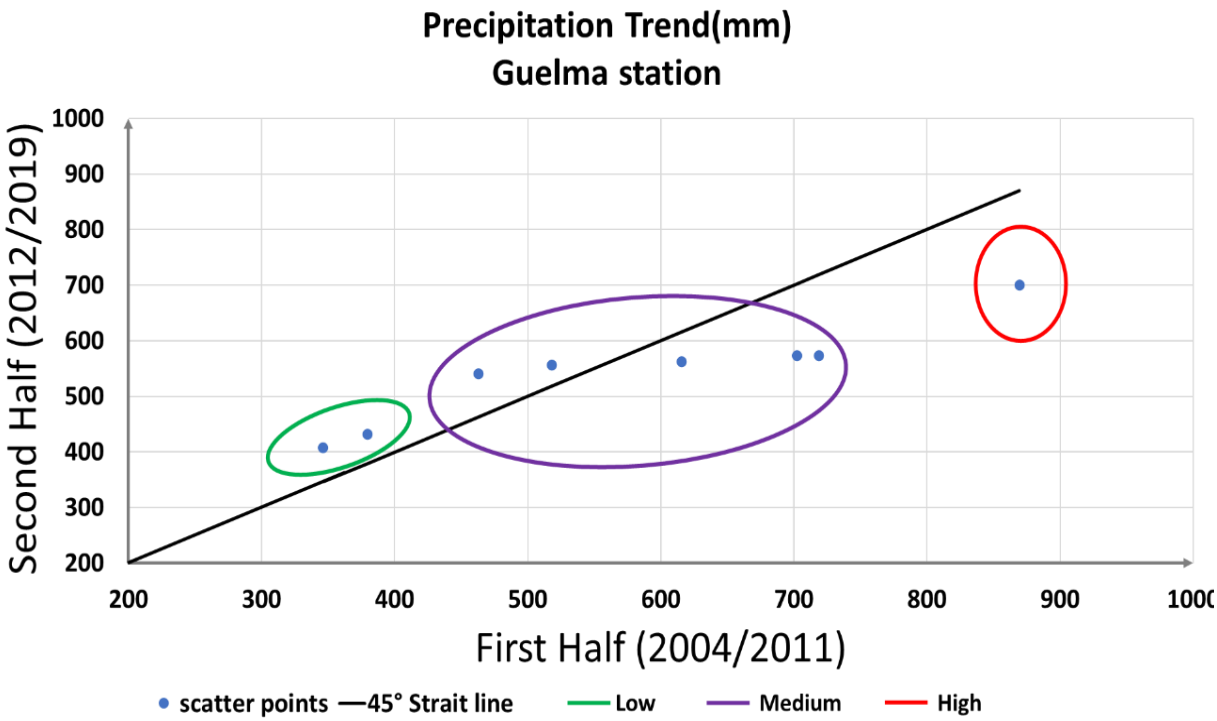
Precipitation Trend(mm)
Guelma station
Second Half (2012/2019)
1000
900
800
700
600
500
400
300
200
200
300
400
500
600
700
800
900
1000
First Half (2004/2011)
scatter points
45° Strait line
Low
Medium
High

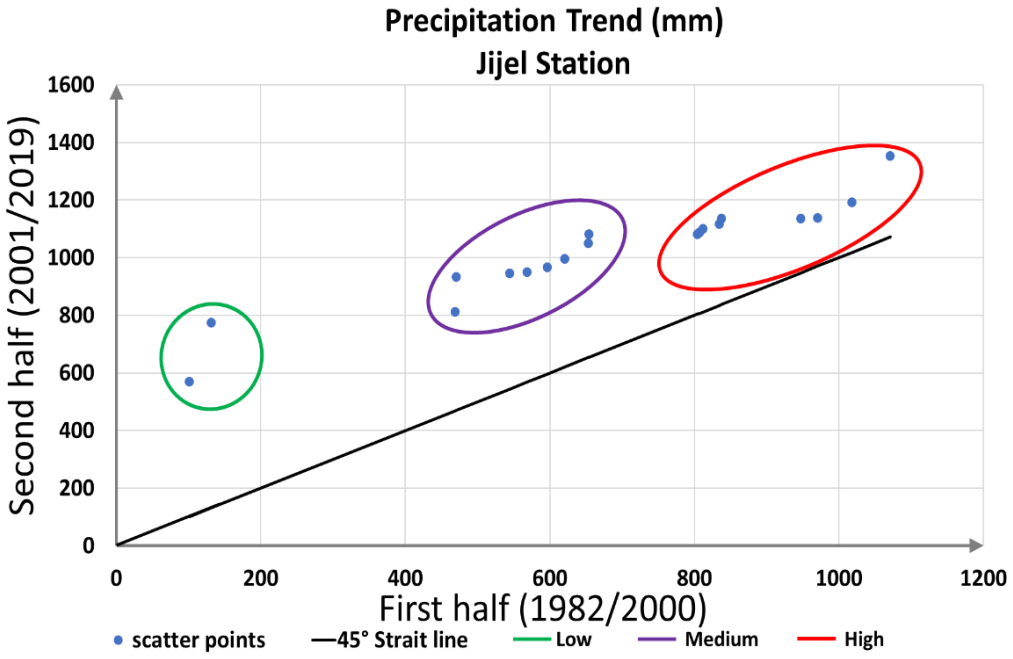
Precipitation Trend (mm)
Jijel Station
Second half (2001/2019)
First half (1982/2000)
1600
1400
1200
1000
800
600
400
200
0
0
200
400
600
800
1000
1200
scatter points
45° Strait line
Low
Medium
High

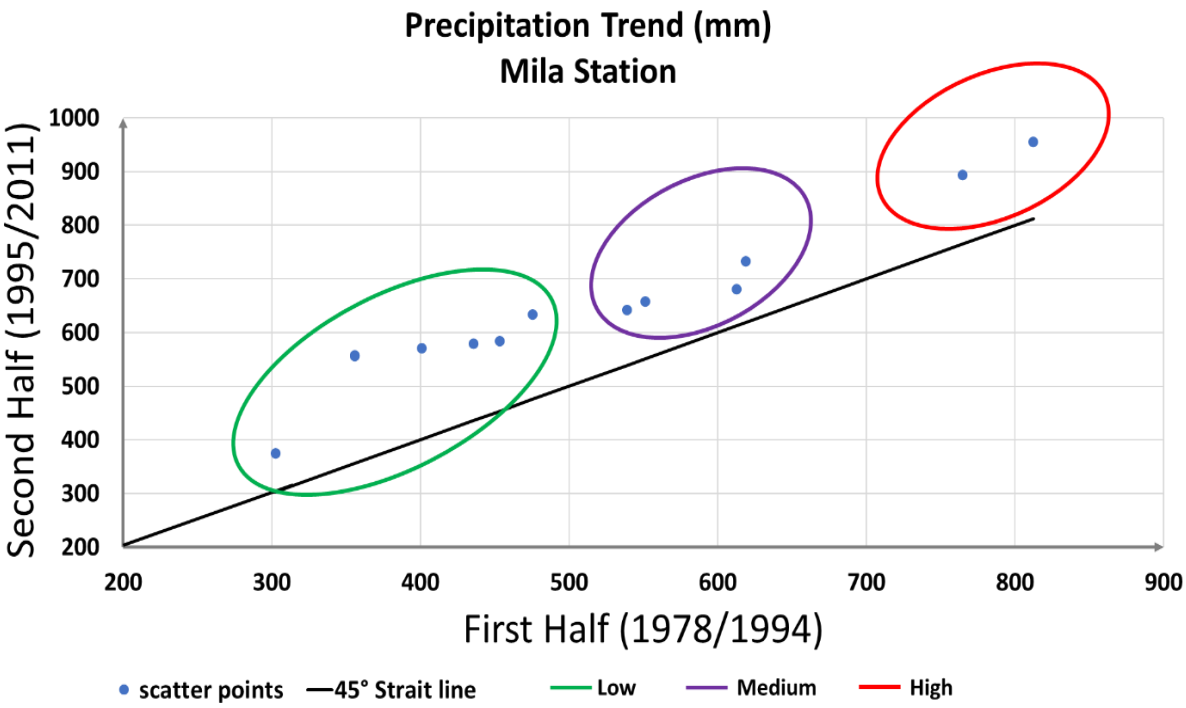
Precipitation Trend (mm)
Mila Station
Second Half (1995/2011)
First Half (1978/1994)
1000
900
800
700
600
500
400
300
200
200
300
400
500
600
700
800
900
scatter points
45° Strait line
Low
Medium
High

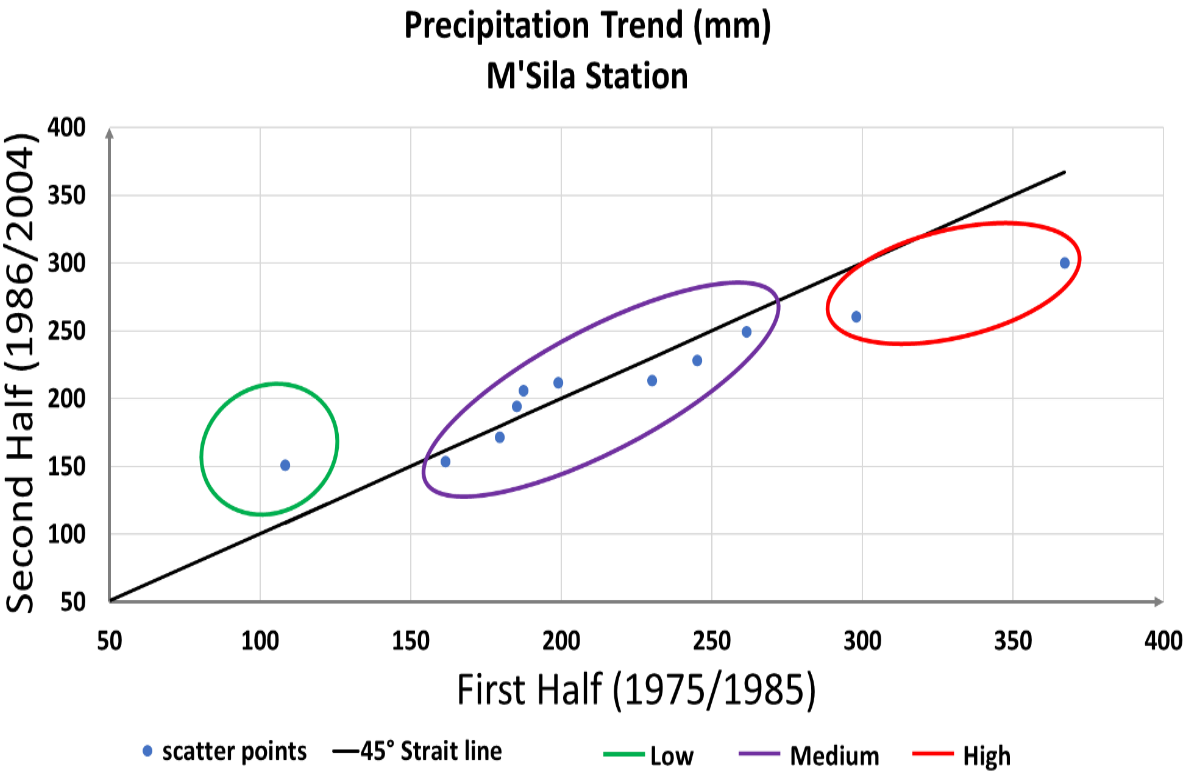
Precipitation Trend (mm)
M'Sila Station
Second Half (1986/2004)
First Half (1975/1985)
400
350
300
250
200
150
100
50
50
100
150
200
250
300
350
400
scatter points
45° Strait line
Low
Medium
High

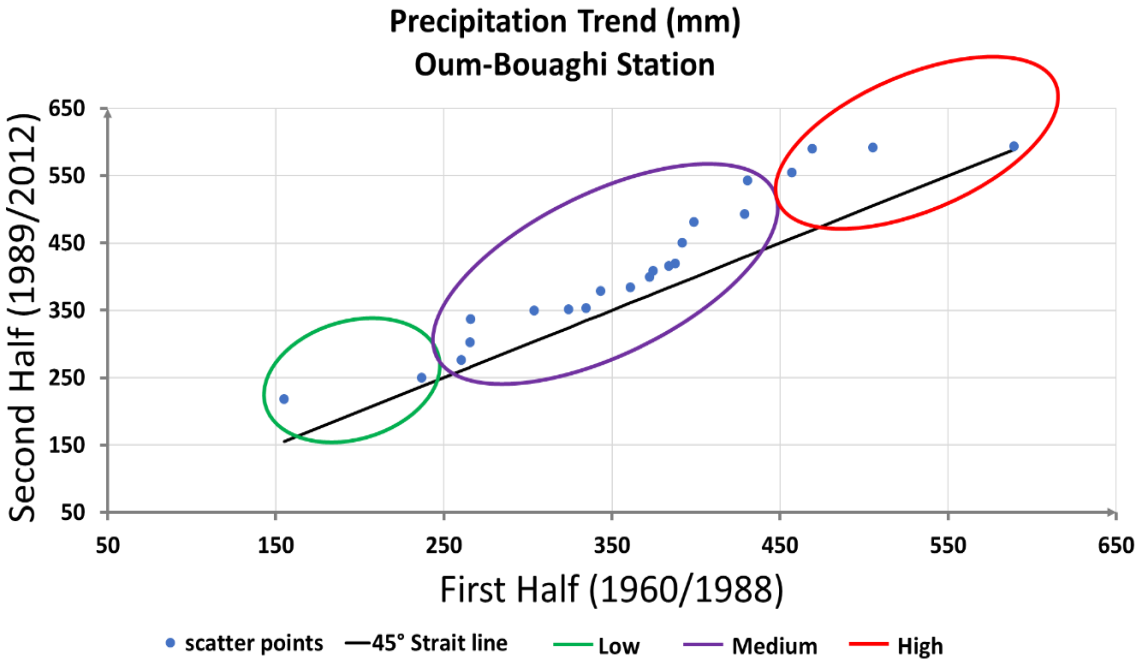
Precipitation Trend (mm)
Oum-Bouaghi Station
Second Half (1989/2012)
650
550
450
350
250
150
50
50
150
250
350
450
550
650
First Half (1960/1988)
scatter points
45° Strait line
Low
Medium
High

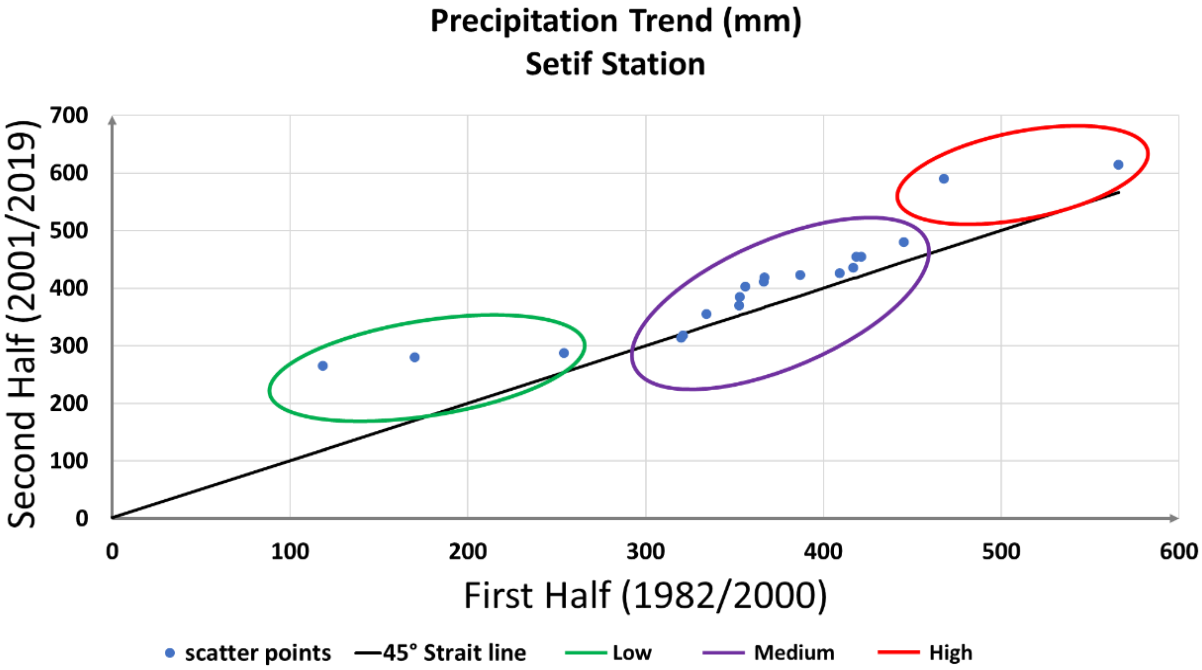
Precipitation Trend (mm)
Setif Station
Second Half (2001/2019)
700
600
500
400
300
200
100
0
0
100
200
300
400
500
600
First Half (1982/2000)
scatter points
45° Strait line
Low
Medium
High

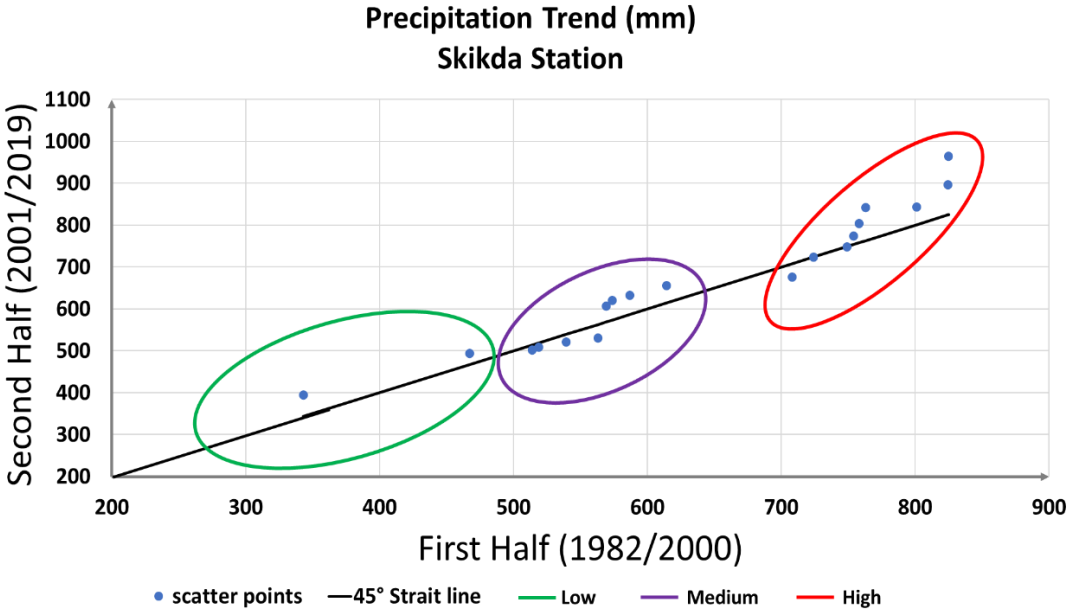
Precipitation Trend (mm)
Skikda Station
Second Half (2001/2019)
First Half (1982/2000)
1100
1000
900
800
700
600
500
400
300
200
200
300
400
500
600
700
800
900
scatter points
45° Strait line
Low
Medium
High

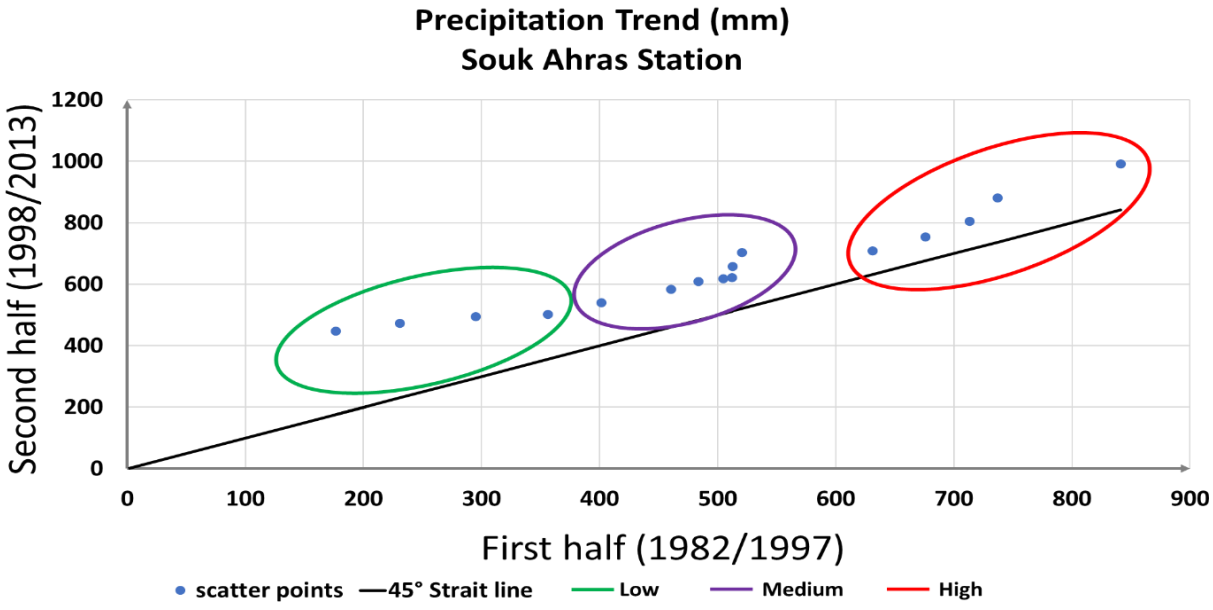
Precipitation Trend (mm)
Souk Ahras Station
Second half (1998/2013)
First half (1982/1997)
1200
1000
800
600
400
200
0
0
100
200
300
400
500
600
700
800
900
scatter points
45° Strait line
Low
Medium
High

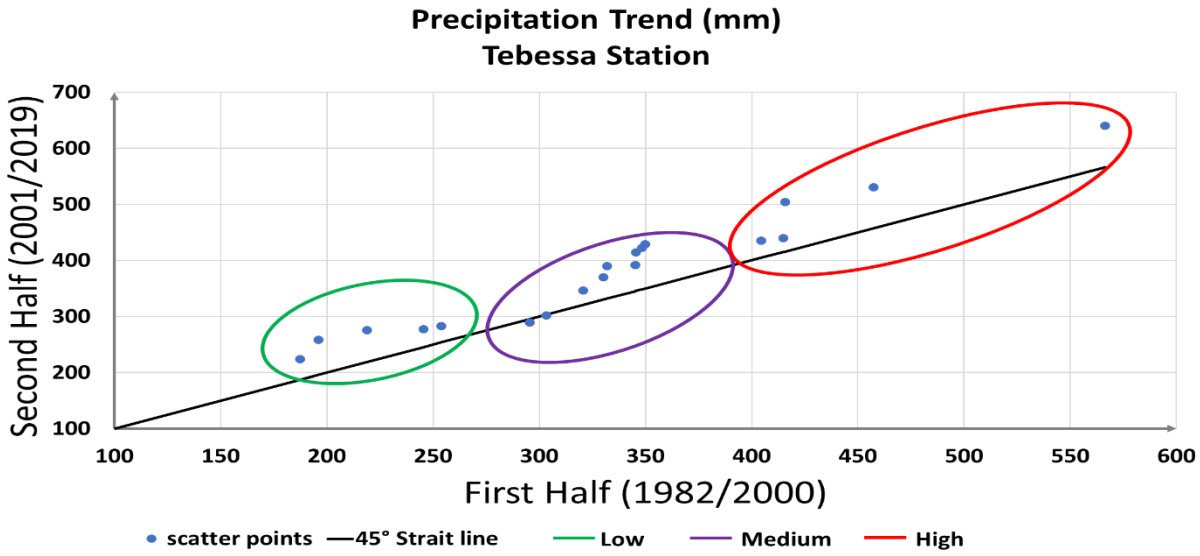
Precipitation Trend (mm)
Tebessa Station
Second Half (2001/2019)
700
600
500
400
300
200
100
100
150
200
250
300
350
400
450
500
550
600
First Half (1982/2000)
scatter points
45° Strait line
Low
Medium
High

8.3 APPENDIX OF THE CHAPTER V

8.3.1 MATLAB program

```
function
[TrendLength,TrendSlope,MidDistance]=LengthSlopeDistanceTrendPolygons(X,I,Title,
Xtitle,Ytitle)
% Bu program 23 Nisan 2015 günü Zekâi Þen tarafýndan yazýlmýþtýr
%   Detailed explanation goes here
% X = 12 ay satýr ve kayýt yýllarý sütun olan eþleþi, X(Yýl+12Ay)
% I      : Indicator. If I = 1 arithmetic average polygon, otherwise
%          standard deviation polygon
% Title   : 'Station name    monthly average precipitation (mm)'
% Xtitle  : 'InitialYear - MiddleYear', For instance, '2150 - 1980'
% Ytitle  : 'MiddleYear - FinalYear'
% IMPORTANT NOTE: One must define Xtitle and Ytitle according to the record years
L=length(X(:,1));
L2=floor(L/2);
IY=X(1,1);
FY=X(end,1);
MY=floor((IY+FY)/2);
for i=2:13
   Onceki(i-1,1:L2)=sort(X(1:L2,i));
   Sonraki(i-1,L2+1:L)=sort(X(L2+1:L,i));
   if I == 1
      OncekiOrt(i-1)=mean(Onceki(i-1,1:L2));
      SonrakiOrt(i-1)=mean(Sonraki(i-1,L2+1:L));
   else
      OncekiOrt(i-1)=std(Onceki(i-1,1:L2));
      SonrakiOrt(i-1)=std(Sonraki(i-1,L2+1:L));
   end
end
% Polygon plot
figure
scatter(OncekiOrt(1),SonrakiOrt(1),'k*')
text(OncekiOrt(1),SonrakiOrt(1),' J')
hold on
scatter(OncekiOrt(2),SonrakiOrt(2),'k+')
text(OncekiOrt(2),SonrakiOrt(2),' F')
line([OncekiOrt(1) OncekiOrt(2)],[SonrakiOrt(1) SonrakiOrt(2)])
TrendLength(1)=sqrt((OncekiOrt(1)-OncekiOrt(2))^2+(SonrakiOrt(1)-
SonrakiOrt(2))^2);
```

```
TrendSlope(1)=(SonrakiOrt(1)-SonrakiOrt(2))/(OncekiOrt(1)-OncekiOrt(2));
MidDistanceX(1)=(OncekiOrt(1)+OncekiOrt(2))/2;  % Horizontal axis mid-point
MidDistanceY(1)=(SonrakiOrt(1)+SonrakiOrt(2))/2;% Vertical axis mid-point
MidDistance(1)=MidDistanceY(1)-MidDistanceX(1);
scatter(OncekiOrt(3),SonrakiOrt(3),'kx')
text(OncekiOrt(3),SonrakiOrt(3),'  M')
line([OncekiOrt(2) OncekiOrt(3)],[SonrakiOrt(2) SonrakiOrt(3)])
TrendLength(2)=sqrt((OncekiOrt(2)-OncekiOrt(3))^2+(SonrakiOrt(2)-
SonrakiOrt(3))^2);
TrendSlope(2)=(SonrakiOrt(2)-SonrakiOrt(3))/(OncekiOrt(2)-OncekiOrt(3));
MidDistanceX(2)=(OncekiOrt(2)+OncekiOrt(3))/2;  % Horizontal axis mid-point
MidDistanceY(2)=(SonrakiOrt(2)+SonrakiOrt(3))/2;% Vertical axis mid-point
MidDistance(2)=MidDistanceY(2)-MidDistanceX(2);
scatter(OncekiOrt(4),SonrakiOrt(4),'k^')
text(OncekiOrt(4),SonrakiOrt(4),'  A')
line([OncekiOrt(3) OncekiOrt(4)],[SonrakiOrt(3) SonrakiOrt(4)])
TrendLength(3)=sqrt((OncekiOrt(3)-OncekiOrt(4))^2+(SonrakiOrt(3)-
SonrakiOrt(4))^2);
TrendSlope(3)=(SonrakiOrt(3)-SonrakiOrt(4))/(OncekiOrt(3)-OncekiOrt(4));
MidDistanceX(3)=(OncekiOrt(3)+OncekiOrt(4))/2;  % Horizontal axis mid-point
MidDistanceY(3)=(SonrakiOrt(3)+SonrakiOrt(4))/2;% Vertical axis mid-point
MidDistance(3)=MidDistanceY(3)-MidDistanceX(3);
scatter(OncekiOrt(5),SonrakiOrt(5),'ks')
text(OncekiOrt(5),SonrakiOrt(5),'  M')
line([OncekiOrt(4) OncekiOrt(5)],[SonrakiOrt(4) SonrakiOrt(5)])
TrendLength(4)=sqrt((OncekiOrt(4)-OncekiOrt(5))^2+(SonrakiOrt(4)-
SonrakiOrt(5))^2);
TrendSlope(4)=(SonrakiOrt(4)-SonrakiOrt(5))/(OncekiOrt(4)-OncekiOrt(5));
MidDistanceX(4)=(OncekiOrt(4)+OncekiOrt(5))/2;  % Horizontal axis mid-point
MidDistanceY(4)=(SonrakiOrt(4)+SonrakiOrt(5))/2;% Vertical axis mid-point
MidDistance(4)=MidDistanceY(4)-MidDistanceX(4);
scatter(OncekiOrt(6),SonrakiOrt(6),'kd')
text(OncekiOrt(6),SonrakiOrt(6),'  J')
line([OncekiOrt(5) OncekiOrt(6)],[SonrakiOrt(5) SonrakiOrt(6)])
TrendLength(5)=sqrt((OncekiOrt(5)-OncekiOrt(6))^2+(SonrakiOrt(5)-
SonrakiOrt(6))^2);
TrendSlope(5)=(SonrakiOrt(5)-SonrakiOrt(6))/(OncekiOrt(5)-OncekiOrt(6));
MidDistanceX(5)=(OncekiOrt(5)+OncekiOrt(6))/2;  % Horizontal axis mid-point
MidDistanceY(5)=(SonrakiOrt(5)+SonrakiOrt(6))/2;% Vertical axis mid-point
scatter(OncekiOrt(7),SonrakiOrt(7),'kv')
text(OncekiOrt(7),SonrakiOrt(7),'  J')
line([OncekiOrt(6) OncekiOrt(7)],[SonrakiOrt(6) SonrakiOrt(7)])
TrendLength(6)=sqrt((OncekiOrt(6)-OncekiOrt(7))^2+(SonrakiOrt(6)-
SonrakiOrt(7))^2);
```

```
TrendSlope(6)=(SonrakiOrt(6)-SonrakiOrt(7))/(OncekiOrt(6)-OncekiOrt(7));
MidDistanceX(6)=(OncekiOrt(6)+OncekiOrt(7))/2;  % Horizontal axis mid-point
MidDistanceY(6)=(SonrakiOrt(6)+SonrakiOrt(7))/2;% Vertical axis mid-point7
MidDistance(6)=MidDistanceY(6)-MidDistanceX(6);
scatter(OncekiOrt(8),SonrakiOrt(8),'k>')
text(OncekiOrt(8),SonrakiOrt(8),'  A')
line([OncekiOrt(7) OncekiOrt(8)],[SonrakiOrt(7) SonrakiOrt(8)])
TrendLength(7)=sqrt((OncekiOrt(7)-OncekiOrt(8))^2+(SonrakiOrt(7)-
SonrakiOrt(8))^2);
TrendSlope(7)=(SonrakiOrt(7)-SonrakiOrt(8))/(OncekiOrt(7)-OncekiOrt(8));
MidDistanceX(7)=(OncekiOrt(7)+OncekiOrt(8))/2;  % Horizontal axis mid-point
MidDistanceY(7)=(SonrakiOrt(7)+SonrakiOrt(8))/2;% Vertical axis mid-point
MidDistance(7)=MidDistanceY(7)-MidDistanceX(7);
scatter(OncekiOrt(9),SonrakiOrt(9),'k<')
text(OncekiOrt(9),SonrakiOrt(9),'  S')
line([OncekiOrt(8) OncekiOrt(9)],[SonrakiOrt(8) SonrakiOrt(9)])
TrendLength(8)=sqrt((OncekiOrt(8)-OncekiOrt(9))^2+(SonrakiOrt(8)-
SonrakiOrt(9))^2);
TrendSlope(8)=(SonrakiOrt(8)-SonrakiOrt(9))/(OncekiOrt(8)-OncekiOrt(9));
MidDistanceX(8)=(OncekiOrt(8)+OncekiOrt(9))/2;  % Horizontal axis mid-point
MidDistanceY(8)=(SonrakiOrt(8)+SonrakiOrt(9))/2;% Vertical axis mid-point
MidDistance(8)=MidDistanceY(8)-MidDistanceX(8);
scatter(OncekiOrt(10),SonrakiOrt(10),'k')
text(OncekiOrt(10),SonrakiOrt(10),'  O')
line([OncekiOrt(9) OncekiOrt(10)],[SonrakiOrt(9) SonrakiOrt(10)])
TrendLength(9)=sqrt((OncekiOrt(9)-OncekiOrt(10))^2+(SonrakiOrt(9)-
SonrakiOrt(10))^2);
TrendSlope(9)=(SonrakiOrt(9)-SonrakiOrt(10))/(OncekiOrt(9)-OncekiOrt(10));
MidDistanceX(9)=(OncekiOrt(9)+OncekiOrt(10))/2;  % Horizontal axis mid-point
MidDistanceY(9)=(SonrakiOrt(9)+SonrakiOrt(10))/2;% Vertical axis mid-point
MidDistance(9)=MidDistanceY(9)-MidDistanceX(9);
scatter(OncekiOrt(11),SonrakiOrt(11),'rpentagram')
text(OncekiOrt(11),SonrakiOrt(11),'  N')
line([OncekiOrt(10) OncekiOrt(11)],[SonrakiOrt(10) SonrakiOrt(11)])
TrendLength(10)=sqrt((OncekiOrt(10)-OncekiOrt(11))^2+(SonrakiOrt(10)-
SonrakiOrt(11))^2);
TrendSlope(10)=(SonrakiOrt(10)-SonrakiOrt(11))/(OncekiOrt(10)-OncekiOrt(11));
MidDistanceX(10)=(OncekiOrt(10)+OncekiOrt(11))/2;  % Horizontal axis mid-point
MidDistanceY(10)=(SonrakiOrt(10)+SonrakiOrt(11))/2;% Vertical axis mid-point
MidDistance(10)=MidDistanceY(10)-MidDistanceX(10);
scatter(OncekiOrt(12),SonrakiOrt(12),'rhexagram')
text(OncekiOrt(12),SonrakiOrt(12),'  D')
line([OncekiOrt(11) OncekiOrt(12)],[SonrakiOrt(11) SonrakiOrt(12)])
line([OncekiOrt(12) OncekiOrt(1)],[SonrakiOrt(12) SonrakiOrt(1)])
```

```
TrendLength(11)=sqrt((OncekiOrt(11)-OncekiOrt(12))^2+(SonrakiOrt(11)-
SonrakiOrt(12))^2);
TrendSlope(11)=(SonrakiOrt(11)-SonrakiOrt(12))/(OncekiOrt(11)-OncekiOrt(12));
MidDistanceX(11)=(OncekiOrt(11)+OncekiOrt(12))/2;  % Horizontal axis mid-point
MidDistanceY(11)=(SonrakiOrt(11)+SonrakiOrt(12))/2;% Vertical axis mid-point
MidDistance(11)=MidDistanceY(11)-MidDistanceX(11);
TrendLength(12)=sqrt((OncekiOrt(12)-OncekiOrt(1))^2+(SonrakiOrt(12)-
SonrakiOrt(1))^2);
TrendSlope(12)=(SonrakiOrt(12)-SonrakiOrt(1))/(OncekiOrt(12)-OncekiOrt(1));
MidDistanceX(12)=(OncekiOrt(12)+OncekiOrt(1))/2;  % Horizontal axis mid-point
MidDistanceY(12)=(SonrakiOrt(12)+SonrakiOrt(1))/2;% Vertical axis mid-point
MidDistance(12)=MidDistanceY(12)-MidDistanceX(12);
m=min(OncekiOrt,SonrakiOrt);
M=max(OncekiOrt,SonrakiOrt);
line([m M],[m M],'LineWidth',2)
title(Title)
xlabel(Xtitle)
ylabel(Ytitle)
box on
grid on
M=[TrendLength; TrendSlope; MidDistance];
M=M';
T=('TRendLength TrendSlope MidDistance')
M
end
```

8.3.2 IPTA Figures and Tables

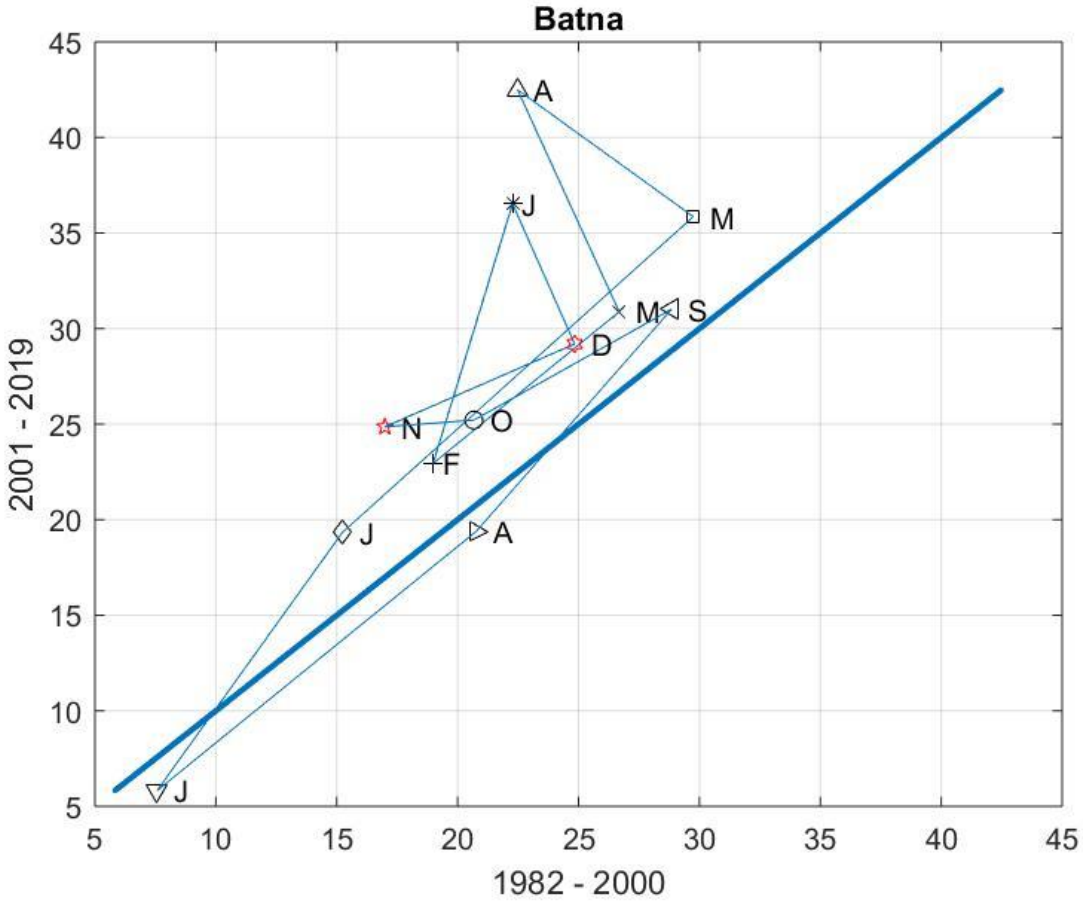

10 months lay in the increasing area supporting the idea of increasing trend in Batna station, the behavior is unsystematic from September to June, March and April show a significant increasing trend recently, summer season (June, July and August) is stable comparing to the rest of the year.

Batna station						
Month	**Jan_Feb**	**Feb_Mar**	**Mar_Apr**	**Apr_May**	**May_Jun**	**Jun_Jul**
TRendLength	14.0	11.1	12.4	9.8	22.0	15.5
TrendSlope	4.1	1.0	-2.8	-0.9	1.1	1.8
MidDistance	9.1	4.1	12.1	13.1	0.0	1.2
Month	**Jul_Aug**	**Aug_Sep**	**Sep_Oct**	**Oct_Nov**	**Nov_Dec**	**Dec_Jan**
TRendLength	18.9	14.2	10.0	3.7	9.0	7.8
TrendSlope	1.0	1.4	0.7	0.1	0.6	-2.9
MidDistance	-1.6	0.4	3.4	6.2	6.1	9.3

The trend lengths are relatively weak, there is no strong shift between passages, based on the slopes results, there is increasing trend in the recent part of the time series from March to April and December to January however from April to May it tend to decrease.

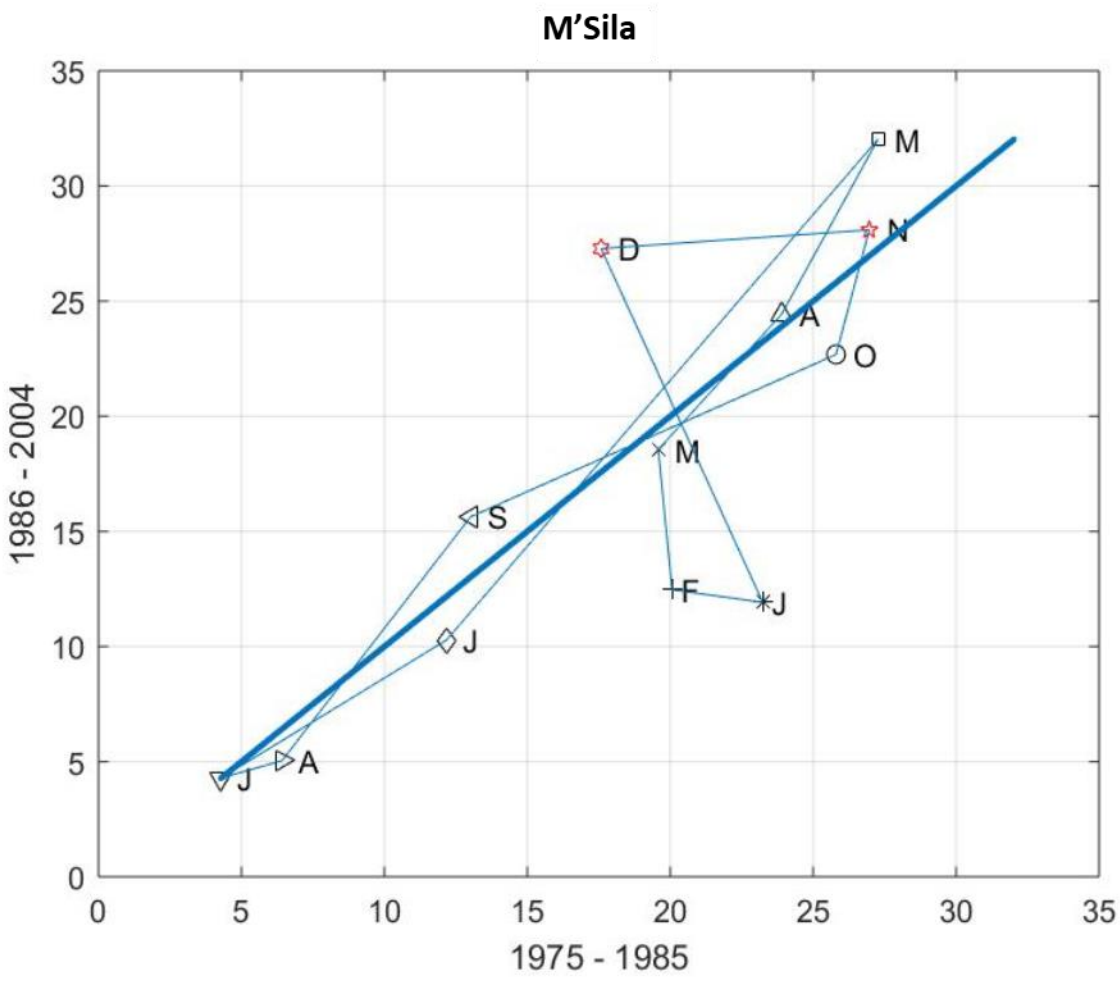

The template contains many loops, sign of unmethodical pursuit caused by December, January, February and May where May is the rainiest month.

March, April November January August July September and October are so close to the trendless zone.

M'Sila Statioin						
Month	**Jan_Feb**	**Feb_Mar**	**Mar_Apr**	**Apr_May**	**May_Jun**	**Jun_Jul**
TRendLength	3.2193	6.1099	7.2967	8.3148	26.4815	9.9202
TrendSlope	-0.1719	-12.6415	1.3621	2.2534	1.4407	0.7595
MidDistance	-9.4591	-4.3136	-0.2455	2.65	0	-0.9409
Month	**Jul_Aug**	**Aug_Sep**	**Sep_Oct**	**Oct_Nov**	**Nov_Dec**	**Dec_Jan**
TRendLength	2.2758	12.4829	14.595	5.5328	9.4166	16.3712
TrendSlope	0.3538	1.6054	0.5512	4.6484	0.0862	-2.717
MidDistance	-0.6841	0.6205	-0.25	-0.9955	5.4136	-0.8091

The longest length is from May to June signify the important decrease in the precipitation amount There is a strong shift from December to January with negative slope (-2) meaning January used to be rainier than December but with time December took over.

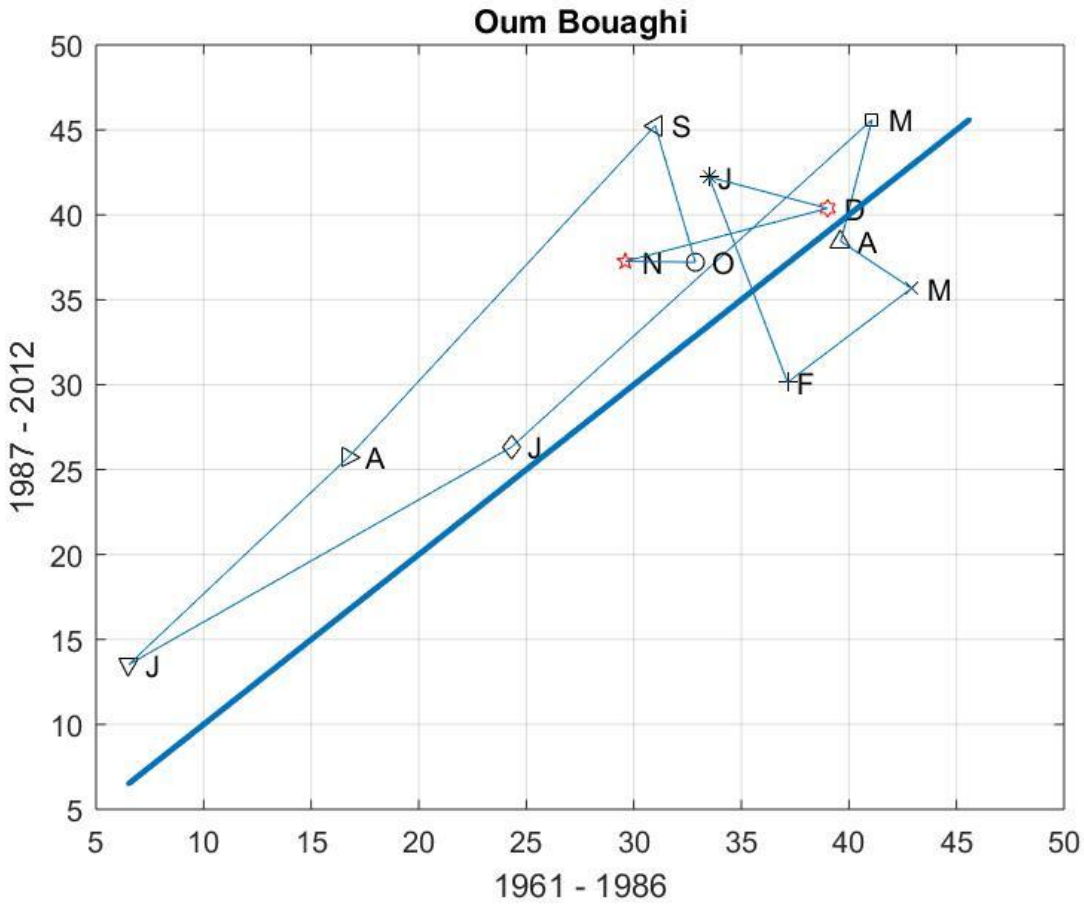

The template shows 9 months located in the increasing trend area, meanwhile, February and march indicate decreasing trend whilst April remain trendless. May and September are the rainiest months.

Oum Bouaghi Station						
Month	**Jan_Feb**	**Feb_Mar**	**Mar_Apr**	**Apr_May**	**May_Jun**	**Jun_Jul**
TRendLength	12.6275	7.9838	4.2912	7.3159	25.5501	21.9128
TrendSlope	-3.3119	0.9606	-0.8407	4.9182	1.1495	0.7194
MidDistance	0.8615	-7.1212	-4.2115	1.6673	0	4.5115
Month	**Jul_Aug**	**Aug_Sep**	**Sep_Oct**	**Oct_Nov**	**Nov_Dec**	**Dec_Jan**
TRendLength	15.9318	24.1612	8.2642	3.2543	9.9028	5.8137
TrendSlope	1.1953	1.3692	-4.3066	-0.0165	0.3314	-0.3357
MidDistance	8.0058	11.6346	9.3058	6	4.5115	5.05

The table show many negative slopes due to the reversible change between the successive months from the first half of the time series to the second half.

May-June represents the longest trend-length followed by August-September, and one can explain that with rapid switch between the wet and dry seasons.

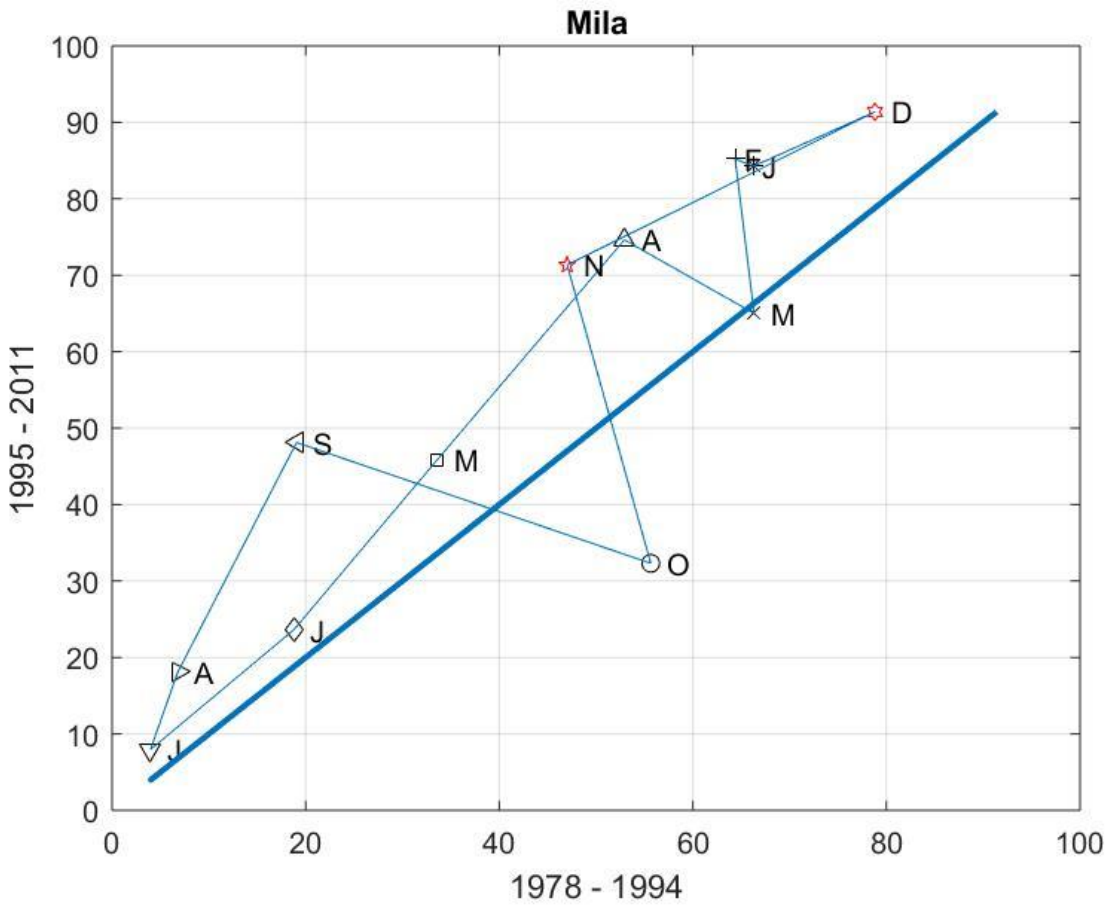

The template reveals generally significant increasing trend, October is the only month that shows a decreasing trend. December the rainiest month, January and February pretty much same amount which tend to increase lately.

Mila Station						
Month	**Jan_Feb**	**Feb_Mar**	**Mar_Apr**	**Apr_May**	**May_Jun**	**Jun_Jul**
TRendLength	2.1	20.3	16.5	34.6	26.8	21.6
TrendSlope	-0.5	-10.3	-0.7	1.5	1.5	1.1
MidDistance	19.4	9.8	10.2	17.0	0.0	4.4
Month	**Jul_Aug**	**Aug_Sep**	**Sep_Oct**	**Oct_Nov**	**Nov_Dec**	**Dec_Jan**
TRendLength	10.5	32.4	39.9	40.0	37.6	14.5
TrendSlope	3.6	2.4	-0.4	-4.5	0.6	0.6
MidDistance	7.6	20.2	2.9	0.5	18.4	15.3

April-May and starting from August to December, all these periods represent medium Trend-Length,

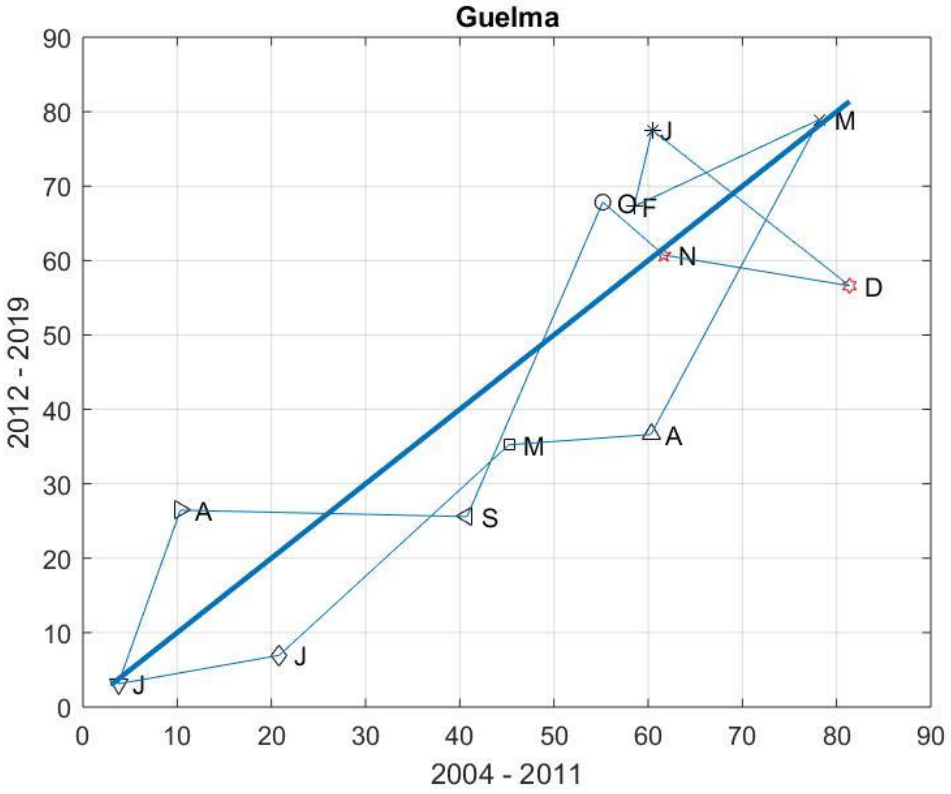

The majority of the months are situated in the decreasing trend area, sing of drought risk in this station. March is the rainiest month, January, February and April trends tend to increase in the last years.

Guelma Station						
Month	**Jan_Feb**	**Feb_Mar**	**Mar_Apr**	**Apr_May**	**May_Jun**	**Jun_Jul**
TRendLength	10.4	22.9	46.0	15.1	37.4	17.5
TrendSlope	5.4	0.6	2.4	0.1	1.2	0.2
MidDistance	12.9	4.8	-11.5	-16.8	0.0	-7.3
Month	**Jul_Aug**	**Aug_Sep**	**Sep_Oct**	**Oct_Nov**	**Nov_Dec**	**Dec_Jan**
TRendLength	24.3	30.4	44.6	9.6	20.1	29.6
TrendSlope	3.5	0.0	2.9	-1.1	-0.2	-1.0
MidDistance	7.7	0.5	-1.3	5.9	-12.8	-3.8

Guelma table present generally weak or medium transition in the whole year, the winter season represent a negative slope [(Oct_Nov), (Nov_Dec) and (Dec_Jan)] which reflect the transition between these months is not in the same direction revealing a perturbation in the precipitation regime in this region in those specific months.

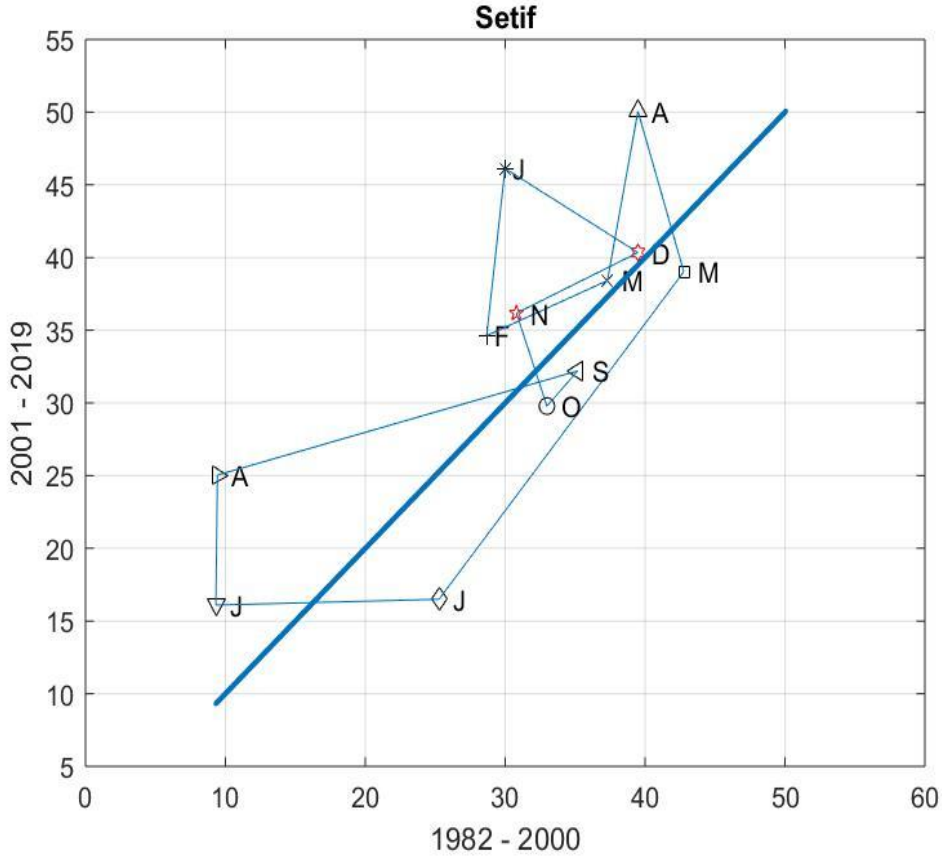

From the template, clearly August tend to increase significantly during the last half of the time series, April is the rainiest month and it tend to increase lately, overall, the behavior is abnormal where many loops are present.

Setif Station						
Month	**Jan_Feb**	**Feb_Mar**	**Mar_Apr**	**Apr_May**	**May_Jun**	**Jun_Jul**
TrendLength	11.6	9.4	11.8	11.5	28.5	16.0
TrendSlope	8.8	0.4	5.3	-3.4	1.3	0.0
MidDistance	11.0	3.5	5.8	3.4	0.0	-1.0
Month	**Jul_Aug**	**Aug_Sep**	**Sep_Oct**	**Oct_Nov**	**Nov_Dec**	**Dec_Jan**
TrendLength	8.9	26.7	3.3	6.8	9.6	11.1
TrendSlope	81.0	0.3	1.1	-2.9	0.5	-0.6
MidDistance	11.2	6.3	-3.1	1.1	3.1	8.5

For Setif table, the trend-length remain in the weak category, (Apr_May), (Oct_Nov) and (Dec_Jan) present a negative trend-slope, only two periods show a negative mid-distance which mean this station is having an increasing trend

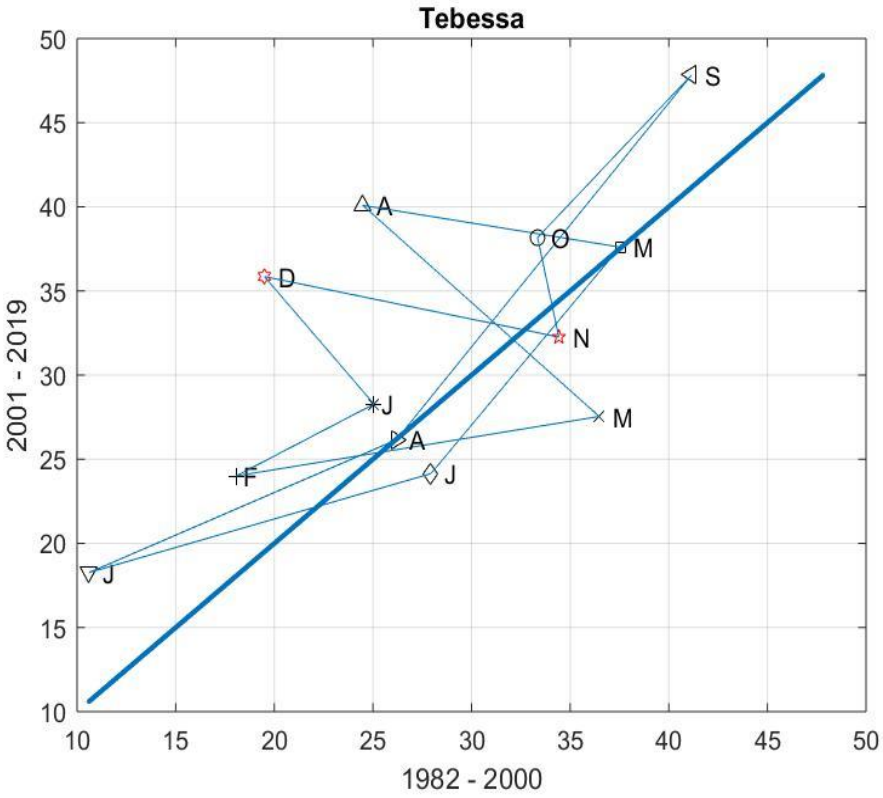

The template shape is very chaotic, the major part positioned above the 45 straight line which indicate the presence of a significant increasing trend. September represents the top rainy month,

Tebessa Station						
Month	**Jan_Feb**	**Feb_Mar**	**Mar_Apr**	**Apr_May**	**May_Jun**	**Jun_Jul**
TrendLength	8.2	18.7	17.4	13.3	16.5	18.3
TrendSlope	0.6	0.2	-1.0	-0.2	1.4	0.3
MidDistance	4.6	-1.5	3.3	7.8	0.0	1.9
Month	**Jul_Aug**	**Aug_Sep**	**Sep_Oct**	**Oct_Nov**	**Nov_Dec**	**Dec_Jan**
TrendLength	17.5	26.3	12.4	6.0	15.4	9.4
TrendSlope	0.5	1.4	1.2	-5.5	-0.2	-1.4
MidDistance	3.8	3.3	5.8	1.3	7.1	9.8

In Tebessa station table, the trend length generally remains indistinguishable, the trend slope shifts often which means the precipitation behavior is not steady, the longest mid distances appear in the rainy month.

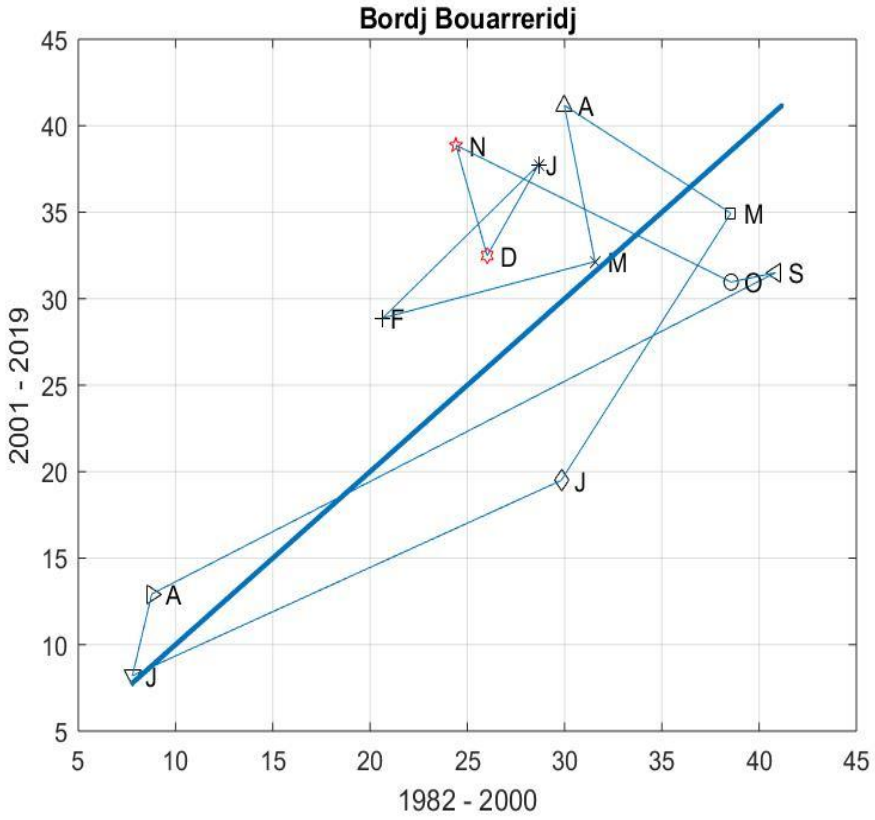

The template contains many loops indicating the unsystematic behavior between the successive months. Especially the wet seasons.

Bordj Bouarreridj Station						
Month	**Jan_Feb**	**Feb_Mar**	**Mar_Apr**	**Apr_May**	**May_Jun**	**Jun_Jul**
TRendLength	12.0	12.0	9.2	10.6	17.7	24.8
TrendSlope	1.1	0.3	-5.7	-0.7	1.8	0.5
MidDistance	8.7	4.4	5.9	3.8	0.0	-5.0
Month	**Jul_Aug**	**Aug_Sep**	**Sep_Oct**	**Oct_Nov**	**Nov_Dec**	**Dec_Jan**
TRendLength	4.8	37.1	2.3	16.2	6.6	5.9
TrendSlope	4.7	0.6	0.2	-0.6	-4.0	2.0
MidDistance	2.3	-2.6	-8.5	3.4	10.5	7.8

For Borj Bouarrerridj, the transition from August to September is the longest among all the others, the trend slope and the mid distance of (Nov_Dec) is the strangest revealing the significance of the change in this particular period.

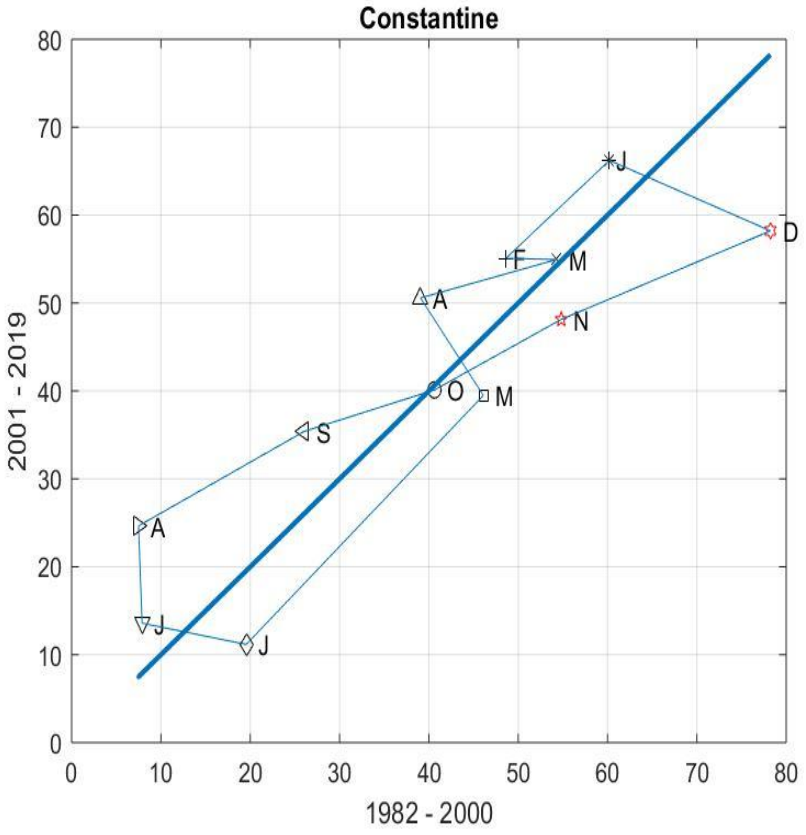

The template stays methodical but it breaks twice (February-March) and (April-May)

Constantine Station						
Month	**Jan_Feb**	**Feb_Mar**	**Mar_Apr**	**Apr_May**	**May_Jun**	**Jun_Jul**
TRendLength	16.1	5.7	15.8	13.1	38.8	11.9
TrendSlope	1.0	0.0	0.3	-1.6	1.1	-0.2
MidDistance	6.2	3.6	6.1	2.5	0.0	-1.3
Month	**Jul_Aug**	**Aug_Sep**	**Sep_Oct**	**Oct_Nov**	**Nov_Dec**	**Dec_Jan**
TRendLength	11.1	21.4	15.3	16.3	25.5	19.7
TrendSlope	-27.4	0.6	0.3	0.6	0.4	-0.4
MidDistance	11.4	13.3	4.4	-3.6	-13.4	-7.0

Constantine station table represent a weak trend length generally, only (May_Jun) is medium, the trend slope of (Jul_Aug) is negative and also significant, the mid distance in noticeable for (Jul_Feb), (Aug_Sep), (Nov_Dec).

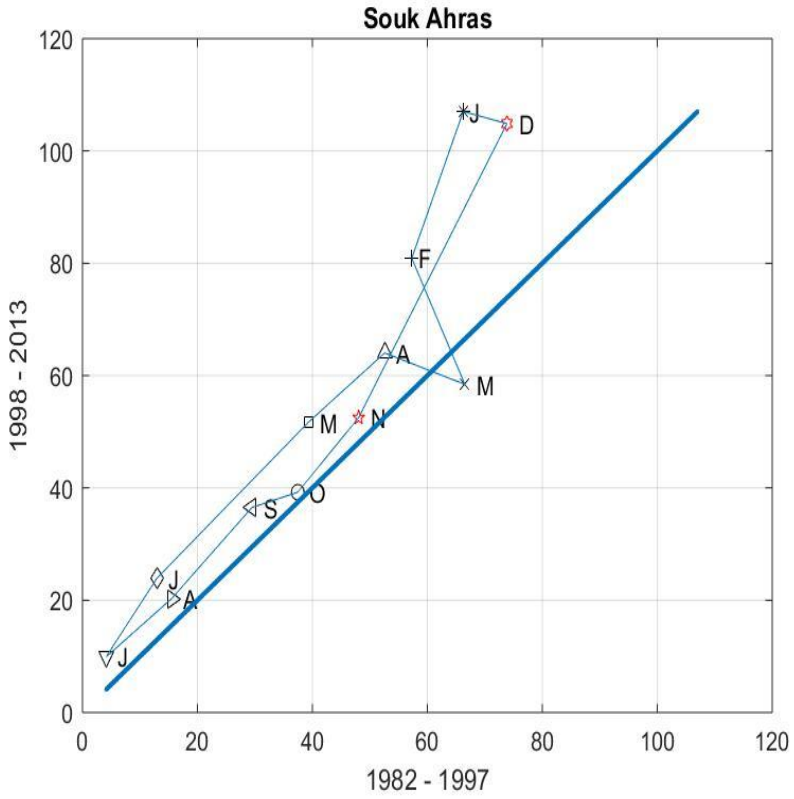

The template is almost systematic, the only month that behave abnormal is March, but generally this station shows an increasing trend.

Souk Ahras Station						
Month	**Jan_Feb**	**Feb_Mar**	**Mar_Apr**	**Apr_May**	**May_Jun**	**Jun_Jul**
TRendLength	27.6	24.3	15.0	18.2	38.3	16.5
TrendSlope	2.9	-2.4	-0.4	0.9	1.1	1.6
MidDistance	32.2	7.8	1.7	11.9	0.0	8.4
Month	**Jul_Aug**	**Aug_Sep**	**Sep_Oct**	**Oct_Nov**	**Nov_Dec**	**Dec_Jan**
TRendLength	15.4	21.4	8.4	17.0	58.4	7.9
TrendSlope	0.9	1.2	0.3	1.3	2.0	-0.3
MidDistance	5.3	5.9	4.4	3.1	17.7	35.9

In Souk Ahras table, (Nov_Dec) is the longest trend length, the slopes does not differ so much, the mid distance is long in both (Jan_Feb) and (Dec_Jan).

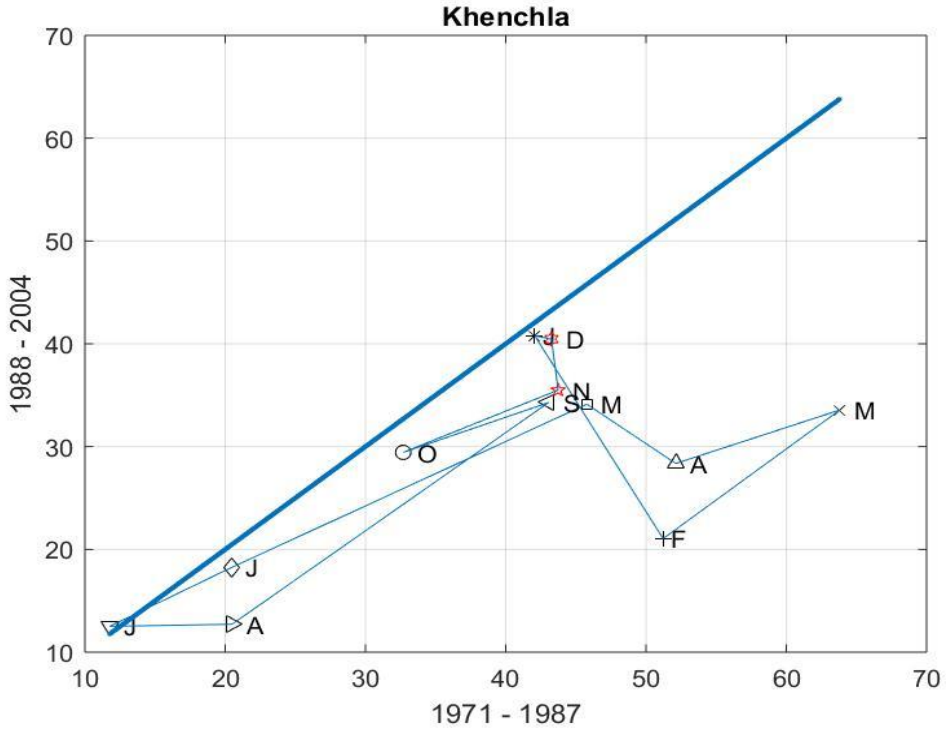

The template is unsystematic and chaotic, all the months appear in the decreasing zone which signify the presence of decreasing trend in rainfall in this station, where Feb, March and April are the most significant.

Khenchla Station						
Month	**Jan_Feb**	**Feb_Mar**	**Mar_Apr**	**Apr_May**	**May_Jun**	**Jun_Jul**
TRendLength	21.8	17.8	12.8	8.6	29.9	10.4
TrendSlope	-2.2	1.0	0.4	-0.9	0.6	0.7
MidDistance	-15.7	-30.2	-27.0	-17.7	0.0	-0.7
Month	**Jul_Aug**	**Aug_Sep**	**Sep_Oct**	**Oct_Nov**	**Nov_Dec**	**Dec_Jan**
TRendLength	8.7	31.2	11.4	12.6	5.0	1.2
TrendSlope	0.0	1.0	0.5	0.5	-10.4	-0.3
MidDistance	-3.5	-8.3	-6.0	-5.7	-5.5	-2.0

Kenchla's table confirm the general decreasing trend where all the mid distances are negative. (Nov_Dec) is the strangest trend slope.

9 SCIENTIFIC CONTRIBUTION

International Publications

- Boudiaf, B., Dabanlı, İ., Boutaghane, H. & Şen, Z. (2020). Temperature and precipitation risk assessment under climate change effect in northeast algeria. Earth Systems and Environment, 4(1), 1-14. https://dx.doi.org/10.1007/s41748-019-00136-7
- Boudiaf, B., Şen, Z. & Boutaghane, H. Climate change impact on rainfall in north-eastern Algeria using innovative trend analyses (ITA). *Arab J Geosci* 14, 511 (2021). https://doi.org/10.1007/s12517-021-06644-z

NATIONAL CONFERENCES

- **Boudiaf B.** & Boutaghane H**,** 2017 The PCA as a decision-making tool for the carcatterization of water quality. Case of industrial discharges of Oued Meboudja. Communication in the framework of the study day: Climate change and water resources: consequences and solutions, held April 19, 2017 in Skikda- Algeria.
- Boutaghane H. & **Boudiaf B**., 2017, Temporal variability of extreme daily rainfall over the north-east of Algeria. Communication in the framework of the study day: Climate change and water resources: consequences and solutions, held on April 19, 2017 in Skikda- Algeria.
- **Boudiaf B**, Dabanli I, Boutaghane H, Şen Z., Temperature and Precipitation Risk Assessment under Climate Change Effect in Bejaia city, Algeria. SNE6-2019-UMMTO « Séminaire sur l'eau », University of Mouloud Mammeri Tizi Ouzou city, 12, 13 and 14 July 2019.
- **Boudiaf B**, Şen Z, Dabanli I, Boutaghane H., Temperature and Precipitation Tendencies in The Rainfall Records in North-East Region Of Algeria (Bejaia city). SNE6-2019-UMMTO « Séminaire sur l'eau », University of Mouloud Mammeri Tizi Ouzou city, 12, 13 et 14 July 2019.